Flavor phenomenology of rare processes in the Standard Model and beyond

Inauguraldissertation
der Philosophisch-naturwissenschaftlichen Fakultät
der Universität Bern

vorgelegt von

Ahmet KOKULU

von Türkei

Leiter der Arbeit:

Prof. Dr. Christoph Greub

Albert Einstein Zentrum für fundamentale Physik
Institut für theoretische Physik, Universität Bern

Flavor phenomenology of rare processes in the Standard Model and beyond

Inauguraldissertation
der Philosophisch-naturwissenschaftlichen Fakultät
der Universität Bern

vorgelegt von

Ahmet KOKULU

von Türkei

Leiter der Arbeit:

Prof. Dr. Christoph Greub

Albert Einstein Zentrum für fundamentale Physik
Institut für theoretische Physik, Universität Bern

Von der Philosophisch-naturwissenschaftlichen Fakultät angenommen.

Der Dekan:

Bern, 26.09.2013

Prof. Dr. S. Decurtins

Abstract

The present work covers several topics including the rare decay $B \to X_s\gamma\gamma$ as well as the study of flavor phenomenology of several other observables. After briefly presenting the methodology used to treat the inclusive rare B-decays, first we study the next-to-leading-logarithmic (NLL) QCD contribution of the electro-magnetic dipole operator $\mathcal{O}_7$ to the double radiative rare process $\bar{B} \to X_s\gamma\gamma$. In this analysis, we supply the first analytical NLL QCD calculation to the decay width of the double-radiative inclusive decay $\bar{B} \to X_s\gamma\gamma$ and find that the numerical impact of the NLL corrections are rather large.

The second study goes beyond the SM. In this work, we point out that a two-Higgs doublet model (2HDM) of type III is capable of explaining the combined 3.4σ discrepancy between the Standard Model predictions for the branching ratios $B \to D\tau\nu$ and $B \to D^*\tau\nu$ and the recent measurements for these observables by BABAR collaboration without fine-tuning. Furthermore, we show that it is also possible to put the theoretical prediction for $B \to \tau\nu$ into an agreement with the 2012 measurements reported by the BABAR and BELLE collaborations.

The last part is devoted to an extensive analysis of the flavor observables in a 2HDM with generic Yukawa structure (of type-III). In this work, in the light of the recent experimental data, we work out all relevant flavor observables and constrain the model both from tree-level processes and from loop observables. Beside this, we give upper limits on the branching ratios of the lepton flavor-violating neutral B meson decays ($B_{s,d} \to \mu e$, $B_{s,d} \to \tau e$ and $B_{s,d} \to \tau\mu$) and correlate the radiative lepton decays ($\tau \to \mu\gamma$, $\tau \to e\gamma$ and $\mu \to e\gamma$) to the corresponding neutral current lepton decays ($\tau^- \to \mu^-\mu^+\mu^-$, $\tau^- \to e^-\mu^+\mu^-$ and $\mu^- \to e^-e^+e^-$), which is of interest to experimentalists working at the LHC and super-B factories.

"Procrastination is the thief of time"

Edward Young

“*Aileme ve Dostlarıma...*“

Contents

Introduction **1**

I Preliminaries **7**

1 The Standard Model **9**
1.1 Overview 11
1.2 Mass generation via Higgs mechanism 12
1.3 The CKM quark mixing matrix 15

2 Two-Higgs-doublet models **18**

3 Effective field theory approach **24**
3.1 Matching procedure 25

4 Calculation techniques **28**
4.1 Integration by parts relations 28
4.2 Method of differential equations 31

II "NLL QCD contribution of the Electromagnetic Dipole operator to $\bar{B} \to X_s\gamma\gamma$", **37**
published in Phys. Rev. D85 (2012) 014020

1 Introduction **39**

2 Leading order result **41**

3 Virtual corrections **44**

4 Bremsstrahlung corrections **46**

5 Final result for the decay width at order α_s **47**

6 Some numerical illustrations **49**

7 Technical details about our calculations **51**
7.1 Details about the calculation of virtual corrections 53
7.2 Details about the calculation of bremsstrahlung corrections 53

8 Summary **54**

A Explicit results for the functions v_i defining the virtual corrections **55**

B Relevant phase-space formulas **56**
B.1 Double differential phase-space for the 3-particle final state 56
B.2 Triple differential phase-space for the 4-particle final state 57

C Renormalization constants 57

III "The $\bar{B} \to X_s\gamma\gamma$ decay: NLL QCD contribution of the Electromagnetic Dipole operator $\mathcal{O}_7$", 61

published in the Proceedings of the conference FPCP 2012 (arXiv:1207.2397 [hep-ph])

1 Introduction 63

2 Leading Order and Final results for the decay width 65

3 Some numerical illustrations 65

4 Concluding remarks 66

IV "Explaining $B \to D\tau\nu$, $B \to D^*\tau\nu$ and $B \to \tau\nu$ in a two Higgs doublet model of type III", 69

published in Phys. Rev. D86 (2012) 054014

1 Introduction 71

2 Effective Field Theory 73

3 Two Higgs doublet model of type III 74

3.1 Experimental constraints 75

3.2 $B \to D\tau\nu$ and $B \to D^*\tau\nu$ 76

3.3 $B \to \tau\nu$ 76

3.4 The quark mass matrix and fine tuning 76

4 Conclusions 77

V "Flavor-phenomenology of two-Higgs-doublet models with generic Yukawa structure", 81

published in Phys. Rev. D87 (2013) 094031

1 Introduction 84

2 Setup 85

3 Constraints on the 2HDM parameter space– overview 88

4 Constraints from 't Hooft's naturalness criterion 92

5 Constraints from tree-level neutral-current processes **93**
5.1 Leptonic neutral meson decays: $B_{s,d} \to \mu^+\mu^-$, $K_L \to \mu^+\mu^-$ and $\bar{D}^0 \to \mu^+\mu^-$. 94
5.1.1 $B_{s,d} \to \mu^+\mu^-$ 95
5.1.2 $K_L \to \mu^+\mu^-$ 96
5.1.3 $\bar{D}^0 \to \mu^+\mu^-$ 96
5.2 Tree-level contributions to $\Delta F = 2$ processes 98
5.3 Lepton-flavor-violating decays: $\tau^- \to \mu^-\mu^+\mu^-$, $\tau^- \to e^-\mu^+\mu^-$ and $\mu \to e^-e^+e^-$ 101

6 Loop-contributions to FCNC processes **103**
6.1 $B_s - \overline{B}_s$, $B_d - \overline{B}_d$ and $K - \overline{K}$ mixing 104
6.2 Radiative B meson decays: $b \to s\gamma$ and $b \to d\gamma$ 104
6.3 Neutral Higgs box contributions to $D - \overline{D}$ mixing 107
6.4 Radiative lepton decays : $\mu \to e\gamma$, $\tau \to e\gamma$ and $\tau \to \mu\gamma$ 108
6.5 $B_s \to \mu^+\mu^-$ 109
6.6 Electric dipole moments and anomalous magnetic moments 109
6.6.1 Charged leptons 109
6.6.2 Electric dipole moment of the neutron 112

7 Tree-level charged current processes **112**
7.1 Tauonic charged B meson decays: $B \to \tau\nu$, $B \to D\tau\nu$ and $B \to D^*\tau\nu$ 114
7.1.1 $B \to D\tau\nu$ and $B \to D^*\tau\nu$ 116
7.1.2 $B \to \tau\nu$ 117
7.2 $D_{(s)} \to \tau\nu$ and $D_{(s)} \to \mu\nu$ 117
7.3 $K \to \mu\nu/\pi \to \mu\nu$ and $K \to e\nu/\pi \to e\nu$ 118
7.4 $\tau \to K\nu/\tau \to \pi\nu$ 118
7.5 Tests for lepton flavour universality: $K(\pi) \to e\nu/K(\pi) \to \mu\nu$ and $\tau \to K(\pi)\nu/K(\pi) \to \mu\nu$ 119
7.5.1 $K \to e\nu/K \to \mu\nu$ and $\pi \to e\nu/\pi \to \mu\nu$ 119
7.5.2 $\tau \to K\nu/K \to \mu\nu$ and $\tau \to \pi\nu/\pi \to \mu\nu$ 120

8 Upper limits and correlation for LFV processes **120**
8.1 Neutral meson decays: $B_{s,d} \to \tau\mu$, $B_{s,d} \to \tau e$ and $B_{s,d} \to \mu e$ 121
8.2 Radiative lepton decays: $\tau \to \mu\gamma$, $\tau \to e\gamma$ and $\mu \to e\gamma$. 123

9 Conclusions **125**

10 Appendix **129**
10.1 Loop functions 129
10.2 Radiative $b \to s(d)\gamma$ decays 130
10.3 Wilson coefficients for $\Delta F = 2$ processes 131
10.3.1 Charged Higgs box contributions 131
10.3.2 Tree-level H_k^0 contribution 132
10.3.3 Neutral Higgs box contribution to D mixing 133
10.4 Semileptonic and leptonic meson decays and tau decays: $B \to (D^{(*)})\tau\nu$, $D_{(s)} \to \ell\nu_\ell$, $K(\pi) \to \ell\nu_\ell$ and $\tau \to K(\pi)\nu$ processes 133
10.5 Lepton flavour violation (LFV): $\ell_i \to \ell_f\gamma$ processes 134

10.6 Wilson coefficients for EDMs and the AMM of the muon 134
10.6.1 Wilson coefficients for EDMs of charged leptons and the anomalous magnetic moment of the muon 134
10.6.2 Wilson coefficients for neutron EDM 135
10.7 Leptonic decays of neutral mesons 136
10.7.1 Wilson coefficients 137
10.8 Flavour-changing lepton decays 138
10.9 Input parameters 138

Acknowledgements **151**

Curriculum vitæ **155**

Introduction

The 21st century has opened an exiting era for particle physicists by the tentative discovery of the Higgs particle[1] at the CMS [1] and ATLAS [2] experiments in 2012. LHC, the world largest and highest energy particle accelerator, is built in a circular tunnel of circumference of 27 km and at a depth ranging from 50 to 175 meters underground and it lies in the Swiss and French border on the outskirts of Geneva [3]. In this great collider, the proton beams are accelerated to reach about 0.999999991 of the speed of light (c) and make a head-on collision in a total collision energy of 14 TeV, the highest energy scales attained ever. By doing so LHC aims to test the Standard Model (SM) of particle physics, which is believed to be the theory of the electro-magnetic, weak and strong interactions. In fact, since its birth in the early 1970s the SM of particle physics has been quite powerful in describing the nature around us by showing excellent agreement with the experimental data. On the other side, there are numerous observed phenomena that the SM is not able to explain. For example, the SM predicts massless neutrinos. However, the recent observation of neutrino oscillations indicates that neutrinos do have mass [4, 5]. Another issue is the difficulty for SM in trying to explain the matter–anti-matter asymmetry of the Universe. The Sakharov's three criteria [6]: baryon number violation, C and CP violation and departure from thermal equilibrium, which explain why the today's Universe is matter dominated, cannot be accounted within the context of SM [7]. Moreover, the hierarchy problem[2] is an example of further problems from which the SM suffers. Therefore, it is widely believed that the SM in its todays form is not the ultimate theory but more like a low-energy-effctive theory (which is powerful up to TeV scales only) of a more fundamental theory and thus it has to be modified in its high energy sector to feed these deficiencies. Enormous work has been devoted by physicists to look for physics beyond SM (SUSY, 2HDMs, extra-dimensions etc.) in order to provide natural explanations to the problems of SM. In this regard, LHC also aims (hopes) to find some "new-physics" (NP) particles.

Beside the direct search for NP at particle accelerators, there is an alternative place where possible NP can exhibit itself indirectly via contributions to well measurable low energy processes. In this perspective, when both the theoretical predictions and the experimental results are precise enough, it is possible to draw constraints on the range of any NP model.

In this context, the inclusive rare B-meson decays gives important information on the indirect search for NP at scales of several hundred GeV as well as they are unique for over-constraining the CKM elements. In the SM all these processes proceed through loop diagrams and thus are relatively suppressed[3]. In the extensions of the SM the contributions stemming from the diagrams with "new" particles in the loops can be comparable or even larger than the contribution from the SM. Thus getting experimental information on rare decays puts strong constraints on the extensions of the SM or can even lead to a disagreement with the SM predictions, providing evidence for "new physics". To make a rigorous comparison between experiment and theory, precise SM calculations for the (differential) decay rates are mandatory. While the branching ratios for $\bar{B} \to X_s\gamma$ [9] and $\bar{B} \to X_s\ell^+\ell^-$ are known today even to next-to-next-to-leading logarithmic (NNLL) precision (for reviews, see [10, 11]), other

[1]The Higgs field is assumed to be responsible for giving mass to all elementary particles.

[2]The hierarchy problem means the large difference between the strengths of the weak force and gravity i.e. it asks why the gravity is 10^{32} times weaker than the weak nuclear force [8].

[3]In the SM, flavor-changing-neutral-current (FCNC) transitions are forbidden at tree-level by definition.

branching ratios, like the one for $\bar{B} \to X_s\gamma\gamma$, has been calculated roughly 10 years ago to leading logarithmic (LL) precision in the SM by several groups [12, 13, 14, 15] and only recently a first step towards next-to-leading-logarithmic (NLL) precision was presented by us in [16]. In contrast to $\bar{B} \to X_s\gamma$, the current-current operator $\mathcal{O}_2$ has a non-vanishing matrix element for $b \to s\gamma\gamma$ at order α_s^0 precision, leading to an interesting interference pattern with the contributions associated with the electromagnetic dipole operator $\mathcal{O}_7$ already at LL precision. As a consequence, potential NP should be clearly visible not only in the total branching ratio, but also in the differential distributions. As the process $\bar{B} \to X_s\gamma\gamma$ is expected to be measured at the planned Super B-factories in Japan and Italy, it is necessary to calculate the differential distributions to NLL precision in the SM, in order to fully exploit its potential concerning new physics.

On the other side, having the precise SM calculations at hand and confronting them with experimental data, one is able to check for any possible deviations between SM predictions and the experiment which might give a sign for a physics beyond the SM. Assuming the existence of new physics, such deviations between the SM and experimental data allow to put constraints on the particular NP model under consideration. As an example of such models are the two-Higgs-doublet-models (2HDMs). The 2HDMs [17] have been under intensive investigation for a long time (see for example Ref. [18] for an introduction or Ref. [19] for a recent review article). There are several reasons for this great interest in 2HDMs: Firstly, 2HDMs are very simple extensions of the SM obtained by just adding an additional scalar $SU(2)_L$ doublet to the SM particle content. This limits the number of new degrees of freedom and makes the model rather predictive. Secondly, motivation for 2HDMs comes from axion models [20] because a possible CP-violating term in the QCD Lagrangian can be rotated away [21] if the Lagrangian has a global $U(1)$ symmetry which is only possible if there are two Higgs doublets. Also the generation of the baryon asymmetry of the Universe motivates the introduction of a second Higgs doublet because in this way the amount of CP violation can be large enough to accommodate for this asymmetry. Finally, probably the best motivation for studying 2HDMs is the Minimal Supersymmetric Standard Model (MSSM) where supersymmetry enforces the introduction of a second Higgs doublet [22] due to the holomorphic superpotential. Furthermore, the 2HDM of type III is also the effective theory obtained by integrating out all super-partners of the SM-like particles from MSSM. 2HDMs are not only interesting for direct searches for additional Higgs bosons at colliders. In addition to these high energy searches at the LHC also low-energy precision flavor observables provide a complementary window to physics beyond the SM, i.e. to the 2HDMs. In this respect, FCNC processes, e.g. neutral meson decays to muon pairs ($B_{s(d)} \to \mu^+\mu^-$, $D \to \mu^+\mu^-$ and $K_L \to \mu^+\mu^-$) are especially interesting because they are very sensitive to flavor changing neutral Higgs couplings. However, also charged current processes like tauonic B-meson decays are affected by the charged Higgs boson and $b \to s\gamma$ provides currently the best lower limit on the charged Higgs mass in the 2HDM of type II. Recently, tauonic B decays received special attention because the BABAR collaboration performed an analysis of the semileptonic B decays $B \to D\tau\nu$ and $B \to D^*\tau\nu$ reporting a discrepancy of $2.0\,\sigma$ and $2.7\,\sigma$ from the SM expectation, respectively. The measurements of both decays exceed the SM predictions, and combining them gives a $3.4\,\sigma$ deviation from the SM [23, 24] expectation, which constitutes first evidence for new physics in semileptonic B decays to tau leptons. This evidence for the violation of lepton flavor universality is further supported by the measurement of $B \to \tau\nu$ by BABAR [25, 26] and BELLE [27, 28] which exceeds the SM prediction by $1.6\,\sigma$ using V_{ub} from the global fit [29]. Assuming that these deviations from the SM are not statistical fluctuations or underestimated theoretical or systematic uncertainties, it is interesting to ask which model of new physics can explain the measured values. Since, a 2HDM of type II cannot explain $B \to \tau\nu$, $B \to D\tau\nu$ and $B \to D^*\tau\nu$ simultaneously [23], one must look at 2HDMs with more general Yukawa structures. Also 2HDMs of type III with Minimal Flavor Violation (MFV) [30] cannot explain these deviations from the SM. These points motivated us to perform a complete analysis of flavor-violation in 2HDMs of type III. For this purpose we took into account all relevant constraints from FCNC processes (both from tree-level contributions and from loop-induced effects) and considered afterwards the possible effects in charged current processes.

Organization of the thesis

This thesis is split into several independent pieces as follows:

- **Part I:** In part-I we give a brief overview of the Standard Model and two-Higgs-doublet-models (2HDMs) and discuss the theoretical framework used to perform perturbative precision calculations in inclusive rare B meson decays.

- **Part II:** Here we present in detail our results in analytical form for the calculation of the NLL QCD contribution of the electromagnetic dipole operator to $\bar{B} \to X_s\gamma\gamma$. In this part, we dealt with numerous loop and d-dimensional phase-space integrals for which the calculation was made possible using the calculation techniques discussed in part I. We published our corresponding results in *Phys. Rev. D85 (2012) 014020 (arXiv:1110.1251 [hep-ph]).*

- **Part III:** *"The $\bar{B} \to X_s\gamma\gamma$ decay:*
  NLL QCD contribution of the Electromagnetic Dipole operator $\mathcal{O}_7$"; C12-05-21 Conference proceedings, hep-ph/1207.2397.
  Presented at Flavor Physics and CP Violation (FPCP 2012), Hefei, China, May 21-25, 2012.

  For completeness, we also include our contribution to the proceedings of the international conference "Flavor Physics and CP Violation (FPCP 2012), Hefei, China, May 21-25, 2012" where I have presented our results on the NLL QCD contribution of the electromagnetic dipole operator to $\bar{B} \to X_s\gamma\gamma$.

- **Part IV**: This part is devoted to the study of charged current processes $B \to D\tau\nu$, $B \to D^*\tau\nu$ and $B \to \tau\nu$ in a two Higgs doublet model of type III. Working, for simplicity, with an MSSM like Higgs potential (which reduces the number of free parameters of the model) we showed that a 2HDM of type III, which allows for FCNC interactions at the tree level, with flavor violation in the up sector can account for the deviations of $B \to D^*\tau\nu$ and $B \to \tau\nu$ from the SM predictions simultaneously without causing conflict with other observables. Furthermore, it is also possible to bring $B \to \tau\nu$ prediction into an agreement with experiment in a type-III 2HDM. We published our corresponding results in *Phys. Rev. D86 (2012) 054014 (arXiv:1206.2634 [hep-ph]).*

- **Part V:** This last piece of the thesis deals with an extensive analysis of the flavor observables in a general 2HDM (of type III). Scanning all relevant flavor observables, we provided stringent constraints on the parameter-space of the model. Furthermore, using the constraints we obtained, we gave upper bounds on the branching ratios of the lepton flavor-violating neutral B meson decays ($B_{s,d} \to \mu e$, $B_{s,d} \to \tau e$ and $B_{s,d} \to \tau\mu$) and correlated the radiative lepton decays ($\tau \to \mu\gamma$, $\tau \to e\gamma$ and $\mu \to e\gamma$) to the corresponding neutral current lepton decays ($\tau^- \to \mu^-\mu^+\mu^-$, $\tau^- \to e^-\mu^+\mu^-$ and $\mu^- \to e^-e^+e^-$). We published our corresponding results in *Phys. Rev. D87 (2013) 094031 (arXiv:1303.5877 [hep-ph])*.

In addition, I recently started a related calculation. Considering the decay channels of the heavy Higgses ($A^0, H^0 \to \bar{t}c$) predicted by the 2HDM of type III together with the top quark decay ($t \to h^0 c$) to the light SM like Higgs, a detailed analysis of the decay rates for these transitions in the type-III 2HDM is planned but not part of this thesis. This work is important in the sense of testing the type-III 2HDM at the LHC.

References

[1] CMS collaboration: http://cms.web.cern.ch/cms/index.html

[2] ATLAS collaboration: http://www.atlas.ch/

[3] Large Hadron Collider: http://lhc.web.cern.ch/lhc/

[4] N. Agafonova *et al.* [OPERA Collaboration], Phys. Lett. B **691** (2010) 138 [arXiv:1006.1623 [hep-ex]].

[5] P. A. R. Ade *et al.* [Planck Collaboration], arXiv:1303.5076 [astro-ph.CO].

[6] A. D. Sakharov, Pisma Zh. Eksp. Teor. Fiz. **5** (1967) 32 [JETP Lett. **5** (1967) 24] [Sov. Phys. Usp. **34** (1991) 392] [Usp. Fiz. Nauk **161** (1991) 61].

[7] M. Trodden, 1998, hep-ph/9805252.

[8] http://profmattstrassler.com/articles-and-posts/particle-physics-basics/the-hierarchy-problem/

[9] M. Misiak, H. Asatrian, K. Bieri, M. Czakon, A. Czarnecki, et al., Phys.Rev.Lett. **98**, 022002 (2007), `hep-ph/0609232`.

[10] T. Hurth and M. Nakao, Ann.Rev.Nucl.Part.Sci. **60**, 645 (2010), `1005.1224`.

[11] A. J. Buras (2011), `1102.5650`.

[12] H. Simma and D. Wyler, Nucl.Phys. **B344**, 283 (1990).

[13] L. Reina, G. Ricciardi, and A. Soni, Phys.Lett. **B396**, 231 (1997), `hep-ph/9612387`.

[14] L. Reina, G. Ricciardi, and A. Soni, Phys.Rev. **D56**, 5805 (1997), `hep-ph/9706253`.

[15] J.-j. Cao, Z.-j. Xiao, and G.-r. Lu, Phys.Rev. **D64**, 014012 (2001), `hep-ph/0103154`.

[16] H. Asatrian, C. Greub, A. Kokulu, and A. Yeghiazaryan, Phys.Rev. **D85**, 014020 (2012), `1110.1251`.

[17] T. Lee, pp. 1226–1239, 1973.

[18] J. F. Gunion, H. E. Haber, G. L. Kane, and S. Dawson, *Front.Phys.*, vol. 80, pp. 1–448, 2000.

[19] G. Branco, P. Ferreira, L. Lavoura, M. Rebelo, M. Sher, *et al.*, *Phys.Rept.*, vol. 516, pp. 1–102, 2012, 1106.0034.

[20] J. E. Kim, *Phys.Rept.*, vol. 150, pp. 1–177, 1987.

[21] R. Peccei and H. R. Quinn, *Phys.Rev.Lett.*, vol. 38, pp. 1440–1443, 1977.

[22] H. E. Haber and G. L. Kane,*Phys.Rept.*, vol. 117, pp. 75–263, 1985.

[23] B. Aubert *et al.*, 2012, 1205.5442.

[24] J. Lees *et al.*, 2013, 1303.0571.

[25] J. Lees *et al.*, 2012, 1207.0698.

[26] B. Aubert *et al.*, *Phys.Rev.*, vol. D81, p. 051101, 2010.

[27] K. Hara *et al.*, *Phys.Rev.*, vol. D82, p. 071101, 2010, 1006.4201.

[28] I. Adachi *et al.*, 2012, 1208.4678.

[29] J. Charles *et al.*, *Eur.Phys.J.*, vol. C41, pp. 1–131, 2005, hep-ph/0406184.

[30] G. D'Ambrosio, G. F. Giudice, G. Isidori, and A. Strumia, *Nucl. Phys.*, vol. B645, pp. 155–187, 2002, hep-ph/0207036.

Part I

Preliminaries

1 The Standard Model

To the best of our knowledge, there exist four fundamental forces in nature: electro-magnetic, weak, strong and gravitational forces. The SM of particle physics is believed to be the theory of the first three forces, while it fails to incorporate gravity. All the matter in the universe is found to be made of a few basic building blocks called fundamental particles, governed by four fundamental forces as shown in Fig. 1. The recent cosmological observations by the Planck satellite [1] further showed that we only know about 4.9% of our universe while we do not currently know much about the rest, which is consisting of the so called *dark matter* (26.8%) and *dark energy* (68.3%).

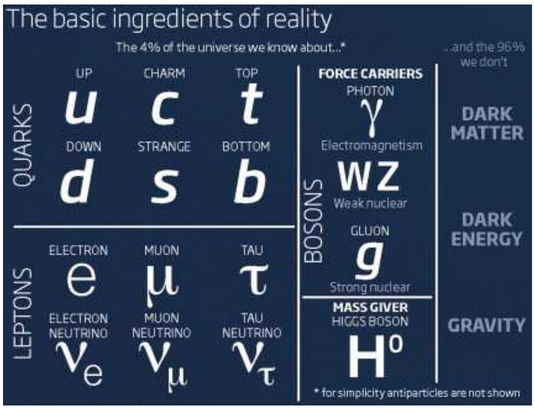

Figure 1: The basic ingredients of reality.

Developed in the late 1960s and early 1970s [2, 3, 4, 5, 6, 7], the SM has been powerful in explaining almost all experimental results and accurately predicted a wide range of phenomena. As an example, in Table 1 we illustrate the precision test of *Quantum Electro Dynamics* (QED) through the quite successful determination of α_{em}. In course of time and through excessive experiments, the SM has become established as a well-tested theory in physics. The great success of unifying the weak and electromagnetic forces into a single theory called *electroweak theory* rewarded Abdus Salam, Sheldon Glashow and Steven Weinberg the nobel prize in physics in 1979. Beside, the prediction of the *asymptotic freedom*[1] property of *Quantum-Choromo-Dynmamics* (QCD) in the early 1970s was another big achievement of the SM and rewarded David Politzer, Frank Wilczek and David Gross the nobel prize in physics in 2004. The experimental confirmations of these predictions together with the discoveries of the bottom quark in 1977, the W and Z in 1983, the top quark in 1995, the tau neutrino in 2000 and the recent tentative discovery of the Higgs particle in 2012 at CMS and ATLAS experiments has brought SM a great confidence and success.

Despite its enormous predictive power, the SM still stays to be inadequate to explain some observed phenomena, which brings physicists to think that the SM is not complete and it should be extended in its high energy sector. Some of the deficiencies of the SM can be summarized as follows:

[1] Asymptotic freedom in QCD means that at sufficiently high energies, the coupling strength of quarks, confined within hadrons, gets weaker to allow them move almost freely.

QED experiments	$\boldsymbol{\alpha_{\mathbf{em}}^{-1}}$
Low-energy QED	
Electron $(g-2)$	137.035 992 35 (73)
Muon $(g-2)$	137.035 5 (11)
Muonium hyperfine splitting	137.035 994 (18)
Lamb shift	137.036 8 (7)
Hydrogen hyperfine splitting	137.036 0 (3)
$2^3S_1 - 1^3S_1$ splitting in positronium	137.034 (16)
$^1S_0$ positronium decay rate	137.00 (6)
$^3S_1$ positronium decay rate	136.971 (6)
Neutron compton wavelength	137.036 010 1 (54)
High-energy QED	
$\sigma\,(e^+e^- \to e^+e^-e^+e^-)$	136.5 (2.7)
$\sigma\,(e^+e^- \to e^+e^-\mu^+\mu^-)$	139.9 (1.2)
Condensed matter	
Quantum Hall effect	137.035 997 9 (32)
AC Josephson effect	137.035 977 0 (77)

Table 1: Table quoted from Ref. [8] showing the values of α_{em} obtained from various precision QED experiments. The shown values of α_{em} are obtained by the fit of the experimental measurement to the corresponding theory side where α_{em} appears as a parameter. These precision tests of the fine structure constant constitutes an evidence for QED to be a strongly tested and enormously successful theory.

- The SM predicts massless neutrinos, while the the recent observation of neutrino oscillations indicates that neutrinos do have mass.
- How can gravity be incorporated in the SM (super-gravity theories, string theory)?
- The SM is not capable of explaining the observed matter-anti matter asymmetry of the universe. The Sakharovs three criteria cannot be accounted for within the context of SM.
- Why is the gravity 10^{32} times weaker than the weak nuclear force (hierarchy problem)?
- There is no natural explanation why the θ_{QCD} parameter has to be small in the SM (strong-CP problem).
- What is the reason for the electroweak sector of SM to be chiral (absence of right-handed W couplings in the SM)?

Generations			$SU(3)_c$	$SU(2)_L$			$U(1)_Y$	$U(1)_Q$
1	2	3	Rep.	T_2	T_2^3	Rep.	Y	Q
$\begin{pmatrix} u \\ d \end{pmatrix}_L$	$\begin{pmatrix} c \\ s \end{pmatrix}_L$	$\begin{pmatrix} t \\ b \end{pmatrix}_L$	**3**	$1/2$ $1/2$	$1/2$ $-1/2$	**2**	$1/6$ $1/6$	$2/3$ $-1/3$
u_R d_R	c_R s_R	t_R b_R	**3**	0 0	0 0	**1**	$2/3$ $-1/3$	$2/3$ $-1/3$
$\begin{pmatrix} \nu_e \\ e \end{pmatrix}_L$	$\begin{pmatrix} \nu_\mu \\ \mu \end{pmatrix}_L$	$\begin{pmatrix} \nu_\tau \\ \tau \end{pmatrix}_L$	**1**	$1/2$ $1/2$	$1/2$ $-1/2$	**2**	$-1/2$ $-1/2$	0 -1
e_R	μ_R	τ_R	**1**	0	0	**1**	-1	-1

Table 2: Quark and lepton families of the SM and their transformation properties under the gauge groups described.

In this chapter, we do not intend to give a thorough discussion of the SM, for which there are many text books, notes or papers discussing it in detail. Instead, we will rather put our focus on the particle content and parameters of the SM, the generation of masses via Higgs mechanism as well as discuss Cabibbo-Kabayashi-Maskawa (CKM) matrix by mentioning the present status of its entries. In the following considerations, we benefit from [9, 10, 11, 12].

1.1 Overview

As mentioned before, the SM of particle physics incorporates the strong, weak and electromagnetic interactions. In the group theory language, it is based on the gauge group

$$G_{SM} = SU(3)_c \otimes SU(2)_L \otimes U(1)_Y . \qquad (1)$$

where $SU(3)_c$ and $SU(2)_L \otimes U(1)_Y$ stand for the strong and the unified electro-weak sectors, respectively.

The SM includes 12 elementary fermions: 6-quarks and 6 leptons appearing in 3 families, 5 elementary bosons: 4 gauge bosons ($\gamma, g, W^{\pm}, Z$)–the so called *force carriers*, and the Higgs. Quarks carry color charges and form composite colorless states like baryons (qqq) or mesons ($q\bar{q}$), which belong to the larger set called hadrons. The quantum numbers (spin, charge, color-charge, etc) which a particle carries determine the transformation properties of that particle under the gauge transformations. In Eq. (1), $SU(3)_c$ only affects the particles having color-charges (index c), $SU(2)_L$ acts only on the left handed fields while it leaves the right handed ones unchanged and lastly the $U(1)_Y$ transformation operates on the fermion fields according to their *hypercharge* quantum number Y.

In the SM there are 18 independent parameters[2], which are not fixed by the model but only determined experimentally. They are called the *free parameters* of the model and read:

- 3 couplings g, g', g_s (or alternatively $e, \sin\theta_{\rm w}, g_s$)
- 4 CKM parameters (3 angles and 1 phase)

[2]Actually, strictly speaking $\theta_{\rm QCD}$ is a free parameter of QCD too, and so is sometimes considered to be the nineteenth free parameter of the Standard Model.

Boson	$SU(3)_c$ Rep.	$SU(2)_L$ Rep.	Y	Q	Role
B_μ	**1**	**1**	-	-	$U(1)_Y$ gauge boson
W_μ	**1**	**3**	-	-	$SU(2)_L$ gauge bosons
G^a_μ	**8**	**1**	0	0	$SU(3)_c$ gauge bosons
$\phi = \begin{pmatrix} \phi^+ \\ \phi^0 \end{pmatrix}_L$	**1**	**2**	1/2 1/2	1 0	Generation of masses

Table 3: Bosonic fields of the SM, their roles and the transformation properties under the gauge groups described.

- 2 boson masses m_Z and m_H (the $W^\pm$ mass can be expressed in terms of m_Z and θ_w)
- 6 quark masses : $m_u, m_d, m_s, m_c, m_b, m_t$
- 3 lepton masses : m_e, m_μ, m_τ (no neutrino masses).

Table 2 and Table 3 presents a summary of the fermionic and bosonic content of the SM, their corresponding quantum numbers together with the representation of the gauge group they belong to.

1.2 Mass generation via Higgs mechanism

In physics, symmetries play a crucial role. According to Noether's theorem, for every continuous symmetry realized in a system there correspond a conserved quantity. For example, time translation invariance of a system leads to conservation of energy, a global $U(1)$ symmetry of QED ensures the conservation of the electric charge (continuity equation), a local gauge invariance guarantees the gauge bosons of QED (photon) and QCD (gluon) to be massless and Lorenz invariance brings along the requirement that the speed of light should be a constant, which is essential in special theory of relativity, etc. Beside these, the condition of renormalizability is crucial as it makes a model more predictive. Writing down by hand mass terms in the Lagrangian for the gauge bosons (or fermions) would explicitly break gauge symmetry, which is not desirable for the reasons discussed above. Hence, in 1967 Weinberg [3] and Salam proposed to generate such mass terms via *spontaneous symmetry breaking* (SSB)[3] by introducing a complex scalar $SU(2)_L$ Higgs doublet

$$\Phi(x) = \begin{pmatrix} \phi^+(x) \\ \phi^0(x) \end{pmatrix}, \tag{2}$$

with the renormalizable Lagrangian

$$\begin{aligned} \mathcal{L}_\Phi &= (\partial_\mu \Phi)^\dagger (\partial^\mu \Phi) - V(\Phi), \\ V(\Phi) &= -\mu^2 \Phi^\dagger \Phi + \lambda \left(\Phi^\dagger \Phi\right)^2, \end{aligned} \tag{3}$$

[3]In fact, SSB is not restricted to gauge symmetries. It can be considered as a subtle way to break a symmetry by still requiring that the Lagrangian remains invariant under the symmetry transformation while the ground state of the system is not invariant i.e. not a singlet under the symmetry transformations.

where $\lambda > 0$ (such that the potential is bounded from below) and μ is a real parameter ($\mu^2 > 0$). In order to keep the local gauge invariance of the Lagrangian intact, one replaces the derivative ∂_μ by a covariant derivative of the form

$$\partial_\mu \longrightarrow D_\mu = \partial_\mu + igT_2^a W_\mu^a + ig'YB_\mu \,. \tag{4}$$

The corresponding potential develops a minimum when $\Phi^\dagger\Phi = \frac{\mu^2}{2\lambda}$ (see Fig. 2) which leads to a constant field configuration of the form

$$\Phi_{\vec{\delta}} = e^{i\delta^i T_2^i} \begin{pmatrix} 0 \\ v \end{pmatrix}, \tag{5}$$

where $v = \mu/\sqrt{2\lambda}$ ($\sim 174\,\mathrm{GeV}$). Since these are infinitely many ground state configurations, one of them has to be chosen spontaneously.

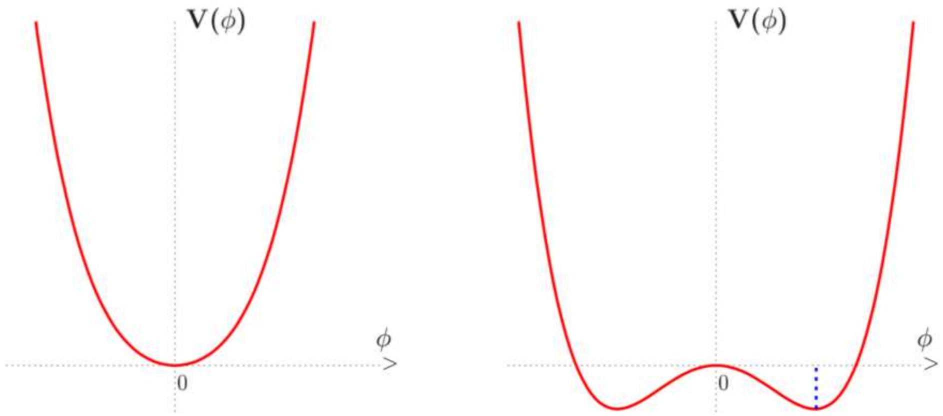

Figure 2: Shape of the scalar potential $V(\Phi)$ for the choices $\mu^2 < 0$ (left) and $\mu^2 > 0$ (right).

There is an infinite number of ground states each with the same lowest energy, i.e. we have a degenerate vacuum. The symmetry breaking occurs in the choice made for the value of $\vec{\delta}$ which represents the "true" vacuum. For a fixed vector $\vec{\delta}$ e.g. $\vec{\delta} = 0$, Eq. (5) is not invariant under $SU(2)_L$ transformations, which spontaneously break the symmetry. For convenience let us work in unitary gauge[4] and choose the Higgs doublet to have the form ($\vec{\delta} = 0$)

$$\Phi(x) = \begin{pmatrix} 0 \\ \chi(x) \end{pmatrix}, \quad \text{such that} \quad \langle 0|\Phi(x)|0\rangle = \begin{pmatrix} 0 \\ v \end{pmatrix}. \tag{6}$$

It is trivial to see that this is not invariant under gauge transformations while invariant under QED gauge group $U(1)_Q$ transformations:

$$e^{i\alpha(x)Q} \begin{pmatrix} 0 \\ v \end{pmatrix} = \begin{pmatrix} 0 \\ v \end{pmatrix} \quad \Longrightarrow \quad Q|0\rangle = 0\,, \tag{7}$$

where the generator of $U(1)_Q$ group is given by $Q = T_2^3 + Y$. This means that the original $SU(2)_L \otimes U(1)_Y$ symmetry of the Lagrangian is not completely broken after the choice of the "true" vacuum but breaks down to $U(1)_Q$ and hence this shows that SM incorporates QED.

[4]In this gauge the unphysical Goldstone bosons fields are set to zero. Namely, they reappear as the longitudinal degrees of freedom of the massive gauge bosons.

To see how to get mass terms for the gauge bosons, let us expand $\Phi(x)$ around its vacuum expectation value as (in unitary gauge)

$$\Phi(x) = \Phi_0 + \Phi'(x) = \begin{pmatrix} 0 \\ v + \frac{H(x)}{\sqrt{2}} \end{pmatrix} \quad \text{with} \quad \Phi_0 = \begin{pmatrix} 0 \\ v \end{pmatrix} . \tag{8}$$

The field H above corresponds to the physical Higgs field and has zero vacuum expectation value.

Expressing the Lagrangian in Eq. (3) in terms of the physical gauge fields

$$\begin{aligned} W_\mu^\pm &= \frac{1}{\sqrt{2}}\left(W_\mu^1 \mp i W_\mu^2\right), \qquad Z_\mu = \frac{1}{\sqrt{g^2+g'^2}}\left(gW_\mu^3 - g'B_\mu\right), \\ A_\mu &= \frac{1}{\sqrt{g^2+g'^2}}\left(g'W_\mu^3 + gB_\mu\right) \end{aligned} \tag{9}$$

gives

$$D_\mu \Phi = \left(\partial_\mu + \frac{ig}{2}\begin{pmatrix} W_\mu^3 & \sqrt{2}W_\mu^- \\ \sqrt{2}W_\mu^+ & -W_\mu^3 \end{pmatrix} + \frac{ig'}{2}B_\mu\right)\begin{pmatrix} 0 \\ v + \frac{H}{\sqrt{2}} \end{pmatrix}, \tag{10}$$

such that

$$\begin{aligned} \mathcal{L}_\Phi &= \frac{1}{2}(\partial_\mu H)^2 - \mu^2 H^2 + \frac{g^2 v^2}{2} W_\mu^- W^{\mu +} + \frac{g^2 v^2}{4\cos^2\theta_{\rm w}} Z_\mu Z^\mu + 0 \cdot A_\mu A^\mu \\ &+ \text{ interaction terms}, \end{aligned} \tag{11}$$

from which we can immediately read the boson masses to be

$$\begin{aligned} m_W &= \frac{gv}{\sqrt{2}}, \qquad m_Z = \frac{gv}{\sqrt{2}\cos\theta_{\rm w}} \\ m_H &= \sqrt{2}\mu = 2v\sqrt{\lambda} \qquad e = g\sin\theta_{\rm w} \ \text{ and } \ m_W/m_Z = \cos\theta_{\rm w}, \end{aligned} \tag{12}$$

where $\theta_{\rm w}$ is the weak mixing angle. As can be seen, we do not have a mass term for the photon field A_μ, which in fact has to be so in order to respect the $U(1)_Q$ gauge symmetry of QED.

Lastly, we turn to the mass generation of the fermion fields. For this aim, we consider a renormalizable and gauge invariant Yukawa Lagrangian involving Higgs-fermion-fermion couplings in the following form

$$\mathcal{L}_{\rm Yukawa} = -y_e \bar{e}_R \Phi^\dagger \begin{pmatrix} \nu_e \\ e \end{pmatrix}_L - y_d \bar{d}_R \Phi^\dagger \begin{pmatrix} u \\ d \end{pmatrix}_L - y_u \bar{u}_R \left(\epsilon^T \Phi^\star\right)^\dagger \begin{pmatrix} u \\ d \end{pmatrix}_L + \text{h.c.}, \tag{13}$$

where $\Phi^\star$ has a hypercharge quantum number of $-1/2$ and the matrix $\epsilon = -2iT_2^2 = \begin{pmatrix} 0 & -1 \\ 1 & 0 \end{pmatrix}$ is constructed such that $\epsilon^T\Phi^\star$ transforms in the same way as Φ which keeps the $SU(2)_L$ symmetry intact. The factors y_e, y_d, and y_u describe the Yukawa couplings in the one-family model, which can be taken to be real and positive. Plugging the Higgs doublet in Eq. (8) into Eq. (13) and considering only the Φ_0 part gives

$$\mathcal{L}_{\rm Yukawa}^{\Phi_0} = -y_e v\, \bar{e}e - y_d v\, \bar{d}d - y_u v\, \bar{u}u, \tag{14}$$

and thus the fermion mass terms read

$$m_u = y_u\, v\,, \quad m_d = y_d\, v\,, \quad m_e = y_e\, v\,. \tag{15}$$

Considering further the physical Higgs $H(x)$ couplings in the Lagrangian gives similar terms as well, which implies that the coupling of the SM Higgs to massive fermions is proportional to their masses.

1.3 The CKM quark mixing matrix

Promoting the spontaneous symmetry breaking mechanism to all three generations works just the same way as we saw in the previous section but with the difference that the mass terms are now 3×3 matrices which are not diagonal in flavor space. Diagonalizing these terms will require the fields to be rotated which in turn will render certain interaction terms non-diagonal.

The Yukawa Lagrangian involving all three generations can be written as

$$\begin{aligned}\mathcal{L}^{\mathrm{SM}}_{\mathrm{Yukawa}} = &- (\bar{e}, \bar{\mu}, \bar{\tau})_R\, Y^{\ell} \begin{pmatrix} \Phi^\dagger \begin{pmatrix} \nu_e \\ e \end{pmatrix}_L \\ \Phi^\dagger \begin{pmatrix} \nu_\mu \\ \mu \end{pmatrix}_L \\ \Phi^\dagger \begin{pmatrix} \nu_\tau \\ \tau \end{pmatrix}_L \end{pmatrix} - \left(\bar{d}, \bar{s}, \bar{b}\right)_R Y^d \begin{pmatrix} \Phi^\dagger \begin{pmatrix} u \\ d \end{pmatrix}_L \\ \Phi^\dagger \begin{pmatrix} c \\ s \end{pmatrix}_L \\ \Phi^\dagger \begin{pmatrix} t \\ b \end{pmatrix}_L \end{pmatrix} \\ &- (\bar{u}, \bar{c}, \bar{t})_R\, Y^u \begin{pmatrix} \left(\epsilon^T \Phi^\star\right)^\dagger \begin{pmatrix} u \\ d \end{pmatrix}_L \\ \left(\epsilon^T \Phi^\star\right)^\dagger \begin{pmatrix} c \\ s \end{pmatrix}_L \\ \left(\epsilon^T \Phi^\star\right)^\dagger \begin{pmatrix} t \\ b \end{pmatrix}_L \end{pmatrix} + \mathrm{h.c.}\end{aligned} \tag{16}$$

Here, the Yukawa couplings Y^ℓ, Y^u and Y^d are now arbitrary complex 3×3 matrices in flavor space. Plugging the Higgs doublet in (8) into Eq. (16) and considering only the Φ_0 part gives

$$\mathscr{L}^{SM}_{\mathrm{mass}} = - (\bar{e}, \bar{\mu}, \bar{\tau})_R\, M_l \begin{pmatrix} e \\ \mu \\ \tau \end{pmatrix}_L - \left(\bar{d}, \bar{s}, \bar{b}\right)_R M_d \begin{pmatrix} d \\ s \\ b \end{pmatrix}_L - (\bar{u}, \bar{c}, \bar{t})_R\, M_u \begin{pmatrix} u \\ c \\ t \end{pmatrix}_L + \mathrm{h.c.}\,, \tag{17}$$

from which the 3×3 mass matrices are extracted to be

$$M_l = v\, Y^\ell, \quad M_u = v\, Y^u, \quad M_d = v\, Y^d. \tag{18}$$

We need to diagonalize these mass matrices in order to arrive at the physical masses measured at experiments, which can be achieved by a bi-unitary transformation of the form $U^\dagger M V = M_{\mathrm{diag.}}$, with U and V themselves being unitary such that all entries in $M_{\mathrm{diag.}}$ are non-negative and real. The wave function rotations, which absorbs the diagonalization matrices, necessary to arrive at the physical basis (primed) are defined as

$$
\begin{aligned}
\begin{pmatrix} e \\ \mu \\ \tau \end{pmatrix}_L &= V_l \begin{pmatrix} e' \\ \mu' \\ \tau' \end{pmatrix}_L , & \begin{pmatrix} e \\ \mu \\ \tau \end{pmatrix}_R &= U_l \begin{pmatrix} e' \\ \mu' \\ \tau' \end{pmatrix}_R , \\
\begin{pmatrix} u \\ c \\ t \end{pmatrix}_L &= V_u \begin{pmatrix} u' \\ c' \\ t' \end{pmatrix}_L , & \begin{pmatrix} u \\ c \\ t \end{pmatrix}_R &= U_u \begin{pmatrix} u' \\ c' \\ t' \end{pmatrix}_R , \\
\begin{pmatrix} d \\ s \\ b \end{pmatrix}_L &= V_d \begin{pmatrix} d' \\ s' \\ b' \end{pmatrix}_L , & \begin{pmatrix} d \\ s \\ b \end{pmatrix}_R &= U_d \begin{pmatrix} d' \\ s' \\ b' \end{pmatrix}_R .
\end{aligned}
\tag{19}
$$

For what concern the Lagrangian, expressing the flavor eigenstates in terms of the mass eigenstates we see that the kinetic terms stay the same except for the exchange of the unprimed fields with the primed ones since the unitary rotation matrices cancel each other. A similar situation is also valid for the couplings of the photon or the Z boson to fermions which leads the neutral currents to stay diagonal i.e. flavor-changing neutral currents (FCNC) to be absent at the tree level in SM. For massless neutrinos, as we do not have a mass matrix that needs to be diagonalized, there is the freedom to rotate the neutrino fields with V_l as in (19) such that in the $W^{\pm}$ couplings involving the lepton fields we do not see rotation matrices. On the other side, considering the charged current interaction with quarks, we see that these rotation matrices form products which leads to the unitary *Cabbibo-Kobayashi-Maskawa* quark mixing matrix

$$
V_{\text{CKM}} = V_u^{\dagger} V_d \quad = \quad \begin{pmatrix} V_{ud} & V_{us} & V_{ub} \\ V_{cd} & V_{cs} & V_{cb} \\ V_{td} & V_{ts} & V_{tb} \end{pmatrix} . \tag{20}
$$

The appearance of this matrix in the charged quark currents has an important consequence: In contrast to the flavor eigenstate basis, the flavor changes can now also cross generations.

As V_{CKM} is a unitary 3×3 matrix we expect that it has nine real parameters. However, five of them can be rotated away by suitable phase transformations on the fields that leave the rest of the Lagrangian invariant and thus only four of these, namely three angles and one phase, remain physical[5].

A standard parametrization for the CKM-matrix was introduced in [15] and is obtained as a product of three rotation matrices, characterized by the three Euler angles θ_{12}, θ_{13} and θ_{23}, and an overall phase δ [6]:

$$
V_{\text{CKM}} = \begin{pmatrix} c_{12}c_{13} & s_{12}c_{13} & s_{13}e^{-i\delta} \\ -s_{12}c_{23} - c_{12}s_{23}s_{13}e^{i\delta} & c_{12}c_{23} - s_{12}s_{23}s_{13}e^{i\delta} & s_{23}c_{13} \\ s_{12}s_{23} - c_{12}s_{23}s_{13}e^{i\delta} & -c_{12}s_{23} - c_{12}s_{23}s_{13}e^{i\delta} & c_{23}c_{13} \end{pmatrix} , \tag{21}
$$

with $c_{ij} = \cos\theta_{ij}$ and $s_{ij} = \sin\theta_{ij}$. The advantage of this parametrization is that the mixing angles are directly related to whether two generations mix, i.e. if a given mixing angle vanishes, there is no mixing between the corresponding generations.

[5] In the case of N generations, one would have $(N-1)^2$ physical parameters which are $N(N-1)/2$ Euler angles and $(N-1)(N-2)/2$ complex phases.

[6] This phase is the central source for all of the CP violation occurring in the SM.

Another popular parametrization was proposed by Wolfenstein in [16] with four parameters A, λ, ρ and η. It uses $\lambda = |V_{us}| \approx 0.22$ as an expansion parameter by which each matrix element is expanded. Phenomenology tells us that c_{13} and c_{23} are $O(1)$. Making further the following definitions ($A \sim O(1)$)

$$\begin{aligned} s_{23} &= A\lambda^2 = \lambda \left|\frac{V_{cb}}{V_{us}}\right| , \\ s_{12} &= \lambda , \\ s_{13}e^{i\delta} &= A\lambda^3(\rho + i\eta) = V^\star_{ub} , \end{aligned} \tag{22}$$

the Wolfenstein parametrization of the V_{CKM} takes the form

$$V_{\mathrm{CKM}} = \begin{pmatrix} 1-\frac{\lambda^2}{2} & \lambda & A\lambda^3(\rho - i\eta) \\ -\lambda & 1-\frac{\lambda^2}{2} & A\lambda^2 \\ A\lambda^3(1-\rho-i\eta) & -A\lambda^2 & 1 \end{pmatrix} + \mathcal{O}\left(\lambda^4\right) , \tag{23}$$

which ensures $\bar\rho + i\bar\eta = -\left(V_{ud}V^\star_{ub}\right) / \left(V_{cd}V^\star_{cb}\right)$ for

$$\rho + i\eta = \frac{(\bar\rho + i\bar\eta)\sqrt{1 - A^2\lambda^4}}{\sqrt{1-\lambda^2}\left[1 - A^2\lambda^4\left(\bar\rho + i\bar\eta\right)\right]} .$$

It can be seen that the entries get smaller as moving away from the diagonal which implies that the W-coupling is stronger in the diagonal while gets suppressed as the flavors are apart from each other. The unitarity of the CKM matrix ($V_{\mathrm{CKM}}V^\dagger_{\mathrm{CKM}} = V^\dagger_{\mathrm{CKM}}V_{\mathrm{CKM}} = \mathrm{I}_{3\times3}$) generates several useful orthogonality and orthonormality relations. The most commonly used unitarity triangle arises from the relation

$$V_{ud}V^\star_{ub} + V_{cd}V^\star_{cb} + V_{td}V^\star_{tb} = 0 , \tag{24}$$

by dividing each side by $V_{cd}V^\star_{cb}$. This results in the three unitarity angles as

$$\begin{aligned} \alpha &= \arg\left(-\frac{V_{td}V^\star_{tb}}{V_{ud}V^\star_{ub}}\right), \qquad \beta = \arg\left(-\frac{V_{cd}V^\star_{cb}}{V_{td}V^\star_{tb}}\right), \\ \gamma &= \arg\left(-\frac{V_{ud}V^\star_{ub}}{V_{cd}V^\star_{cb}}\right), \end{aligned} \tag{25}$$

which are physical and can be independently constrained from B meson decays.

The current best fit to the CKM parameters according to CKM-fitter group read [17]

$$\begin{aligned} A &= 0.802^{+0.048}_{-0.025} , \qquad \lambda = 0.2254^{+0.0013}_{-0.0027} , \\ \bar\eta &= 0.343^{+0.043}_{-0.037} , \qquad \bar\rho = 0.140^{+0.059}_{-0.049} , \\ \alpha &= \left(90.5^{+9.6}_{-7.7}\right)^\circ , \qquad \beta = \left(21.7^{+2.4}_{-1.9}\right)^\circ , \\ \gamma &= \left(67.7^{+7.6}_{-9.1}\right)^\circ , \end{aligned} \tag{26}$$

leading to

$$V_{\mathrm{CKM}} \approx \begin{pmatrix} 0.97 & 0.23 & 0.0014 - i0.0032 \\ -0.23 & 0.97 & 0.04 \\ 0.008 - i0.003 & -0.040 - i0.001 & 1 \end{pmatrix} . \tag{27}$$

Finally, we would like to conclude this chapter by giving the present SM constraints on the CKM parameters based on a global fit result[7] as illustrated in Fig. 3.

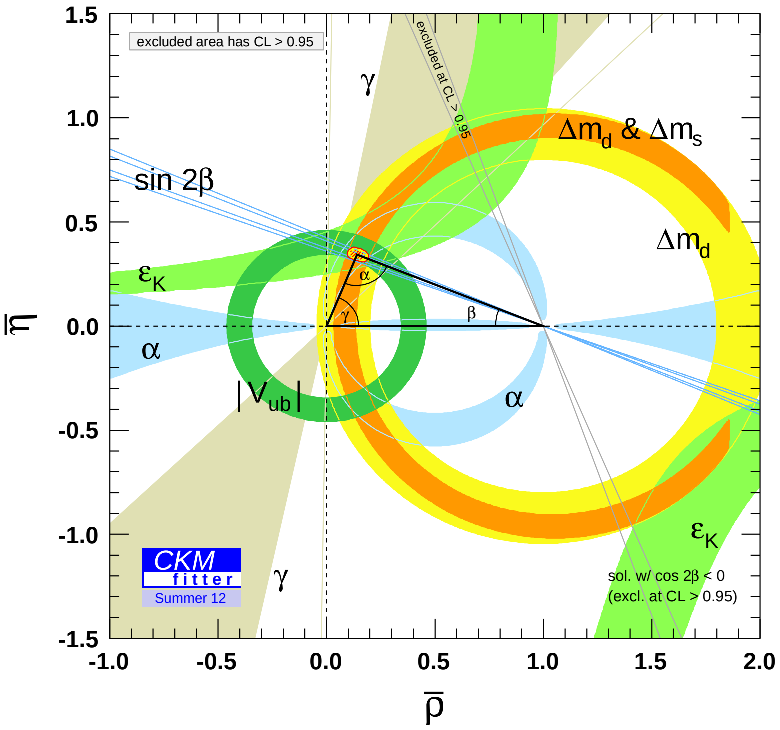

Figure 3: Plot taken from Ref. [17] showing the updated SM constraints (the regions compatible with experiment are superimposed on each other at 95% CL) on the $\bar{\rho} - \bar{\eta}$ plane from various measurements and the global fit result.

2 Two-Higgs-doublet models

The two-Higgs-doublet-models (2HDMs) are simple extension of the SM with a limited number of additional free parameters. As we have seen in Eq. (13) of Sec. 1, in the SM one uses the same scalar doublet Φ to couple the right-handed up- and down-type quarks to the left-handed fermion doublets. This is done using the fact that the combination $\epsilon^T \Phi^\star$ transforms in the same way as Φ, which keeps the $SU(2)_L$ symmetry intact, and that the scalar doublets coupling to right-handed up- and down-type quarks have opposite hypercharge quantum numbers [19].

In 2HDMs, one introduces a second complex SU(2) Higgs doublet and obtains five physical Higgs particles. Assuming a CP conserving Higgs potential one gets: two neutral CP-even Higgses H^0, h^0, a neutral CP-odd Higgs A^0 and two charged Higgses $H^\pm$.

[7]Global fit implies using all available measurements and imposing the SM constraints. The analogous fit results on the CKM parameters can also be seen from the online update of UTfit group [18].

Depending on the couplings of the Higgs doublets to the quarks, different versions of the 2HDM were named [20]. A type-I model describe the coupling of both up and down-type quarks to the same doublet (H_u), whereas the other doublet (H_d) does not couple to any quark. In a type-II model, one doublet (H_d) couples only to down type quarks whereas the second one (H_u) only couples to up type quarks, and in a type-III 2HDM both scalar doublets are assumed to couple to both type of quarks. Beside that, there are several other versions of 2HDMs such as lepton-specific, flipped, inert or Aligned [21] models etc. For a thorough discussion of 2HDMs, we refer the reader to see e.g. a recent comprehensive review by [22] or [23].

The early history concerning the formulation of 2HDMs can be summarized as follows [24]:

- The first formulation of a 2HDM comes by T. D. Lee in 1973 [25] with the motivation to find extra sources of CP violation. He uses the fact that in a model with two doublets the vacuum could break the CP symmetry spontaneously [22].

- S.L. Glashow and S. Weinberg in 1977 [26] put forward the idea of *natural flavor conservation* stating that the tree-level flavor-changing-neutral Higgs interactions can be avoided if fermions of a given quantum number couple to at most one of the Higgs doublets.

- N.G. Deshpande and E. Ma in 1978 [27] showed that in order to keep the $U(1)_{\text{em}}$ symmetry intact, the parameters of the Higgs potential should lie in an appropriate region of parameter space.

- H.E. Haber, G.L. Kane and T. Sterling in 1979 [28] invented the 2HDM of type-I in which one Higgs doublet couples to up and down-type quarks at the same time, while the other Higgs doublet does not couple to the quarks at all.

- J.F. Donoghue and L. F. Li in 1979 invented the 2HDM of type-II [29] in which one Higgs doublet couples to down-type quarks and the other Higgs doublet couples to up-type quarks.

- L.J. Hall and M.B. Wise in 1981 invented the type-I and type-II terminology [30].

- T.P. Cheng and M. Sher in 1987 [31] founded the first realistic type-III 2HDM in which all possible Higgs-fermion couplings are allowed.

Among these types, the 2HDM of type-II is the most studied one since it shares many features with the Higgs sector of the super-symmetric models (like MSSM) [22]. Hence, in the following considerations we would like to focus on the type-II model by examining its Higgs sector and the Yukawa structure[8].

The gauge invariant and renormalizable (allowing at most quartic couplings of the Higgs fields) scalar potential of a 2HDM (motivated by the corresponding MSSM Higgs potential)

[8] The more general type-III 2HDM will be discussed first briefly in Part IV and later in more detail in Part V of this thesis.

can be written as[9] [32]:

$$\begin{aligned} V\left(H_u, H_d\right) &= m_{H_d}^2 \left|H_d\right|^2 + m_{H_u}^2 \left|H_u\right|^2 + \frac{\lambda_1}{2}\left(H_d^\dagger H_u\right)\left(H_u^\dagger H_d\right) + \frac{\lambda_2}{8}\left(\left|H_u\right|^2 - \left|H_d\right|^2\right)^2 \\ &+ \left(b\left(\epsilon^T H_d^\star\right)^\dagger H_u + \text{h.c.}\right), \end{aligned} \tag{28}$$

where the Higgs doublets read

$$\begin{aligned} H_d &= \begin{pmatrix} H_d^1 \\ H_d^2 \end{pmatrix} = \begin{pmatrix} \tilde{H}_d^0 \\ H_d^- \end{pmatrix}, \\ H_u &= \begin{pmatrix} H_u^1 \\ H_u^2 \end{pmatrix} = \begin{pmatrix} H_u^+ \\ \tilde{H}_u^0 \end{pmatrix}. \end{aligned} \tag{29}$$

Minimizing this potential yields $\langle H_u \rangle = \begin{pmatrix} 0 \\ v_u \end{pmatrix}$ and $\langle H_d \rangle = \begin{pmatrix} v_d \\ 0 \end{pmatrix}$ with $v_u = \sin\beta v,\ v_d = \cos\beta v$ such that $\tan\beta = v_u/v_d$ is the ratio of these vev's. After expanding around these minima the Higgs doublets take the form:

$$\begin{aligned} H_d &= \begin{pmatrix} H_d^1 \\ H_d^2 \end{pmatrix} = \begin{pmatrix} v_d + H_d^0 \\ H_d^- \end{pmatrix} \text{ with } H_d^0 = \rho_d + i\eta_d\,, \\ H_u &= \begin{pmatrix} H_u^1 \\ H_u^2 \end{pmatrix} = \begin{pmatrix} H_u^+ \\ v_u + H_u^0 \end{pmatrix} \text{ with } H_u^0 = \rho_u + i\eta_u\,. \end{aligned} \tag{30}$$

After SSB, plugging the doublets given in Eq. (30) into Eq. (28) gives

$$\begin{aligned} V &= m_{H_d}^2\left[\left(v_d+\rho_d+i\eta_d\right)\left(v_d+\rho_d-i\eta_d\right)+H_d^+H_d^-\right] \\ &+ m_{H_u}^2\left[\left(v_u+\rho_u+i\eta_u\right)\left(v_u+\rho_u-i\eta_u\right)+H_u^+H_u^-\right] \\ &+ \frac{\lambda_1}{2}\left[\left(\left(v_d+\rho_d-i\eta_d\right)H_u^+ + \left(v_u+\rho_u+i\eta_u\right)H_d^+\right)\left(\left(v_d+\rho_d+i\eta_d\right)H_u^- + \left(v_u+\rho_u-i\eta_u\right)H_d^-\right)\right] \\ &+ \frac{\lambda_2}{8}\left[H_u^+H_u^- - H_d^+H_d^- + \left(v_u+\rho_u+i\eta_u\right)\left(v_u+\rho_u-i\eta_u\right) - \left(v_d+\rho_d+i\eta_d\right)\left(v_d+\rho_d-i\eta_d\right)\right]^2 \\ &+ b\left[H_u^+H_d^- + H_u^-H_d^+ - \left(v_u+\rho_u+i\eta_u\right)\left(v_d+\rho_d+i\eta_d\right) - \left(v_u+\rho_u-i\eta_u\right)\left(v_d+\rho_d-i\eta_d\right)\right]. \end{aligned} \tag{31}$$

At this stage, setting to zero the derivatives of the potential in Eq. (31) with respect to the real parts of the neutral up and down components as $\partial V/\partial\rho_u = \partial V/\partial\rho_d = 0$ allows us to

[9]This choice of the potential assumes a discrete Z_2 symmetry (with $H_u \to -H_u$ and all other SM fields are unaffected) which eliminates quartic terms odd in either of the doublets [22] such that it avoids dangerous CP violation due to the potential itself, while leaving a b-term (dimension-two term) to break this symmetry softly. The b-term is known as soft-supersymmetry breaking scale. Moreover, with appropriate requirements on the parameters involved (such as $v_{u,d} > 0$ etc.), this potential induce a correct SSB leaving $U(1)_{\text{em}}$ intact as desired [32].

relate some of the parameters in the potential to the vev's $(v_{u,d})$ in the following way[10]

$$m_{H_u}^2 = b\frac{v_d}{v_u} + \frac{\lambda_2}{4}\left(v_d^2 - v_u^2\right) \ , \quad m_{H_d}^2 = b\frac{v_u}{v_d} + \frac{\lambda_2}{4}\left(v_u^2 - v_d^2\right) \ . \tag{32}$$

Working out explicitly all quadratic terms together with the mixing terms of the fields in Eq. (31) define the corresponding mass matrices in the following way:

$$\mathcal{L}_{\rm mass}^{\rm Higgs} = \mathcal{L}_{\rm mass}^{\rm H_u^\pm, H_d^\pm} + \mathcal{L}_{\rm mass}^{\rho_u,\rho_d} + \mathcal{L}_{\rm mass}^{\eta_u,\eta_d} \ , \tag{33}$$

where the individual pieces read:

$$\begin{aligned}
\mathcal{L}_{\rm mass}^{\rm H_u^\pm, H_d^\pm} &= -\left(b + \frac{\lambda_1 v^2}{4}\sin(2\beta)\right)\left(H_u^-\,,H_d^-\right)\begin{pmatrix}\cot\beta & 1\\ 1 & \tan\beta\end{pmatrix}\begin{pmatrix}H_u^+\\ H_d^+\end{pmatrix} \ ,\\
\mathcal{L}_{\rm mass}^{\rho_u,\rho_d} &= -\left(\rho_u\,,\rho_d\right)\underbrace{\begin{pmatrix} b\cot\beta + \frac{\lambda_2 v^2}{2}\sin^2\beta & -b - \frac{\lambda_2 v^2}{4}\sin(2\beta)\\ -b - \frac{\lambda_2 v^2}{4}\sin(2\beta) & b\tan\beta + \frac{\lambda_2 v^2}{2}\cos^2\beta\end{pmatrix}}_{\mathcal{M}^{\rho_u,\rho_d}}\begin{pmatrix}\rho_u\\ \rho_d\end{pmatrix} \ ,\\
\mathcal{L}_{\rm mass}^{\eta_u,\eta_d} &= -\left(\eta_u\,,\eta_d\right)\begin{pmatrix} b\cot\beta & b\\ b & b\tan\beta\end{pmatrix}\begin{pmatrix}\eta_u\\ \eta_d\end{pmatrix} \ .
\end{aligned} \tag{34}$$

As can be seen, these mass matrices squared are symmetric and real valued. Thus, it is possible to diagonalize them by orthogonal 2×2 matrices ($O^T = O^{-1}$), which corresponds to perform field transformations of the form:

$$\begin{aligned}
\begin{pmatrix}H_u^1\\ H_d^{2\star}\end{pmatrix} &= \begin{pmatrix}H_u^+\\ H_d^+\end{pmatrix} = \begin{pmatrix}\cos\beta & -\sin\beta\\ \sin\beta & \cos\beta\end{pmatrix}\begin{pmatrix}H^+\\ G^+\end{pmatrix} \ ,\\
\begin{pmatrix}\rho_u\\ \rho_d\end{pmatrix} &= \frac{1}{\sqrt{2}}\begin{pmatrix}\cos\alpha & \sin\alpha\\ -\sin\alpha & \cos\alpha\end{pmatrix}\begin{pmatrix}h^0\\ H^0\end{pmatrix} \ ,\\
\begin{pmatrix}\eta_u\\ \eta_d\end{pmatrix} &= \frac{1}{\sqrt{2}}\begin{pmatrix}\cos\beta & -\sin\beta\\ \sin\beta & \cos\beta\end{pmatrix}\begin{pmatrix}A^0\\ G^0\end{pmatrix} \ .
\end{aligned} \tag{35}$$

These transformations project the old fields $(H^\pm_{u,(d)}, \rho_{u,d}, \eta_{u,d})$ onto the physical $(H^\pm, h^0, H^0, A^0)$ and un-physical Goldstone boson $(G^\pm, G^0)$ mass eigenstates in the following way:

$$\begin{aligned}
H_u^0 &= \rho_u + i\eta_u = \frac{1}{\sqrt{2}}\left(H^0\sin\alpha + h^0\cos\alpha + iA^0\cos\beta - i\sin\beta G^0\right) \ ,\\
H_d^0 &= \rho_d + i\eta_d = \frac{1}{\sqrt{2}}\left(H^0\cos\alpha - h^0\sin\alpha + iA^0\sin\beta + i\cos\beta G^0\right) \ ,\\
H_u^1 &= H_u^+ = \cos\beta\, H^+ - \sin\beta G^+ \ ,\\
H_d^2 &= H_d^- = \sin\beta\, H^- + \cos\beta G^- \ ,
\end{aligned} \tag{36}$$

where α is the mixing angle necessary to diagonalize the neutral CP-even Higgs mass matrix (see e.g. [33]) and β is the rotation angle[11] doing the same job for the corresponding charged

[10] At the minimum, all the components of the doublets are set to zero as $H_u^\pm = H_d^\pm = \rho_{u,d} = \eta_{u,d} = 0$.

[11] Since $v_{u,d} > 0$, β can be chosen to lie in the range $\beta \in [0, \pi/2]$.

scalars and of the CP-odd Higgses. These angles are important phenomenologically since they define the interactions of various Higgses with fermions and gauge bosons [22].

Diagonalization of the mass matrices given in Eq. (34) results in the following mass terms for the physical and the Goldstone boson fields[12]:

$$
\begin{aligned}
m_{H^\pm}^2 &= \frac{2b}{\sin 2\beta} + \frac{\lambda_1 v^2}{2}, \quad m_{G^\pm}^2 = 0, \quad m_{A^0}^2 = \frac{2b}{\sin 2\beta}, \quad m_{G^0}^2 = 0\,, \\
m_{H^0,h^0}^2 &= \frac{1}{2}\left(m_{A^0}^2 + \frac{\lambda_2 v^2}{2} \pm \sqrt{\left(m_{A^0}^2 - \lambda_2 v^2/2\right)^2 + 2\lambda_2 v^2 m_{A^0}^2 \sin^2 2\beta}\right).
\end{aligned}
\tag{37}
$$

Next, the gauge boson masses simply follow from the Higgs kinetic terms

$$
\mathcal{L}_{\text{kinetic}} = \left(D_\mu H_u\right)^\dagger \left(D^\mu H_u\right) + \left(D_\mu H_d\right)^\dagger \left(D^\mu H_d\right)\,, \tag{38}
$$

with D_μ and $H_{u,d}$ being defined as in Eq. (10) and Eq. (30), respectively. Working out explicitly the quadratic terms in the gauge fields, we find

$$
m_W^2 = \frac{g^2(v_u^2 + v_d^2)}{2}, \quad m_Z^2 = \frac{(g^2 + g'^2)(v_u^2 + v_d^2)}{2}, \quad m_\gamma^2 = 0\,, \tag{39}
$$

where $v_u^2 + v_d^2$ plays the role of v^2 in the SM and is therefore fixed at $v_u^2 + v_d^2 = v^2 \approx (174\,\text{GeV})^2$. Furthermore, using the orthogonal matrix given in the second line of Eq. (35) and setting to zero the non-diagonal entries of the matrix product

$$
\begin{pmatrix} \cos\alpha & \sin\alpha \\ -\sin\alpha & \cos\alpha \end{pmatrix}^T \mathcal{M}^{\rho_u,\rho_d} \begin{pmatrix} \cos\alpha & \sin\alpha \\ -\sin\alpha & \cos\alpha \end{pmatrix}\,, \tag{40}
$$

allows us to relate the angles α and β as

$$
\tan(2\alpha) = -\frac{2\mathcal{M}_{12}^{\rho_u,\rho_d}}{\mathcal{M}_{11}^{\rho_u,\rho_d} - \mathcal{M}_{22}^{\rho_u,\rho_d}}\,. \tag{41}
$$

With little bit algebra this yields

$$
\tan(2\alpha) = \frac{2\,m_{A^0}^2 + \lambda_2 v^2}{2\,m_{A^0}^2 - \lambda_2 v^2}\tan(2\beta)\,. \tag{42}
$$

This equation has a unique solution for α, if α is restricted to be in the range $\alpha \in [-\pi/2, 0]$. Using the SUSY conditions $\lambda_1 = g^2$ and $\lambda_2 = g^2 + g'^2$ (see e.g. [23] for the corresponding discussion), Eq. (42) can further be expressed as

$$
\tan(2\alpha) = \frac{m_{A^0}^2 + m_Z^2}{m_{A^0}^2 - m_Z^2}\tan(2\beta) = \frac{m_{H^0}^2 + m_{h^0}^2}{m_{A^0}^2 - m_Z^2}\tan(2\beta)\,. \tag{43}
$$

Having derived all these relations above, we can now look at some useful limit of them. In the phenomenologically interesting limit of large $\tan\beta$ and $v^2 = v_u^2 + v_d^2 \ll m_{A^0}^2$, it is easy to

[12]Being directly proportional to the soft SUSY breaking scale b, the masses of $H^\pm$, A^0 and H^0 are a priori assumed to be large compared to the SM like Higgs h^0 mass.

see from Eq. (37) that all the heavy Higgs masses become equal ($m_{H^0} \approx m_{H^\pm} \approx m_{A^0} \equiv m_H$) and additionally the following useful relation between the angles α and β exist[13]

$$\boxed{\cot\alpha \simeq -\tan\beta} \, ,$$

when choosing α to be in the range $\alpha \in [-\pi/2, 0]$.

As a result, under these assumptions, the degrees of freedom of the model reduce drastically and thus the type-II 2HDM would only have two free parameters to be fixed via experiment: $\tan\beta$ and m_H.

As a next step, let us discuss the Yukawa Lagrangian of the type II model. Following the notations used in Ref. [34] the Lagrangian governing the Yukawa interactions, in the electroweak basis, reads

$$\mathcal{L}_Y = \bar{Q}^a_{f\,L}\left[Y^{d\,\mathrm{ew}}_{fi}\epsilon_{ba}H^{b\star}_d\right] d_{i\,R} + \bar{Q}^a_{f\,L}\left[Y^{u\,\mathrm{ew}}_{fi}\epsilon_{ab}H^{b\star}_u\right] u_{i\,R} + \mathrm{h.c.}\ . \tag{44}$$

Here a, b denote $SU(2)_L$ - indices, ϵ_{ab} is again the two-dimensional antisymmetric tensor with $\epsilon_{12} = -1$. Writing Eq. (44) down explicitly in component form and after performing the wave-function rotations necessary to arrive at the physical basis with diagonal quark mass matrices, the Yukawa Lagrangian takes the form:

$$\begin{aligned}\mathcal{L}_Y = \ & - \ \bar{d}_{f\,L}\left[\left(\frac{m_{d_i}}{v_d}\delta_{fi}\right) H^{0\star}_d\right] d_{i\,R} - \bar{u}_{f\,L}\left[\left(\frac{m_{u_i}}{v_u}\delta_{fi}\right) H^{0\star}_u\right] u_{i\,R} \\ & + \ \bar{u}_{f\,L}V^{\mathrm{CKM}}_{fi}\left(\frac{m_{d_i}}{v_d}\right) H^+_d\, d_{i\,R} + \bar{d}_{f\,L}V^{\star\mathrm{CKM}}_{if}\left(\frac{m_{u_i}}{v_u}\right) H^-_u u_{i\,R} + \mathrm{h.c.}\ . \end{aligned} \tag{45}$$

Here, m_{q_i} are the physical running quark masses, $H^\pm_q$ and H^0_q are the components of the Higgs doublets as given in Eq. (30). These Higgs fields can be replaced by the corresponding mass eigenstates using Eq. (36). As can be seen, there is no flavor-changing-neutral Higgs interactions at the tree-level in 2HDM of type II so it is a model which respect natural flavor conservation.

In part IV and part V of this thesis, we will analyze the flavor phenomenology of the type-III 2HDM. We will see that the type II model discussed above will not be competent to explain some recent experimental data and thus one has to work with more general models. In the 2HDM of type III, in addition to the number of free parameters of the type II model, we will have extra free parameters, the so called non-holomorphic couplings ϵ^f_{ij}, which generates FCNC transitions at the tree-level[14].

Before closing this chapter, we would like to make a final remark concerning the choice of the Higgs potential. In fact most phenomenological studies of 2HDMs makes several simplifying assumptions. In order for distinguishing between scalar and pesudoscalar particles, it is usually assumed that the Higgs sector respect CP symmetry (a CP-conserving Higgs potential) [22] as we also did in writing the Higgs potential in Eq. (28). Moreover, a non-vanishing b term in Eq. (28) would allow a finite FCNC at one-loop level indicating FCNCs to be small[15] [35].

[13]For large values of $\tan\beta$ this relation implies; $\sin\beta \to 1$, $\cos\beta \to 0$, $\sin\alpha \to 0$ and $\cos\alpha \to 1$.

[14]There is a straightforward correlation between the type-II and type-III models. The results obtained in a type III model are more general and one can simply translate these results to the results of type II model by setting all ϵ^f_{ij} textures (see Part V for the corresponding discussion) to zero.

[15]FCNCs can be avoided if the same Higgs multiplet is used to couple all fermions sharing the same quantum

3 Effective field theory approach

In physics, an effective field theory is described as the theory that contains the appropriate degrees of freedom to describe physical phenomena occurring at a chosen energy scale, while ignores the degrees of freedom at higher energies (or, equivalently, shorter distances). If we want to examine a specific physical system within the great features of the surrounding nature, we need to isolate some parts of the system from the others. By doing so, we would get a description adapted to that particular system without trying to learn everything related to it. The basic idea for doing that is to specify the relevant parameters which are assumed to be adequate to describe the physics at the chosen energy scale [37].

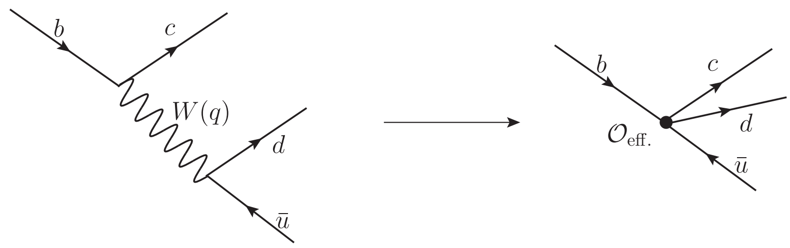

Figure 4: Left: Quark level $b \to cd\bar{u}$ transition in the full SM. Right: $b \to cd\bar{u}$ transition in the effective theory framework governed by local effective operators.

Applied to Feynman diagrams this approach means to identify the light and the heavy particles in a given diagram and to study the dynamics of the diagram after *integrating out* the heavy scales, which is formally performed within the concept of *operator product expansion* (OPE) introduced by Wilson in 1969 [38]. This way the heavy scales are treated as frozen-static sources and the physics describing them is absorbed in the so called Wilson coefficients (short range) while the low energy effects are hidden inside effective operators (long ranges). To illustrate the construction of such an effective theory let us take the simple tree-level $b \to cd\bar{u}$ transition depicted in the left frame of Fig. 4. The SM amplitude for this transition is

$$\mathcal{A}_{\rm SM} = -i\left(\frac{-ig_2}{\sqrt{2}}\right)^2 V_{cb}V_{ud}^* \frac{g^{\mu\nu} - \frac{q^\mu q^\nu}{m_W^2}}{q^2 - m_W^2} \left(\bar{d}\gamma_\mu L u\right)\left(\bar{c}\gamma_\nu L b\right), \tag{46}$$

where q refers to the momentum transfer through the W. Since $q \sim \mathcal{O}(m_b) \ll m_W$, it is possible to expand the W-propagator in q^2/m_W^2 as

$$\frac{g^{\mu\nu} - \frac{q^\mu q^\nu}{m_W^2}}{q^2 - m_W^2} = -\frac{g^{\mu\nu}}{m_W^2} + \mathcal{O}\left(\frac{q^2}{m_W^4}\right), \tag{47}$$

numbers (thus capable of mixing) [22]. According to Paschos-Glashow-Weinberg theorem (see [22] and references therein), "a necessary and sufficient condition for controlling the presence of FCNC at the tree-level is that all fermions of a given charge and helicity transforms according to the same irreducible representation of $SU(2)$, correspond to the same eigenvalue of T_2^3 and that a basis exist in which they receive their contributions in the mass matrix from a single source". In the 2HDMs, this can be achieved by imposing discrete (like Z_2 symmetry) or continues symmetries (like Peccei-Quinn symmetry [36]).

Plugging Eq. (47) into Eq. (46) gives rise to series of local operators of ascending mass dimension

$$\mathcal{A}_{\rm SM} = \frac{-ig_2^2}{2} V_{cb} V_{ud}^* \left[\frac{1}{m_W^2} \underbrace{\left(\bar{d}\gamma_\mu L u\right)\left(\bar{c}\gamma^\mu L b\right)}_{\text{dim-6 operator}} + \frac{1}{m_W^4} \underbrace{(..........)}_{\text{dim-8 operator}} + \ldots \right]. \tag{48}$$

The operators with mass dimension higher than 6 are suppressed by appropriate inverse powers of m_W^2. For example a dimension-8 operator would have a suppression factor of m_b^2/m_W^2 relative to a dimension-6 one. Hence, neglecting the higher dimensional operators in Eq. (48) allows us to construct an effective amplitude of the form

$$\mathcal{A}_{\rm eff} = \frac{-ig_2^2}{2} V_{cb} V_{ud}^* \frac{1}{m_W^2} \left(\bar{d}\gamma_\mu L u\right)\left(\bar{c}\gamma^\mu L b\right), \tag{49}$$

which is equivalent to throw away the $\mathcal{O}\left(q^2/m_W^4\right)$ terms in the full SM side in Eq. (47). As we have seen, integrating out the W in the SM resulted in a local four fermion interaction operator on the effective theory side (pictorially shown in the right frame of Fig. 4).

In the next subsection, we will briefly illustrate how to do matching for the electromagnetic-dipole operator $\mathcal{O}_7$, which is the most important operator throughout this work, by taking into account the $b \to s\gamma$ decay at the lowest order in QCD, i.e., α_s^0. Therefore, before closing this section let us give the effective Hamiltonian $\mathcal{H}_{\rm eff}$ governing the $b \to s\gamma$ ($b \to sg$, $b \to s\gamma\gamma$) decay(s)[16]. After integrating out the heavy particles in the SM we have

$$\mathcal{H}_{eff} = \frac{4G_F}{\sqrt{2}} \left[\sum_{i=1}^{2} C_i(\mu) \left(\lambda_c \mathcal{O}_i^c(\mu) + \lambda_u \mathcal{O}_i^u(\mu)\right) - \lambda_t \sum_{i=3}^{8} C_i(\mu) \mathcal{O}_i(\mu) \right], \tag{50}$$

where $\lambda_q = V_{qb} V_{qs}^\star$ and the set of dimension-6 operators read [41]:

$$\begin{aligned}
\mathcal{O}_1 &= (\bar{s}_L \gamma_\mu T^a c_L)(\bar{c}_L \gamma^\mu T_a b_L)\,, & \mathcal{O}_2 &= (\bar{s}_L \gamma_\mu c_L)(\bar{c}_L \gamma^\mu b_L)\,, \\
\mathcal{O}_3 &= (\bar{s}_L \gamma_\mu b_L) \textstyle\sum_q (\bar{q}\gamma^\mu q)\,, & \mathcal{O}_4 &= (\bar{s}_L \gamma_\mu T^a b_L) \textstyle\sum_q (\bar{q}\gamma^\mu T_a q)\,, \\
\mathcal{O}_5 &= (\bar{s}_L \gamma_\mu \gamma_\nu \gamma_\rho b_L) \textstyle\sum_q (\bar{q}\gamma^\mu \gamma^\nu \gamma^\rho q)\,, & \mathcal{O}_6 &= (\bar{s}_L \gamma_\mu \gamma_\nu \gamma_\rho T^a b_L) \textstyle\sum_q (\bar{q}\gamma^\mu \gamma^\nu \gamma^\rho T_a q)\,, \\
\mathcal{O}_7 &= \tfrac{e}{16\pi^2} \left(\bar{s}\sigma^{\mu\nu} \left[\bar{m}_b R + \bar{m}_s L\right] b\right) F_{\mu\nu}\,, & \mathcal{O}_8 &= \tfrac{g_s}{16\pi^2} \left(\bar{s}\sigma^{\mu\nu} \left[\bar{m}_b R + \bar{m}_s L\right] T^a b\right) G^a_{\mu\nu}\,.
\end{aligned} \tag{51}$$

The symbols T^a ($a = 1, 8$) denote the $SU(3)$ color generators; g_s and e, the strong and electromagnetic coupling constants. In Eq. (51), $\bar{m}_q$ are the running quark masses in the $\overline{\rm MS}$-scheme at the renormalization scale μ. When the aim is to compute the decay rates (but not the CP violation effects), concerning the decays $b \to s\gamma$, $b \to s\gamma\gamma$ and $b \to sg$, one can make use of the hierarchy $V_{ub} V_{us}^* \ll V_{tb} V_{ts}^*$ to further simplify Eq. (50).

3.1 Matching procedure

The idea of doing matching lies in the calculation of the transition amplitude of corresponding process both in the full and in the effective theory and then extracting the corresponding Wilson coefficients after confronting both results. For this aim, let us consider the quark-level $b \to s\gamma$ decay at the lowest order in QCD and try to extract in the effective theory the Wilson

[16]For a detailed discussion of the derivation of the Hamiltonian for these transitions see e.g. [39, 40].

coefficient C_7 associated with the electro-magnetic dipole operator $\mathcal{O}_7$ (see e.g. [42] for a two-loop matching of the dipole operators; matching procedures of other operators such as the chromo-magnetic dipole operator $\mathcal{O}_8$ or current-current operators $\mathcal{O}_{1,2}$ can be found e.g. in [9, 10, 11, 43, 44]). For a detailed discussion of this procedure and the extraction of all Wilson coefficients we refer to [39, 40].

In lowest order of QCD, the relevant diagram[17] for $b \to s\gamma$ is given by Fig. 5 with t and c-quarks circulating in the loop. The diagram with an internal u-quark circulating in the loop is proportional to $\lambda_u = V_{ub}V_{us}^\star$ which is much smaller in magnitude than the corresponding top and charm loop contributions and thus can be safely neglected. Therefore, there remain two cases to consider: i-) the graphs with internal top–loop and ii) the ones with internal charm–loop.

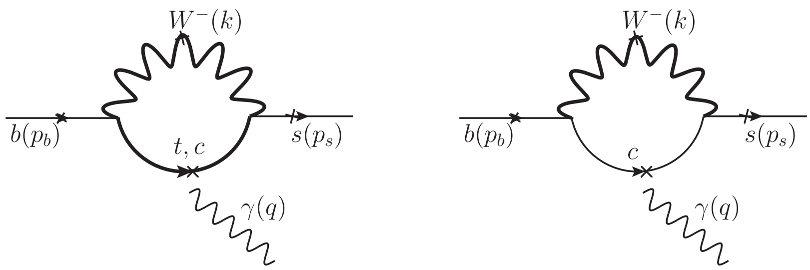

Figure 5: Diagrams contributing to $b \to s\gamma$ in the full theory according to HME. The bold lines describe the sub-graphs which should be expanded in their external momenta and masses. In the right frame, the loop-momentum k flowing through the W-line should be treated as an external momentum and thus an expansion of the W propagator in k should be considered.

Let us tackle the former case first. In this case, since all internal scales (m_t, m_W) are heavy and the external momenta (p_b, p_s) are of $\mathcal{O}(m_b)$, one can naively Taylor expand the occurring propagators in the light scales p_b, p_s, m_b and m_s. For the top-quark propagator involving p_b this would simply imply to make the following geometric expansion

$$\frac{1}{(k+p_b)^2 - m_t^2} = \frac{1}{k^2 - m_t^2} \sum_{n\geq 0} \left(-\frac{p_b^2 + 2kp_b}{k^2 - m_t^2} \right)^n , \tag{52}$$

and same expansion holds for the propagators involving p_s. The top-loop diagram, where the photon is emitted from the internal top quark, alone turns out to develop a $1/\varepsilon$ singularity. However, combined with the other three diagrams where the photon is emitted from the W, b or s-quark[18], the total top-loop amplitude $\mathcal{A}^t_{\text{total}}$ gives a finite result.

Now, we turn to the calculation of the diagrams where an internal c quark is propagating in the loop. According to the heavy-mass-expansion (HME) rules defined in [45, 46], there are two types of (sub)diagrams that we should calculate in this case. The first one is the full

[17] We work in the unitary gauge such that we do not have additional non-physical Higgs interactions.

[18] In fact, gauge invariance already determines the structure of the result. To make the job simpler, it can be adequate just to calculate the sum of two diagrams where γ is emitted from the internal top and from W, which are the only ones contributing to $\epsilon.p_b$ structure while the remaining two-diagrams contribute to $\not\epsilon$ structure. Eventually, matching the $\epsilon.p_b$ structures in the full and the effective theory enable us to fix C_7.

diagram where the corresponding propagators are again expanded in a naive way in the light external momenta and masses (p_b, p_s, m_b, m_c and m_s). In addition, due to the light mass of the c-quark compared to m_t, we need to consider a second type of diagram (subdiagram) as shown in the right frame of Fig. 5. In this case, the momentum of the W is considered as an external one and thus the W propagator should also be expanded in the loop momentum k as

$$\frac{1}{k^2 - m_W^2} = -\frac{1}{m_W^2}\left[1 + \frac{k^2}{m_W^2} + \mathcal{O}\left(\frac{1}{m_W^4}\right)\right]. \tag{53}$$

However, performing the relevant algebra the calculations show that for an on-shell photon ($q^2 = 0$) the contribution shown in the right frame of Fig. 5 vanishes and one only gets a contribution from the naively expanded full diagrams with an internal c-quark circulating in the loop (left frame of Fig. 5).

Therefore, summing up all the non-vanishing contributions from the top and charm-loop amplitudes we arrive at the following finite result for the complete SM amplitude[19] in the leading order of QCD

$$\begin{aligned} \mathcal{A}_{\text{full}} &= i\,\frac{4G_F\,\lambda_t}{\sqrt{2}}\frac{e}{16\pi^2}\underbrace{\frac{x}{24}\left[\frac{-8x^3+3x^2+12x-7+(18x^2-12x)\ln(\mathrm{x})}{(x-1)^4}\right]} \\ &\times\; \bar{u}(p_s)2\left[R(\not{\epsilon}(q)(m_b^2+m_s^2) - 2m_b\,p_b.\epsilon(q)) + L\,(2m_bm_s\not{\epsilon}(q) - 2m_s\,p_b.\epsilon(q))\right]u(p_b)\,, \end{aligned} \tag{54}$$

where x is given by $x = m_t^2/m_W^2$.

Having completed the calculation on the full theory side, now we can turn to effective theory framework and identify all the operators involved in the transition $b \to s\gamma$. At the leading order in α_s, the contributions from the operators $\mathcal{O}_1$ and $\mathcal{O}_3 - \mathcal{O}_6$ vanish as their corresponding Wilson coefficients are zero. Due to another reason, the contribution of $\mathcal{O}_2$ identically vanishes[20]. Moreover, a possible contribution from $\mathcal{O}_8$ to $b \to s\gamma$ can only come through higher-order QCD corrections and so it is not relevant for our case. As a result, on the effective theory side we are solely left with the contribution of $\mathcal{O}_7$ to the matrix element of $b \to s\gamma$. Decomposing the $\sigma_{\mu\nu}F^{\mu\nu}$ structure involved in $\mathcal{O}_7$ in terms of the commutator $\left[\not{\epsilon}, \not{q}\right]$ and making use of the Dirac equation we arrive at the following amplitude on the effective theory side

$$\begin{aligned} \mathcal{A}_{\text{eff}} &= \frac{4iG_F\,\lambda_t}{\sqrt{2}}\,C_7\langle s\gamma|\mathcal{O}_7|b\rangle = \frac{4iG_FC_7\,\lambda_t}{\sqrt{2}}\frac{e}{16\pi^2} \\ &\times\; \bar{u}(p_s)2\left[R(\not{\epsilon}(q)(m_b^2+m_s^2) - 2m_b\,p_b.\epsilon(q)) + L\,(2m_bm_s\not{\epsilon}(q) - 2m_s\,p_b.\epsilon(q))\right]u(p_b)\,. \end{aligned} \tag{55}$$

Hence, requiring that the amplitudes both in the full and effective theory are equal completes our matching procedure and fixes the Wilson coefficient C_7 to be

$$C_7 = \frac{x}{24}\left[\frac{-8x^3+3x^2+12x-7+(18x^2-12x)\ln(\mathrm{x})}{(x-1)^4}\right]. \tag{56}$$

[19]In order to arrive at this result, we exploited the unitarity of the CKM matrix to write $|V_{cb}V_{cs}^\star| \simeq -|V_{tb}V_{ts}^\star|$.

[20]Up to a constant factor, the $\mathcal{O}_2$ contribution to $b \to s\gamma$ on the effective theory side corresponds to the calculation of the diagram in the right frame of Fig. 5 by integrating out the W.

At this stage, a final remark concerning the scale dependence of the Wilson coefficients is worth mentioning. For arbitrary order m in α_s the Wilson coefficients obtained from matching posses a structure of the form:

$$\begin{aligned} C_m(\mu) &= c_m^{(0)}\left[\alpha_s(\mu)\ln\left(\frac{\mu}{m_W}\right)\right]^m + c_m^{(1)}\alpha_s(\mu)\left[\alpha_s(\mu)\ln\left(\frac{\mu}{m_W}\right)\right]^{m-1} \\ &+ c_m^{(2)}\alpha_s(\mu)^2\left[\alpha_s(\mu)\ln\left(\frac{\mu}{m_W}\right)\right]^{m-2} + \ldots + c_m^{(m)}\alpha_s(\mu)^m\,, \end{aligned} \tag{57}$$

where μ is the renormalization scale and c_m^n are some constant factors. Hence, it turns out that the Wilson coefficients obtained after a matching calculation forces us to choose the scale $\mu = \mu_W \approx m_W$ in order to respect the perturbation theory. On the other side, the matrix elements of the effective operators depend on the external momenta and the small mass scales and thus they posses a dependence proportional to $\ln(\mu/m_b)$ which on contrary requires the scale to be $\mu = \mu_b \approx m_b$. This situation at the first glance seem to be puzzling. However, the remedy for this puzzle is provided by the so-called *renormalization group equation* (RGE) technique by which the Wilson coefficients are evolved from the high (matching scale) down to the low scale. At the leading-order, RGE does the job of summing all the terms of the form $[\alpha_s(\mu_b)\ln(\mu_b/m_W)]^m$, at the next-to-leading order it sums the terms $\alpha_s(\mu_b)\,[\alpha_s(\mu_b)\ln(\mu_b/m_W)]^{m-1}$ and it goes in this way for higher orders such that the large logarithms are under control. A thorough discussion of RGE procedure and its applications can be found e.g. in [39, 47].

4 Calculation techniques

In elementary particle physics, while performing perturbative calculations one deals with solving loop-integrals. A particular Feynman diagram creates its own Feynman integrals[21] and depending on the complexity of the integrand computations of such integrals might become quite cumbersome. Especially, when computing multi-loop Feynman diagram(s) for a particular process with several kinematical variables, where the number of scalar integrals can be hundreds or more, it might turn out to be that the traditional techniques of using Feynman parametrization or Mellin-Barnes representations might not be fully competent to obtain analytic results. In order to handle them, the optimal strategy is first to derive some *recurrence* relations between the particular set of Feynman integrals using integration by parts (IBP) relations leading to master integrals (MI) which then can be tackled making use of differential equation technique. In Part II of this thesis, we encountered numerous challenging loop and phase-space integrals which we computed by applying the techniques mentioned above together with other known methods. In the following sections we discuss these methods briefly and illustrate how to use them by giving basic examples.

4.1 Integration by parts relations

The particular loop integrals which we encountered in Part II through the loop-diagrams under consideration are tackled using integration-by-parts[22] (IBPs) identities [49, 50]. The

[21] Here, Feynman integral is meant to refer to integrals over loop momenta and not a path integral.

[22] The meaning of IBP identities in this case is different than the usual meaning known from integral calculus. In the case of Feynman integrals, it means only that the integral of a total divergence is zero, which means

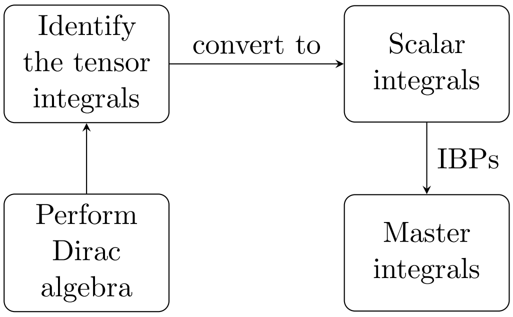

Figure 6: Steps to be followed to obtain the MIs of a particular loop diagram.

large set of complicated scalar loop integrals featuring the the same propagators of different powers are reduced to the so-called *master integrals* [23] (MIs). Another alternative way for computing loop-integrals is exploiting the fact that any scalar integral is invariant under Lorenz transformations [51]. This method, however, is not effective when considering multi-loop integrals.

The central idea of IBP identities is based on setting to zero any loop integrals of a total divergence within dimensional regularization. By doing so, one can correlate the Feynman integrals of some propagators to others which have the same structure of propagators, but raised to different powers. This procedure continues until one express a given Feynman integral as a linear combination of some *master* integrals with much simplified structure. However, when the number and complexity of the loop-integrals gets high, it becomes quite hard to obtain such relations manually. Instead, one makes use of some computer algorithms which does this job systematically. The Laporta algorithm [52], described by Laporta in 2000, is such an algorithm which is used to express complicated Feynman integrals as linear combinations of simpler MIs using IBPs identities. There are some implementations of this identities in a computer algebra system e.g. the `MAPLE` implementation `AIR` [53] and the `MATHEMATICA` implementation called `FIRE` [54]. In Part II of this thesis, we checked the correctness of our results by making use of both implementations. The strategy for obtaining the MIs out of a particular loop-diagram is sketched in Fig. 6.

To illustrate how to make use of IBP relations let us employ a simple example by considering the one-loop scalar self energy diagram shown in Fig. 7 [48]. Fig. 7 with appropriate "insertions of dots" in the loop lines, gives rise to class of two-point Feynman integrals with scalar propagators of the following form

$$F(\nu_1,\nu_2) = \int \frac{d^dl}{(2\pi)^d} \underbrace{\frac{1}{(l^2-m_1^2)^{\nu_1}\left[(l-p)^2-m_2^2\right]^{\nu_2}}}_{\chi(\nu_1,\nu_2)} . \tag{58}$$

Let us assume for simplicity $m_2 \ll m_1 = m$ such that we neglect the mass of the lighter line.

that one neglects the surface terms. Thus, though it is commonly accepted in this way in physics, the name can be misleading [48].

[23]MIs refer to the integrals of a simplified structure typically with low powers of propagators. Within a given family (topology) of integrals, MIs are those which cannot be reduced any further.

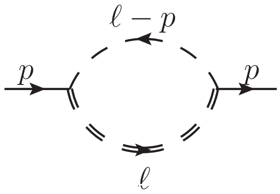

Figure 7: Scalar one-loop self energy diagram.

Setting to zero the dimensionally regularized integrals of the form

$$\int \frac{d^d l}{(2\pi)^d} \frac{\partial}{\partial l_\mu} \left[\eta^\mu \chi(\nu_1, \nu_2)\right] = 0\,,$$

with $\eta = \ell, p$ [24], one arrives at the following two IBP identities:

$$\begin{aligned}(d - \nu_2 - 2\nu_1)F(\nu_1, \nu_2) + \nu_2(p^2 - m^2)F(\nu_1, \nu_2 + 1)\\ -2m^2\nu_1 F(\nu_1 + 1, \nu_2) - \nu_2 F(\nu_1 - 1, \nu_2 + 1) = 0\,,\end{aligned} \tag{59}$$

$$\begin{aligned}(\nu_2 - \nu_1)F(\nu_1, \nu_2) + \nu_2(p^2 - m^2)F(\nu_1, \nu_2 + 1) - \nu_1(p^2 + m^2)F(\nu_1 + 1, \nu_2)\\ -\nu_2 F(\nu_1 - 1, \nu_2 + 1) + \nu_1 F(\nu_1 + 1, \nu_2 - 1) = 0\,.\end{aligned} \tag{60}$$

In the relations above the space-time dimension d arises due to the derivative acting on $\eta = l$ and the invariant quantities m^2 and p^2 originate after expressing the possible scalar products in terms of the two propagators. Note that alternative adjustment of Eq. (59) and Eq. (60) allows to obtain further relations among integrals with propagators of arbitrary powers of ν_1 and ν_2. Subtracting Eq. (60) from Eq. (59) gives

$$(d - \nu_1 - 2\nu_2)F(\nu_1, \nu_2) + \nu_1(p^2 - m^2)F(\nu_1 + 1, \nu_2) - \nu_1 F(\nu_1 + 1, \nu_2 - 1) = 0\,. \tag{61}$$

For the particular choice of $\nu_1, \nu_2 = 1$, which is corresponding to the Feynman integral originating from Fig. 7 without extra dots, Eq. (61) gives ($d = 4 - 2\epsilon$)

$$F(2, 1) = \frac{1}{m^2 - p^2}\left[(1 - 2\epsilon)F(1, 1) - F(2, 0)\right]\,. \tag{62}$$

The integrals with $\nu_2 \leq 0$ are simpler objects and can be computed directly in terms of the Γ-functions. In fact, setting $\nu_1 = 1, \nu_2 = 0$ in Eq. (59) helps us to express $F(2, 0)$ in terms of the simpler integral $F(1, 0)$ as[25]

$$F(2, 0) = \frac{1 - \epsilon}{m^2} F(1, 0)\,, \tag{63}$$

[24]For more general situations involving e.g. L–loops and N–external legs, one has $N + L - 1$ choices for η^μ which yield $(N + L - 1)L$ possible identities [11].

[25]In writing Eq. (63), we made use of the fact that within dimensional regularization any integral $F(\nu_1, \nu_2)$ (for $m_2 = 0$) with $\nu_1 \leq 0$ will vanish since it will correspond to a massless tadpole.

which further simplifies Eq. (62) to give

$$F(2,1) = \frac{1}{m^2 - p^2}\left[(1-2\epsilon)F(1,1) - \frac{1-\epsilon}{m^2}F(1,0)\right]. \tag{64}$$

As a result, we see that following this way it is possible to express any integral of a given structure as a linear combination of some master integrals and in our particular example the only-non vanishing MIs are $F(1,1)$ and $F(1,0)$ appearing on the RHS of Eq. (64).

4.2 Method of differential equations

The differential equations (DE) technique to evaluate MIs by making use of IBP relations was first proposed in [55] and later developed in [56]. The idea of this method uses the fact that taking some derivative of a particular MI with respect to its scales (invariants of the kinematics, masses) will generate a linear combination of integrals of the same family but with different powers ν_i of the denominators. As a next step, the resulting new integrals can be decomposed to MIs applying IBP identities. Repeating this procedure to some or all master integrals then generates a system of linear first-order differential equations satisfied by these MIs which can be evaluated by using convenient boundary conditions (see e.g. Ref. [48] for more detail). In some cases it can be more difficult to solve the DEs rather than computing the given MI directly, nevertheless the DEs give useful information about the analytic features or the asymptotic behavior of the integral [11]. Solving DEs requires fixing the integration constants which can be achieved by computing the integral for particular limit of its kinematical scales (which is often much easier than solving the original integral directly) and then confronting this result with the one obtained from DEs for the same limit.

To describe the basic recipes of this technique let us again follow our favorite example from the previous subsection and try to compute the MI $F(1,1)$ in Eq. (64). Taking the derivative of $F(1,1)$ with respect to $m^2 = \hat{t}$ gives nothing but $F(2,1)$ which we already know how to relate it to the MIs through Eq. (64). Doing so, we arrive at the following differential equation for $F(1,1)$

$$\frac{dF(1,1)}{d\hat{t}} = \frac{1}{\hat{t} - p^2}\left[(1-2\epsilon)F(1,1) - \frac{1-\epsilon}{\hat{t}}F(1,0)\right], \tag{65}$$

where $F(1,0)$ is a simple one-scale master integral which can easily be evaluated in terms of Γ-functions to give

$$F(1,0) = -\frac{i}{(4\pi)^{d/2}}\Gamma\left(1-\frac{d}{2}\right)(\hat{t})^{d/2-1}.$$

Defining $F(1,1) = \frac{i}{(4\pi)^{d/2}}(\hat{t})^{-\epsilon}\, y(\hat{t})$ we obtain

$$y' - \frac{\hat{t}(1-\epsilon) - \epsilon p^2}{(\hat{t}-p^2)\hat{t}}y = -\frac{\Gamma(\epsilon)}{\hat{t}-p^2}, \tag{66}$$

which is a first-order linear inhomogeneous DE for y, the right hand side being the inhomogeneity, and can be solved by the variation of constant technique. The corresponding homogenous solution of Eq. (66) (i.e., with zero at the right hand side) reads

$$y_{\text{hom}}(\hat{t}) = C\,(\hat{t}-p^2)^{1-2\epsilon}(\hat{t})^{\epsilon}. \tag{67}$$

Then, varying the constant C to be dependent on $\hat{t}$ as $C \to C_p(\hat{t})$ we assume a particular solution of the form $y_{\text{part}}(\hat{t}) = C_p(\hat{t})\,(\hat{t}-p^2)^{1-2\epsilon}(\hat{t})^{\epsilon}$. Plugging this to the full DE in Eq. (66) generates a linear DE for $C_p(\hat{t})$ as

$$C_p(\hat{t})' = -\hat{t}^{-\epsilon}(\hat{t}-p^2)^{-2+2\epsilon}\,\Gamma(\epsilon)\,, \tag{68}$$

and for which the solution reads

$$C_p(\hat{t}) = -\Gamma(\epsilon)\int_0^{\hat{t}} dx \frac{x^{-\epsilon}}{(x-p^2)^{2-2\epsilon}}\,. \tag{69}$$

Combining the homogenous and particular solutions we arrive at the general solution for $F(1,1)$ to be

$$F(1,1) = \frac{i}{(4\pi)^{d/2}}\,(\hat{t}-p^2)^{1-2\epsilon}\left[-\Gamma(\epsilon)\int_0^{\hat{t}} dx \frac{x^{-\epsilon}}{(x-p^2)^{2-2\epsilon}} + C\right]\,, \tag{70}$$

where C is the integration constant which can be fixed by evaluating the integral in the limit $\hat{t} \to 0$. In this asymptotic limit it is easier to calculate the behavior of $F(1,1)$ and equating this result with Eq. (70) for $\hat{t} \to 0$ (notice that the first term vanishes) fixes the constant C to be

$$C = \frac{\Gamma(\epsilon)\Gamma(1-\epsilon)^2}{\Gamma(2-2\epsilon)(-p^2)^{1-\epsilon}}\,.$$

Thus, we conclude that the solution for the integral $F(1,1)$ is[26]

$$\boxed{F(1,1) = \frac{i}{(4\pi)^{d/2}}\,(\hat{t}-p^2)^{1-2\epsilon}\left[-\Gamma(\epsilon)\int_0^{\hat{t}} dx \frac{x^{-\epsilon}}{(x-p^2)^{2-2\epsilon}} + \frac{\Gamma(\epsilon)\Gamma(1-\epsilon)^2}{\Gamma(2-2\epsilon)(-p^2)^{1-\epsilon}}\right]}\,. \tag{71}$$

Notice that in this particular example we solved the DE in an exact way with respect to ϵ, however depending on the complexity of the DEs, solutions order by order in ϵ can be preferable. In some cases an integral is evaluated as an expansion in a certain parameter, in such a case one has to be aware of the fact that this parameter can also be present in the denominator of the master integrals' coefficients. For example, if there is a factor of $1/\epsilon$ in front of a master integral, this would tell us to evaluate this integral up to $\mathcal{O}(\epsilon)$ in order to obtain the correct finite piece.

Remark on computational tools: In this thesis, most of the calculations (mainly the ones in Part II) are performed using the program `MATHEMATICA` [57]. In the intermediate steps of the calculations two custom software packages are employed. In order to tackle the complicated Dirac algebra the `MATHEMATICA` package `Fermions.m` [43], originally written by Patric Liniger, is used. At another stage, the reduction to master integrals was made possible using the `MAPLE` implementation `AIR` [53] by C. Anastasiou and A. Lazopoulos and the `MATHEMATICA` implementation `FIRE` [54] by A. V. Smirnov. Lastly, all Feynman diagrams are generated using the `Java` program `Jaxodraw` written by D. Binosi and L. Theussl [58].

[26]Note that in order to maintain the correct dimensionality of the result when going from 4 to d space-time dimensions one has to introduce a renormalization scale. For example in the so-called $\overline{MS}$ scheme, this would simply correspond multiplying the result in Eq. (71) by a factor $\bar{\mu}^{2\epsilon} = \mu^{2\epsilon}(e^{\gamma_E}/4\pi)^{\epsilon}$.

References

[1] http://www.symmetrymagazine.org/article/march-2013/planck-reveals-new-insight-into-universe.

[2] S. L. Glashow, Nucl. Phys. **22** (1961) 579.

[3] S. Weinberg, Phys. Rev. Lett. **19** (1967) 1264.

[4] H. Fritzsch, M. Gell-Mann and H. Leutwyler, Phys. Lett. B **47** (1973) 365.

[5] S. L. Glashow, J. Iliopoulos and L. Maiani, Phys. Rev. D **2** (1970) 1285.

[6] N. Cabibbo, Phys. Rev. Lett. **10** (1963) 531.

[7] M. Kobayashi and T. Maskawa, Prog. Theor. Phys. **49** (1973) 652.

[8] M. E. Peskin and D. V. Schroeder, "An introduction to Quantum Feild Theory," Westview Press, 1995.

[9] Manuel Philipp Walker, Ph.D Thesis, University of Bern, 2002.

[10] Kay Axel Bieri, Ph.D Thesis, University of Bern, 2004.

[11] Christof Schuepbach, Ph.D Thesis, University of Bern, 2011.

[12] Uwe-Jens Wiese, *The Standard Model of Particle Physics*, Lecture notes, March 2010.

[13] P. W. Higgs, Phys. Lett. **12** (1964) 132.

[14] T. W. B. Kibble, Phys. Rev. **155** (1967) 1554.

[15] L. L. Chau and W. Y. Keung, Phys. Rev. Lett. **53** (1984) 1802.

[16] L. Wolfenstein, Phys. Rev. Lett. **51** (1983) 1945.

[17] CKM-Fitter home page: $http://ckmfitter.in2p3.fr/www/html/ckm_main.html$

[18] UTfit home page: http://www.utfit.org/UTfit/WebHome

[19] O. Deschamps, S. Descotes-Genon, S. Monteil, V. Niess, S. T'Jampens and V. Tisserand, Phys. Rev. D **82** (2010) 073012 [arXiv:0907.5135 [hep-ph]].

[20] W. S. Hou, Phys. Rev. D **48** (1993) 2342.

[21] A. Pich and P. Tuzon, Phys. Rev. D **80** (2009) 091702 [arXiv:0908.1554 [hep-ph]].

[22] G. C. Branco, P. M. Ferreira, L. Lavoura, M. N. Rebelo, M. Sher and J. P. Silva, Phys. Rept. **516** (2012) 1 [arXiv:1106.0034 [hep-ph]].

[23] J. F. Gunion, H. E. Haber, G. Kane, S. Dawson, *The Higgs Hunter's Guide*, Addison Wesley, 1990.

[24] Howard Haber, *The Two Higgs-Doublet Model: Past, Present and Future*, Talk given at Kane Symposium, University of Michigan, 2007.

[25] T. D. Lee, *A Theory of Spontaneous T Violation*, Phys. Rev. D8, 1226 (1973).

[26] S. L. Glashow and S. Weinberg, *Natural Conservation Laws For Neutral Currents*, Phys. Rev. D15, 1958 (1977).

[27] N. G. Deshpande and E. Ma, *Pattern Of Symmetry Breaking With Two Higgs Doublets*, Phys. Rev. D18, 2574 (1978).

[28] H. E. Haber, G. L. Kane and T. Sterling, *The Fermion Mass Scale And Possible Effects Of Higgs Bosons On Experimental Observables*, Nucl. Phys. B161, 493 (1979).

[29] J. F. Donoghue and L. F. Li, *Properties Of Charged Higgs Bosons*, Phys. Rev. D19, 945 (1979).

[30] L. J. Hall and M. B. Wise, *Flavor Changing Higgs Boson Couplings*, Nucl. Phys. B187, 397 (1981).

[31] T. P. Cheng and M. Sher, *Mass Matrix Ansatz and Flavor Nonconservation in Models with Multiple Higgs Doublets*, Phys. Rev. D35, 3484 (1987).

[32] Christopher Smith, *Minimal Flavor Violation*, Lecture notes.

[33] J. Rosiek, hep-ph/9511250.

[34] A. Crivellin, A. Kokulu and C. Greub, arXiv:1303.5877 [hep-ph].

[35] J. F. Gunion and H. E. Haber, Phys. Rev. D **67** (2003) 075019 [hep-ph/0207010].

[36] R. Peccei and H. Quinn, Phys. Rev. D **16** (1977) 1791.

[37] A. Pich, hep-ph/9806303.

[38] K. G. Wilson, Phys. Rev. **179** (1969) 1499.

[39] A. J. Buras, hep-ph/9806471.

[40] C. Bobeth, M. Misiak and J. Urban, Nucl. Phys. B **574** (2000) 291 [hep-ph/9910220].

[41] K. G. Chetyrkin, M. Misiak and M. Munz, Phys. Lett. B **400** (1997) 206 [Erratum-ibid. B **425** (1998) 414] [hep-ph/9612313].

[42] C. Greub and T. Hurth, Phys. Rev. D **56** (1997) 2934 [hep-ph/9703349].

[43] Patric Liniger, Ph.D Thesis, University of Bern, 2001.

[44] Peter Kienholz, M.Sc Thesis, University of Bern, 2008.

[45] V. A. Smirnov, Mod. Phys. Lett. A **10** (1995) 1485 [hep-th/9412063].

[46] V. A. Smirnov, Phys. Lett. B **394** (1997) 205 [hep-th/9608151].

[47] G. Buchalla, A. J. Buras and M. E. Lautenbacher, Rev. Mod. Phys. **68** (1996) 1125 [arXiv:hep-ph/9512380].

[48] V. A. Smirnov, “ Feynman Integral Calculus,” Springer edition, 2006.

[49] K. G. Chetyrkin and F. V. Tkachov, Nucl. Phys. B **192** (1981) 159.

[50] F. V. Tkachov, Phys. Lett. B **100** (1981) 65.

[51] T. Gehrmann and E. Remiddi, Nucl. Phys. B **580** (2000) 485 [arXiv:hep-ph/9912329].

[52] S. Laporta, Int. J. Mod. Phys. A **15** (2000) 5087 [arXiv:hep-ph/0102033].

[53] C. Anastasiou and A. Lazopoulos, JHEP **0407** (2004) 046 [arXiv:hep-ph/0404258].

[54] A. V. Smirnov, JHEP **0810** (2008) 107 [arXiv:0807.3243 [hep-ph]].

[55] A. V. Kotikov, Phys. Lett. B **254** (1991) 158; B **259** (1991) 314; B **267** (1991) 123; Mod. Phys. Lett. A **6** (1991) 677; 3133; Int. J. Mod. Phys. A **7** (1992) 1977.

[56] E. Remiddi, Nuovo Cim. A **110** (1997) 1435 [arXiv:hep-th/9711188].

[57] M. Kofler: *Mathematica. Introduction, application, Reference*, (1998), Addison-Wesley, Bonn, ISBN: 3827312086.

[58] D. Binosi, L. Theussl: *Jaxodraw. A graphical user interface for drawing Feynman diagrams*, (2004), Comp. Phys. Comm. **161** 76.

Part II

NLL QCD contribution of the Electromagnetic Dipole operator to $\bar{B} \to X_s\gamma\gamma$

published in

Phys. Rev. D85 (2012) 014020
(arXiv:1110.1251 [hep-ph])

NLL QCD contribution of the Electromagnetic Dipole operator to $\bar{B} \to X_s\gamma\gamma$

H.M. Asatrian[a], C. Greub[b], A. Kokulu[b], A. Yeghiazaryan[a]

[a] *Yerevan Physics Institute, 0036 Yerevan, Armenia*

[b] *Albert Einstein Center for Fundamental Physics, Institute for Theoretical Physics, Univ. of Bern, CH-3012 Bern, Switzerland*

Abstract

We calculate the set of $O(\alpha_s)$ corrections to the double differential decay width $d\Gamma_{77}/(ds_1\, ds_2)$ for the process $\bar{B} \to X_s\gamma\gamma$ originating from diagrams involving the electromagnetic dipole operator $\mathcal{O}_7$. The kinematical variables s_1 and s_2 are defined as $s_i = (p_b - q_i)^2/m_b^2$, where p_b, q_1, q_2 are the momenta of b-quark and two photons. While the (renormalized) virtual corrections are worked exactly for a certain range of s_1 and s_2, we retain in the gluon bremsstrahlung process only the leading power w.r.t. the (normalized) hadronic mass $s_3 = (p_b - q_1 - q_2)^2/m_b^2$ in the underlying triple differential decay width $d\Gamma_{77}/(ds_1 ds_2 ds_3)$. The double differential decay width, based on this approximation is free of infrared- and collinear singularities when combining virtual- and bremsstrahlung corrections. The corresponding results are obtained analytically. When retaining all powers in s_3, the sum of virtual- and bremstrahlung corrections contains uncanceled $1/\epsilon$ singularities (which are due to collinear *photon* emission from the s-quark) and other concepts, which go beyond perturbation theory, like parton fragmentation functions of a quark or a gluon into a photon, are needed which is beyond the scope of our paper.

1 Introduction

Inclusive rare B-meson decays are known to be a unique source of indirect information about physics at scales of several hundred GeV. In the Standard Model (SM) all these processes proceed through loop diagrams and thus are relatively suppressed. In the extensions of the SM the contributions stemming from the diagrams with “new” particles in the loops can be comparable or even larger than the contribution from the SM. Thus getting experimental information on rare decays puts strong constraints on the extensions of the SM or can even lead to a disagreement with the SM predictions, providing evidence for some “new physics”.

To make a rigorous comparison between experiment and theory, precise SM calculations for the (differential) decay rates are mandatory. While the branching ratios for $\bar{B} \to X_s\gamma$ [1] and $\bar{B} \to X_s\ell^+\ell^-$ are known today even to next-to-next-to-leading logarithmic (NNLL) precision (for reviews, see [2, 3]), other branching ratios, like the one for $\bar{B} \to X_s\gamma\gamma$ discussed in this paper, are only known to leading logarithmic (LL) precision in the SM [4, 5, 6, 7]. In contrast to $\bar{B} \to X_s\gamma$, the current-current operator $\mathcal{O}_2$ has a non-vanishing matrix element for $b \to s\gamma\gamma$ at order α_s^0 precision, leading to an interesting interference pattern with the contributions associated with the electromagnetic dipole operator $\mathcal{O}_7$ already at LL precision. As a consequence, potential new physics should be clearly visible not only in the total branching ratio, but also in the differential distributions.

As the process $\bar{B} \to X_s\gamma\gamma$ is expected to be measured at the planned Super B-factories in Japan and Italy, it is necessary to calculate the differential distributions to NLL precision in the SM, in order to fully exploit its potential concerning new physics. The starting point of our calculation is the effective Hamiltonian, obtained by integrating out the heavy particles in the SM, leading to

$$\mathcal{H}_{eff} = -\frac{4G_F}{\sqrt{2}}\, V_{ts}^\star V_{tb} \sum_{i=1}^{8} C_i(\mu)\mathcal{O}_i(\mu)\,, \tag{1}$$

where we use the operator basis introduced in [8]:

$$\begin{array}{llll} \mathcal{O}_1 = (\bar{s}_L\gamma_\mu T^a c_L)\,(\bar{c}_L\gamma^\mu T_a b_L)\,, & \mathcal{O}_2 = (\bar{s}_L\gamma_\mu c_L)\,(\bar{c}_L\gamma^\mu b_L)\,, \\ \mathcal{O}_3 = (\bar{s}_L\gamma_\mu b_L)\sum_q(\bar{q}\gamma^\mu q)\,, & \mathcal{O}_4 = (\bar{s}_L\gamma_\mu T^a b_L)\sum_q(\bar{q}\gamma^\mu T_a q)\,, \\ \mathcal{O}_5 = (\bar{s}_L\gamma_\mu\gamma_\nu\gamma_\rho b_L)\sum_q(\bar{q}\gamma^\mu\gamma^\nu\gamma^\rho q)\,, & \mathcal{O}_6 = (\bar{s}_L\gamma_\mu\gamma_\nu\gamma_\rho T^a b_L)\sum_q(\bar{q}\gamma^\mu\gamma^\nu\gamma^\rho T_a q)\,, \\ \mathcal{O}_7 = \frac{e}{16\pi^2}\,\bar{m}_b(\mu)\,(\bar{s}_L\sigma^{\mu\nu}b_R)\,F_{\mu\nu}\,, & \mathcal{O}_8 = \frac{g_s}{16\pi^2}\,\bar{m}_b(\mu)\,(\bar{s}_L\sigma^{\mu\nu}T^a b_R)\,G^a_{\mu\nu}\,. \end{array} \tag{2}$$

The symbols T^a $(a = 1, 8)$ denote the $SU(3)$ color generators; g_s and e, the strong and electromagnetic coupling constants. In eq. (2), $\bar{m}_b(\mu)$ is the running b-quark mass in the $\overline{\text{MS}}$-scheme at the renormalization scale μ. As we are not interested in CP-violation effects in the present paper, we made use of the approximation $V_{ub}V_{us}^* \ll V_{tb}V_{ts}^*$ when writing eq. (1). Furthermore, we also put $m_s = 0$.

While the Wilson coefficients $C_i(\mu)$ appearing in eq. (1) are known to sufficient precision at the low scale $\mu \sim m_b$ since a long time (see e.g. the reviews [2, 3] and references therein), the matrix elements $\langle s\gamma\gamma|\mathcal{O}_i|b\rangle$ and $\langle s\gamma\gamma\, g|\mathcal{O}_i|b\rangle$, which in a NLL calculation are needed to order g_s^2 and g_s, respectively, are not known yet. To calculate the $(\mathcal{O}_i, \mathcal{O}_j)$-interference contributions for the differential distributions at order α_s is in many respects of similar complexity as the calculation of the photon energy spectrum in $\bar{B} \to X_s\gamma$ at order α_s^2 needed for the NNLL computation. There, the individual interference contributions, which all involve extensive calculations, were published in separate papers, sometimes even by two independent groups (see e.g. [9] and [10]). It therefore cannot be expected that the NLL results for the differential distributions related to $\bar{B} \to X_s\gamma\gamma$ are given in a single paper. As a first step in this NLL enterprise, we derive in the present paper the $O(\alpha_s)$ corrections to the $(\mathcal{O}_7, \mathcal{O}_7)$-interference contribution to the double differential decay width $d\Gamma/(ds_1 ds_2)$ at the partonic level. The variables s_1 and s_2 are defined as $s_i = (p_b - q_i)^2/m_b^2$, where p_b and q_i denote the four-momenta of the b-quark and the two photons, respectively.

At order α_s there are contributions to $d\Gamma_{77}/(ds_1 ds_2)$ with three particles (s-quark and two photons) and four particles (s-quark, two photons and a gluon) in the final state. These contributions correspond to specific cuts of the b-quarks self-energy at order $\alpha^2 \times \alpha_s$, involving twice the operator $\mathcal{O}_7$. As there are additional cuts, which contain for example only one photon, our observable cannot be obtained using the optical theorem, i.e., by taking the absorptive part of the b-quark self-energy at three-loop. We therefore calculate the mentioned contributions with three and four particles in the final state individually.

As discussed in section 2, we work out the QCD corrections to the double differential decay width in the kinematical range

$$0 < s_1 < 1 \quad ; \quad 0 < s_2 < 1 - s_1 \, .$$

Concerning the virtual corrections, all singularities (after ultra-violet renormalization) are due to **soft gluon** exchanges and/or **collinear gluon** exchanges involving the s-quark. Concerning the bremsstrahlung corrections (restricted to the same range of s_1 and s_2), there are in addition kinematical situations where **collinear photons** are emitted from the s-quark. The corresponding singularities are not canceled when combined with the virtual corrections, as discussed in detail in section 4. We found, however, that there are no singularities associated with collinear photon emission in the double differential decay width when only retaining the leading power w.r.t to the (normalized) hadronic mass $s_3 = (p_b - q_1 - q_2)^2/m_b^2$ in the underlying triple differential distribution $d\Gamma_{77}/(ds_1 ds_2 ds_3)$. Our results of this paper are obtained within this "approximation". When going beyond, other concepts which go beyond perturbation theory, like parton fragmentation functions of a quark or a gluon into a photon, are needed [11].

Before moving to the detailed organization of our paper, we should mention that the inclusive double radiative process $\bar{B} \to X_s \gamma\gamma$ has also been explored in several extensions of the SM [5, 7, 12]. Also the corresponding exclusive modes, $B_s \to \gamma\gamma$ and $B \to K\gamma\gamma$, have been examined before, both in the SM [6, 13, 14, 15, 16, 17, 18, 19, 20, 21] and in its extensions [12, 17, 18, 22, 23, 24, 25, 26, 27, 28, 29, 30]. We should add that the long-distance resonant effects were also discussed in the literature (see e.g. [6] and the references therein). Finally, the effects of photon emission from the spectator quark in the B-meson were discussed in [13, 17, 31].

The remainder of this paper is organized as follows. In section 2 we work out the double differential distribution $d\Gamma_{77}/(ds_1 ds_2)$ in leading order, i.e., without taking into account QCD corrections to the matrix element $\langle s\gamma\gamma|\mathcal{O}_7|b\rangle$. We retain, however, terms up to order ϵ^1, with ϵ being the dimensional regulator ($d = 4 - 2\epsilon$). Section 3 is devoted to the calculation of the virtual corrections of order α_s to the double differential decay width. In section 4 the corresponding gluon bremsstrahlung corrections to the double differential width are worked out in the approximation where only the leading power w.r.t. the (normalized) hadronic mass s_3 is retained at the level of the triple differential decay width $d\Gamma_{77}/(ds_1 ds_2 ds_3)$. In section 5 virtual- and bremsstrahlung corrections are combined and the result for the double differential decay width, which is free of infrared- and collinear singularities, is given in analytic form. In section 6 we illustrate the numerical impact of the NLL corrections and in section 7 we present the technical details of our calculations. The paper ends with a short summary in section 8.

2 Leading order result

In this section we discuss the double differential decay width $d\Gamma_{77}/(ds_1 ds_2)$ at lowest order in QCD, i.e. α_s^0. The dimensionless variables s_1 and s_2 are defined everywhere in this paper as

$$s_1 = \frac{(p_b - q_1)^2}{m_b^2} \quad ; \quad s_2 = \frac{(p_b - q_2)^2}{m_b^2} \, . \tag{3}$$

At lowest order the double differential decay width is based on the diagrams shown in Fig. 1. The variables s_1 and s_2 form a complete set of kinematically independent variables for the

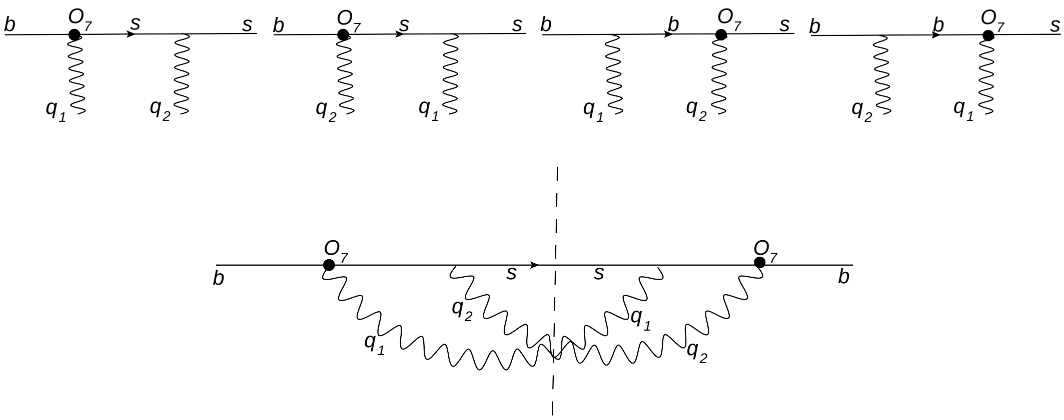

Figure 1: On the first line the diagrams defining the tree-level amplitude for $b \to s\gamma\gamma$ associated with $\mathcal{O}_7$ are shown. The four-momenta of the b-quark, the s-quarks and the two photons are denoted by p_b, p_s, q_1 and q_2, respectively. On the second line the contribution to the decay width corresponding to the interference of first and second diagram is shown.

three-body decay $b \to s\gamma\gamma$. Their kinematical range is as follows:

$$0 \le s_1 \le 1 \quad ; \quad 0 \le s_2 \le 1 - s_1 \, .$$

The energies E_1 and E_2 in the rest-frame of the b-quark of the two photons are related to s_1 and s_2 in a simple way: $s_i = 1 - 2\,E_i/m_b$. As the energies E_i of the photons have to be away from zero in order to be observed, the values of s_1 and s_2 can be considered to be smaller than one. By additionally requiring s_1 and s_2 to be larger than zero, we exclude collinear photon emission from the s-quark, because $2p_sq_1 = (p_s+q_1)^2 = (p_b-q_2)^2 = s_2\,m_b^2 > 0$ and $2p_sq_2 = (p_s+q_2)^2 = (p_b-q_1)^2 = s_1\,m_b^2 > 0$. It is also easy to implement a lower cut on the invariant mass squared s of the of the two photons by observing that $s = (q_1+q_2)^2 = 1-s_1-s_2$. To parametrize all the mentioned conditions in terms of one parameter c (with $c > 0$), one can proceed as suggested in [5]:

$$s_1 \ge c \, , \quad s_2 \ge c \, , \quad 1 - s_1 - s_2 \ge c \, . \tag{4}$$

Applying such cuts, the relevant phase-space region in the (s_1, s_2)-plane is shown by the shaded area in Fig. 2. Our aim in this paper is to work out the double differential decay width in this restricted area of the s_1 and the s_2 variable also when discussing the gluon bremsstrahlung corrections[1]. In this restricted region of the phase-space, the tree-level amplitude is free of infrared- and collinear singularities. To exhibit the singularity structure of the virtual corrections discussed in the next section in a transparent way, it is useful to give the leading-order spectrum in $d = 4 - 2\epsilon$ dimensions. We obtain

$$\frac{d\Gamma_{77}^{(0,d)}}{ds_1\,ds_2} = \frac{\alpha^2\,\bar{m}_b^2(\mu)\,m_b^3\,|C_{7,eff}(\mu)|^2\,G_F^2\,|V_{tb}V_{ts}^*|^2\,Q_d^2}{1024\,\pi^5} \left(\frac{\mu}{m_b}\right)^{4\epsilon} r \tag{5}$$

[1]In this case, the normalized invariant mass squared s of the two photons reads $s = 1 - s_1 - s_2 + s_3$, where s_3 is the normalized hadronic mass squared. The condition $1 - s_1 - s_2 \ge c$ then still eliminates two-photon configurations with small invariant mass.

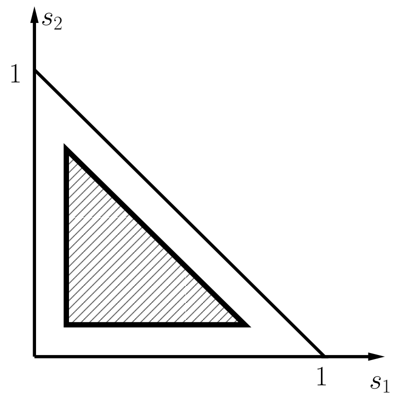

Figure 2: The relevant phase-space region for (s_1, s_2) used in this paper is shown by the shaded area.

with

$$r = \frac{[r_0 + \epsilon(r_1 + r_2 + r_3 + r_4)]\,(1 - s_1 - s_2)}{(1 - s_1)^2\, s_1\, (1 - s_2)^2\, s_2} \,. \tag{6}$$

In r we retained terms of order ϵ^1, while discarding terms of higher order. The individual pieces $r_0, \ldots, r_4$ read

$$\begin{aligned} r_0 \;&=\; -48 s_2^3 s_1^3 + 96 s_2^2 s_1^3 - 56 s_2 s_1^3 + 8 s_1^3 + 96 s_2^3 s_1^2 - 192 s_2^2 s_1^2 + 112 s_2 s_1^2 - 56 s_2^3 s_1 + \\ &\quad\; 112 s_2^2 s_1 - 96 s_2 s_1 + 8 s_1 + 8 s_2^3 + 8 s_2 \end{aligned}$$

$$\begin{aligned} r_1 \;&=\; -16 s_2^2 s_1^3 + 16 s_2 s_1^3 - 16 s_2^3 s_1^2 + 48 s_2^2 s_1^2 - 32 s_2 s_1^2 + 16 s_1^2 + 16 s_2^3 s_1 - \\ &\quad\; 32 s_2^2 s_1 - 16 s_2 s_1 + 16 s_2^2 \end{aligned}$$

$$\begin{aligned} r_2 \;&=\; \big(48 s_2^3 s_1^3 - 96 s_2^2 s_1^3 + 56 s_2 s_1^3 - 8 s_1^3 - 96 s_2^3 s_1^2 + 192 s_2^2 s_1^2 - \\ &\quad\; 112 s_2 s_1^2 + 56 s_2^3 s_1 - 112 s_2^2 s_1 + 96 s_2 s_1 - 8 s_1 - 8 s_2^3 - 8 s_2\big) \log(s_1) \end{aligned}$$

$$r_3 \;=\; r_2(s_1 \leftrightarrow s_2)$$

$$\begin{aligned} r_4 \;&=\; \big[48 s_2^3 s_1^3 - 96 s_2^2 s_1^3 + 56 s_2 s_1^3 - 8 s_1^3 - 96 s_2^3 s_1^2 + 192 s_2^2 s_1^2 - 112 s_2 s_1^2 + 56 s_2^3 s_1 - \\ &\quad\; 112 s_2^2 s_1 + 96 s_2 s_1 - 8 s_1 - 8 s_2^3 - 8 s_2\big] \log(1 - s_1 - s_2) \end{aligned}$$

In eq. (5) the symbols $\bar{m}_b(\mu)$ and m_b denote the mass of the b-quark in the $\overline{\text{MS}}$-scheme and in the on-shell scheme, respectively.

In $d = 4$ dimensions, the leading-order spectrum (in our restricted phase-space) is obtained by simply putting ϵ to zero, obtaining

$$\frac{d\Gamma_{77}^{(0)}}{ds_1\, ds_2} = \frac{\alpha^2\, \bar{m}_b^2(\mu)\, m_b^3\, |C_{7,eff}(\mu)|^2\, G_F^2\, |V_{tb} V_{ts}^*|^2\, Q_d^2}{1024\, \pi^5}\, \frac{(1 - s_1 - s_2)}{(1 - s_1)^2 s_1 (1 - s_2)^2 s_2}\, r_0 \,. \tag{7}$$

3 Virtual corrections

We now turn to the calculation of the virtual QCD corrections, i.e. to the contributions of order α_s with three particles in the final state. The diagrams defining the (unrenormalized) virtual corrections at the amplitude level are shown on the first four lines of Fig. 3. As the diagrams with a self-energy insertion on the external b- and s-quark legs are taken into account in the renormalization process, these diagrams are not shown in Fig. 3. In order to get the (unrenormalized) virtual corrections $d\Gamma_{77}^{\rm bare}/(ds_1 ds_2)$ of order α_s to the decay width, we have to work out the interference of the diagrams on the first four lines in Fig. 3 with the leading order diagrams in Fig. 1. One of these interference contributions is shown on the last line in Fig. 3. To illustrate the calculational procedure for getting the virtual corrections to the decay width, we describe in section 7.1 the relevant steps for the particular interference shown in Fig. 3.

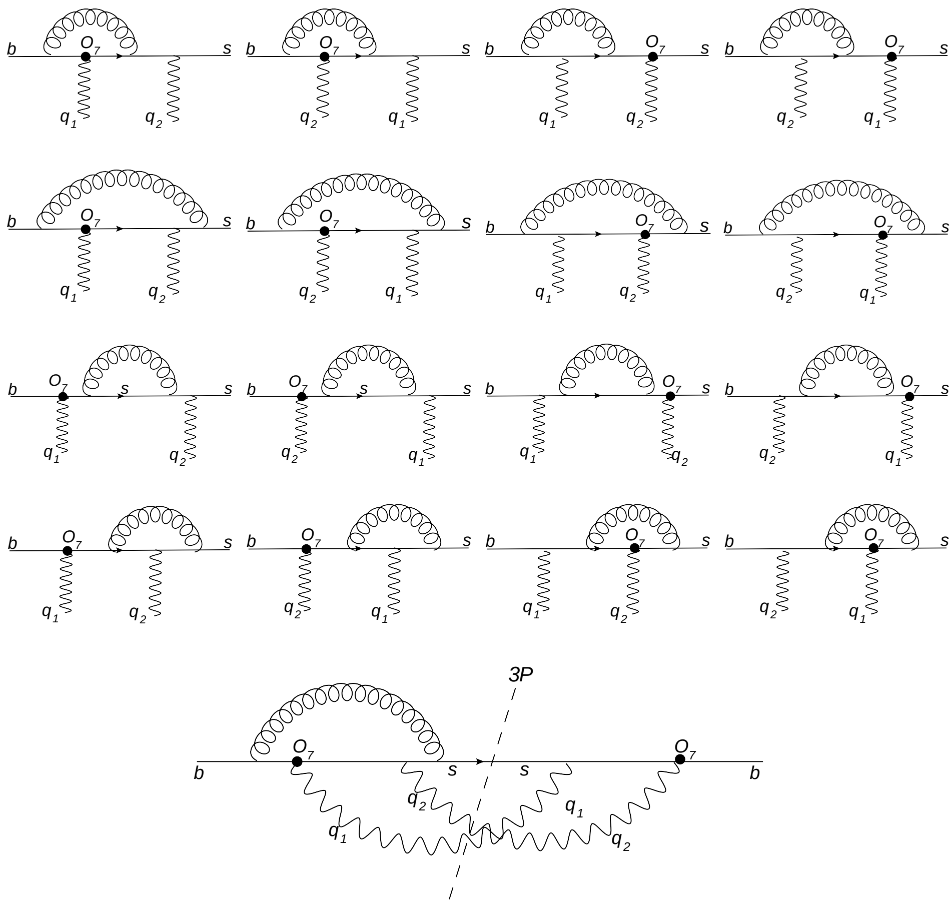

Figure 3: On the first four lines the diagrams defining the one-loop amplitude for $b \to s\gamma\gamma$ associated with $\mathcal{O}_7$ are shown. Diagrams with self-energy insertions on the external quark-legs are not shown. On the last line the contribution to the decay width corresponding to the interference of the first diagram on the second line with the second (tree-level) diagram in Fig. 1 is shown.

In addition, we have to work out the counterterm contributions to the decay width. They can be split into two parts, according to

$$\frac{d\Gamma_{77}^{\mathrm{ct}}}{ds_1 ds_2} = \frac{d\Gamma_{77}^{\mathrm{ct},(A)}}{ds_1 ds_2} + \frac{d\Gamma_{77}^{\mathrm{ct},(B)}}{ds_1 ds_2} \,. \tag{8}$$

Part (A) involves the LSZ factors $\sqrt{Z_{2b}^{\mathrm{OS}}}$ and $\sqrt{Z_{2s}^{\mathrm{OS}}}$ for the b- and s-quark field, as well as the self-renormalization constant $Z_{77}^{\overline{\mathrm{MS}}}$ of the operator $\mathcal{O}_7$ and $Z_{m_b}^{\overline{\mathrm{MS}}}$ renormalizing the factor $\bar{m}_b(\mu)$ present in the operator $\mathcal{O}_7$. The explicit results for these Z-factors are given to relevant precision in Appendix C. For part (A) we get

$$\frac{d\Gamma_{77}^{\mathrm{ct},(A)}}{ds_1 ds_2} = \left[\delta Z_{2b}^{\mathrm{OS}} + \delta Z_{2s}^{\mathrm{OS}} + 2\,\delta Z_{m_b}^{\overline{\mathrm{MS}}} + 2\,\delta Z_{77}^{\overline{\mathrm{MS}}}\right] \frac{d\Gamma_{77}^{(0,d)}}{ds_1 ds_2} \,, \tag{9}$$

where $d\Gamma_{77}^{(0,d)}/(ds_1 ds_2)$ is the leading order double differential decay width in d-dimensions, as given in eq. (5).

Figure 4: Counterterm diagrams with a δm_b insertion, see text.

The counterterms defining part (B) are due to the insertion of $-i\delta m_b \bar{b}b$ in the internal b-quark line in the leading order diagrams as indicated in Fig. 4, where

$$\delta m_b = (Z_{m_b}^{\mathrm{OS}} - 1)\, m_b \,.$$

More precisely, Part (B) consists of the interference of the diagrams in Fig. 4 with the leading order diagrams in Fig. 1.

By adding $d\Gamma_{77}^{\mathrm{bare}}/(ds_1 ds_2)$ and $d\Gamma_{77}^{\mathrm{ct}}/(ds_1 ds_2)$, we get the result for the renormalized virtual corrections to the spectrum, $d\Gamma_{77}^{(1),virt}/(ds_1\, ds_2)$. It is useful to decompose this result into two pieces,

$$\frac{d\Gamma_{77}^{(1),virt}}{ds_1\, ds_2} = \frac{d\Gamma_{77}^{(1,a),virt}}{ds_1\, ds_2} + \frac{d\Gamma_{77}^{(1,b),virt}}{ds_1\, ds_2} \,. \tag{10}$$

The infrared- and collinear singularities are completely contained in $d\Gamma_{77}^{(1,a),virt}/(ds_1\, ds_2)$. Explicitly, we obtain

$$\frac{d\Gamma_{77}^{(1,a),virt}}{ds_1\, ds_2} = \frac{\alpha_s}{4\pi}\, C_F \left(-\frac{2}{\epsilon^2} + \frac{4\log(s_1+s_2) - 5}{\epsilon}\right) \left(\frac{\mu}{m_b}\right)^{2\epsilon} \frac{d\Gamma_{77}^{(0,d)}}{ds_1\, ds_2} \tag{11}$$

where $d\Gamma_{77}^{(0,d)}/(ds_1\, ds_2)$ is understood to be taken exactly as given in eqs. (5) and (6), i.e., by including the terms of order ϵ^1 in r. From the explicit expression $d\Gamma_{77}^{(1,a),virt}/(ds_1\, ds_2)$ we see that the singularity structure consists of a simple singular factor multiplying the corresponding tree-level decay width in d-dimensions. We stress that singularities (represented by $1/\epsilon^2$ and

$1/\epsilon$ poles) are entirely due to soft- and/or collinear **gluon** exchange. The infrared finite piece $d\Gamma_{77}^{(1,b),virt}/(ds_1\, ds_2)$ can be written as

$$\frac{d\Gamma_{77}^{(1,b),virt}}{ds_1\, ds_2} = \frac{\alpha^2\, \bar{m}_b^2(\mu)\, m_b^3\, |C_{7,eff}(\mu)|^2\, G_F^2\, |V_{tb}V_{ts}^*|^2\, Q_d^2}{1024\,\pi^5} \times$$
$$\frac{\alpha_s}{4\pi}\, C_F\, \left(\frac{-4\, r_0\, (1-s_1-s_2)}{(1-s_1)^2\, s_1\, (1-s_2)^2\, s_2}\, \log\frac{\mu}{m_b} + \frac{\sum_{i=1}^{20} v_i}{3\,(1-s_1)^3\, s_1\, (1-s_2)^3\, s_2} \right) \quad (12)$$

where the individual quantites $v_1, \ldots, v_{20}$ are relegated to Appendix A.

4 Bremsstrahlung corrections

We now turn to the calculation of the bremsstrahlung QCD corrections, i.e. to the contributions of order α_s with four particles in the final state. Before going into details, we mention that the kinematical range of the variables s_1 and s_2 defined in eq. (3) is given in this case by $0 \le s_1 \le 1\,;\, 0 \le s_2 \le 1$. Nevertheless, we consider in this paper only the range which is also accessible to the three-body decay $b \to s\gamma\gamma$, i.e., $0 \le s_1 \le 1\,;\, 0 \le s_2 \le 1 - s_1$ or, more precisely, by its restricted version specified in eq. (4).

The diagrams defining the bremsstrahlung corrections at the amplitude level are shown in the first line of Fig. 5. The amplitude squared, needed to get the (double differential) decay

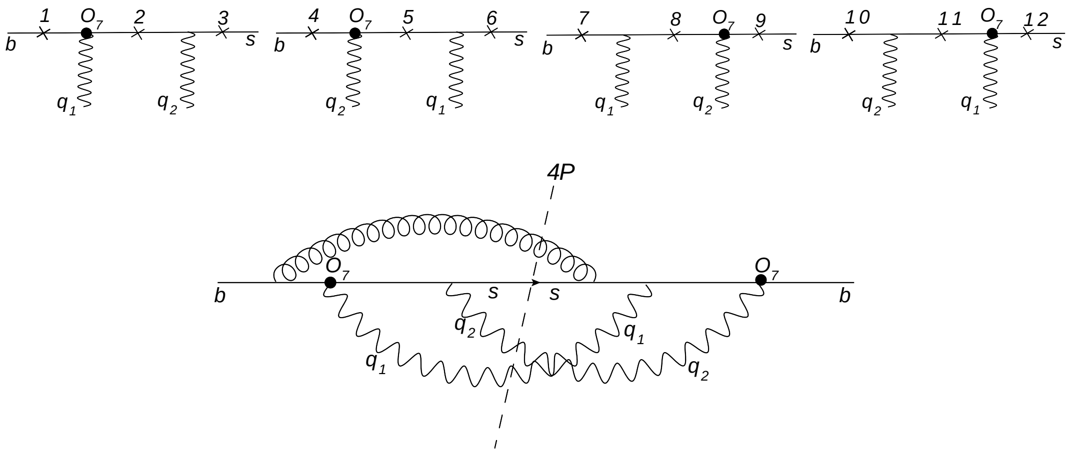

Figure 5: On the first line the diagrams defining the gluon-bremsstrahlung corrections to $b \to s\gamma\gamma$ are shown at the amplitude level. The crosses in the graphs stand for the possible emission places of the gluon. On the second line the contribution to the decay width corresponding to the interference of diagram 1 with diagram 6 is illustrated.

width, can be written as a sum of interferences of the different diagrams on the first line in Fig. 5. One such interference is shown on the second line of the same figure. The four particle final state is described by five independent kinematical variables. In a first attempt we worked out the decay width by keeping s_1 and s_2 differential and integrating over the three remaining variables. Proceeding in this way, we found that the infrared- and collinear singularities in the bremsstrahlung spectrum do not cancel when adding the virtual corrections. The sum still contains $1/\epsilon$-poles, but no $1/\epsilon^2$-poles. While, as already mentioned in section 3, the only source of the singularities in the virtual corrections in our restricted range of s_1 and s_2 are due to soft **gluon**-emission and/or collinear emission of **gluons** from the s-quark, we found after analyzing the bremsstrahlung kinematics more carefully that there are situations where one of the **photons** can become collinear with the s-quark. This is the reason why there is no cancellation of singularities when combining virtual- and bremsstrahlung corrections. Realizing that for (formally) zero hadronic mass of the (s,g)-system collinear photon emission is kinematically impossible, led us to the idea that we should first look at the triple differential decay width $d\Gamma_{77}/(ds_1 ds_2 ds_3)$, where $s_3 = (p_s + p_g)^2/m_b^2$ is the normalized hadronic mass squared. Our conjecture was that the double differential decay width, based on the triple differential decay width in which only the leading power terms w.r.t. s_3 are retained, should lead to a finite result when combined with the virtual corrections.

We therefore worked out the leading power of this quantity w.r.t s_3, denoting it by $d\Gamma_{77}^{\text{leading power}}/(ds_1 ds_2 ds_3)$. The leading power, which is of order $1/s_3$ (modified by epsilontic dimensional regulators), is supposed to be a good approximation for low values of the hadronic mass. An approximation to the double-differential decay width $d\Gamma_{77}^{(1),brems}/(ds_1 ds_2)$ due to gluon bremsstrahlung corrections is then obtained by integrating $d\Gamma_{77}^{\text{leading power}}/(ds_1 ds_2 ds_3)$ over s_3, which runs in the range $s_3 \in [0, s_1 \cdot s_2]$. The approximation is obviously accurate for small values of $s_1 \cdot s_2$. As $s_1 \cdot s_2$ is at most $1/4$, the approximation is expected not to be bad in the full region of s_1 and s_2 considered in this paper. The technical details of the calculation of the leading power w.r.t. s_3 in the triple differential decay width are illustrated in section 7.2 for the interference of diagram 1 with diagram 6, as shown in the second line of Fig. 5.

Indeed, we find that the infrared- and collinear singularities cancel when combining the approximated version of $d\Gamma_{77}^{(1),brems}/(ds_1 ds_2)$ with the virtual corrections $d\Gamma_{77}^{(1),virt}/(ds_1 ds_2)$.

When going beyond this approximation other concepts, which go beyond perturbation theory, like parton fragmentation functions of a quark or a gluon into a photon, are needed [11]. We do not enter this issue in this paper.

The result of combined virtual- and bremsstrahlung corrections is explicitly presented in the next section.

5 Final result for the decay width at order α_s

The complete order α_s correction to the double differential decay width $d\Gamma_{77}/(ds_1\, ds_2)$ is obtained by adding the renormalized virtual corrections from section 3 and the bremsstrahlung corrections discussed in section 4. Explicitly we get

$$\frac{d\Gamma_{77}^{(1)}}{ds_1\, ds_2} = \frac{\alpha^2\, \bar{m}_b^2(\mu)\, m_b^3\, |C_{7,eff}(\mu)|^2\, G_F^2\, |V_{tb}V_{ts}^*|^2\, Q_d^2}{1024\, \pi^5} \times \frac{\alpha_s}{4\pi}\, C_F\, \left[\frac{-4\, r_0\, (1-s_1-s_2)}{(1-s_1)^2\, s_1\, (1-s_2)^2\, s_2}\, \log\frac{\mu}{m_b} + f \right], \tag{13}$$

where f is decomposed as

$$f = \frac{(1-s_1-s_2)\,(f_1+f_2+f_3+f_4+f_5+f_6+f_7+f_8+f_9+f_{15}+f_{16}+f_{17})}{3\,(1-s_1)^3\, s_1\, (1-s_2)^3\, s_2} + \frac{f_{10}+f_{11}+f_{12}+f_{13}+f_{14}}{3\,(1-s_1)^3\, s_1\, (1-s_2)^3\, s_2} \tag{14}$$

The individual quantities $f_1, \ldots, f_{17}$ read

$$
\begin{aligned}
f_1 \;=\;& -16\pi^2 s_2^3 s_1^5 - 16\pi^2 s_2^5 s_1^3 + 48\pi^2 s_2^2 s_1^5 + 48\pi^2 s_2^5 s_1^2 - 48\pi^2 s_2 s_1^5 - 48\pi^2 s_2^5 s_1 + \\
& 16\pi^2 s_1^5 + 16\pi^2 s_2^5 - 168 s_1^3 - 168 s_2^3 + \left(1104 + 160\pi^2\right) s_2^4 s_1^4 + \\
& \left(-3360 - 400\pi^2\right) s_2^3 s_1^4 + \left(3432 + 304\pi^2\right) s_2^2 s_1^4 + \left(-1296 - 64\pi^2\right) s_2 s_1^4 + \\
& \left(120 - 16\pi^2\right) s_1^4 + \left(-3360 - 400\pi^2\right) s_2^4 s_1^3 + \left(10416 + 1152\pi^2\right) s_2^3 s_1^3 + \\
& \left(-10872 - 1056\pi^2\right) s_2^2 s_1^3 + \left(3984 + 368\pi^2\right) s_2 s_1^3 + \left(3432 + 304\pi^2\right) s_2^4 s_1^2 + \\
& \left(-10872 - 1056\pi^2\right) s_2^3 s_1^2 + \left(12096 + 1088\pi^2\right) s_2^2 s_1^2 + \\
& \left(-4872 - 448\pi^2\right) s_2 s_1^2 + \left(216 + 16\pi^2\right) s_1^2 + \left(-1296 - 64\pi^2\right) s_2^4 s_1 + \\
& \left(3984 + 368\pi^2\right) s_2^3 s_1 + \left(-4872 - 448\pi^2\right) s_2^2 s_1 + \left(2352 + 224\pi^2\right) s_2 s_1 + \\
& \left(-168 - 16\pi^2\right) s_1 + \left(120 - 16\pi^2\right) s_2^4 + \left(216 + 16\pi^2\right) s_2^2 + \left(-168 - 16\pi^2\right) s_2
\end{aligned}
$$

$$
\begin{aligned}
f_2 \;=\;& 48 s_2 \left(1 - s_1\right) \left(1 - s_2\right)^2 \left(6 s_2 s_1^3 - 6 s_1^3 - 11 s_2 s_1^2 + 15 s_1^2 + 3 s_2 s_1 - 9 s_1 + 2\right) \times \\
& \log\left(1 - s_1\right)
\end{aligned}
$$

$$
\begin{aligned}
f_3 \;=\;& 24 \left(1 - s_1\right) \left(1 - s_2\right) \left(30 s_2^3 s_1^3 - 64 s_2^2 s_1^3 + 41 s_2 s_1^3 - 7 s_1^3 - 60 s_2^3 s_1^2 + 128 s_2^2 s_1^2 - \right. \\
& \left. 82 s_2 s_1^2 + 37 s_2^3 s_1 - 78 s_2^2 s_1 + 76 s_2 s_1 - 7 s_1 - 7 s_2^3 - 7 s_2\right) \log\left(s_1\right)
\end{aligned}
$$

$$
\begin{aligned}
f_4 \;=\;& -48 \left(1 - s_1\right) \left(1 - s_2\right) \left(s_2^2 s_1^4 - s_2 s_1^4 - 5 s_2^3 s_1^3 + 9 s_2^2 s_1^3 - 5 s_2 s_1^3 + s_1^3 + 9 s_2^3 s_1^2 - \right. \\
& \left. 20 s_2^2 s_1^2 + 13 s_2 s_1^2 - 5 s_2^3 s_1 + 12 s_2^2 s_1 - 12 s_2 s_1 + s_1 + s_2^3 + s_2\right) \log^2\left(s_1\right)
\end{aligned}
$$

$$
\begin{aligned}
f_7 \;=\;& 96 \left(1 - s_1\right) \left(1 - s_2\right) \left(6 s_2^3 s_1^3 - 12 s_2^2 s_1^3 + 7 s_2 s_1^3 - s_1^3 - 12 s_2^3 s_1^2 + 24 s_2^2 s_1^2 - \right. \\
& \left. 14 s_2 s_1^2 + 7 s_2^3 s_1 - 14 s_2^2 s_1 + 12 s_2 s_1 - s_1 - s_2^3 - s_2\right) \log\left(s_1\right) \log\left(s_2\right)
\end{aligned}
$$

$$
\begin{aligned}
f_9 \;=\;& -96 \left(1 - s_1\right) \left(1 - s_2\right) \left(6 s_2^3 s_1^3 - 12 s_2^2 s_1^3 + 7 s_2 s_1^3 - s_1^3 - 12 s_2^3 s_1^2 + 24 s_2^2 s_1^2 - \right. \\
& \left. 14 s_2 s_1^2 + 7 s_2^3 s_1 - 14 s_2^2 s_1 + 12 s_2 s_1 - s_1 - s_2^3 - s_2\right) \log\left(s_1 + s_2\right)
\end{aligned}
$$

$$
\begin{aligned}
f_{10} \;=\;& 96 \left(1 - s_1\right) \left(1 - s_2\right)^2 \left(s_2 s_1^5 - s_1^5 + 2 s_2^2 s_1^4 - 5 s_2 s_1^4 + 3 s_1^4 + s_2^3 s_1^3 - 5 s_2^2 s_1^3 + \right. \\
& 8 s_2 s_1^3 - 2 s_1^3 - s_2^3 s_1^2 + 4 s_2^2 s_1^2 - 4 s_2 s_1^2 + s_1^2 - 4 s_2^2 s_1 + 3 s_2 s_1 - s_1 - \\
& \left. s_2^2 + s_2\right) \log\left(1 - s_1\right) \log\left(s_1 + s_2\right)
\end{aligned}
$$

$$
\begin{aligned}
f_{11} \;=\;& -96 \left(1 - s_1\right) \left(1 - s_2\right) \left(s_2^2 s_1^5 - s_2 s_1^5 - 10 s_2^3 s_1^4 + 19 s_2^2 s_1^4 - 11 s_2 s_1^4 + 2 s_1^4 - \right. \\
& 11 s_2^4 s_1^3 + 53 s_2^3 s_1^3 - 77 s_2^2 s_1^3 + 41 s_2 s_1^3 - 2 s_1^3 + 21 s_2^4 s_1^2 - 76 s_2^3 s_1^2 + 94 s_2^2 s_1^2 - \\
& 49 s_2 s_1^2 + 2 s_1^2 - 11 s_2^4 s_1 + 38 s_2^3 s_1 - 46 s_2^2 s_1 + 25 s_2 s_1 - 2 s_1 + s_2^4 - s_2^3 + \\
& \left. s_2^2 - s_2\right) \log\left(s_1\right) \log\left(s_1 + s_2\right)
\end{aligned}
$$

$$
\begin{aligned}
f_{14} \;=\;& 48 \left(1 - s_1\right) \left(1 - s_2\right) \left(s_2^2 s_1^5 - s_2 s_1^5 - 21 s_2^3 s_1^4 + 40 s_2^2 s_1^4 - 22 s_2 s_1^4 + 3 s_1^4 - \right. \\
& 21 s_2^4 s_1^3 + 106 s_2^3 s_1^3 - 153 s_2^2 s_1^3 + 79 s_2 s_1^3 - 3 s_1^3 + s_2^5 s_1^2 + 40 s_2^4 s_1^2 - 153 s_2^3 s_1^2 + \\
& 188 s_2^2 s_1^2 - 95 s_2 s_1^2 + 3 s_1^2 - s_2^5 s_1 - 22 s_2^4 s_1 + 79 s_2^3 s_1 - 95 s_2^2 s_1 + 50 s_2 s_1 - \\
& \left. 3 s_1 + 3 s_2^4 - 3 s_2^3 + 3 s_2^2 - 3 s_2\right) \log^2\left(s_1 + s_2\right)
\end{aligned}
$$

$$f_{15} = 96 s_1 (1-s_2)^2 \left(s_2 s_1^4 - s_1^4 + s_2^2 s_1^3 - 4 s_2 s_1^3 + 3 s_1^3 - 5 s_2^2 s_1^2 + 8 s_2 s_1^2 - 2 s_1^2 + 7 s_2^2 s_1 - 11 s_2 s_1 + s_1 - 2 s_2^2 + 5 s_2 - 1\right) \mathrm{Li}_2(s_1)$$

$$f_{16} = 96 (1-s_1)(1-s_2) \left(s_2^2 s_1^4 - 2 s_2 s_1^4 + s_1^4 + 8 s_2^3 s_1^3 - 17 s_2^2 s_1^3 + 12 s_2 s_1^3 - 3 s_1^3 + s_2^4 s_1^2 - 17 s_2^3 s_1^2 + 32 s_2^2 s_1^2 - 20 s_2 s_1^2 - 2 s_2^4 s_1 + 12 s_2^3 s_1 - 20 s_2^2 s_1 + 20 s_2 s_1 - 2 s_1 + s_2^4 - 3 s_2^3 - 2 s_2\right) \mathrm{Li}_2(1 - s_1 - s_2)$$

$$f_5 = f_2(s_1 \leftrightarrow s_2) \qquad f_6 = f_3(s_1 \leftrightarrow s_2) \qquad f_8 = f_4(s_1 \leftrightarrow s_2)$$
$$f_{12} = f_{10}(s_1 \leftrightarrow s_2) \qquad f_{13} = f_{11}(s_1 \leftrightarrow s_2) \qquad f_{17} = f_{15}(s_1 \leftrightarrow s_2)$$

The order α_s correction $d\Gamma_{77}^{(1)}/(ds_1 ds_2)$ in Eq. (13) to the double differential decay width for $b \to X_s \gamma\gamma$ is the main result of our paper.

6 Some numerical illustrations

In the previous sections we calculated the virtual- and bremsstrahlung QCD corrections which were the missing ingredient in order to obtain the $(\mathcal{O}_7, \mathcal{O}_7)$ contribution to the double differential decay width for $\bar{B} \to X_s \gamma\gamma$ at NLL precision. The Wilson coefficient $C_{7,eff}(\mu)$ at the low scale ($\mu \sim m_b$) which is needed up to order α_s, i.e.,

$$C_{7,eff}(\mu) = C_{7,eff}^0(\mu) + \frac{\alpha_s(\mu)}{4\pi} C_{7,eff}^1(\mu) \tag{15}$$

is known for a long time (see ref. [8] and references therein). Numerical values for the input parameters and for this Wilson coefficient at various values for the scale μ, together with the numerical values of $\alpha_s(\mu)$, are given in Table 4 and Table 5, respectively. The NLL prediction reads

Parameter	Value
m_b	4.8 GeV
m_t	175 GeV
m_W	80.4 GeV
m_Z	91.19 GeV
G_F	1.16637×10^{-5} GeV^{-2}
$V_{tb}V_{ts}^*$	0.04
α^{-1}	137
$\alpha_s(M_Z)$	0.119

Table 4: Values of the relevant input parameters

$$\frac{d\Gamma_{77}}{ds_1 ds_2} = \frac{d\Gamma_{77}^{(0)}}{ds_1 ds_2} + \frac{d\Gamma_{77}^{(1)}}{ds_1 ds_2} \tag{16}$$

where the first- and second term of the r.h.s. are given in eqs. (7) and (13), respectively.

	$\alpha_s(\mu)$	$C^0_{7,eff}(\mu)$	$C^1_{7,eff}(\mu)$
$\mu = m_W$	0.1213	-0.1957	-2.3835
$\mu = 2\,m_b$	0.1818	-0.2796	-0.1788
$\mu = m_b$	0.2175	-0.3142	0.4728
$\mu = m_b/2$	0.2714	-0.3556	1.0794

Table 5: $\alpha_s(\mu)$ and the Wilson coefficient $C_{7,eff}(\mu)$ at different values of the scale μ

To illustrate our results, we first rewrite the $\overline{\mathrm{MS}}$ mass $\bar{m}_b(\mu)$ in eq. (16) in terms of the pole mass m_b, using the one-loop relation

$$\bar{m}_b(\mu) = m_b \left[1 - \frac{\alpha_s(\mu)}{4\pi}\left(8\log\frac{\mu}{m_b} + \frac{16}{3}\right)\right] .$$

We then insert $C_{7,eff}(\mu)$ in the expanded form (15) and expand the resulting expression for $d\Gamma_{77}/(ds_1 ds_2)$ w.r.t. α_s, discarding terms of order α_s^2. This defines the NLL result. The corresponding LL result is obtained by also discarding the order α_s^1 term. In Fig. 6 the LL- and the NLL- result is shown by the short-dashed- and the solid line, respectively.

In our procedure the NLL corrections have three sources: (a) α_s corrections to the Wilson coefficient $C_{7,eff}(\mu)$, (b) expressing $\bar{m}_b(\mu)$ in terms of the pole mass m_b and (c) virtual- and real- order α_s corrections to the matrix elements. To illustrate the effect of source (c), which is worked out for the first time in this paper, we show in Fig. 6 (by the long-dashed line) the (partial) NLL result in which source (c) is switched off. We conclude that the effect (c) is roughly of equal importance as the combined effects of (a) and (b).

For completeness we show in this figure (by the dash-dotted line) also the result when QCD is completely switched off, which amounts to put $\mu = m_W$ in the LL result.

From Fig. 6 we see that the NLL results are substantially smaller (typically by 50% or slightly more) than those at LL precision, which is also the case when choosing other values for s_2.

In the numerical discussion above, we have systematically converted the running b-quark mass $\bar{m}_b(\mu)$ in terms of the pole mass m_b. As perturbative expansions often behave better when expressed in terms of the running mass, we also studied the results obtained when systematically converting m_b in terms of $\bar{m}_b(\mu)$. After doing also this version, we observe the following: Generally speaking, NLL corrections are not small for both cases, when taking into account the full range of μ, i.e., $m_b/2 < \mu < 2\,m_b$. More precisely, in the $\overline{\mathrm{MS}}$ version they are large for $\mu = m_b/2$ and smaller for larger values of μ, while in the pole mass version they are large for all values of μ.

We stress that the numerically important contributions involving the operator O_2 are not discussed in our paper. Therefore, the issue concerning the reduction of the μ dependence at NLL precision cannot be addressed at this level. Our main point in this section was to illustrate that the NLL corrections to the process $\bar{B} \to X_s\gamma\gamma$ are expected to be rather large.

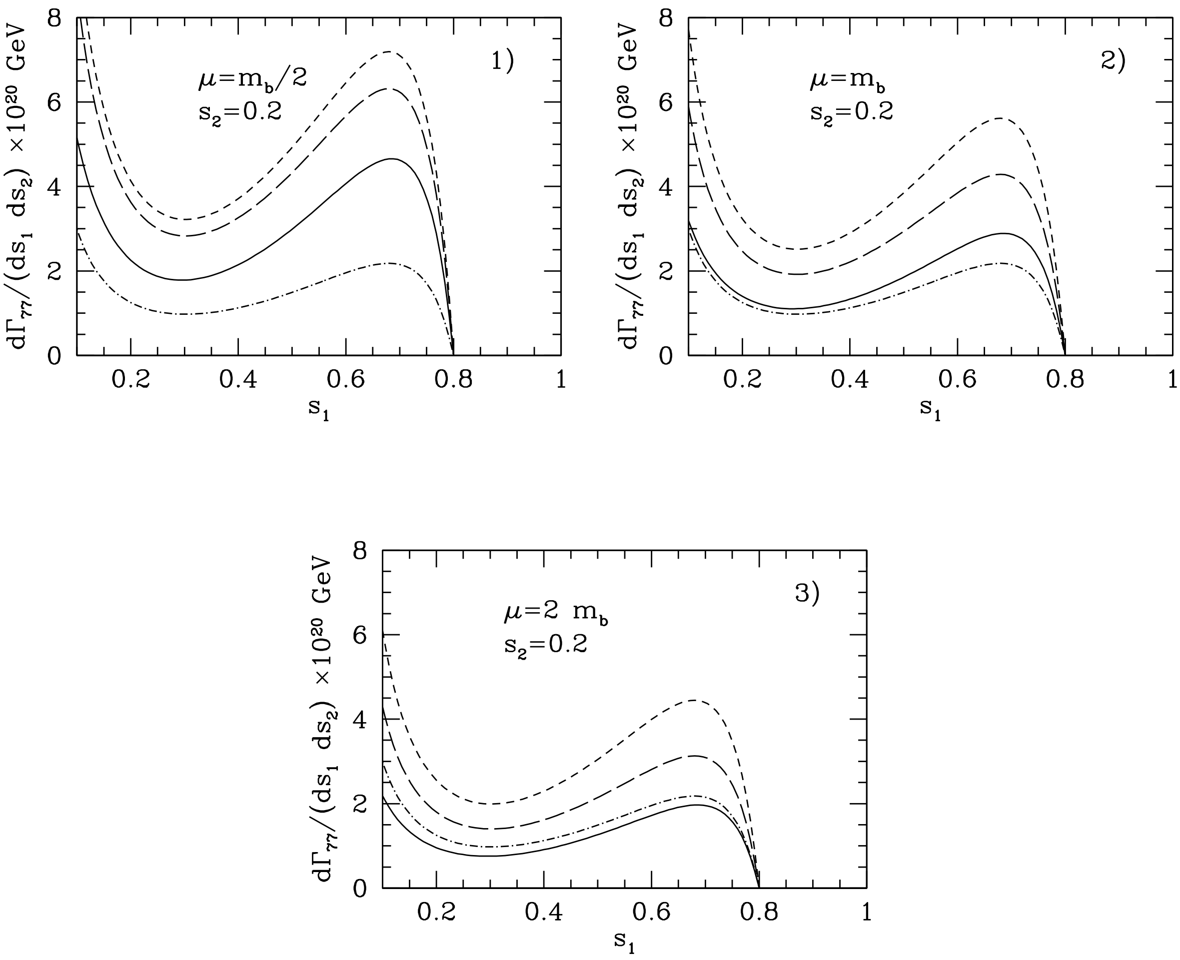

Figure 6: Double differential decay width $d\Gamma_{77}/(ds_1 ds_2)$ as a function of s_1 for s_2 fixed at $s_2 = 0.2$. The dash-dotted, the short-dashed and the solid line shows the result when neglecting QCD-effects, the LL result and the NLL result, respectively. The long-dashed line represents the (partial) NLL result in which the virtual- and bremsstrahlung corrections worked out in this paper are switched off (see text for more details). In the frames 1), 2) and 3) the renormalization scale is chosen to be $\mu = m_b/2$, $\mu = m_b$ and $\mu = 2\,m_b$, respectively.

7 Technical details about our calculations

We first describe the general setup of our calculations and then discuss in the subsections 7.1 and 7.2 the calculation of the virtual- and the bremsstrahlung corrections for the interference diagrams shown in the last lines of Fig. 3 and Fig. 5, respectively.

The starting point is the general expression for the total decay width of the massive b quark with momentum p_b decaying into $3 \leq n \leq 4$ massless final-state particles with momenta k_i,

$$\Gamma_{1\to n} = \frac{1}{2m_b} \left(\prod_{i=1}^{n} \int \frac{d^{d-1}k_i}{(2\pi)^{d-1} 2E_i} \right) (2\pi)^d \, \delta^{(d)} \left(p_b - \sum_{i=1}^{n} k_i \right) \, |M_n|^2$$

$$= \frac{1}{2m_b}(2\pi)^n \left(\prod_{i=1}^{n-1} \int \frac{d^d k_i}{(2\pi)^d} \, \delta(k_i^2) \, \theta(k_i^0) \right)$$
$$\times \, \delta\left(\left(p_b - \sum_{i=1}^{n-1} k_i \right)^2 \right) \theta\left(p_b^0 - \sum_{i=1}^{n-1} k_i^0 \right) |M_n|^2 \,, \tag{17}$$

where the squared Feynman amplitude $|M_n|^2$ is always understood to be summed over final spin-, polarization- and color states, and averaged over the spin directions and colors of the decaying b quark. It also includes a factor of 1/2 for the two identical particles in the final state, i.e. the photons. Furthermore, $d = 4 - 2\epsilon$ denotes the space-time dimension that we use to regulate the ultraviolet, infrared and collinear singularities.

The double differential decay rate $d\Gamma_{77}/(ds_1 ds_2)$ is obtained from eq. (17) by multiplying the integrand on the r.h.s. with the delta functions $\delta\left(s_1 - (p_b - q_1)^2/m_b^2\right)$ and $\delta\left(s_2 - (p_b - q_2)^2/m_b^2\right)$ [32], where p_b and q_1, q_2 denote the four momenta of the b quark and the photons, respectively. For the bremsstrahlung corrections, as mentioned in section 4, we need to consider also the triple differential decay width $d\Gamma_{77}/(ds_1 ds_2 ds_3)$, where $s_3 = (p_b - q_1 - q_2)^2/m_b^2$ is the normalized hadronic mass squared. The triple differential decay width is obtained by multiplying the integrand with the additional delta-function $\delta\left(s_3 - (p_b - q_1 - q_2)^2/m_b^2\right)$. Finally, the delta functions just mentioned and all of the delta functions present in eq. (17) can be rewritten as differences of propagators as follows [33, 34],

$$\delta\left(q^2 - m^2\right) = \frac{1}{2\pi i}\left(\frac{1}{q^2 - m^2 - i0} - \frac{1}{q^2 - m^2 + i0} \right) . \tag{18}$$

In this step the phase-space integrations are converted into loop integrations (which can be combined with possible loop integrations already present in $|M_n|^2$). By subsequently doing tensor reductions, the (differential) decay width can be written as a linear combination of scalar integrals. The systematic Laporta algorithm [35], based on integration-by-part techniques first proposed in [36, 37], can then be applied to reduce the scalar integrals to a small number of simpler integrals, usually referred to as the master integrals (MIs). For this reduction we used the AIR and FIRE implementations [38, 39] of the Laporta algorithm. After the reduction process, it usually happens that some MIs contain propagators which were introduced via (18) with zero or negative power. In this case the $\pm i0$ prescription becomes irrelevant and as a consequence these MIs are zero. In the remaining MIs we convert the propagators introduced via (18) back to delta-functions. Thus, we are left with phase-space MIs (which can contain loop integrations as well). The final task is then to calculate these MIs, i.e. to perform possible loop integrations together with the phase-space integrations.

Very often we had to deal with MIs which we were not able to evaluate by direct integration of their integral representation in terms of Feynman parameters and/or phase-space parameters. A powerful tool to be used in these cases is the differential equation method [33, 34, 40, 41]. The goal of this method is to employ the output of the reduction procedure for a given topology to build differential equations which are satisfied by the MIs of that topology. In our case, we consider differential equations w.r.t. s_1 and s_2 and also w.r.t. s_3 for case of bremsstrahlung corrections. With these methods we were able to obtain analytic expressions for all master integrals appearing in the calculation of the various diagrams.

7.1 Details about the calculation of virtual corrections

To illustrate our methods for the virtual corrections, we take as an example the interference diagram shown on the last line of Figure 3. In this case we have five MIs. Four of them can be solved by means of direct integration on Feynman parameters. To calculate the last one (called P_{1111}), we solve the differential equations w.r.t. s_1 and s_2 and get the solution which we denote as Q_{1111}. At this level Q_{1111} contains integration constants (which are not fixed by the differential equations). To get the integration constants, we proceed in the following way. Using Feynman parametrization for the loop integral, we write the MI P_{1111} as

$$P_{1111} = s_1^{-\epsilon} s_2^{-\epsilon} (1 - s_1 - s_2)^{-\epsilon} \int_0^1 g_0(s_1, s_2, \epsilon, u, v, y)\, du\, dv\, dy\,, \tag{19}$$

where u, v and y are Feynman parameters (all of them running from 0 to 1). The factor $s_1^{-\epsilon} s_2^{-\epsilon}(1 - s_1 - s_2)^{-\epsilon}$ is coming from the phase-space (see eq. (23) in Appendix B.1). One then can put $s_2 = 0$ in $g_0(s_1, s_2, \epsilon, u, v, y)$ and integrate on the Feynman parameters, which defines the new function

$$g_1(s_1, \epsilon) = \int_0^1 g_0(s_1, 0, \epsilon, u, v, y)\, du\, dv\, dy\,. \tag{20}$$

We managed to work out the leading term of the expansion of $g_1(s_1, \epsilon)$ on s_1 around zero, which is proportional to s_1^{-2}. From this, we immediately get the leading term of the expansion of P_{1111} on s_2 and s_1 (which is proportional to s_2^0/s_1^2). Comparing the result of this calculation with the corresponding expansion of the solution Q_{1111} of the differential equations, we could determine all integration constants.

7.2 Details about the calculation of bremsstrahlung corrections

To illustrate our methods for the bremsstrahlung corrections, we take as an example the interference diagram shown on the last line of Figure 5. In this case we obtain three MIs, denoted by P_{00}, P_{10} and P_{11}. Writing the diagram as a linear combination of the MIs, we see that the leading power (w.r.t. s_3) of all three coefficients (in front of the MIs) is of the order $1/s_3$. Keeping in mind that we are taking into account only terms proportional to the leading power in s_3 at the level of the triple differential decay width (as extensively discussed in section 4), it is sufficient to work out the MIs to zero-th power in s_3, including the epsilontic regulator, i.e., $s_3^{0-n\epsilon}$ (in our case only $n = 1$ and $n = 2$ occur).

The simplest MI, P_{00}, which corresponds to the pure phase-space (see eq. (25) in Appendix B.2), can be easily solved by means of direct integration. For P_{10} the solution of the differential equation w.r.t. s_3 can be represented in the limit $s_3 \to 0$ in the form

$$P_{10} = a_1(s_1, s_2, \epsilon)\, s_3^{-\epsilon} + a_2(s_1, s_2, \epsilon)\, s_3^{-2\epsilon}\,, \tag{21}$$

where the function $a_1(s_1, s_2, \epsilon)$ is fully determined. To find the function $a_2(s_1, s_2, \epsilon)$, we use differential equations w.r.t. s_1 and s_2. In this way, we could find $a_2(s_1, s_2, \epsilon)$ up to integration constants. To determine these constants, we managed to calculate the MI for specific values of s_1, s_2 and $s_3 \to 0$. In the same way we also calculated the MI P_{11}.

8 Summary

In the present work we calculated the set of the $O(\alpha_s)$ corrections to the decay process $\bar{B} \to X_s\gamma\gamma$ originating from diagrams involving the electromagnetic dipole operator $\mathcal{O}_7$. To perform this calculation it is necessary to work out diagrams with three particles (s-quark and two photons) and four particles (s-quark, two photons and a gluon) in the final state. From the technical point of view, the calculation was made possible by the use of the Laporta Algorithm to identify the needed Master Integrals and by applying the differential equation method to solve the Master Integrals. When calculating the bremsstrahlung corrections, we take into account only terms proportional to the leading power of the hadronic mass. We find that the infrared and collinear singularities cancel when combining the above mentioned approximated version of bremsstrahlung corrections with the virtual corrections. The numerical impact of the NLL corrections is not small: for $d\Gamma_{77}/(ds_1\, ds_2)$ the NLL results are approximately 50% smaller than those at LL precision.

Acknowledgments

C.G. and A.K. were partially supported by the Swiss National Foundation and by the Helmholz Association through funds provided to the virtual institute "Spin and strong QCD" (VH-VI-231). The Albert Einstein Center for Fundamental Physics (Bern), to which C.G. and A.K. are affiliated, is supported by the "Innovations- und Kooperationsprojekt C-13 of the Schweizerische Universitätskonferenz SUK/CRUS".
H.A. and A.Y. were supported by the Armenian State Committee of Science under contract 11-1c014.
Finally, we thank A.V. Smirnov for helpful email exchanges concerning his program FIRE [39].

A Explicit results for the functions v_i defining the virtual corrections

The functions v_i appearing in eq. (12) read

$$\begin{aligned}
v_1 \;=\;& (1-s_1-s_2)\big(-16\pi^2 s_2^3 s_1^5-16\pi^2 s_2^5 s_1^3+48\pi^2 s_2^2 s_1^5+48\pi^2 s_2^5 s_1^2-48\pi^2 s_2 s_1^5-\\
&48\pi^2 s_2^5 s_1+16\pi^2 s_1^5+16\pi^2 s_2^5+\big(2112-104\pi^2\big)s_2^4 s_1^4+\big(392\pi^2-6384\big)s_2^3 s_1^4+\\
&\big(6672-532\pi^2\big)s_2^2 s_1^4+\big(288\pi^2-2736\big)s_2 s_1^4+\big(336-60\pi^2\big)s_1^4+\\
&\big(392\pi^2-6384\big)s_2^4 s_1^3+\big(19584-1224\pi^2\big)s_2^3 s_1^3+\big(1452\pi^2-20784\big)s_2^2 s_1^3+\\
&\big(7872-600\pi^2\big)s_2 s_1^3+\big(44\pi^2-288\big)s_1^3+\big(6672-532\pi^2\big)s_2^4 s_1^2+\\
&\big(1452\pi^2-20784\big)s_2^3 s_1^2+\big(23904-1728\pi^2\big)s_2^2 s_1^2+\big(740\pi^2-10128\big)s_2 s_1^2+\\
&\big(336-28\pi^2\big)s_1^2+\big(288\pi^2-2736\big)s_2^4 s_1+\big(7872-600\pi^2\big)s_2^3 s_1+\\
&\big(740\pi^2-10128\big)s_2^2 s_1+\big(5376-392\pi^2\big)s_2 s_1+\big(28\pi^2-384\big)s_1+\\
&\big(336-60\pi^2\big)s_2^4+\big(44\pi^2-288\big)s_2^3+\big(336-28\pi^2\big)s_2^2+\big(28\pi^2-384\big)s_2\big)
\end{aligned}$$

$$\begin{aligned}
v_2 \;=\;& -96\,(1-s_1)\,(1-s_2)\,(1-s_1-s_2)\big(3s_2^3 s_1^3-4s_2^2 s_1^3+s_2 s_1^3-5s_2^3 s_1^2+7s_2^2 s_1^2-\\
&2s_2 s_1^2-s_1^2+2s_2^3 s_1-3s_2^2 s_1+3s_2 s_1-s_2^2\big)\log(s_1)
\end{aligned}$$

$$\begin{aligned}
v_3 \;=\;& -24\,(1-s_1)\,(1-s_2)\,(1-s_1-s_2)\big(2s_2^2 s_1^4-2s_2 s_1^4-4s_2^3 s_1^3+6s_2^2 s_1^3-\\
&3s_2 s_1^3+s_1^3+6s_2^3 s_1^2-16s_2^2 s_1^2+12s_2 s_1^2-3s_2^3 s_1+10s_2^2 s_1-12s_2 s_1+\\
&s_1+s_2^3+s_2\big)\log^2(s_1)
\end{aligned}$$

$$\begin{aligned}
v_4 \;=\;& 48\,(1-s_1)\,(1-s_2)\,(1-s_1-s_2)\big(6s_2^3 s_1^3-12s_2^2 s_1^3+7s_2 s_1^3-s_1^3-12s_2^3 s_1^2+\\
&24s_2^2 s_1^2-14s_2 s_1^2+7s_2^3 s_1-14s_2^2 s_1+12s_2 s_1-s_1-s_2^3-s_2\big)\log(s_1)\log(s_2)
\end{aligned}$$

$$\begin{aligned}
v_5 \;=\;& 48\,(1-s_1)\,(1-s_2)\,(1-s_1-s_2)\big(6s_2^3 s_1^3-12s_2^2 s_1^3+7s_2 s_1^3-s_1^3-12s_2^3 s_1^2+\\
&24s_2^2 s_1^2-14s_2 s_1^2+7s_2^3 s_1-14s_2^2 s_1+12s_2 s_1-s_1-s_2^3-s_2\big)\log(s_1)\times\\
&\log(1-s_1-s_2)
\end{aligned}$$

$$\begin{aligned}
v_6 \;=\;& -96\,(1-s_1)^2\,(1-s_2)^2 s_2\big(s_1^4+2s_2 s_1^3-2s_1^3+s_2^2 s_1^2-4s_2 s_1^2+s_1^2-2s_2^2 s_1+\\
&3s_2 s_1-2s_1+s_2^2+1\big)\log(s_1)\log(s_1+s_2)
\end{aligned}$$

$$\begin{aligned}
v_7 \;=\;& 48\,(1-s_1)\,(s_2-1)^2 s_2\,(1-s_1-s_2)\big(6s_2 s_1^3-6s_1^3-11s_2 s_1^2+15s_1^2+\\
&3s_2 s_1-9s_1+2)\log(1-s_1)
\end{aligned}$$

$$\begin{aligned}
v_8 \;=\;& 96\,(1-s_1)\,(s_2-1)^2\big(s_2 s_1^5-s_1^5+2s_2^2 s_1^4-5s_2 s_1^4+3s_1^4+s_2^3 s_1^3-5s_2^2 s_1^3+\\
&8s_2 s_1^3-2s_1^3-s_2^3 s_1^2+4s_2^2 s_1^2-4s_2 s_1^2+s_1^2-4s_2^2 s_1+3s_2 s_1-s_1-s_2^2+s_2\big)\times\\
&\log(1-s_1)\log(s_1+s_2)
\end{aligned}$$

$$\begin{aligned} v_9 \;=\;& 48\,(1-s_1)\,(1-s_2)\,\big(s_2^2 s_1^5 - s_2 s_1^5 - 9 s_2^3 s_1^4 + 16 s_2^2 s_1^4 - 8 s_2 s_1^4 + s_1^4 - 9 s_2^4 s_1^3 + \\ & 46 s_2^3 s_1^3 - 67 s_2^2 s_1^3 + 35 s_2 s_1^3 - s_1^3 + s_2^5 s_1^2 + 16 s_2^4 s_1^2 - 67 s_2^3 s_1^2 + 84 s_2^2 s_1^2 - \\ & 43 s_2 s_1^2 + s_1^2 - s_2^5 s_1 - 8 s_2^4 s_1 + 35 s_2^3 s_1 - 43 s_2^2 s_1 + 22 s_2 s_1 - s_1 + s_2^4 - s_2^3 + \\ & s_2^2 - s_2\big) \log^2(s_1+s_2) \end{aligned}$$

$$\begin{aligned} v_{10} \;=\;& -96\,(1-s_1)\,(1-s_2)\,(1-s_1-s_2)\,\big(s_2^2 s_1^3 - s_2 s_1^3 + s_2^3 s_1^2 - 3 s_2^2 s_1^2 + 2 s_2 s_1^2 - \\ & s_1^2 - s_2^3 s_1 + 2 s_2^2 s_1 + s_2 s_1 - s_2^2\big) \log(1-s_1-s_2) \end{aligned}$$

$$\begin{aligned} v_{11} \;=\;& 24\,(1-s_1)\,(1-s_2)\,(1-s_1-s_2)\,\big(6 s_2^3 s_1^3 - 12 s_2^2 s_1^3 + 7 s_2 s_1^3 - s_1^3 - 12 s_2^3 s_1^2 + \\ & 24 s_2^2 s_1^2 - 14 s_2 s_1^2 + 7 s_2^3 s_1 - 14 s_2^2 s_1 + 12 s_2 s_1 - s_1 - s_2^3 - s_2\big) \times \\ & \log^2(1-s_1-s_2) \end{aligned}$$

$$\begin{aligned} v_{12} \;=\;& 96 s_1\,(1-s_2)^2\,(1-s_1-s_2)\,\big(s_2 s_1^4 - s_1^4 + s_2^2 s_1^3 - 4 s_2 s_1^3 + 3 s_1^3 - 5 s_2^2 s_1^2 + \\ & 8 s_2 s_1^2 - 2 s_1^2 + 7 s_2^2 s_1 - 11 s_2 s_1 + s_1 - 2 s_2^2 + 5 s_2 - 1\big) \mathrm{Li}_2(s_1) \end{aligned}$$

$$\begin{aligned} v_{13} \;=\;& 96\,(1-s_1)\,(1-s_2)\,(1-s_1-s_2)\,\big(s_2^2 s_1^4 - 2 s_2 s_1^4 + s_1^4 + 8 s_2^3 s_1^3 - 17 s_2^2 s_1^3 + \\ & 12 s_2 s_1^3 - 3 s_1^3 + s_2^4 s_1^2 - 17 s_2^3 s_1^2 + 32 s_2^2 s_1^2 - 20 s_2 s_1^2 - 2 s_2^4 s_1 + 12 s_2^3 s_1 - \\ & 20 s_2^2 s_1 + 20 s_2 s_1 - 2 s_1 + s_2^4 - 3 s_2^3 - 2 s_2\big) \mathrm{Li}_2(1-s_1-s_2) \end{aligned}$$

$$\begin{array}{llll} v_{14} = v_2(s_1 \leftrightarrow s_2) & v_{15} = v_3(s_1 \leftrightarrow s_2) & v_{16} = v_5(s_1 \leftrightarrow s_2) & \\ v_{17} = v_6(s_1 \leftrightarrow s_2) & v_{18} = v_7(s_1 \leftrightarrow s_2) & v_{19} = v_8(s_1 \leftrightarrow s_2) & v_{20} = v_{12}(s_1 \leftrightarrow s_2) \end{array}$$

B Relevant phase-space formulas

B.1 Double differential phase-space for the 3-particle final state

The kinematical variables s_1 and s_2 are defined as

$$s_1 = \frac{(p_b - q_1)^2}{m_b^2} \quad ; \quad s_2 = \frac{(p_b - q_2)^2}{m_b^2}\,, \tag{22}$$

where p_b and q_i denote the four-momenta of the b-quark and the photons, respectively. The kinematics of the process $b \to s\gamma\gamma$ is fully described by s_1 and s_2. The formula for double differential decay width is therefore free of additional phase-space integration variables. It reads

$$\frac{d\Gamma_{1\to 3}}{ds_1\, ds_2} = \frac{1}{4}\,\frac{(4\pi)^{-3+2\epsilon}}{\Gamma[2-2\epsilon]}\, m_b^{1-4\epsilon}\, s_1^{-\epsilon}\, s_2^{-\epsilon}\,(1-s_1-s_2)^{-\epsilon}\,|M_3|^2\,. \tag{23}$$

The variables s_1 and s_2 vary in the range

$$0 \le s_1 \le 1\,; \quad 0 \le s_2 \le 1 - s_1\,.$$

B.2 Triple differential phase-space for the 4-particle final state

The kinematical variables s_1, s_2 and s_3 are defined as

$$s_1 = \frac{(p_b - q_1)^2}{m_b^2} \quad ; \quad s_2 = \frac{(p_b - q_2)^2}{m_b^2} \quad ; \quad s_3 = \frac{(p_s + k)^2}{m_b^2} \tag{24}$$

where p_b, p_s, k and q_i denote the four-momenta of the b-quark, the s-quark, the gluon and the photons, respectively. The kinematics is fully described in terms of five phase-space variables x_1, x_2, x_3, x_4 and x_5 as given explicitly in eqs. (3.6), (3.9) and (3.10) in ref. [42]. By identifying k_1, k_2, k_3 and k_4 given there with the four-momenta of the two photons, the s-quark and the gluon, respectively, we easily derive from the information in [42] the formula for the triple differential decay width. We remind the reader that in this paper we consider only the range in s_1 and s_2 with

$$0 \le s_1 \le 1 \, ; \quad 0 \le s_2 \le 1 - s_1 \, ,$$

which is also accessible to the three-body decay $b \to s\gamma\gamma$. For this case we obtain

$$\begin{aligned} \frac{d\Gamma_{1\to 4}}{ds_1\, ds_2\, ds_3} = \quad & \frac{(4\pi)^{-6+3\epsilon}\, 2^{-4\epsilon}\, \Gamma[1-\epsilon]}{(1-2\epsilon)\, \Gamma^2[1-2\epsilon]}\, m_b^{3-6\epsilon}\, s_3^{-\epsilon}\, (s_1 s_2 - s_3)^{-\epsilon}\, (1 - s_1 - s_2 + s_3)^{-\epsilon} \times \\ & \int dx_4\, dx_5\, [x_4\,(1-x_4)]^{-\epsilon}\, [x_5\,(1-x_5)]^{-1/2-\epsilon}\, |M_4|^2 \, , \end{aligned} \tag{25}$$

where x_1, x_2 and x_3 (appearing in $|M_4|^2$) are understood to be expressed in terms of s_1, s_2 and s_3 according to

$$x_1 = s_1 \, ; \quad x_2 = \frac{s_3}{s_1} \, ; \quad x_3 = \frac{s_1 s_2 - s_3}{(1-s_1)\,(s_1 - s_3)} \, . \tag{26}$$

x_4 and x_5 vary between zero and one, while $s_3 \in [0, s_1\, s_2]$.

C Renormalization constants

In this appendix, we collect the explicit expressions of the renormalization constants needed for the ultraviolet renormalization in our calculation (see section 3).
The operator $\mathcal{O}_7$, as well as the b-quark mass contained in this operator are renormalized in the $\overline{\text{MS}}$ scheme [43]:

$$Z_{77}^{\overline{\text{MS}}} = 1 + \frac{4\, C_F}{\epsilon} \frac{\alpha_s(\mu)}{4\pi} + O(\alpha_s^2) \quad ; \quad Z_{m_b}^{\overline{\text{MS}}} = 1 - \frac{3\, C_F}{\epsilon} \frac{\alpha_s(\mu)}{4\pi} + O(\alpha_s^2) \, . \tag{27}$$

All the remaining fields and parameters are renormalized in the on-shell scheme. The on-shell renormalization constant for the b-quark mass is given by

$$Z_{m_b}^{\text{OS}} = 1 - C_F\, \Gamma(\epsilon)\, e^{\gamma\epsilon}\, \frac{3-2\epsilon}{1-2\epsilon} \left(\frac{\mu}{m_b}\right)^{2\epsilon} \frac{\alpha_s(\mu)}{4\pi} + O(\alpha_s^2) \, . \tag{28}$$

while the renormalization constants for the s- and b-quark fields are

$$\begin{aligned} Z_{2s}^{\text{OS}} &= 1 + O(\alpha_s^2) \, , \\ Z_{2b}^{\text{OS}} &= 1 - C_F\, \Gamma(\epsilon)\, e^{\gamma\epsilon}\, \frac{3-2\epsilon}{1-2\epsilon} \left(\frac{\mu}{m_b}\right)^{2\epsilon} \frac{\alpha_s(\mu)}{4\pi} + O(\alpha_s^2) \, . \end{aligned} \tag{29}$$

The various quantities δZ appearing in section 3 are defined to be $\delta Z = Z - 1$.

References

[1] M. Misiak *et al.*, Phys. Rev. Lett. **98** (2007) 022002, [hep-ph/0609232].

[2] T. Hurth, M. Nakao, Ann. Rev. Nucl. Part. Sci. **60** (2010) 645, [arXiv:1005.1224 [hep-ph]].

[3] A. J. Buras, arXiv:1102.5650 [hep-ph].

[4] H. Simma, D. Wyler, Nucl. Phys. **B344** (1990) 283.

[5] L. Reina, G. Ricciardi, A. Soni, Phys. Lett. **B396** (1997) 231, [hep-ph/9612387].

[6] L. Reina, G. Ricciardi, A. Soni, Phys. Rev. **D56** (1997) 5805, [hep-ph/9706253].

[7] J. J. Cao, Z.J. Xiao, G. R. Lu, Phys. Rev. **D64** (2001) 014012, [hep-ph/0103154].

[8] K. G. Chetyrkin, M. Misiak and M. Munz, Phys. Lett. B **400** (1997) 206 [Erratum-ibid. B **425** (1998) 414], [arXiv:hep-ph/9612313].

[9] K. Melnikov and A. Mitov, Phys. Lett. B **620** (2005) 69, [arXiv:hep-ph/0505097].

[10] H. M. Asatrian, T. Ewerth, A. Ferroglia, P. Gambino, C. Greub, Nucl. Phys. **B762** (2007) 212, [hep-ph/0607316].

[11] A. Kapustin, Z. Lint and H. D. Politzer, Phys. Lett. B **357** (1995) 653, [arXiv:hep-ph/9507248].

[12] A. Gemintern, S. Bar-Shalom, G. Eilam, Phys. Rev. **D70** (2004) 035008, [hep-ph/0404152].

[13] C. -H. V. Chang, G. -L. Lin, Y. -P. Yao, Phys. Lett. **B415** (1997) 395, [hep-ph/9705345].

[14] G. Hiller, E. O. Iltan, Phys. Lett. **B409** (1997) 425, [hep-ph/9704385].

[15] S. W. Bosch, G. Buchalla, JHEP **0208** (2002) 054, [hep-ph/0208202].

[16] S. W. Bosch, hep-ph/0208203.

[17] G. Hiller, A. S. Safir, JHEP **0502** (2005) 011, [hep-ph/0411344].

[18] G. Hiller, A. S. Safir, PoS **HEP2005** (2006) 277, [hep-ph/0511316].

[19] G. L. Lin, J. Liu and Y. P. Yao, Phys. Rev. Lett. **64** (1990) 1498.

[20] S. Herrlich and J. Kalinowski, Nucl. Phys. B **381** (1992) 501.

[21] S. R. Choudhury, G. C. Joshi, N. Mahajan, B. H. J. McKellar, Phys. Rev. **D67** (2003) 074016, [hep-ph/0210160].

[22] T. M. Aliev, G. Hiller, E. O. Iltan, Nucl. Phys. **B515** (1998) 321, [hep-ph/9708382].

[23] S. Bertolini, J. Matias, Phys. Rev. **D57** (1998) 4197, [hep-ph/9709330].

[24] I. I. Bigi, G. Chiladze, G. Devidze, C. Hanhart, A. Liparteliani, U. -G. Meissner, hep-ph/0603160.

[25] G. G. Devidze, G. R. Jibuti, hep-ph/9810345.

[26] T. M. Aliev, G. Turan, Phys. Rev. **D48** (1993) 1176.

[27] Z. J. Xiao, C. D. Lu, W. J. Huo, Phys. Rev. **D67** (2003) 094021, [hep-ph/0301221].

[28] Q. XiuMei, W. Huo, X. Yang, Chin. Phys. **C33** (2009) 252, [arXiv:1101.2437 [hep-ph]].

[29] W. J. Huo, C. D. Lu, Z. J. Xiao, hep-ph/0302177.

[30] H. Chen, W. Huo, arXiv:1101.4660 [hep-ph].

[31] A. Y. Ignatiev, G. C. Joshi, B. H. J. McKellar, Int. J. Mod. Phys. **A20** (2005) 4079, [hep-ph/0308126].

[32] C. Anastasiou, L. J. Dixon and K. Melnikov, Nucl. Phys. Proc. Suppl. **116** (2003) 193, [arXiv:hep-ph/0211141].

[33] C. Anastasiou and K. Melnikov, Nucl. Phys. B **646** (2002) 220, [arXiv:hep-ph/0207004].

[34] C. Anastasiou, L. J. Dixon, K. Melnikov and F. Petriello, Phys. Rev. D **69** (2004) 094008, [arXiv:hep-ph/0312266].

[35] S. Laporta, Int. J. Mod. Phys. A **15**, 5087 (2000), [arXiv:hep-ph/0102033].

[36] F. V. Tkachov, Phys. Lett. B **100**, 65 (1981).

[37] K. G. Chetyrkin and F. V. Tkachov, Nucl. Phys. B **192**, 159 (1981).

[38] C. Anastasiou and A. Lazopoulos, JHEP **0407**, (2004) 046, [arXiv:hep-ph/0404258].

[39] A. V. Smirnov, JHEP **0810** (2008) 107, [arXiv:0807.3243 [hep-ph]].

[40] E. Remiddi, Nuovo Cim. A **110**, (1997) 1435, [arXiv:hep-th/9711188].

[41] M. Argeri and P. Mastrolia, Int. J. Mod. Phys. A **22** (2007) 4375, [arXiv:0707.4037].

[42] H. M. Asatrian, A. Hovhannisyan, V. Poghosyan, T. Ewerth, C. Greub and T. Hurth, Nucl. Phys. B **749** (2006) 325, [arXiv:hep-ph/0605009].

[43] M. Misiak and M. Munz, Phys. Lett. B **344** (1995) 308, [arXiv:hep-ph/9409454].

Part III

The $\bar{B} \to X_s\gamma\gamma$ decay: NLL QCD contribution of the Electromagnetic Dipole operator $\mathcal{O}_7$

published in

Proceedings of the conference FPCP 2012
(arXiv:1207.2397 [hep-ph])

The $\bar{B} \to X_s\gamma\gamma$ decay:
NLL QCD contribution of the Electromagnetic Dipole operator $\mathcal{O}_7$

Ahmet Kokulu
Albert Einstein Center for Fundamental Physics,
Institute for Theoretical Physics,
University of Bern,
CH-3012 Bern, Switzerland

Abstract

We calculate the set of $O(\alpha_s)$ corrections to the double differential decay width $d\Gamma_{77}/(ds_1\, ds_2)$ for the process $\bar{B} \to X_s\gamma\gamma$ originating from diagrams involving the electromagnetic dipole operator $\mathcal{O}_7$. The kinematical variables s_1 and s_2 are defined as $s_i = (p_b - q_i)^2/m_b^2$, where p_b, q_1, q_2 are the momenta of b-quark and two photons. While the (renormalized) virtual corrections are worked out exactly for a certain range of s_1 and s_2, we retain in the gluon bremsstrahlung process only the leading power w.r.t. the (normalized) hadronic mass $s_3 = (p_b - q_1 - q_2)^2/m_b^2$ in the underlying triple differential decay width $d\Gamma_{77}/(ds_1 ds_2 ds_3)$. The double differential decay width, based on this approximation, is free of infrared- and collinear singularities when combining virtual- and bremsstrahlung corrections. The corresponding results are obtained analytically. When retaining all powers in s_3, the sum of virtual- and bremstrahlung corrections contains uncanceled $1/\epsilon$ singularities (which are due to collinear *photon* emission from the s-quark) and other concepts, which go beyond perturbation theory, like parton fragmentation functions of a quark or a gluon into a photon, are needed which is beyond the scope of our paper.

1 Introduction

Inclusive rare B-meson decays are known to be a unique source of indirect information about physics at scales of several hundred GeV. In the Standard Model (SM) all these processes proceed through loop diagrams and thus are relatively suppressed. In the extensions of the SM the contributions stemming from the diagrams with “new” particles in the loops can be comparable or even larger than the contribution from the SM. Thus getting experimental information on rare decays puts strong constraints on the extensions of the SM or can even lead to a disagreement with the SM predictions, providing evidence for some “new physics”.

To make a rigorous comparison between experiment and theory, precise SM calculations for the (differential) decay rates are mandatory. While the branching ratios for $\bar{B} \to X_s\gamma$ [1] and $\bar{B} \to X_s\ell^+\ell^-$ are known today even to next-to-next-to-leading logarithmic (NNLL) precision (for reviews, see [2, 3]), other branching ratios, like the one for $\bar{B} \to X_s\gamma\gamma$ discussed in these proceedings, has been calculated before to leading logarithmic (LL) precision in the SM by several groups [4, 5, 6, 7] and only recently a first step towards next-to-leading-logarithmic (NLL) precision was presented by us in [8]. In contrast to $\bar{B} \to X_s\gamma$, the current-current operator $\mathcal{O}_2$ has a non-vanishing matrix element for $b \to s\gamma\gamma$ at order α_s^0 precision, leading to an interesting interference pattern with the contributions associated with the electromagnetic dipole operator $\mathcal{O}_7$ already at LL precision. As a consequence, potential new physics should be clearly visible not only in the total branching ratio, but also in the differential distributions.

As the process $\bar{B} \to X_s\gamma\gamma$ is expected to be measured at the planned Super B-factories in Japan and Italy, it is necessary to calculate the differential distributions to NLL precision in the SM, in order to fully exploit its potential concerning new physics. The starting point of our calculation is the effective Hamiltonian, obtained by integrating out the heavy particles in the SM, leading to

$$\mathcal{H}_{eff} = -\frac{4G_F}{\sqrt{2}} V_{ts}^{\star} V_{tb} \sum_{i=1}^{8} C_i(\mu)\mathcal{O}_i(\mu) \,, \tag{1}$$

where we use the operator basis introduced in [9]:

$$\begin{array}{llll} \mathcal{O}_1 = (\bar{s}_L\gamma_\mu T^a c_L)\,(\bar{c}_L\gamma^\mu T_a b_L)\,, & \mathcal{O}_2 = (\bar{s}_L\gamma_\mu c_L)\,(\bar{c}_L\gamma^\mu b_L)\,, \\ \mathcal{O}_3 = (\bar{s}_L\gamma_\mu b_L)\sum_q(\bar{q}\gamma^\mu q)\,, & \mathcal{O}_4 = (\bar{s}_L\gamma_\mu T^a b_L)\sum_q(\bar{q}\gamma^\mu T_a q)\,, \\ \mathcal{O}_5 = (\bar{s}_L\gamma_\mu\gamma_\nu\gamma_\rho b_L)\sum_q(\bar{q}\gamma^\mu\gamma^\nu\gamma^\rho q)\,, & \mathcal{O}_6 = (\bar{s}_L\gamma_\mu\gamma_\nu\gamma_\rho T^a b_L)\sum_q(\bar{q}\gamma^\mu\gamma^\nu\gamma^\rho T_a q)\,, \\ \mathcal{O}_7 = \frac{e}{16\pi^2}\,\bar{m}_b(\mu)\,(\bar{s}_L\sigma^{\mu\nu}b_R)\,F_{\mu\nu}\,, & \mathcal{O}_8 = \frac{g_s}{16\pi^2}\,\bar{m}_b(\mu)\,(\bar{s}_L\sigma^{\mu\nu}T^a b_R)\,G^a_{\mu\nu}\,. \end{array} \tag{2}$$

The symbols T^a $(a = 1, 8)$ denote the $SU(3)$ color generators; g_s and e, the strong and electromagnetic coupling constants. In eq. (2), $\bar{m}_b(\mu)$ is the running b-quark mass in the $\overline{\text{MS}}$-scheme at the renormalization scale μ. As we are not interested in CP-violation effects in the present paper, we made use of the hierarchy $V_{ub}V_{us}^* \ll V_{tb}V_{ts}^*$ when writing eq. (1). Furthermore, we also put $m_s = 0$.

While the Wilson coefficients $C_i(\mu)$ appearing in eq. (1) are known to sufficient precision at the low scale $\mu \sim m_b$ since a long time (see e.g. the reviews [2, 3] and references therein), the matrix elements $\langle s\gamma\gamma|\mathcal{O}_i|b\rangle$ and $\langle s\gamma\gamma\, g|\mathcal{O}_i|b\rangle$, which in a NLL calculation are needed to order g_s^2 and g_s, respectively, are not known yet. To calculate the $(\mathcal{O}_i, \mathcal{O}_j)$-interference contributions to the differential distributions at order α_s is in many respects of similar complexity as the calculation of the photon energy spectrum in $\bar{B} \to X_s\gamma$ at order α_s^2 needed for the NNLL computation. As a first step in this NLL enterprise, we derived in our paper [8], the $O(\alpha_s)$ corrections to the $(\mathcal{O}_7, \mathcal{O}_7)$-interference contribution to the double differential decay width $d\Gamma/(ds_1 ds_2)$ at the partonic level. The variables s_1 and s_2 are defined as $s_i = (p_b - q_i)^2/m_b^2$, where p_b and q_i denote the four-momenta of the b-quark and the two photons, respectively.

At order α_s there are contributions to $d\Gamma_{77}/(ds_1 ds_2)$ with three particles (s-quark and two photons) and four particles (s-quark, two photons and a gluon) in the final state. These contributions correspond to specific cuts of the b-quarks self-energy at order $\alpha^2 \times \alpha_s$, involving twice the operator $\mathcal{O}_7$. As there are additional cuts, which contain for example only one photon, our observable cannot be obtained using the optical theorem, i.e., by taking the absorptive part of the b-quark self-energy at three-loop. We therefore calculate the mentioned contributions with three and four particles in the final state individually.

We work out the QCD corrections to the double differential decay width in the kinematical range

$$0 < s_1 < 1 \quad ; \quad 0 < s_2 < 1 - s_1 \,.$$

Concerning the virtual corrections, all singularities (after ultra-violet renormalization) are due to **soft gluon** exchanges and/or **collinear gluon** exchanges involving the s-quark. Concerning the bremsstrahlung corrections (restricted to the same range of s_1 and s_2), there are in addition kinematical situations where **collinear photons** are emitted from the s-quark. The corresponding singularities are not canceled when combined with the virtual corrections. We found, however, that there are no singularities associated with collinear photon emission in the double differential decay width when only retaining the leading power w.r.t to the (normalized) hadronic mass $s_3 = (p_b - q_1 - q_2)^2/m_b^2$ in the underlying triple differential distribution $d\Gamma_{77}/(ds_1 ds_2 ds_3)$. Our results of our paper are obtained within this "approximation". When going beyond, other concepts which go beyond perturbation theory, like parton fragmentation functions of a quark or a gluon into a photon, are needed [10].

2 Leading Order and Final results for the decay width

In $d = 4$ dimensions, the leading-order spectrum (in our restricted phase-space) is given by

$$\frac{d\Gamma_{77}^{(0)}}{ds_1\, ds_2} = \frac{\alpha^2\, \bar{m}_b^2(\mu)\, m_b^3\, |C_{7,eff}(\mu)|^2\, G_F^2\, |V_{tb}V_{ts}^*|^2\, Q_d^2}{1024\, \pi^5} \, \frac{(1-s_1-s_2)}{(1-s_1)^2 s_1 (1-s_2)^2 s_2}\, r_0\,. \qquad (3)$$

where

$$r_0 = -48s_2^3 s_1^3 + 96s_2^2 s_1^3 - 56s_2 s_1^3 + 8s_1^3 + 96s_2^3 s_1^2 - 192s_2^2 s_1^2 + 112s_2 s_1^2 - 56s_2^3 s_1 + 112s_2^2 s_1 - 96s_2 s_1 + 8s_1 + 8s_2^3 + 8s_2$$

The complete order α_s correction to the double differential decay width $d\Gamma_{77}/(ds_1\, ds_2)$ is obtained by adding the renormalized virtual corrections and the bremsstrahlung corrections. Explicitly we obtain

$$\begin{aligned} \frac{d\Gamma_{77}^{(1)}}{ds_1\, ds_2} &= \frac{\alpha^2\, \bar{m}_b^2(\mu)\, m_b^3\, |C_{7,eff}(\mu)|^2\, G_F^2\, |V_{tb}V_{ts}^*|^2\, Q_d^2}{1024\, \pi^5} \\ &\times \frac{\alpha_s}{4\pi}\, C_F \left[\frac{-4\, r_0\, (1-s_1-s_2)}{(1-s_1)^2\, s_1\, (1-s_2)^2\, s_2} \log\frac{\mu}{m_b} + f \right], \end{aligned} \qquad (4)$$

where f can be found explicitly in [8].

The order α_s correction $d\Gamma_{77}^{(1)}/(ds_1 ds_2)$ in Eq. (4) to the double differential decay width for $b \to X_s\gamma\gamma$ was the main result of our paper [8].

3 Some numerical illustrations

In our procedure the NLL corrections have three sources: (a) α_s corrections to the Wilson coefficient $C_{7,eff}(\mu)$, (b) expressing $\bar{m}_b(\mu)$ in terms of the pole mass m_b and (c) virtual- and real- order α_s corrections to the matrix elements. To illustrate the effect of source (c), which is worked out for the first time in our paper [8], we show in Fig. 1 (by the long-dashed line) the (partial) NLL result in which source (c) is switched off. We conclude that the effect (c) is roughly of equal importance as the combined effects of (a) and (b).

For completeness we show in this figure (by the dotted line) also the result when QCD is completely switched off, which amounts to put $\mu = m_W$ in the LL result.

From Fig. 1 we see that the NLL results are substantially smaller (typically by 50% or slightly more) than those at LL precision, which is also the case when choosing other values for s_2.

In the numerical discussion above, we have systematically converted the running b-quark mass $\bar{m}_b(\mu)$ in terms of the pole mass m_b. As perturbative expansions often behave better when expressed in terms of the running mass, we also studied the results obtained when systematically converting m_b in terms of $\bar{m}_b(\mu)$. After doing also this version, we observe the following: Generally speaking, NLL corrections are not small for both cases, when taking into account the full range of μ, i.e., $m_b/2 < \mu < 2\,m_b$. More precisely, in the $\overline{\rm MS}$ version they are large for $\mu = m_b/2$ and smaller for larger values of μ, while in the pole mass version they are large for all values of μ.

We stress that the numerically important contributions involving the operator O_2 are not discussed in our paper. Therefore, the issue concerning the reduction of the μ dependence at NLL precision cannot be addressed at this level. Finally, the relevant input parameters that we used in our analysis together with the values of the Wilson coefficient C_7 and the strong coupling α_s at different values of the scale μ are listed in Table 6.

Parameter	Value
$\mathrm{m_b}$(pole)	4.8 GeV
$\mathrm{m_t}$(pole)	175 GeV
$\mathrm{M_W}$	80.4 GeV
$\mathrm{M_Z}$	91.19 GeV
$\mathrm{G_F}$	1.16637×10^{-5} GeV^{-2}
$\mathrm{V_{tb}V^*_{ts}}$	0.04
α^{-1}	137
$\alpha_\mathrm{s}(\mathrm{M_Z})$	0.119

	$\alpha_s(\mu)$	$C^0_{7,eff}(\mu)$	$C^1_{7,eff}(\mu)$
$\mu = \mathrm{M_W}$	0.1213	-0.1957	-2.3835
$\mu = 2\,m_b$	0.1818	-0.2796	-0.1788
$\mu = m_b$	0.2175	-0.3142	0.4728
$\mu = m_b/2$	0.2714	-0.3556	1.0794

Table 6: **Left:** Relevant input parameters. **Right:** $\alpha_s(\mu)$ and the Wilson coefficient $C_{7,eff}(\mu)$ at different values of the scale μ.

4 Concluding remarks

In the present work we calculated the set of the $O(\alpha_s)$ corrections to the decay process $\bar{B} \to X_s\gamma\gamma$ originating from diagrams involving $\mathcal{O}_7$. To perform this calculation, it is necessary to work out diagrams with three particles (s-quark and two photons) and four particles (s-quark, two photons and a gluon) in the final state. From the technical point of view, the calculation was made possible by the use of the Laporta Algorithm to identify the needed master integrals and by applying the differential equation method to solve the master integrals. When calculating the bremsstrahlung corrections, we take into account only terms proportional to the leading power of the hadronic mass. We find that the infrared and collinear singularities cancel when combining the above mentioned approximated version of bremsstrahlung corrections with the virtual corrections. The numerical impact of the NLL corrections is large: for $d\Gamma_{77}/(ds_1\,ds_2)$ the NLL result is approximately 50% smaller than the LL prediction.

Acknowledgments.— I wish to thank to the organizers of the conference FPCP 2012 for their efforts to make it very pleasant. This work is partially supported by the Swiss National Foundation and by the Helmholz Association through funds provided to the virtual institute "Spin and strong QCD" (VH-VI-231).

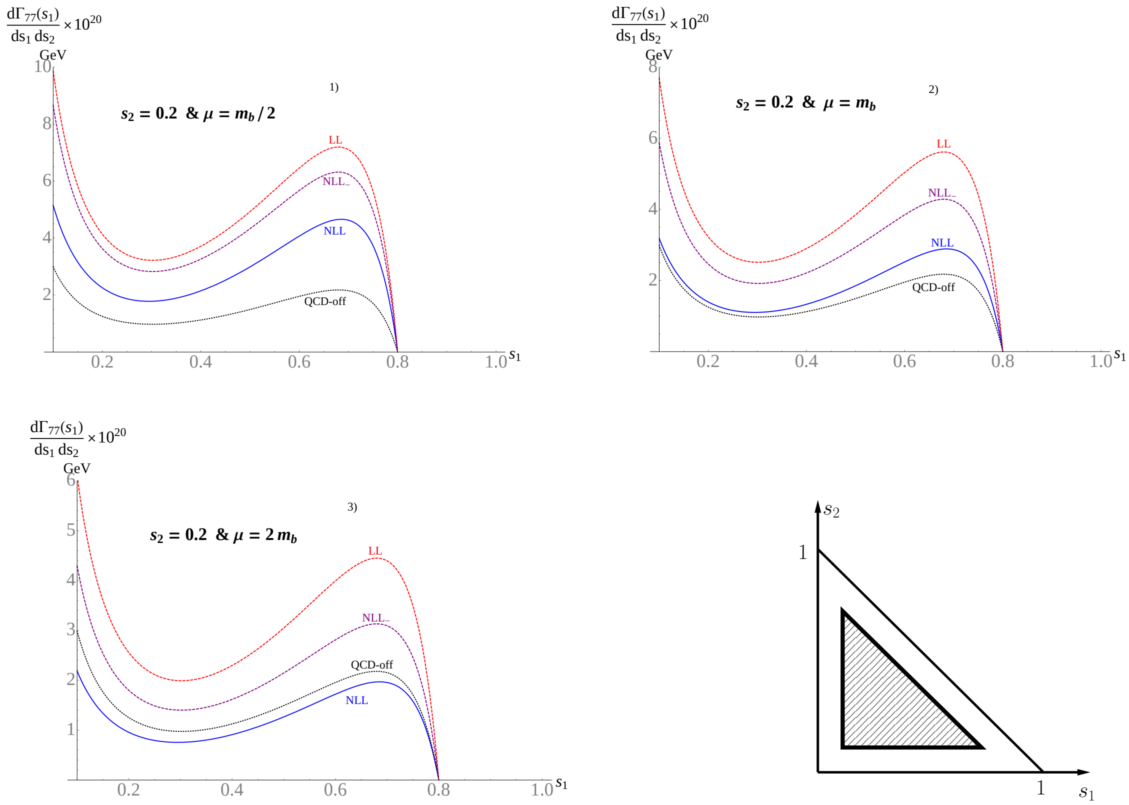

Figure 1: **Frames 1)-3)**: Double differential decay width $d\Gamma_{77}/(ds_1 ds_2)$ as a function of s_1 for s_2 fixed at $s_2 = 0.2$. The dotted(black), the short-dashed(red) and the solid line(blue) shows the result when neglecting QCD-effects, the LL and the NLL result, respectively. The long-dashed line(purple) represents the (partial) NLL result in which the virtual- and bremsstrahlung corrections worked out in our paper [8] are switched off. In the frames 1), 2) and 3) the renormalization scale is chosen to be $\mu = m_b/2$, $\mu = m_b$ and $\mu = 2\,m_b$, respectively. **Down right:** The relevant phase-space region for s_1 and s_2.

References

[1] M. Misiak, H. Asatrian, K. Bieri, M. Czakon, A. Czarnecki, et al., Phys.Rev.Lett. **98**, 022002 (2007), `hep-ph/0609232`.

[2] T. Hurth and M. Nakao, Ann.Rev.Nucl.Part.Sci. **60**, 645 (2010), `1005.1224`.

[3] A. J. Buras (2011), `1102.5650`.

[4] H. Simma and D. Wyler, Nucl.Phys. **B344**, 283 (1990).

[5] L. Reina, G. Ricciardi, and A. Soni, Phys.Lett. **B396**, 231 (1997), `hep-ph/9612387`.

[6] L. Reina, G. Ricciardi, and A. Soni, Phys.Rev. **D56**, 5805 (1997), `hep-ph/9706253`.

[7] J.-j. Cao, Z.-j. Xiao, and G.-r. Lu, Phys.Rev. **D64**, 014012 (2001), `hep-ph/0103154`.

[8] H. Asatrian, C. Greub, A. Kokulu, and A. Yeghiazaryan, Phys.Rev. **D85**, 014020 (2012), `1110.1251`.

[9] K. G. Chetyrkin, M. Misiak, and M. Munz, Phys.Lett. **B400**, 206 (1997), `hep-ph/9612313`.

[10] A. Kapustin, Z. Ligeti, and H. D. Politzer, Phys.Lett. **B357**, 653 (1995), `hep-ph/9507248`.

Part IV

Explaining $B \to D\tau\nu$, $B \to D^*\tau\nu$ and $B \to \tau\nu$ in a two Higgs doublet model III

published in

Phys. Rev. D86 (2012) 054014
(arXiv:1206.2634 [hep-ph])

Explaining $B \to D\tau\nu$, $B \to D^{*}\tau\nu$ and $B \to \tau\nu$ in a two Higgs doublet model of type III

Andreas Crivellin, Christoph Greub and Ahmet Kokulu
Albert Einstein Center for Fundamental Physics,
Institute for Theoretical Physics,
University of Bern,
CH-3012 Bern, Switzerland

Abstract

Recently, the BABAR Collaboration reported first evidence for new physics in $B \to D\tau\nu$ and $B \to D^{*}\tau\nu$. Combining both processes, the significance is $3.4\,\sigma$. This result cannot be explained in a two Higgs doublet model of type II. Furthermore, the CKMfitter Group finds a $2.9\,\sigma$ discrepancy between the Standard Model prediction for $\mathrm{Br}[B \to \tau\nu]$ (using V_{ub} from a global fit to the unitary triangle) and the measurements of the B factories. Altogether, these measurements are strong indications for physics beyond the Standard Model in B-meson decays to taus.

We show that in a two Higgs doublet model of type III it is possible to simultaneously explain $B \to D\tau\nu$ and $B \to D^{*}\tau\nu$ using a single free parameter ϵ^{u}_{32}. Also, $\mathrm{Br}[B \to \tau\nu]$ can be brought into agreement with experiment using ϵ^{u}_{31}. Furthermore, for Higgs ($A^0, H^0, H^{\pm}$) masses around 500 GeV, as preferred by recent CMS results, all bounds from FCNC processes are satisfied and $B \to D\tau\nu$, $B \to D^{*}\tau\nu$ and $B \to \tau\nu$ can be explained without a significant degree of fine tuning.

1 Introduction

In addition to the direct searches for new physics (performed at very high energies) at the LHC, low-energy precision flavour observables provide a complementary window to physics beyond the Standard Model (SM). Tauonic B-meson decays are an excellent probe of new physics: they test lepton flavor universality satisfied in the Standard Model (SM) and are sensitive to new particles which couple proportionally to the mass of the involved particles (e.g. Higgs bosons) due to the heavy τ lepton involved. The single decay modes still suffer from large hadronic uncertainties related to the form factors and from the uncertainties of the CKM elements. However, in normalizing the τ decay mode to the corresponding decay with light leptons in the final state, these uncertainties are reduced and the sensitivity to new physics is significantly improved.

Recently, the BABAR Collaboration performed an analysis of the semileptonic B decays $B \to D\tau\nu$ and $B \to D^{*}\tau\nu$ using the full available data set [1]. They find for the ratios

$$\mathcal{R}(D^{(*)}) \;=\; \mathcal{B}(B \to D^{(*)}\tau\nu)/\mathcal{B}(B \to D^{(*)}\ell\nu)\,, \tag{1}$$

the following results:

$$\mathcal{R}(D) \;=\; 0.440 \pm 0.058 \pm 0.042\,, \tag{2}$$
$$\mathcal{R}(D^{*}) \;=\; 0.332 \pm 0.024 \pm 0.018\,. \tag{3}$$

Here the first error is statistical and the second one is systematic. Comparing these measurements to the SM predictions

$$\mathcal{R}_{\rm SM}(D) = 0.297 \pm 0.017\,, \tag{4}$$
$$\mathcal{R}_{\rm SM}(D^*) = 0.252 \pm 0.003\,, \tag{5}$$

we see that there is a discrepancy of $2.2\,\sigma$ for $\mathcal{R}(D)$ and $2.7\,\sigma$ for $\mathcal{R}(D^*)$. For these theory predictions we again used the updated results of [1], which rely on the calculations of Refs. [2, 3] based on the previous results of Refs. [4, 5, 6, 7, 8]. Both processes exceed the SM prediction, and combining them gives a $3.4\,\sigma$ deviation from the SM [1], which constitutes the first evidence for new physics in semileptonic B decays to tau leptons.

This evidence for new physics in B-meson decays to taus is further supported by the measurement of $B \to \tau\nu$ by BABAR [9] and BELLE [10]. Averaging both measurements, one obtains the branching ratio [11]

$$\mathcal{B}[B \to \tau\nu] = (1.67 \pm 0.3) \times 10^{-4}\,. \tag{6}$$

This also disagrees with the SM prediction by $2.9\,\sigma$ [12] or $2.5\,\sigma$ [13], using the global fit of the CKM matrix performed by CKMfitter or UTfit, respectively.

Thus, combining $\mathcal{R}(D)$, $\mathcal{R}(D^*)$ and $B \to \tau\nu$, we have rather solid evidence for violation of lepton flavor universality. Assuming that these deviations from the SM are not statistical fluctuations or underestimated theoretical or systematic errors, it is interesting to ask which model of new physics can explain the measured values. Since these processes are all tree-level decays in the SM, it is difficult to explain these deviations with a model of new physics (NP), since one in general also needs a tree-level exchange of a new particle in order to get sizable effects. This then generates the difficulty to explain the absence of NP effects in other observables.

A widely studied possibility is the introduction of a charged scalar particle which couples proportionally to the masses of the fermions involved in the interaction: a charged Higgs boson. Such a charged Higgs boson is introduced in the MSSM or in general in any two Higgs doublet model (2HDM), and affects $B \to \tau\nu$ [14, 15], $B \to D\tau\nu$ and $B \to D^*\tau\nu$ [16, 17, 18]. This is a reasonable model: because the Higgs couples only significantly to the tau, it can explain the absence of NP effects in B decays to light leptons and gives rise to lepton flavor universality violation.

In a 2HDM of type II (like the MSSM[1]), one Higgs doublet couples to down quarks and charged leptons, while the other one gives masses to the up quarks. Then the only free additional parameters are $\tan\beta = v_u/v_d$ (the ratio of the two vacuum expectation values) and the charged Higgs mass $m_{H^\pm}$ (the heavy CP even Higgs mass m_{H^0} and the CP odd Higgs mass m_{A^0} can be expressed in terms of the charged Higgs mass and differ only by electroweak corrections). In this setup the charged Higgs contribution to $B \to \tau\nu$ interferes necessarily destructively with the SM [14]. Thus, an enhancement of $\mathcal{B}[B \to \tau\nu]$ is only possible if the absolute value of the charged Higgs contribution is bigger than two times the SM one, which is in conflict with $B \to D\tau\nu$. Furthermore, a 2HDM of type II cannot explain $\mathcal{R}(D)$ and $\mathcal{R}(D^*)$ simultaneously [1].

Another possibility to explain $B \to \tau\nu$ is the introduction of a right-handed W-coupling [19] or new physics in B mixing [20] (meaning that the actual value of V_{ub} is bigger than

[1]At the loop-level non-holomorphic couplings are induced, but for constructive interference they have to exceed the tree-level Yukawa coupling, which is very difficult.

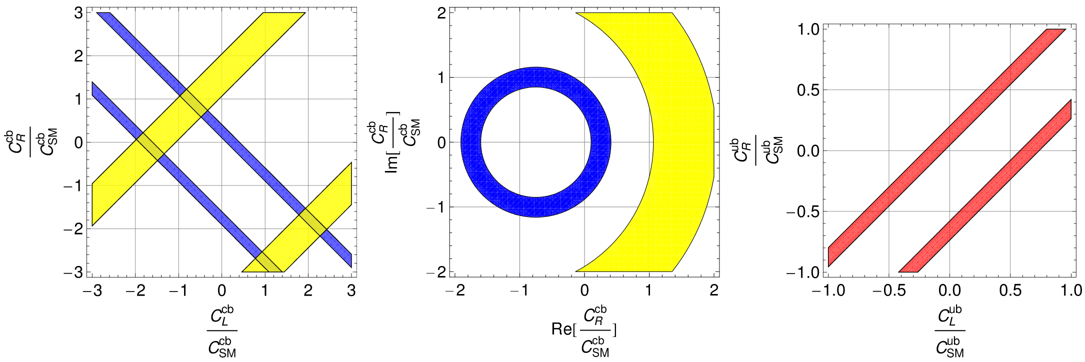

Figure 1: Left and middle: Allowed $1\,\sigma$ regions from $\mathcal{R}(D)$ (blue) and $\mathcal{R}(D^*)$ (yellow), adding the experimental uncertainty and theoretical uncertainty linear. Left: Constraints in the $C_L^{cb}/C_{\rm SM}^{cb}$–$C_R^{cb}/C_{\rm SM}^{cb}$ plane for real values of $C_L^{cb}/C_{\rm SM}^{cb}$ and $C_R^{cb}/C_{\rm SM}^{cb}$. Middle: C_R^{cb} complex for C_L^{cb}=0. Right: Allowed $1\,\sigma$ regions from $B\to\tau\nu$ in the $C_L^{ub}/C_{\rm SM}^{ub}$–$C_R^{ub}/C_{\rm SM}^{ub}$ plane for real values of $C_L^{ub}/C_{\rm SM}^{ub}$ and $C_R^{ub}/C_{\rm SM}^{ub}$. All Wilson coefficients are understood to be at the scale m_b.

the one extracted from the global fit). Anyway, neither possibilities can help to explain the deviation from the SM in $\mathcal{R}(D)$ and $\mathcal{R}(D^*)$.

Thus, we need another model to explain $\mathcal{R}(D)$ and $\mathcal{R}(D^*)$. Our choice in this article is a 2HDM of type III (where both Higgs doublets couple to up quarks and down quarks as well) with MSSM-like Higgs potential. Since a 2HDM of type III with minimal flavor violation (MFV) can only explain $B\to\tau\nu$ in some fine-tuned regions of parameter space [21] and cannot explain $\mathcal{R}(D)$ and $\mathcal{R}(D^*)$ simultaneously, we consider a more generic flavor structure with flavor violation in the up sector. As we will see, this model is capable to explain $B\to\tau\nu$, $\mathcal{R}(D)$ and $\mathcal{R}(D^*)$ without fine tuning.

2 Effective Field Theory

Since the NP we are interested in must be far above the scale of the B meson, we can integrate out the heavy degrees of freedom (including the SM W boson). The SM contribution and the NP contribution are then contained within the effective Hamiltonian

$$\mathcal{H}_{\rm eff} = C_{\rm SM}^{qb} O_{\rm SM}^{qb} + C_R^{qb} O_R^{qb} + C_L^{qb} O_L^{qb}\,, \tag{7}$$

with (for massless neutrinos)

$$\begin{aligned} O_{\rm SM}^{qb} &= \bar{q}\gamma_\mu P_L b\, \bar{\tau}\gamma_\mu P_L \nu_\tau\,,\\ O_R^{qb} &= \bar{q} P_R b\, \bar{\tau} P_L \nu_\tau\,,\\ O_L^{qb} &= \bar{q} P_L b\, \bar{\tau} P_L \nu_\tau\,. \end{aligned} \tag{8}$$

In Eq. (7) and Eq. (8) $q=u$ for $B\to\tau\nu$ and $q=c$ for $B\to D\tau\nu$ and $B\to D^*\tau\nu$. The SM Wilson coefficient is given by $C_{\rm SM}^{qb} = 4G_F\, V_{qb}/\sqrt{2}$. The corresponding Wilson coefficients C_R^{qb}

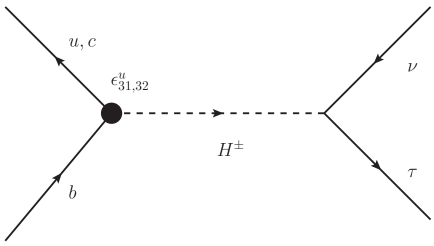

Figure 2: Feynman diagram with a charged Higgs contributing to $B \to \tau\nu$ and $B \to D^{(*)}\tau\nu$. The dot represents the flavor-violating interaction containing the 2HDM of type III parameters ϵ^u_{31} and ϵ^u_{32}, which affect $B \to \tau\nu$ and $B \to D^{(*)}\tau\nu$, respectively.

and C_L^{qb} (given at the B meson scale), which parametrize the effect of NP, affect our three physical observables in the following way [3, 15, 22]:

$$\mathcal{R}(D) = \mathcal{R}_{\rm SM}(D)\left(1 + 1.5\Re\left[\frac{C_R^{cb}+C_L^{cb}}{C_{SM}^{cb}}\right] + 1.0\left|\frac{C_R^{cb}+C_L^{cb}}{C_{SM}^{cb}}\right|^2\right), \tag{9}$$

$$\mathcal{R}(D^*) = \mathcal{R}_{\rm SM}(D^*)\left(1 + 0.12\Re\left[\frac{C_R^{cb}-C_L^{cb}}{C_{SM}^{cb}}\right] + 0.05\left|\frac{C_R^{cb}-C_L^{cb}}{C_{SM}^{cb}}\right|^2\right), \tag{10}$$

$$\mathcal{B}[B \to \tau\nu] = \frac{G_F^2|V_{ub}|^2}{8\pi} m_\tau^2 f_B^2 m_B\left(1 - \frac{m_\tau^2}{m_B^2}\right)^2 \tau_B \times \left|1 + \frac{m_B^2}{\overline{m}_b m_\tau}\frac{(C_R^{ub}-C_L^{ub})}{C_{SM}^{ub}}\right|^2. \tag{11}$$

Let us consider first $B \to D\tau\nu$ and $B \to D^*\tau\nu$, where the ratios $\mathcal{R}(D)$ and $\mathcal{R}(D^*)$ are affected by the two Wilson coefficients C_R^{cb} and C_L^{cb}. For our analysis we add the experimental errors in quadrature and the theoretical uncertainty linear on top of this. From the left plot in Fig. 1, we see that both $\mathcal{R}(D)$ and $\mathcal{R}(D^*)$ can be brought into agreement with the experimental values within the $1\,\sigma$ error by C_L^{cb} only. Note that C_R^{cb} is not capable of achieving this without a simultaneous contribution from C_L^{cb}. Since (neglecting small mass ratios) only C_R^{cb} is generated in a 2HDM of type II or in a 2HDM of type III with MFV [23] (neglecting small quark mass ratios), these models cannot explain $\mathcal{R}(D)$ and $\mathcal{R}(D^*)$ simultaneously. This is still true if we allow for complex values of C_R^{cb}, as we can see from the middle plot in Fig. 1. Note that the Wilson coefficients in the plots are given at the scale m_b.

On the other hand, $B \to \tau\nu$ can be explained either with C_R^{ub} or with C_L^{ub} (or with a combination of both of them). However, as we will see in the next section, in the context of the 2HDM of type III, C_L^{ub} is the more natural choice.

3 Two Higgs doublet model of type III

The SM contains only one scalar isospin doublet, the Higgs doublet. After electroweak symmetry breaking, this gives masses to up quarks, down quarks and charged leptons. The charged component of this doublet becomes the longitudinal component of the W boson, and thus we have only one physical neutral Higgs particle. In a 2HDM we introduce a second Higgs doublet and obtain four additional physical Higgs particles (in the case of a CP conserving Higgs potential): the neutral CP-even Higgs H, a neutral CP-odd Higgs A and the two charged Higgses $H^\pm$.

Two Higgs doublet models have been studied for many years with focus on the type II models [17, 24, 25] or type III models with MFV [21, 23, 26], and on alignment [27, 28] or natural flavour conservation [26, 29]. As outlined in the introduction, these models cannot explain $\mathcal{R}(D)$ and $\mathcal{R}(D^*)$ simultaneously [1] (and for $B \to \tau\nu$ fine tuning is needed); we will study a 2HDM of type III with generic flavour-structure [30], but for simplicity, with MSSM-like Higgs potential [2].

In the 2HDM of type III, we have the Yukawa Lagrangian (see for example [32] for details):

$$\begin{aligned} \mathcal{L}_Y^{eff} &= \bar{Q}^a_{f\,L}\left[Y^d_{fi}\epsilon_{ab}H^{b\star}_d \,-\, \epsilon^d_{fi}H^a_u\right] d_{i\,R} \\ &- \bar{Q}^a_{f\,L}\left[Y^u_{fi}\epsilon_{ab}H^{b\star}_u \,+\, \epsilon^u_{fi}H^a_d\right] u_{i\,R} \,+\, \text{H.c.}\,, \end{aligned} \tag{12}$$

where ϵ_{ab} is the totally antisymmetric tensor, and ϵ^q_{ij} parametrizes the non-holomorphic corrections which couple up (down) quarks to the down (up) type Higgs doublet. After electroweak symmetry breaking, this Lagrangian gives rise to the following Feynman-rule:

$$i\left(\Gamma^{H^\pm\,LR\,\text{eff}}_{u_f d_i} P_R + \Gamma^{H^\pm\,RL\,\text{eff}}_{u_f d_i} P_L\right)\,, \tag{13}$$

with

$$\begin{aligned} \Gamma^{H^\pm\,LR\,\text{eff}}_{u_f d_i} &= \sum_{j=1}^{3} \sin\beta\, V_{fj}\left(\frac{m_{d_i}}{v_d}\delta_{ji} - \epsilon^d_{ji}\tan\beta\right)\,, \\ \Gamma^{H^\pm\,RL\,\text{eff}}_{u_f d_i} &= \sum_{j=1}^{3} \cos\beta\left(\frac{m_{u_f}}{v_u}\delta_{jf} - \epsilon^{u\star}_{jf}\tan\beta\right) V_{ji}\,. \end{aligned} \tag{14}$$

Thus, the Wilson coefficients C^{qb}_L and C^{qb}_R at the matching scale are given by

$$C^{qb}_{R(L)} = \frac{-1}{M^2_{H^\pm}}\,\Gamma^{LR(RL),H^\pm}_{qb}\,\frac{m_\tau}{v}\tan\beta\,, \tag{15}$$

with the vacuum expectation value $v \approx 174\text{GeV}$. Here we assumed that the Peccei-Quinn breaking for leptons is negligible, which means that the lepton-Higgs coupling are like in the 2HDM of type II. Note that for large Higgs masses and large values $\tan(\beta)$, the CP-odd and the heavy CP-even Higgs mass approach the charged one.

3.1 Experimental constraints

First, note that all flavor-changing elements ϵ^d_{ij} are stringently constrained from FCNC processes in the down sector because of tree-level neutral Higgs exchange. Thus, they cannot have any significant impact on the decays we are interested in, and therefore we are left with ϵ^d_{33}.

Concerning the elements ϵ^u_{ij} we see that only ϵ^u_{31} (ϵ^u_{32}) significantly effects $B \to \tau\nu$ ($\mathcal{R}(D)$ and $\mathcal{R}(D^*)$) without any CKM suppression. Furthermore, since flavor-changing top-to-up (or charm) transitions are not measured with sufficient accuracy, we can only constrain these elements from charged Higgs-induced FCNCs in the down sector. However, since in this case an up (charm) quark always propagates inside the loop, the contribution is suppressed by the

[2]Flavor-observables in type III models have been considered before [31], but with focus on the flavor-changing elements in the down sector.

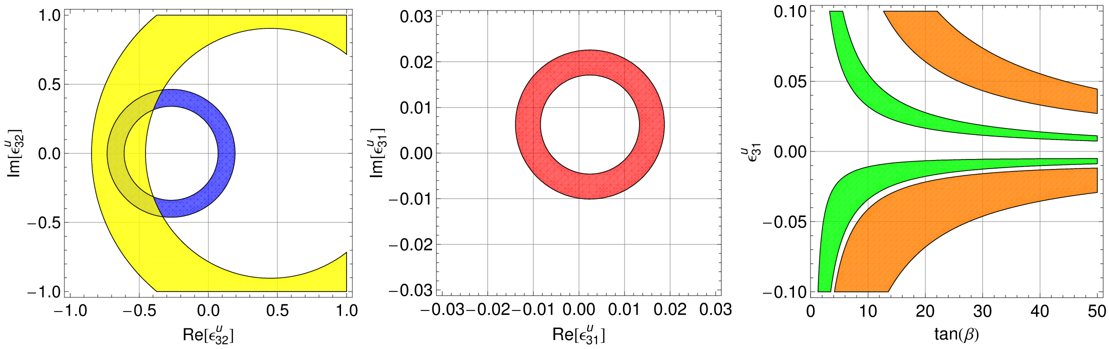

Figure 3: Left: Allowed regions in the complex ϵ^u_{32}-plane from $\mathcal{R}(D)$ (blue) and $\mathcal{R}(D^*)$ (yellow) for $\tan\beta = 50$ and $m_H = 500$ GeV. Middle: Allowed regions in the complex ϵ^u_{31}-plane from $B \to \tau\nu$. Right: Allowed regions in the $\tan\beta$–ϵ^u_{31} plane from $B \to \tau\nu$ for real values of ϵ^u_{31} and $m_H = 400$ GeV (green), $m_H = 800$ GeV (orange). The scaling of the allowed region for ϵ^u_{32} with $\tan\beta$ and m_H is the same as for ϵ^u_{31}. ϵ^u_{32} and ϵ^u_{31} are given at the matching scale m_H.

small Yukawa couplings of the up-down-Higgs (charm-strange-Higgs) vertex involved in the corresponding diagrams. Thus, the constraints from FCNC processes are weak, and $\epsilon^u_{32,31}$ can be sizable.

Of course, the lower bounds on the charged Higgs mass for a 2HDM of type II from $b \to s\gamma$ of 300 GeV [33] must still be respected by our model, and also the results from direct searches at the LHC [34] are in principle unchanged. Note that the recent CMS results even welcome a heavy Higgs $(H^0, A^0, H^\pm)$ mass around 500 GeV.

3.2 $B \to D\tau\nu$ and $B \to D^*\tau\nu$

ϵ^d_{33} contributes to C^{cb}_R, and thus (as we see from Fig. 1) cannot simultaneously explain $\mathcal{R}(D)$ and $\mathcal{R}(D^*)$. Thus, we are left with ϵ^u_{32}, which contributes to $B \to D\tau\nu$ and $B \to D^*\tau\nu$ via the Feynman diagram shown in Fig. 2. In Fig. 3 we see the allowed region in the complex ϵ^u_{32}-plane, which gives the correct values for $\mathcal{R}(D)$ and $\mathcal{R}(D^*)$ within the $1\,\sigma$ uncertainties for $\tan\beta = 50$ and $M_H = 500$ GeV.

3.3 $B \to \tau\nu$

In principle, $B \to \tau\nu$ can be explained either by using ϵ^d_{33} (as in 2HDMs with MFV) or by ϵ^u_{31}, or by a combination of both (see right plot in Fig. 1). However, ϵ^d_{33} alone cannot explain the deviation from the SM without fine tuning, while ϵ^u_{31} is capable of doing this. We see this from the right plot in Fig. 3, keeping in mind that ϵ^d_{33} generates C^{ub}_R, while ϵ^u_{31} generates C^{ub}_L.

3.4 The quark mass matrix and fine tuning

The naturalness criterion of 't Hooft states that the smallness of a quantity is only natural if a symmetry is gained in the limit in which this quantity is zero. This means, on the other hand, that large accidental cancellations, which are not enforced by a symmetry, are unnatural and thus not desirable. Let us apply this reasoning to the quark masses and CKM elements in the 2HDM. The quark mass matrices in the 2HDM of type III are given by

$$m_{ij}^{d(u)} = v_{d(u)} Y_{ij}^{d(u)} + v_{u(d)} \epsilon_{ij}^{d(u)} \,. \tag{16}$$

Diagonalizing these quark mass matrices gives the physical quark masses and the CKM matrix. Using 't Hooft's naturalness criterion we can demand the absence of fine-tuned cancellations between $v_d Y_{ij}^d$ ($v_u Y_{ij}^u$) and $v_u \epsilon_{ij}^d$ ($v_d \epsilon_{ij}^u$). Thus, we require that the contributions of $v_u \epsilon_{ij}^d$ and $v_d \epsilon_{ij}^u$ to the quark masses and CKM matrix not exceed the physical measured quantities:

$$|v_{u(d)} \epsilon_{ij}^{d(u)}| \leq |V_{ij}| \max \left[m_{d_i(u_i)}, m_{d_j(u_j)} \right] . \tag{17}$$

From Fig. 3, we see that 't Hooft's naturalness criterion is satisfied if $\mathcal{R}(D)$, $\mathcal{R}(D^*)$ and $B \to \tau\nu$ are explained using ϵ_{32}^u and ϵ_{31}^u, respectively. However, if $B \to \tau\nu$ is explained using ϵ_{33}^d, 't Hooft's naturalness criterion is violated either because the SM contribution to $B \to \tau\nu$ is overcompensated or because $\left|v_u \epsilon_{33}^d\right| > m_b$.

4 Conclusions

The decays $B \to \tau\nu$, $B \to D\tau\nu$ and $B \to D^*\tau\nu$ are an excellent probe of physics beyond the SM (complementary to the direct searches at the LHC), since they are sensitive to lepton flavor universality violating new physics, e.g., Higgs bosons. The BABAR Collaboration recently reported an excess both in $B \to D\tau\nu$ and $B \to D^*\tau\nu$ compared to the SM predictions [1]. This evidence for new physics cannot be explained with a 2HDM of type II. Therefore, we proposed a 2HDM of type III with MSSM-like Higgs potential and flavor-violation in the up sector in order to explain these deviations from the SM. In fact, our model can account for the deviation of $\mathcal{R}(D)$ and $\mathcal{R}(D^*)$ from the SM predictions simultaneously and also bring $B \to \tau\nu$ into agreement with experiment. This is even possible without significant fine tuning. Furthermore, all experimental constraints from other processes can be satisfied, and recent CMS results [34] even welcome a mass around 500 GeV for the non-SM-like Higgs bosons of a 2HDM. In order to test the model, we propose to search for $A^0, H^0 \to \bar{t} + c$ at the LHC.

Acknowledgments.— We are grateful M. Procura for proofreading the article. A.C. thanks Eugenio Paoloni for useful discussions and bringing the $B \to D^{(*)}\tau\nu$ problem to his attention. This work is supported by the Swiss National Science Foundation. The Albert Einstein Center for Fundamental Physics is supported by the "Innovations- und Kooperationsprojekt C-13" of the Schweizerische Universitätskonferenz SUK/CRUS.

References

[1] B. Aubert et al. (BABAR Collaboration) (2012), 1205.5442.

[2] J. F. Kamenik and F. Mescia, Phys.Rev. **D78**, 014003 (2008), 0802.3790.

[3] S. Fajfer, J. F. Kamenik, and I. Nisandzic (2012), 1203.2654.

[4] J. Korner and G. Schuler, Z.Phys. **C38**, 511 (1988).

[5] J. Korner and G. Schuler, Phys.Lett. **B231**, 306 (1989).

[6] J. Korner and G. Schuler, Z.Phys. **C46**, 93 (1990).

[7] P. Heiliger and L. Sehgal, Phys.Lett. **B229**, 409 (1989).

[8] X.-Y. Pham, Phys.Rev. **D46**, R1909 (1992).

[9] B. Aubert et al. (BABAR Collaboration), Phys.Rev. **D81**, 051101 (2010).

[10] K. Hara et al. (Belle collaboration), Phys.Rev. **D82**, 071101 (2010), 1006.4201.

[11] D. Asner et al. (Heavy Flavor Averaging Group) (2010), 1010.1589.

[12] J. Charles et al. (CKMfitter Group), Eur.Phys.J. **C41**, 1 (2005), hep-ph/0406184.

[13] M. Bona et al. (UTfit Collaboration), Phys.Lett. **B687**, 61 (2010), 0908.3470.

[14] W.-S. Hou, Phys.Rev. **D48**, 2342 (1993).

[15] A. Akeroyd and S. Recksiegel, J.Phys.G **G29**, 2311 (2003), hep-ph/0306037.

[16] M. Tanaka, Z.Phys. **C67**, 321 (1995), hep-ph/9411405.

[17] T. Miki et al., pp. 116–124 (2002), hep-ph/0210051.

[18] U. Nierste, S. Trine, and S. Westhoff, Phys.Rev. **D78**, 015006 (2008), 0801.4938.

[19] A. Crivellin, Phys. Rev. **D81**, 031301 (2010), 0907.2461.

[20] A. Lenz et al. (2012), 1203.0238.

[21] G. Blankenburg and G. Isidori (2011), 1107.1216.

[22] Y. Sakaki and H. Tanaka (2012), 1205.4908.

[23] G. D'Ambrosio, G. F. Giudice, G. Isidori, and A. Strumia, Nucl. Phys. **B645**, 155 (2002), hep-ph/0207036.

[24] A. Wahab El Kaffas, P. Osland, and O. M. Ogreid, Phys.Rev. **D76**, 095001 (2007), 0706.2997.

[25] O. Deschamps et al., Phys.Rev. **D82**, 073012 (2010), 0907.5135.

[26] A. J. Buras, M. V. Carlucci, S. Gori, and G. Isidori, JHEP **1010**, 009 (2010), 1005.5310.

[27] A. Pich and P. Tuzon, Phys.Rev. **D80**, 091702 (2009), 0908.1554.

[28] M. Jung, A. Pich, and P. Tuzon, JHEP **1011**, 003 (2010), 1006.0470.

[29] S. L. Glashow and S. Weinberg, Phys.Rev. **D15**, 1958 (1977).

[30] T. Cheng and M. Sher, Phys.Rev. **D35**, 3484 (1987).

[31] F. Mahmoudi and O. Stal, Phys.Rev. **D81**, 035016 (2010), 0907.1791.

[32] A. Crivellin, Phys. Rev. **D83**, 056001 (2011), 1012.4840.

[33] M. Misiak et al., Phys.Rev.Lett. **98**, 022002 (2007), hep-ph/0609232.

[34] S. Chatrchyan et al. (CMS Collaboration), Phys.Lett. **B713**, 68 (2012), 1202.4083.

Part V

Flavor-phenomenology of two-Higgs-doublet models with generic Yukawa structure

published in

Phys. Rev. D87 (2013) 094031
(arXiv:1303.5877 [hep-ph])

Flavor-phenomenology of two-Higgs-doublet models with generic Yukawa structure

Andreas Crivellin, Christoph Greub and Ahmet Kokulu

Albert Einstein Center for Fundamental Physics,
Institute for Theoretical Physics,
University of Bern,
CH-3012 Bern, Switzerland

Abstract

In this article, we perform an extensive study of flavor observables in a two-Higgs-doublet model (2HDM) with generic Yukawa structure (of type III). This model is interesting not only because it is the decoupling limit of the Minimal Supersymmetric Standard Model (MSSM) but also because of its rich flavor phenomenology which also allows for sizable effects not only in FCNC processes but also in tauonic B decays. We examine the possible effects in flavor physics and constrain the model both from tree-level processes and from loop-observables. The free parameters of the model are the heavy Higgs mass, $\tan\beta$ (the ratio of vacuum expectation values) and the "non-holomorphic" Yukawa couplings ϵ^f_{ij} $(f = u, d, \ell)$. In our analysis we constrain the elements ϵ^f_{ij} in various ways: In a first step we give order of magnitude constraints on ϵ^f_{ij} from 't Hooft's naturalness criterion, finding that all ϵ^f_{ij} must be rather small unless the third generation is involved. In a second step, we constrain the Yukawa structure of the type-III 2HDM from tree-level FCNC processes ($B_{s,d} \to \mu^+\mu^-$, $K_L \to \mu^+\mu^-$, $\bar{D}^0 \to \mu^+\mu^-$, $\Delta F = 2$ processes, $\tau^- \to \mu^-\mu^+\mu^-$, $\tau^- \to e^-\mu^+\mu^-$ and $\mu^- \to e^-e^+e^-$) and observe that all flavor off-diagonal elements of these couplings, except $\epsilon^u_{32,31}$ and $\epsilon^u_{23,13}$ must be very small in order to satisfy the current experimental bounds. In a third step, we consider Higgs mediated loop contributions to FCNC processes ($b \to s(d)\gamma$, $B_{s,d}$ mixing, $K-\overline{K}$ mixing and $\mu \to e\gamma$) finding that also ϵ^u_{13} and ϵ^u_{23} must be very small, while the bounds on ϵ^u_{31} and ϵ^u_{32} are especially weak. Furthermore, considering the constraints from electric dipole moments (EDMs) we obtain constrains on some parameters $\epsilon^{u,\ell}_{ij}$. Taking into account the constraints from FCNC processes we study the size of possible effects in the tauonic B decays ($B \to \tau\nu$, $B \to D\tau\nu$ and $B \to D^*\tau\nu$) as well as in $D_{(s)} \to \tau\nu$, $D_{(s)} \to \mu\nu$, $K(\pi) \to e\nu$, $K(\pi) \to \mu\nu$ and $\tau \to K(\pi)\nu$ which are all sensitive to tree-level charged Higgs exchange. Interestingly, the unconstrained $\epsilon^u_{32,31}$ are just the elements which directly enter the branching ratios for $B \to \tau\nu$, $B \to D\tau\nu$ and $B \to D^*\tau\nu$. We show that they can explain the deviations from the SM predictions in these processes without fine tuning. Furthermore, $B \to \tau\nu$, $B \to D\tau\nu$ and $B \to D^*\tau\nu$ can even be explained simultaneously. Finally, we give upper limits on the branching ratios of the lepton flavor-violating neutral B meson decays ($B_{s,d} \to \mu e$, $B_{s,d} \to \tau e$ and $B_{s,d} \to \tau\mu$) and correlate the radiative lepton decays ($\tau \to \mu\gamma$, $\tau \to e\gamma$ and $\mu \to e\gamma$) to the corresponding neutral current lepton decays ($\tau^- \to \mu^-\mu^+\mu^-$, $\tau^- \to e^-\mu^+\mu^-$ and $\mu^- \to e^-e^+e^-$). A detailed appendix contains all relevant information for the considered processes for general scalar-fermion-fermion couplings.

1 Introduction

Two-Higgs-doublet models (2HDMs) [1] have been under intensive investigation for a long time (see for example Ref. [2] for an introduction or Ref. [3] for a recent review article). There are several reasons for this great interest in 2HDMs: Firstly, 2HDMs are very simple extensions of the Standard Model (SM) obtained by just adding an additional scalar $SU(2)_L$ doublet to the SM particle content. This limits the number of new degrees of freedom and makes the model rather predictive. Secondly, motivation for 2HDMs comes from axion models [4] because a possible CP-violating term in the QCD Lagrangian can be rotated away [5] if the Lagrangian has a global $U(1)$ symmetry which is only possible if there are two Higgs doublets. Also the generation of the baryon asymmetry of the Universe motivates the introduction of a second Higgs doublet because in this way the amount of CP violation can be large enough to accommodate for this asymmetry, while the CP violation in the SM is too small [6]. Finally, probably the best motivation for studying 2HDMs is the Minimal Supersymmetric Standard Model (MSSM) where supersymmetry enforces the introduction of a second Higgs doublet [7] due to the holomorphic superpotential. Furthermore, the 2HDM of type III is also the effective theory obtained by integrating out all super-partners of the SM-like particles (the SM fermion, the gauge boson and the Higgs particles of the 2HDM) from MSSM.

2HDMs are not only interesting for direct searches for additional Higgs bosons at colliders. In addition to these high energy searches at the LHC also low-energy precision flavor observables provide a complementary window to physics beyond the SM, i.e. to the 2HDMs. In this respect, FCNC processes, e.g. neutral meson decays to muon pairs ($B_{s(d)} \to \mu^+\mu^-$, $D \to \mu^+\mu^-$ and $K_L \to \mu^+\mu^-$) are especially interesting because they are very sensitive to flavor changing neutral Higgs couplings. However, also charged current processes like tauonic B-meson decays are affected by the charged Higgs boson and $b \to s\gamma$ provides currently the best lower limit on the charged Higgs mass in the 2HDM of type II.

Recently, tauonic B decays received special attention because the BABAR collaboration performed an analysis of the semileptonic B decays $B \to D\tau\nu$ and $B \to D^*\tau\nu$ reporting a discrepancy of $2.0\,\sigma$ and $2.7\,\sigma$ from the SM expectation, respectively. The measurements of both decays exceed the SM predictions, and combining them gives a $3.4\,\sigma$ deviation from the SM [8, 9] expectation, which constitutes first evidence for new physics in semileptonic B decays to tau leptons. This evidence for the violation of lepton flavor universality is further supported by the measurement of $B \to \tau\nu$ by BABAR [10, 11] and BELLE [12, 13] which exceeds the SM prediction by $1.6\,\sigma$ using V_{ub} from the global fit [14]. Assuming that these deviations from the SM are not statistical fluctuations or underestimated theoretical or systematic uncertainties, it is interesting to ask which model of new physics can explain the measured values. Since, a 2HDM of type II cannot explain $B \to \tau\nu$, $B \to D\tau\nu$ and $B \to D^*\tau\nu$ simultaneously [8], one must look at 2HDMs with more general Yukawa structures. Also 2HDMs of type III with Minimal Flavor Violation (MFV) [15] cannot explain these deviations from the SM but a 2HDM of type III (where both Higgs doublets couple to up quarks and down quarks as well) with flavor-violation in the up sector, is capable of explaining $B \to \tau\nu$, $B \to D\tau\nu$ and $B \to D^*\tau\nu$ without fine tuning [16].

These points motivate us to perform a complete analysis of flavor-violation in 2HDMs of type III in this article. For this purpose we take into account all relevant constraints from FCNC processes (both from tree-level contributions and from loop-induced effects) and consider afterwards the possible effects in charged current processes.

This article is structured as follows: In Sec. 2, we review the Yukawa Lagrangian of the 2HDM of type III. In Sec. 3 we give a general overview on the constraints on 2HDMs and update the bounds on the 2HDM of type II. The following sections discuss in detail the constraints on the 2HDM of type III parameter space from 't Hooft's naturalness argument (Sec. 4), from tree-level FCNC processes (Sec. 5) and from loop-induced charged and neutral Higgs mediated contributions to the flavor observables (Sec. 6). Sec. 7 studies the possible effects in charged current decays ($B \to \tau\nu$, $B \to D\tau\nu$, $B \to D^*\tau\nu$, $D_{(s)} \to \tau\nu$, $D_{(s)} \to \mu\nu$, $K(\pi) \to e\nu$, $K(\pi) \to \mu\nu$, $\tau \to K(\pi)\nu$) and Sec. 8 is denoted to the study of the upper limits on the branching ratios $B_{s,d} \to \tau\mu$, $B_{s,d} \to \tau e$, $B_{s,d} \to \mu e$ and the correlations among $\tau^- \to \mu^-\mu^+\mu^-$, $\tau^- \to e^-\mu^+\mu^-$, $\mu^- \to e^-e^+e^-$ and $\tau \to \mu\gamma$, $\tau \to e\gamma$, $\mu \to e\gamma$. Finally, we conclude. A detailed appendix contains some of the input parameters used in our analysis, general expressions for some branching ratios as well as all the relevant Wilson coefficients for $b \to s(d)\gamma$, $\Delta F = 2$ processes, leptonic neutral meson decays ($\Delta F = 1$), LFV transitions, EDMs, anamolous magnetic moment (AMM) of muon and (semi-) leptonic charged meson decays for general charged and/or neutral scalar-fermion-fermion couplings.

2 Setup

The SM contains only one scalar weak-isospin doublet, the Higgs doublet. After electroweak symmetry breaking its vacuum expectation value (”vev”) gives masses to up quarks, down quarks and charged leptons. The charged (CP-odd neutral) component of this doublet becomes the longitudinal component of the W (Z) boson, and thus we have only one physical CP-even neutral Higgs particle in the SM. In a 2HDM we introduce a second Higgs doublet and obtain four additional physical Higgs particles (in the case of a CP conserving Higgs potential): the neutral heavy CP-even Higgs H^0, a neutral CP-odd Higgs A^0 and the two charged Higgses $H^{\pm}$.

As outlined in the introduction we consider a 2HDM with generic Yukawa structure (2HDM of type III). One motivation is that a 2HDM with natural flavor-conservation (like type I or type II) cannot explain $B \to D\tau\nu$, $B \to D^*\tau\nu$ and $B \to \tau\nu$ simultaneously, while the type III model is capable of doing this [16]. Beside this, our calculations in the 2HDM III are the most general ones in the sense that they can be applied to models with specific flavor-structures like 2HDMs with MFV[15, 17, 18]. In this sense also our bounds are model independent, because they apply to any 2HDM with specific Yukawa structures as well (in the absence of large cancellations which are unlikely). Finally the type-III 2HDM is the decoupling limit of the MSSM and the calculated bounds can be translated to limits on the MSSM parameter space.

The fact that the 2HDM III is the decoupling limit of the MSSM also motivates us to choose for definiteness a MSSM like Higgs potential [1] which automatically avoids dangerous CP violation. The matching of the MSSM on the 2HDM Yukawa sector has been considered in detail. For the MSSM with MFV it was calculated in Ref. [19, 20, 21, 22, 23, 24] and for the MSSM with generic flavor structure in Ref. [25] (neglecting the effects of the A-terms) and in Ref. [26] (including the A-terms). Even the next-to-leading order corrections were

[1] If we would require that the Higgs potential possesses a Z_2 symmetry the results would be very similar (for $v \ll m_H$). The heavy Higgs masses squared would still differ by terms of the order of v^2 and only Higgs self-couplings would be different, but they do not enter the flavor-processes at the loop-level under consideration.

calculated for the flavor-conserving case in [27] and for the flavor-changing one in the general MSSM in Ref. [28]. Also the one-loop corrections to the Higgs potential have been considered [29, 30, 31, 32, 33, 34, 35, 36, 37], but their effects on flavor-observables were found to be small [38].

Following the notation of Ref. [26, 28, 39] we have the following Yukawa Lagrangian in the 2HDM of type III starting in an electroweak basis:

$$\mathcal{L}_Y = \bar{Q}^a_{f\,L}\left[Y^{d\,\mathrm{ew}}_{fi}\epsilon_{ba}H^{b\star}_d - \epsilon^{d\,\mathrm{ew}}_{fi}H^a_u\right]d_{i\,R} + \bar{Q}^a_{f\,L}\left[Y^{u\,\mathrm{ew}}_{fi}\epsilon_{ab}H^{b\star}_u - \epsilon^{u\,\mathrm{ew}}_{fi}H^a_d\right]u_{i\,R} + h.c. \;. \tag{1}$$

Here a, b denote $SU(2)_L$ - indices, ϵ_{ab} is the two-dimensional antisymmetric tensor with $\epsilon_{12} = -1$ and the Higgs doublets are defined as :

$$\begin{aligned} H_d &= \begin{pmatrix} H^1_d \\ H^2_d \end{pmatrix} = \begin{pmatrix} H^0_d \\ H^-_d \end{pmatrix} \text{ with } \langle H_d\rangle = \begin{pmatrix} v_d \\ 0 \end{pmatrix}, \\ H_u &= \begin{pmatrix} H^1_u \\ H^2_u \end{pmatrix} = \begin{pmatrix} H^+_u \\ H^0_u \end{pmatrix} \text{ with } \langle H_u\rangle = \begin{pmatrix} 0 \\ v_u \end{pmatrix}. \end{aligned} \tag{2}$$

Apart from the holomorphic Yukawa-couplings $Y^{u\,\mathrm{ew}}_{fi}$ and $Y^{d\,\mathrm{ew}}_{fi}$, we included the non-holomorphic couplings $\epsilon^{q\,\mathrm{ew}}_{fi}$ $(q = u, d)$ as well.

As a next step we decompose the $SU(2)$ doublets into their components and switch to a basis in which the holomorphic Yukawa couplings are diagonal:

$$\begin{aligned} \mathcal{L}_Y = &-\bar{d}_{f\,L}\left[Y^{d_i}\delta_{fi}H^{0\star}_d + \tilde{\epsilon}^d_{fi}\,H^0_u\right]d_{i\,R} - \bar{u}_{f\,L}\left[Y^{u_i}\delta_{fi}H^{0\star}_u + \tilde{\epsilon}^u_{fi}\,H^0_d\right]u_{i\,R} \\ &+\bar{u}_{f\,L}V_{fj}\left[Y^{d_i}\delta_{ji} - \cot\beta\,\tilde{\epsilon}^d_{ji}\right]H^{2\star}_d d_{i\,R} \\ &+\bar{d}_{f\,L}V^\star_{jf}\left[Y^{u_i}\delta_{ji} - \tan\beta\,\tilde{\epsilon}^u_{ji}\right]H^{1\star}_u u_{i\,R} + h.c. \;. \end{aligned} \tag{3}$$

where, $\tan\beta = v_u/v_d$ is the ratio of the vacuum expectation values v_u and v_d acquired by H_u and H_d, respectively. We perform this intermediate step, because this is the basis which corresponds to the super-CKM basis of the MSSM and the couplings $\tilde{\epsilon}^d_{ij}$ can be directly related to loop-induced non-holomorphic Higgs coupling. The wave-function rotations $U^{q\,L,R}_{fi}$ necessary to arrive at the physical basis with diagonal quark mass matrices are defined by

$$U^{q\,L\star}_{jf} m^q_{jk} U^{q\,R}_{ki} = m_{q_i}\delta_{fi}\,. \tag{4}$$

They modify the Yukawa Lagrangian as follows:

$$\begin{aligned} \mathcal{L}_Y = \; &- \; \bar{d}_{f\,L}\left[\left(\frac{m_{d_i}}{v_d}\delta_{fi} - \epsilon^d_{fi}\tan\beta\right)H^{1\star}_d + \epsilon^d_{fi}\,H^2_u\right]d_{i\,R} \\ &- \; \bar{u}_{f\,L}\left[\left(\frac{m_{u_i}}{v_u}\delta_{fi} - \epsilon^u_{fi}\cot\beta\right)H^{2\star}_u + \epsilon^u_{fi}\,H^1_d\right]u_{i\,R} \\ &+ \; \bar{u}_{f\,L}V_{fj}\left[\frac{m_{d_i}}{v_d}\delta_{ji} - (\cot\beta + \tan\beta)\,\epsilon^d_{ji}\right]H^{2\star}_d\; d_{i\,R} \\ &+ \; \bar{d}_{f\,L}V^\star_{jf}\left[\frac{m_{u_i}}{v_u}\delta_{ji} - (\tan\beta + \cot\beta)\,\epsilon^u_{ji}\right]H^{1\star}_u u_{i\,R} + h.c. \;. \end{aligned} \tag{5}$$

Here, m_{q_i} are the physical running quark masses, H_q^1 and H_q^2 are the components of the Higgs doublets, and

$$V_{fi} = U_{jf}^{u\,L*} U_{ji}^{d\,L}\,, \tag{6}$$

is the CKM matrix. The Higgs doublets H_u and H_d project onto the physical mass eigenstates H^0 (heavy CP-even Higgs), h^0 (light CP-even Higgs), A^0 (CP-odd Higgs) and $H^\pm$ in the following way:

$$\begin{aligned} H_u^0 &= \frac{1}{\sqrt{2}}\left(H^0 \sin\alpha + h^0 \cos\alpha + iA^0 \cos\beta\right)\,, \\ H_d^0 &= \frac{1}{\sqrt{2}}\left(H^0 \cos\alpha - h^0 \sin\alpha + iA^0 \sin\beta\right)\,, \\ H_u^1 &= \cos\beta\, H^+\,, \\ H_d^2 &= \sin\beta\, H^-\,, \end{aligned} \tag{7}$$

where, α is the mixing angle necessary to diagonalize the neutral CP-even Higgs mass matrix (see e.g. [40]) [2]. Since we assume a MSSM-like Higgs potential[3] we have

$$\begin{aligned} &\tan\beta = \frac{v_u}{v_d}\,, \\ &\tan 2\alpha = \tan 2\beta\, \frac{m_{A^0}^2 + M_Z^2}{m_{A^0}^2 - M_Z^2}\,, \\ &m_{H^\pm}^2 = m_{A^0}^2 + M_W^2\,, \quad m_{H^0}^2 = m_{A^0}^2 + M_Z^2 - m_{h^0}^2\,, \end{aligned} \tag{8}$$

with $\dfrac{-\pi}{2} < \alpha < 0$ and $0 < \beta < \dfrac{\pi}{2}$.

This means that in the phenomenologically interesting and viable limit of large values of $\tan\beta$ and $v \ll m_{A^0}$ we have to a good approximation[4]:

$$\begin{aligned} &\tan\beta \approx -\cot\alpha\,, \\ &m_{H^0} \approx m_{H^\pm} \approx m_{A^0} \equiv m_H\,. \end{aligned} \tag{9}$$

Without the non-holomorphic corrections ϵ_{ij}^q, the rotation matrices $U_{fi}^{q\,L,R}$ would simultaneously diagonalize the mass terms and the neutral Higgs couplings in Eq. (5). However, in the presence of non-holomorphic corrections, this is no longer the case and flavor changing neutral Higgs couplings are present in the basis in which the physical quark mass matrices are diagonal.

The Yukawa Lagrangian in Eq. (5) leads to the following Feynman rules[5] for Higgs-quark-quark couplings

$$i\left(\Gamma_{q_f q_i}^{LR\,H} P_R + \Gamma_{q_f q_i}^{RL\,H} P_L\right) \tag{10}$$

[2]Note that we defined α as common in the MSSM. In the 2HDM also a convention with a doubled range for α is used.

[3]MSSM-like Higgs potential implies that in the large $\tan\beta$ limit and for $v \ll m_H$ the charged Higgs mass $m_{H^\pm}$, the heavy CP even Higgs mass m_{H^0} and the CP odd Higgs mass m_{A^0} are equal.

[4]For the SM-like Higgs boson h^0 we use $m_{h^0} \approx 125$ GeV in our numerical analysis.

[5]Hermiticity of the Lagrangian implies the relation $\Gamma_{q_f q_i}^{RL\,H} = \Gamma_{q_i q_f}^{LR\,H\,\star}$.

with

$$
\begin{aligned}
\Gamma^{LR\,H_k^0}_{u_f u_i} &= x_u^k \left(\frac{m_{u_i}}{v_u} \delta_{fi} - \epsilon^u_{fi} \cot\beta \right) + x_d^{k\star} \epsilon^u_{fi} \,, \\
\Gamma^{LR\,H_k^0}_{d_f d_i} &= x_d^k \left(\frac{m_{d_i}}{v_d} \delta_{fi} - \epsilon^d_{fi} \tan\beta \right) + x_u^{k\star} \epsilon^d_{fi} \,, \\
\Gamma^{LR\,H^\pm}_{u_f d_i} &= \sum_{j=1}^{3} \sin\beta\, V_{fj} \left(\frac{m_{d_i}}{v_d} \delta_{ji} - \epsilon^d_{ji} \tan\beta \right) \,, \\
\Gamma^{LR\,H^\pm}_{d_f u_i} &= \sum_{j=1}^{3} \cos\beta\, V^\star_{jf} \left(\frac{m_{u_i}}{v_u} \delta_{ji} - \epsilon^u_{ji} \tan\beta \right) \,.
\end{aligned} \tag{11}
$$

Similarly, for the lepton case, the non-vanishing effective Higgs vertices are

$$
\begin{aligned}
\Gamma^{LR\,H_k^0}_{\ell_f \ell_i} &= x_d^k \left(\frac{m_{\ell_i}}{v_d} \delta_{fi} - \epsilon^\ell_{fi} \tan\beta \right) + x_u^{k\star} \epsilon^\ell_{fi} \,, \\
\Gamma^{LR\,H^\pm}_{\nu_f \ell_i} &= \sum_{j=1}^{3} \sin\beta\, V^{\rm PMNS}_{fj} \left(\frac{m_{\ell_i}}{v_d} \delta_{ji} - \epsilon^\ell_{ji} \tan\beta \right) \,.
\end{aligned} \tag{12}
$$

Here, $H_k^0 = (H^0, h^0, A^0)$ and the coefficients x_q^k are given by

$$
\begin{aligned}
x_u^k &= \left(-\frac{1}{\sqrt{2}} \sin\alpha,\ -\frac{1}{\sqrt{2}} \cos\alpha,\ \frac{i}{\sqrt{2}} \cos\beta \right) \,, \\
x_d^k &= \left(-\frac{1}{\sqrt{2}} \cos\alpha,\ \frac{1}{\sqrt{2}} \sin\alpha,\ \frac{i}{\sqrt{2}} \sin\beta \right) \,.
\end{aligned} \tag{13}
$$

This means that flavor-violation (beyond the one already present in the 2HDM of type II) is entirely governed by the couplings $\epsilon^{q,\ell}_{ij}$. If one wants to make the connection to the MSSM, the parameters $\epsilon^{q,\ell}_{ij}$ will depend only on SUSY breaking parameters and $\tan\beta$.

3 Constraints on the 2HDM parameter space– general discussion and overview

In this section we give an overview on flavor observables sensitive to charged Higgs contributions. We review the constraints on the 2HDM of type II and discuss to which extent these bounds will hold in the 2HDM of type III. A detailed analysis of flavor constraints on the type-III 2HDM parameter space will be given in the following sections.

The most common version of 2HDMs, concerning its Yukawa sector, is the 2HDM of type II which respects natural flavor conservation [41] by requiring that one Higgs doublet couples only to up-quarks while the other one gives masses to down-type quarks and charged leptons (like the MSSM at tree-level). Flavor-observables in 2HDMs of type II have been studied in detail [42, 43, 44]. In the type II model there are no tree-level flavor-changing neutral currents and all flavor violation is induced by the CKM matrix entering the charged Higgs vertex. In this way the constraints from FCNC processes can be partially avoided. This is true for $\Delta F = 2$ processes where the charged Higgs contribution is small, for $K_L \to \mu^+\mu^-$, $D^0 \to \mu^+\mu^-$ (due to the tiny Higgs couplings to light quarks) and all flavor observables in the lepton sector. However, the FCNC processes $b \to s\gamma$ (also to less extent $b \to d\gamma$) and $B_s \to \mu^+\mu^-$ are sensitive the charged Higgs contributions. In addition, direct searches at the LHC and charged current processes restrict the type-II 2HDM parameter space.

Among the FCNC processes, the constraints from $b \to s\gamma$ are most stringent due to the necessarily constructive interference with the SM contribution [45, 46, 47, 48]. The most recent lower bound on the charged Higgs mass obtained in Ref. [49] is $m_{H^\pm} \geq 360\,\mathrm{GeV}$ which includes NNLO QCD corrections and is rather independent of $\tan\beta$. In the type-III 2HDM this lower bound on the charged Higgs mass can be weakened due to destructive interference with contributions involving ϵ^q_{ij}. Also in $B_s \to \mu^+\mu^-$ (and $B_d \to \mu^+\mu^-$) a sizable loop-induced effect is possible in the 2HDM II, but the constrains are still not very stringent even if the new LHCb measurement are used. The reason for this is that, taking into account the constraints from $b \to s\gamma$ on the charged Higgs mass, the branching ratio for $B_s \to \mu^+\mu^-$ in the 2HDM II is even below the SM expectation for larger values of $\tan\beta$ [50, 51, 52] due to the destructive interference between the charged Higgs and the SM contribution.

Regarding charged current processes, tauonic B decays are currently most sensitive to charged Higgs effects. Here, the charged-Higgs contribution in the type-II 2HDM to $B \to \tau\nu$ interferes destructively with the SM contribution [53, 54]. The same is true for $B \to D^*\tau\nu$ [55] and $B \to D\tau\nu$ [42, 56, 57]. As outlined in the introduction this leads to the fact that the 2HDM II cannot explain $B \to \tau\nu$, $B \to D\tau\nu$ and $B \to D^*\tau\nu$ simultaneously [8]. Other charged current observables sensitive to charged Higgses are $D_{(s)} \to \mu\nu$, $D_{(s)} \to \tau\nu$ [58, 59, 60], $\tau \to K(\pi)\nu$ and $K \to \mu\nu/\pi \to \mu\nu$ [61] (see [44] for a global analysis).

Fig. 1 shows our updated constraints on the 2HDM II parameters space from $b \to s\gamma$, $B \to \tau\nu$, $B \to D\tau\nu$, $B \to D^*\tau\nu$, $B_s \to \mu^+\mu^-$ and $K \to \mu\nu/\pi \to \mu\nu$. We see that in order to get agreement within $2\,\sigma$ between the theory prediction and the measurement of $B \to D^*\tau\nu$, large values of $\tan\beta$ and light Higgs masses would be required which is in conflict with all other processes under consideration.

Concerning direct searches the bounds on the charged Higgs mass are rather weak due to the large background from W events. The search for neutral Higgs bosons is easier and the CMS bounds[6] on m_{A^0} from $A^0 \to \tau^+\tau^-$ are shown in Fig. 2. These bounds were obtained in the MSSM, but since the MSSM corrections to $A^0 \to \tau^+\tau^-$ are rather small and since we consider a MSSM-like Higgs potential, these bounds also hold in the 2HDM III as long as the Peccei-Quinn symmetry breaking in the lepton sector is small [7].

Going beyond the simple Yukawa structure of the 2HDM of type II, also 2HDMs of type III with MFV [15, 17, 18], alignment [64, 65] or natural flavor conservation [17, 41] have been analyzed in detail. However, flavor-observables in type III models with generic flavor-structure have received much less attention. Ref. [66] considered the possible effects of the flavor-diagonal terms and Ref. [67] considers leptonic observables. As outlined in the introduction, 2HDMs of type II (or type III with MFV) cannot explain $B \to D\tau\nu$ and $B \to D^*\tau\nu$ simultaneously [8] (and for $B \to \tau\nu$ fine tuning is needed [18]).

In the following sections we will study in detail the flavor-observables in the 2HDM with generic flavor-structure [68], but for definiteness, with MSSM-like Higgs potential. For this

[6] Note that we did not use the bounds from unpublished CMS update of the $A^0 \to \tau^+\tau^-$ analysis.

[7] For a global analysis of electroweak precision constraints see for example Ref. [62].

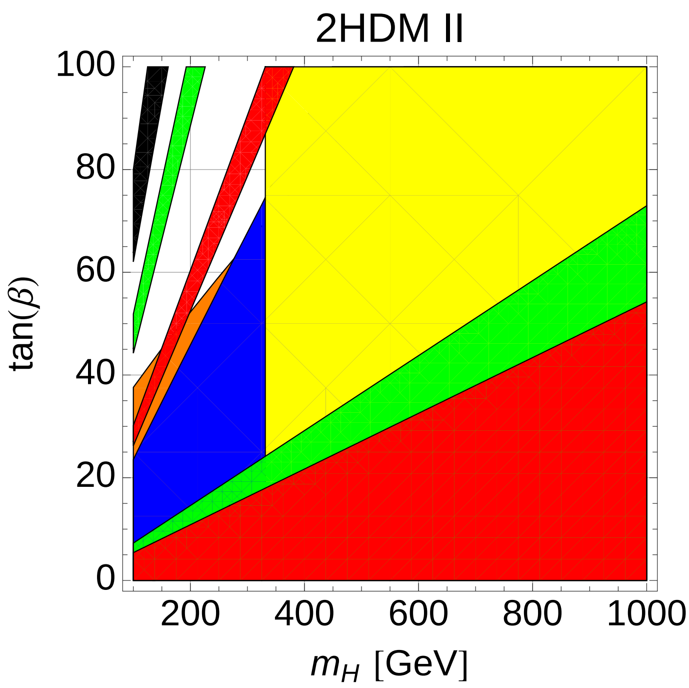

Figure 1: Updated constraints on the 2HDM of type II parameter space. The regions compatible with experiment are shown (the regions are superimposed on each other): $b \to s\gamma$ (yellow), $B \to D\tau\nu$ (green), $B \to \tau\nu$ (red), $B_s \to \mu^+\mu^-$ (orange), $K \to \mu\nu/\pi \to \mu\nu$ (blue) and $B \to D^*\tau\nu$ (black). Note that no region in parameter space is compatible with all processes. Explaining $B \to D^*\tau\nu$ would require very small Higgs masses and large values of $\tan\beta$ which is not compatible with the other observables. To obtain this plot, we added the theoretical uncertainty linear on the top of the $2\,\sigma$ experimental error.

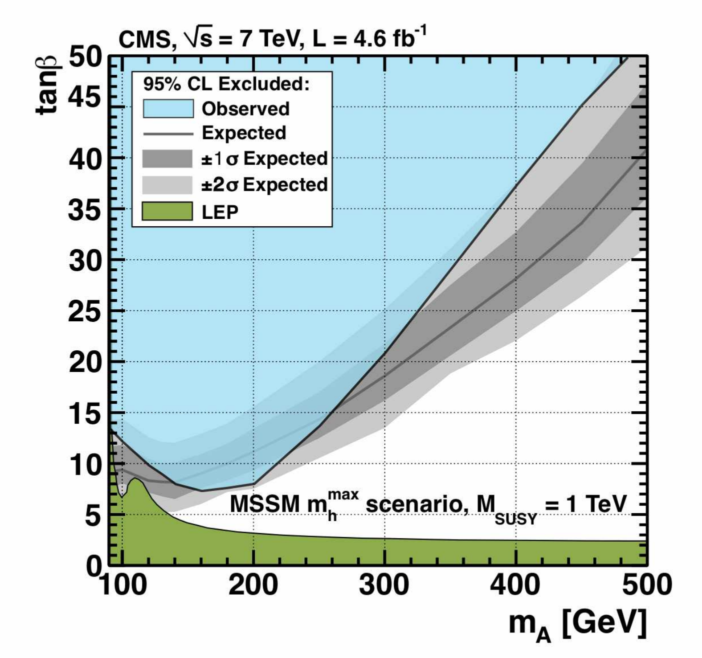

Figure 2: Plot from the CMS collaboration taken from Ref. [63]: Exclusion limts in the m_{A^0}–$\tan\beta$ plane from $A^0 \to \tau^+\tau^-$. The analysis was done in the MSSM, but since we consider a 2HDM with MSSM-like Higgs potential and the MSSM corrections to the $A^0\tau\tau$ vertex are small, we can apply this bound to our model. However, a large value of ϵ^{ℓ}_{33} in the 2HDM of type III could affect the conclusions. Note that in the limit $v \ll m_H$ all heavy Higgs masses (m_{H^0}, m_{A^0} and $m_{H^\pm}$) are approximately equal.

purpose, all processes described above are relevant. In addition, $\Delta F = 2$ processes, lepton flavor violating observables (LFV), EDMs, $\tau \to K(\pi)\nu/K(\pi) \to \mu\nu$ and $K \to \mu(e)\nu/\pi \to \mu(e)\nu$ will turn out to give information on the flavor structure of the 2HDM of type III. Furthermore, we will investigate to which extent contributions to $B_{s,d} \to \tau\mu$, $B_{s,d} \to \tau e$, $B_{s,d} \to \mu e$ and muon anomalous magnetic moment are possible.

4 Constraints from 't Hooft's naturalness criterion

The naturalness criterion of 't Hooft states that the smallness of a quantity is only natural if a symmetry is gained in the limit in which this quantity is zero. This means on the other hand that large accidental cancellations, which are not enforced by a symmetry, are unnatural and thus not desirable. Let us apply this reasoning to the fermion mass matrices in the 2HDM. We recall from the last section the expressions for the fermion mass matrices in the electroweak basis:

$$\begin{aligned} m_{ij}^{d} &= v_d Y_{ij}^{d\,\mathrm{ew}} + v_u \epsilon_{ij}^{d\,\mathrm{ew}} \,, \\ m_{ij}^{u} &= v_u Y_{ij}^{u\,\mathrm{ew}} + v_d \epsilon_{ij}^{u\,\mathrm{ew}} \,, \\ m_{ij}^{\ell} &= v_d Y_{ij}^{\ell\,\mathrm{ew}} + v_u \epsilon_{ij}^{\ell\,\mathrm{ew}} \,. \end{aligned} \tag{14}$$

Diagonalizing these fermion mass matrices gives the physical fermion masses and the CKM matrix. Using 't Hooft's naturalness criterion we can demand the absence of fine-tuned cancellations between $v_d Y_{ij}^{d,\ell}$ ($v_u Y_{ij}^{u}$) and $v_u \epsilon_{ij}^{d,\ell}$ ($v_d \epsilon_{ij}^{u}$). Thus, we require that the contributions of $v_u \epsilon_{ij}^{d,\ell}$ and $v_d \epsilon_{ij}^{u}$ to the fermion masses and CKM matrix do not exceed the physical measured quantities.

In first order of a perturbative diagonalization of the fermion mass matrices, the diagonal elements m_{ii}^{f} give rise to the fermion masses, while (in our conventions) the elements m_{ij}^{f} with $i < j$ ($i > j$) affect the left-handed (right-handed) rotations necessary to diagonalize the fermion mass matrices. The left-handed rotations of the quark fields are linked to the CKM matrix and can therefore be constrained by demanding that the physical CKM matrix is generated without a significant degree of fine-tuning. However, the right-handed rotations of the quarks are not known and the mixing angles of the PMNS matrix are big so that for these two cases we can only demand that the fermion masses are generated without too large accidental cancellations. Note, that in Eq. (14) the elements $\epsilon_{ij}^{f\,\mathrm{ew}}$ enter, while the elements ϵ_{ij}^{f} which we want to constrain from flavor observables are given in the physical basis with diagonal fermion masses. This means that in order to constrain ϵ_{ij}^{f} from 't Hooft's naturalness criterion we have to assume in addition that no accidental cancellation occur by switching between the electroweak basis and the physical basis. In conclusion this leads to the following upper bounds

$$\begin{aligned} \left| v_{u(d)} \epsilon_{ij}^{d(u)} \right| &\leq \left| V_{ij}^{\mathrm{CKM}} \right| \times \max\left[m_{d_i(u_i)}, m_{d_j(u_j)} \right] \;\text{ for } i < j \,, \\ \left| v_{u(d)} \epsilon_{ij}^{d(u)} \right| &\leq \max\left[m_{d_i(u_i)}, m_{d_j(u_j)} \right] \;\text{ for } i \geq j \,, \\ \left| v_u \epsilon_{ij}^{\ell} \right| &\leq \max\left[m_{\ell_i}, m_{\ell_j} \right] \,. \end{aligned} \tag{15}$$

In the large $\tan\beta$ limit, inserting the quark masses $m_q(\mu)$ at the Higgs scale (which we choose here to be $\mu_{\rm Higgs} = 500\,{\rm GeV}$), we can immediately read off the upper bounds on $\epsilon^{u,d,\ell}_{ij}$ from Eq. (15):

$$
\begin{aligned}
\left|\epsilon^d_{ij}\right| &\leq \begin{pmatrix} 1.3\times10^{-4} & 5.8\times10^{-5} & 5.1\times10^{-5} \\ 2.6\times10^{-4} & 2.6\times10^{-4} & 5.9\times10^{-4} \\ 1.4\times10^{-2} & 1.4\times10^{-2} & 1.4\times10^{-2} \end{pmatrix}_{ij}, \\
\left|\epsilon^u_{ij}\right| &\leq (\tan\beta/50) \begin{pmatrix} 3.4\times10^{-4} & 3.2\times10^{-2} & 1.6\times10^{-1} \\ 1.4\times10^{-1} & 1.4\times10^{-1} & 1.9 \\ - & - & - \end{pmatrix}_{ij}, \\
\left|\epsilon^\ell_{ij}\right| &\leq \begin{pmatrix} 2.9\times10^{-6} & 6.1\times10^{-4} & 1.0\times10^{-2} \\ 6.1\times10^{-4} & 6.1\times10^{-4} & 1.0\times10^{-2} \\ 1.0\times10^{-2} & 1.0\times10^{-2} & 1.0\times10^{-2} \end{pmatrix}_{ij}.
\end{aligned}
\tag{16}
$$

Of course, these constraints are not strict bounds in the sense that they must be respected in any viable model. Anyway, big violation of naturalness is not desirable and Eq. (16) gives us a first glance on the possible structure of the elements ϵ^f_{ij}. As we will see later, it is possible to explain $B\to\tau\nu$, $B\to D\tau\nu$ and $B\to D^*\tau\nu$ using $\epsilon^u_{31,32}$ without violating Eq. (16), while if one wants to explain $B\to\tau\nu$ with ϵ^d_{33} 't Hooft's naturalness criterion is violated.

5 Constraints from tree-level neutral-current processes

The flavor off-diagonal elements ϵ^f_{ij} (with $i\neq j$) give rise to flavor-changing neutral currents (FCNCs) already at the tree-level. Comparing the Higgs contributions to the loop-suppressed SM contributions, large effects are in principle possible. However, all experimental results are in very good agreement with SM predictions, which put extremely stringent constraints on the non-holomorphic terms ϵ^f_{ij}.

In this section we consider three different kinds of processes:

- Muonic decays of neutral mesons ($B_{s,d}\to\mu^+\mu^-$, $K_L\to\mu^+\mu^-$ and $\bar{D}^0\to\mu^+\mu^-$).
- $\Delta F=2$ processes ($D-\overline{D}$, $K-\overline{K}$, $B_s-\overline{B}_s$ and $B_d-\overline{B}_d$ mixing).
- Flavor changing lepton decays ($\tau^-\to\mu^-\mu^+\mu^-$, $\tau^-\to e^-\mu^+\mu^-$ and $\mu^-\to e^-e^+e^-$).

As we will see in detail in Sec. 5.1, the leptonic neutral meson decays $B_{s,d}\to\mu^+\mu^-$, $K_L\to\mu^+\mu^-$ and $\bar{D}^0\to\mu^+\mu^-$ put constraints on the elements ϵ^d_{ij} (with $i\neq j$) and $\epsilon^u_{12,21}$ already if one of these elements is non-zero, while $B_d-\overline{B}_d$, $B_s-\overline{B}_s$, $K-\overline{K}$ and $D-\overline{D}$ mixing only provide constraints on the products $\epsilon^d_{ij}\epsilon^{d\star}_{ji}$ and $\epsilon^u_{12}\epsilon^{u\star}_{21}$ (Sec. 5.2). This means that the constraints on $\Delta F=2$ processes can be avoided if one element of the product $\epsilon^q_{ij}\epsilon^{q\star}_{ji}$ is zero, while the constraints from the leptonic neutral meson decays can only be avoided if the Peccei Quinn symmetry breaking for the leptons is large such that $\epsilon^\ell_{22}\approx m_\mu/v_u$ is possible.

In Sec. 5.3 we will consider the flavor changing lepton decays $\tau^-\to\mu^-\mu^+\mu^-$, $\tau^-\to e^-\mu^+\mu^-$ and $\mu^-\to e^-e^+e^-$ which constrain the off-diagonal elements $\epsilon^\ell_{23,32}$, $\epsilon^\ell_{13,31}$ and $\epsilon^\ell_{12,21}$, respectively.

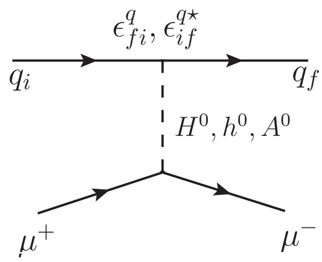

Figure 3: Feynman diagram showing the neutral Higgs contribution to $B_{s,d} \to \mu^+\mu^-$, $K_L \to \mu^+\mu^-$ and $\bar{D}^0 \to \mu^+\mu^-$.

5.1 Leptonic neutral meson decays: $B_{s,d} \to \mu^+\mu^-$, $K_L \to \mu^+\mu^-$ and $\bar{D}^0 \to \mu^+\mu^-$

Muonic decays of neutral mesons ($B_s \to \mu^+\mu^-$, $B_d \to \mu^+\mu^-$, $K_L \to \mu^+\mu^-$ and $\bar{D}^0 \to \mu^+\mu^-$) are strongly suppressed in the SM for three reasons: they are loop-induced, helicity suppressed and they involve small CKM elements. Therefore, their branching ratios (in the SM) are very small and in fact only $K_L \to \mu^+\mu^-$ and recently also $B_s \to \mu^+\mu^-$ [69] have been measured, while for the other decays only upper limits on the branching ratios exist (see Table 7). We do not consider decays to electrons (which are even stronger helicity suppressed) nor $B_{d,s} \to \tau^+\tau^-$ (where the tau leptons are difficult to reconstruct) because the experimental limits are even weaker. The study of meson decays to lepton flavor-violating final states is postponed to Sec. 8.

Process	Experimental value	SM prediction
$\mathcal{B}\,[B_s \to \mu^+\mu^-]$	$3.2^{+1.5}_{-1.2} \times 10^{-9}$ [69]	$(3.23 \pm 0.27) \times 10^{-9}$ [70]
$\mathcal{B}\,[B_d \to \mu^+\mu^-]$	$\leq\ 9.4 \times 10^{-10}$ (95% CL) [69]	$(1.07 \pm 0.10) \times 10^{-10}$ [70]
$\mathcal{B}\,[K_L \to \mu^+\mu^-]_{\text{short}}$	$\leq 2.5 \times 10^{-9}$ [71]	$\approx 0.9 \times 10^{-9}$ [71]
$\mathcal{B}\,\left[D^0 \to \mu^+\mu^-\right]$	$\leq\ 1.4 \times 10^{-7}$ (90% CL) [72]	–

Table 7: Experimental values and SM predictions for the branching ratios of neutral meson decays to muon pairs. For $K_L \to \mu^+\mu^-$ we only give the upper limit on the computable short distance contribution [71] extracted from the experimental value $(6.84\ \pm\ 0.11) \times 10^{-9}$ (90% CL) [72]. The SM prediction for $D^0 \to \mu^+\mu^-$ cannot be reliably calculated due to hadronic uncertainties.

We see from Fig. 3 that the off-diagonal elements of $\epsilon^d_{13,31}$, $\epsilon^d_{23,32}$, $\epsilon^d_{12,21}$ and $\epsilon^u_{12,21}$ directly give rise to tree-level neutral Higgs contributions to $B_d \to \mu^+\mu^-$, $B_s \to \mu^+\mu^-$, $K_L \to \mu^+\mu^-$ and $\bar{D}^0 \to \mu^+\mu^-$, respectively.

In principle, the constraints from these processes could be weakened, or even avoided, if $\epsilon^\ell_{22} \approx m_{\ell_2}/v_u$. Anyway, in this section we will assume that the Peccei Quinn breaking for the leptons is small and neglect the effect of ϵ^ℓ_{22} in our numerical analysis for setting limits on ϵ^q_{ij}.

5.1.1 $B_{s,d} \to \mu^+\mu^-$

For definiteness, consider the decay of a neutral $B_s\,(\bar{b}s)$ meson (the corresponding decay of a B_d meson follow trivially by replacing s with d and 2 with 1) to a muon pair. The effective Hamiltonian governing this transition is[8]

$$\mathcal{H}_{\rm eff}^{B_s\to\mu^+\mu^-} = -\frac{G_F^2 M_W^2}{\pi^2}\left[C_A^{bs}O_A^{bs} + C_S^{bs}O_S^{bs} + C_P^{bs}O_P^{bs} + C_A^{\prime bs}O_A^{\prime bs} + C_S^{\prime bs}O_S^{\prime bs} + C_P^{\prime bs}O_P^{\prime bs}\right] + h.c.\,, \tag{17}$$

where the operators are defined as

$$\begin{aligned} O_A^{bs} &= \left(\bar{b}\gamma_\mu P_L s\right)\left(\bar{\mu}\gamma^\mu\gamma_5\mu\right)\,, \\ O_S^{bs} &= \left(\bar{b}P_L s\right)\left(\bar{\mu}\mu\right)\,, \\ O_P^{bs} &= \left(\bar{b}P_L s\right)\left(\bar{\mu}\gamma_5\mu\right)\,, \end{aligned} \tag{18}$$

and the primed operators are obtained replacing P_L with P_R. The corresponding expression for the branching ratio in terms of the Wilson coefficients reads

$$\begin{aligned} \mathcal{B}\left[B_s \to \mu^+\mu^-\right] = &\frac{G_F^4 M_W^4}{8\pi^5}\sqrt{1-4\frac{m_\mu^2}{M_{B_s}^2}}\,M_{B_s}\,f_{B_s}^2\,m_\mu^2\,\tau_{B_s} \\ &\times\left[\left|\frac{M_{B_s}^2\left(C_P^{bs}-C_P^{\prime bs}\right)}{2\left(m_b+m_s\right)m_\mu} - \left(C_A^{bs}-C_A^{\prime bs}\right)\right|^2 + \left|\frac{M_{B_s}^2\left(C_S^{bs}-C_S^{\prime bs}\right)}{2\left(m_b+m_s\right)m_\mu}\right|^2 \times\left(1-4\frac{m_\mu^2}{m_{B_s}^2}\right)\right]\,. \end{aligned} \tag{19}$$

Concerning the running of the Wilson coefficients due to the strong interaction, the operators O_A^{bs} and $O_A^{\prime bs}$ correspond to conserved vector currents with vanishing anomalous dimensions. This means that their Wilson coefficients are scale independent. The scalar and pseudo-scalar Wilson coefficients C_S^{bs} and C_P^{bs} ($C_S^{\prime bs}$ and $C_P^{\prime bs}$) have the same anomalous dimension as quark masses in the SM which means that their scale dependence is given by:

$$C_{S,P}^{(\prime)bs}\left(\mu_{low}\right) = \frac{m_q(\mu_{low})}{m_q(\mu_{high})}\,C_{S,P}^{(\prime)bs}\left(\mu_{high}\right), \tag{20}$$

where m_q is the running quark mass with the appropriate number of active flavors. In the SM, C_A is the only non-vanishing Wilson coefficient

$$C_A^{bs} = -V_{tb}^\star V_{ts} Y\left(\frac{m_t^2}{M_W^2}\right) - V_{cb}^\star V_{cs} Y\left(\frac{m_c^2}{M_W^2}\right)\,, \tag{21}$$

where, the function Y is defined as $Y = \eta_Y Y_0$ such that the NLO QCD effects are included in $\eta_Y = 1.0113$ [70] and the one loop Inami-Lim function Y_0 reads [73]

$$Y_0(x) = \frac{x}{8}\left[\frac{4-x}{1-x} + \frac{3\,x}{(1-x)^2}\ln(x)\right]\,. \tag{22}$$

The complete Wilson coefficients for general quark-quark-scalar couplings are given in the appendix. In the 2HDM of type III, in the case of large $\tan\beta$ and $v \ll m_H$, the terms

[8] The complete expression for the Hamiltonian and the branching ratio including lepton flavor-violating final states is given in the appendix.

involving ϵ^q_{ij} simplify to

$$\begin{aligned} C_S^{bs} &= C_P^{bs} = -\frac{\pi^2}{G_F^2 M_W^2}\frac{1}{2m_H^2}\frac{m_{\ell_2} - v_u\epsilon^\ell_{22}}{v}\epsilon^{d\star}_{23}\tan^2\beta\,, \\ C_S^{\prime bs} &= -C_P^{\prime bs} = -\frac{\pi^2}{G_F^2 M_W^2}\frac{1}{2m_H^2}\frac{m_{\ell_2} - v_u\epsilon^\ell_{22}}{v}\epsilon^{d}_{32}\tan^2\beta\,. \end{aligned} \tag{23}$$

To these Wilson coefficients the well known loop-induced type II 2HDM contributions[9]

$$C_S^{bs} = C_P^{bs} = -\frac{m_b V_{tb}^\star V_{ts}}{2}\frac{m_\mu}{2M_W^2}\tan^2\beta\,\frac{\log\left(m_H^2/m_t^2\right)}{m_H^2/m_t^2 - 1}\,, \tag{24}$$

have to be added as well [52]. Note that since we give the Wilson coefficients at the matching scale, also m_b and m_t must be evaluated at this scale.

We can now constrain the elements $\epsilon^d_{23,32}$ and $\epsilon^d_{13,31}$ by demanding that the experimental bounds are satisfied within two standard deviations for $B_s \to \mu^+\mu^-$ or equivalently at the 95% CL concerning $B_d \to \mu^+\mu^-$. The results for the constraints on ϵ^d_{23} and ϵ^d_{32} (ϵ^d_{13} and ϵ^d_{31}) from $B_s \to \mu^+\mu^-$ ($B_d \to \mu^+\mu^-$) are shown in Fig. 4 (Fig. 5).

All constraints on $\epsilon^d_{13,31}$ and $\epsilon^d_{23,32}$ are very stringent; of the order of 10^{-5}. Both an enhancement or a suppression of $\mathcal{B}\left[B_{d,s} \to \mu^+\mu^-\right]$ compared to the SM prediction is possible. While in the 2HDM II the minimal value for $\mathcal{B}\left[B_{d,s} \to \mu^+\mu^-\right]$ is half the SM prediction, in the 2HDM III also a bigger suppression of $B_{d,s} \to \mu^+\mu^-$ is possible if $\epsilon^d_{13,23} \neq 0$. In principle, the constraints on ϵ^d_{23} (ϵ^d_{13}) from $B_{s(d)} \to \mu^+\mu^-$ are not independent of ϵ^d_{32} (ϵ^d_{31}). Anyway, in the next section it will turn out that the constraints from $\Delta F = 2$ processes are more stringent if both ϵ^d_{32} and ϵ^d_{23} are different from zero (the same conclusions hold for $\epsilon^d_{31,13}$, $\epsilon^d_{21,12}$ and $\epsilon^u_{21,12}$).

$B_s \to \mu^+\mu^-$ and $B_d \to \mu^+\mu^-$ can also be used to constrain the leptonic parameter ϵ^ℓ_{22}. We will discuss the corresponding subject in Sec.6.

5.1.2 $K_L \to \mu^+\mu^-$

Concerning $K_L \to \mu^+\mu^-$, the branching ratio and the Wilson coefficients can be obtained by a simple replacement of indices from Eq. (19), Eq. (21) and Eq. (23). Due to the presence of large non-perturbative QCD effects, we require that the 2HDM III contribution together with the short distance piece of the SM contribution does not exceed the upper limit on the short distance contribution to the branching ratio calculated in Ref. [71]. The resulting constraints on $\epsilon^d_{12,21}$ are shown in Fig. 6. They are found to be extremely stringent (of the order of 10^{-6}).

5.1.3 $\bar{D}^0 \to \mu^+\mu^-$

The analogous expressions for the branching ratio for $\bar{D}^0 \to \mu^+\mu^-$ ($\bar{D}^0(\bar{c}u)$) follow by a straightforward replacement of indices in Eq. (19) but the Wilson coefficients in the type-III

[9] Since we want to put constraints on the elements $\epsilon^d_{13,23}$ we assume that the loop-induced 2HDM II contribution is not changed by elements ϵ^u_{i3} or ϵ^d_{33}.

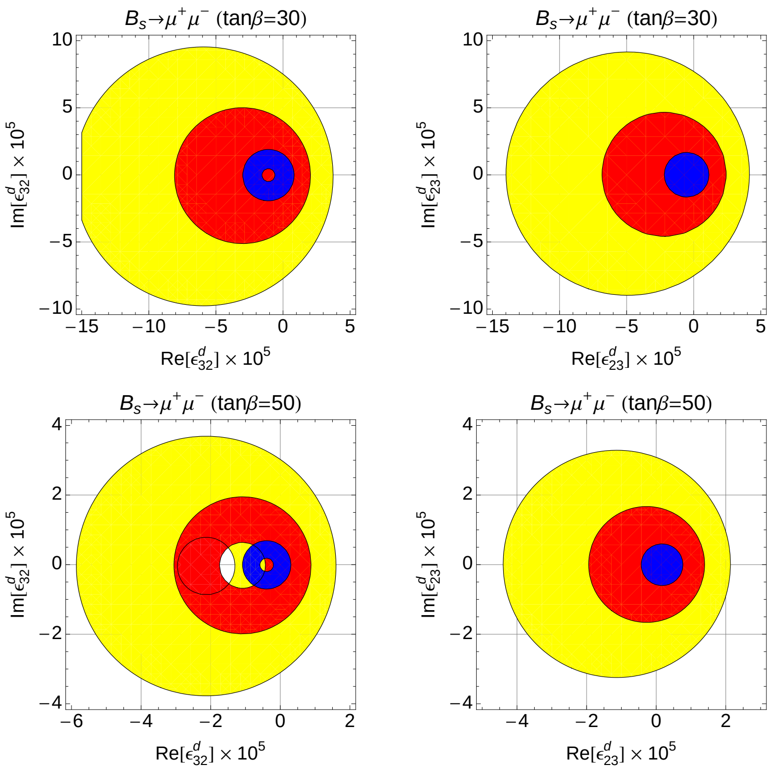

Figure 4: Allowed regions in the complex $\epsilon^d_{23,32}$–plane from $B_s \to \mu^+\mu^-$ for $\tan\beta = 30$, $\tan\beta = 50$ and $m_H = 700$ GeV (yellow), $m_H = 500$ GeV (red) and $m_H = 300$ GeV (blue). Note that the allowed regions for ϵ^d_{32}–plane are not full circles because in this case a suppression of $\mathcal{B}\,[B_s \to \mu^+\mu^-]$ below the experimental lower bound is possible.

2HDM for $\bar{D}^0 \to \mu^+\mu^-$ have a different dependence on $\tan\beta$:

$$\begin{aligned} C_S^{cu} = -C_P^{cu} &= \frac{\pi^2}{G_F^2 M_W^2} \frac{1}{2m_H^2} \frac{m_{\ell_2} - v_u \epsilon^\ell_{22}}{v} \epsilon^{u\star}_{12} \tan\beta \,, \\ C_S^{\prime cu} = C_P^{\prime cu} &= \frac{\pi^2}{G_F^2 M_W^2} \frac{1}{2m_H^2} \frac{m_{\ell_2} - v_u \epsilon^\ell_{22}}{v} \epsilon^{u}_{21} \tan\beta \,. \end{aligned} \tag{25}$$

Differently than for $B_{d,s} \to \mu^+\mu^-$ the SM contribution cannot be calculated due to non-perturbative effects and the 2HDM II contribution is numerically irrelevant. Since we do not know the SM contribution, we require that the 2HDM III contribution alone does not generate more than the experimental upper limit on this branching ratio.

It is then easy to express the constraints on $\epsilon^u_{12,21}$ in terms of the parameters m_H and $\tan\beta$:

$$\left|\epsilon^u_{12,21}\right| \;\leq\; 3.0 \times 10^{-2} \frac{\left(m_H/500\,\mathrm{GeV}\right)^2}{\tan\beta/50} \,. \tag{26}$$

The resulting bounds on $\epsilon^u_{12,21}$ (setting one of these elements to zero) are shown in Fig. 7.

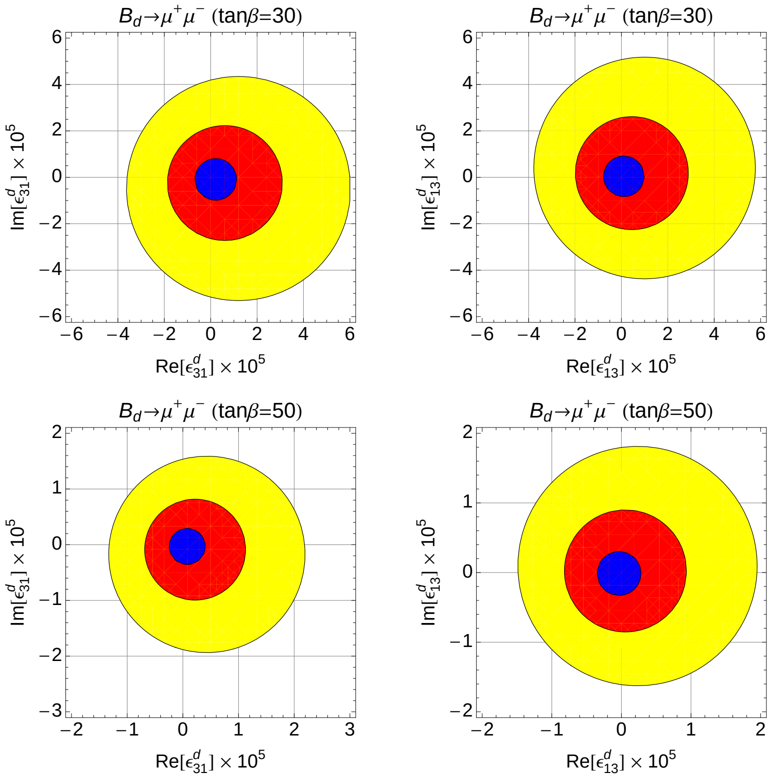

Figure 5: Allowed regions in the complex $\epsilon^d_{13,31}$–plane from $B_d \to \mu^+\mu^-$ for $\tan\beta = 30$, $\tan\beta = 50$ and $m_H = 700$ GeV(yellow), $m_H = 500$ GeV(red) and $m_H = 300$ GeV(blue).

5.2 Tree-level contributions to $\Delta F = 2$ processes

In the presence of non-zero elements ϵ^q_{ij} neutral Higgs mediated contributions to neutral meson mixing ($B_{d,s}$–$\overline{B}_{d,s}$, K–$\overline{K}$ and D–$\overline{D}$ mixing) arise (see Fig. 8). In these processes, the 2HDM contribution vanishes if the $U(1)_{\rm PQ}$ symmetry is conserved. This has the consequence that the leading $\tan\beta$-enhanced tree-level contribution to the $\Delta F = 2$ processes (shown in Fig. 8) is only non-vanishing if ϵ^q_{ij} and ϵ^q_{ji} are simultaneously different from zero (in the approximation $m_{A^0} = m_{H^0}$ and $\cot\beta = 0$). Making use of the effective Hamiltonian defined in Eq. (84) of the appendix we get the following contributions to B_s–$\overline{B}_s$ mixing (the expressions for B_d–$\overline{B}_d$ and K–$\overline{K}$ mixing again follow by a simple replacement of indices):

$$C_4 = -\frac{\epsilon^d_{23}\epsilon^{d\star}_{32}}{m_H^2}\tan^2\beta\,. \tag{27}$$

All other Wilson coefficients are sub-leading in $\tan\beta$. For D mixing, again only C_4 is non-zero and given by

$$C_4 = -\frac{\epsilon^u_{12}\epsilon^{u\star}_{21}}{m_H^2}\,. \tag{28}$$

After performing the renormalization group evolution [74, 75, 76, 77, 78] (here we used $\mu_H = 500$ GeV at the high scale) it turns out that the dominant contribution to the hadronic matrix elements stems from O_4. Inserting the bag factors [79, 80] and decay constants from

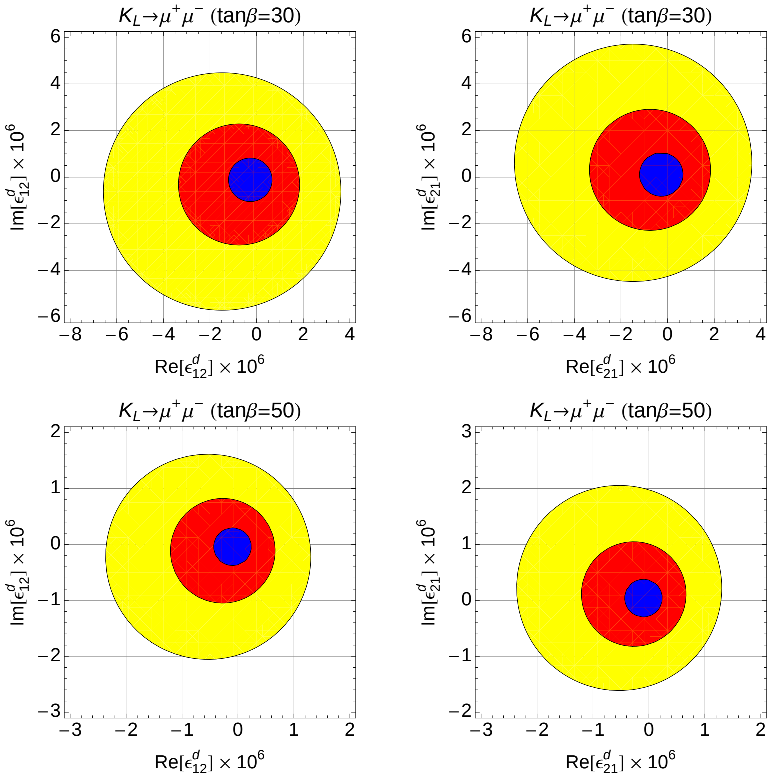

Figure 6: Allowed regions in the complex $\epsilon^d_{12,21}$-plane from $K_L \to \mu^+\mu^-$ for $\tan\beta = 30$, $\tan\beta = 50$ and $m_H = 700$ GeV(yellow), $m_H = 500$ GeV(red) and $m_H = 300$ GeV(blue).

lattice QCD (see Table. 10.9), we get for the 2HDM of type III contribution

$$\begin{aligned}
\left\langle B^0_d\right| C_4 O_4 \left|\bar{B}^0_d\right\rangle &\approx 0.26\, C_4\, \text{GeV}^3, \\
\left\langle B^0_s\right| C_4 O_4 \left|\bar{B}^0_s\right\rangle &\approx 0.37\, C_4\, \text{GeV}^3, \\
\left\langle K^0\right| C_4 O_4 \left|\bar{K}^0\right\rangle &\approx 0.30\, C_4\, \text{GeV}^3, \\
\left\langle D^0\right| C_4 O_4 \left|\bar{D}^0\right\rangle &\approx 0.18\, C_4\, \text{GeV}^3,
\end{aligned} \tag{29}$$

where, we used the normalization of the meson states as defined for example in [77]. In Eq. (29) the Wilson coefficients within the matrix elements are at the corresponding meson scale while C_4 on the right-handed side is given at the matching scale m_H. For computing the constraints on $\epsilon^d_{13}\epsilon^{d\star}_{31}$, $\epsilon^d_{23}\epsilon^{d\star}_{32}$ and $\epsilon^d_{12}\epsilon^{d\star}_{21}$ we use the online update of the analysis of the UTfit collaboration [81][10]. For this purpose we define

$$C_{B_q} e^{2i\varphi_{B_q}} = 1 + \frac{\left\langle B^0_q\right| \mathcal{H}^{NP}_{eff} \left|\bar{B}^0_q\right\rangle}{\left\langle B^0_q\right| \mathcal{H}^{SM}_{eff} \left|\bar{B}^0_q\right\rangle}\,, \tag{30}$$

[10] See also the online update of the CKMfitter group for an analogous analysis [14].

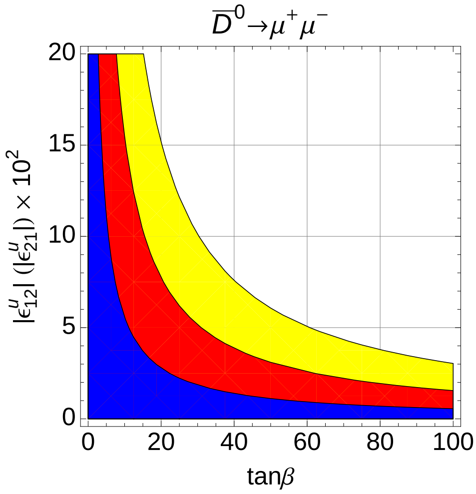

Figure 7: Allowed regions in the complex $\epsilon^u_{12,21}$–$\tan\beta$ plane from $\bar{D}^0 \to \mu^+\mu^-$ for $m_H =$ 700 GeV (yellow), $m_H = 500$ GeV (red) and $m_H = 300$ GeV (blue).

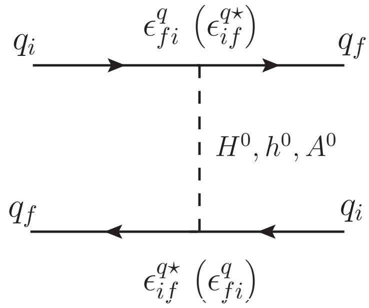

Figure 8: Feynman diagram contributing to $B_{d,s}$–$\overline{B}_{d,s}$, K–$\overline{K}$ and D–$\overline{D}$ mixing.

for $B_d - \overline{B}_d$ and $B_s - \overline{B}_s$ mixing and

$$\begin{aligned} C_{\epsilon_K} &= 1 + \frac{\text{Im}\left[\left\langle K^0\right| \mathcal{H}^{NP}_{eff} \left|\bar{K}^0\right\rangle\right]}{\text{Im}\left[\left\langle K^0\right| \mathcal{H}^{SM}_{eff} \left|\bar{K}^0\right\rangle\right]}\,, \\ C_{\Delta M_K} &= 1 + \frac{\text{Re}\left[\left\langle K^0\right| \mathcal{H}^{NP}_{eff} \left|\bar{K}^0\right\rangle\right]}{\text{Re}\left[\left\langle K^0\right| \mathcal{H}^{SM}_{eff} \left|\bar{K}^0\right\rangle\right]}\,, \end{aligned} \tag{31}$$

for $K - \overline{K}$ mixing. Using for the matrix elements of the SM Hamiltonian[11] [82]

$$\begin{aligned} \left\langle B^0_d\right| \mathcal{H}^{\Delta F=2}_{SM} \left|\bar{B}^0_d\right\rangle &\approx (1.08 + 1.25i) \times 10^{-13}\,\text{GeV}\,, \\ \left\langle B^0_s\right| \mathcal{H}^{\Delta F=2}_{SM} \left|\bar{B}^0_s\right\rangle &\approx (59 - 2.2i) \times 10^{-13}\,\text{GeV}\,, \\ \left\langle K^0\right| \mathcal{H}^{\Delta F=2}_{SM} \left|\bar{K}^0\right\rangle &\approx (115 + 1.16i) \times 10^{-17}\,\text{GeV}\,, \end{aligned} \tag{32}$$

[11] To obtain a value consistent with the NP analysis of the UTfit collaboration, we also used their input for computing the matrix elements of the SM $\Delta F = 2$ Hamiltonian in Eq. (32).

we can directly read off the bounds on C_4 and thus on $\epsilon^d_{12}\epsilon^{d\star}_{21}$, $\epsilon^d_{13}\epsilon^{d\star}_{31}$ and $\epsilon^d_{23}\epsilon^{d\star}_{32}$:

$$-2.0\times 10^{-10} \leq \quad \mathrm{Re}\left[\epsilon^d_{23}\epsilon^{d\star}_{32}\right]\left(\frac{\tan\beta/50}{m_H/500\,\mathrm{GeV}}\right)^2 \leq 6.0\times 10^{-10}\,, \tag{33}$$

$$-3.0\times 10^{-10} \leq \quad \mathrm{Im}\left[\epsilon^d_{23}\epsilon^{d\star}_{32}\right]\left(\frac{\tan\beta/50}{m_H/500\,\mathrm{GeV}}\right)^2 \leq 7.0\times 10^{-10}\,, \tag{34}$$

$$-3.0\times 10^{-11} \leq \quad \mathrm{Re}\left[\epsilon^d_{13}\epsilon^{d\star}_{31}\right]\left(\frac{\tan\beta/50}{m_H/500\,\mathrm{GeV}}\right)^2 \leq 1.5\times 10^{-11}\,, \tag{35}$$

$$-1.5\times 10^{-11} \leq \quad \mathrm{Im}\left[\epsilon^d_{13}\epsilon^{d\star}_{31}\right]\left(\frac{\tan\beta/50}{m_H/500\,\mathrm{GeV}}\right)^2 \leq 2.5\times 10^{-11}\,, \tag{36}$$

$$-1.0\times 10^{-12} \leq \quad \mathrm{Re}\left[\epsilon^d_{12}\epsilon^{d\star}_{21}\right]\left(\frac{\tan\beta/50}{m_H/500\,\mathrm{GeV}}\right)^2 \leq 3.0\times 10^{-13}\,, \tag{37}$$

$$-4.0\times 10^{-15} \leq \quad \mathrm{Im}\left[\epsilon^d_{12}\epsilon^{d\star}_{21}\right]\left(\frac{\tan\beta/50}{m_H/500\,\mathrm{GeV}}\right)^2 \leq 2.5\times 10^{-15}\,. \tag{38}$$

We see that if ϵ^d_{ij} is of the same order as ϵ^d_{ji} these bound are even more stringent than the ones from $B_{d,s}\to\mu^+\mu^-$ and $K_L\to\mu^+\mu^-$ computed in the last subsection.

For D–$\overline{D}$ mixing, the SM predictions is not known due to very large hadronic uncertainties. In order to constrain the NP effects we demand the absence of fine tuning, which means that the NP contribution, which are calculable short distance contributions, should not exceed the measured values. Concerning the 2HDM III contribution, there is no $\tan\beta$ enhancement and taking into account the recent analysis of UTfit collaboration [83] we arrive at the following constraints (for $m_H = 500$ GeV):

$$|\epsilon^u_{12}\epsilon^{u\star}_{21}| < 2.0\times 10^{-8}\,. \tag{39}$$

Note that although these bounds look more stringent than the corresponding $\Delta F = 1$ constraints, they scale differently with $\tan\beta$ and also involve products of pairs of ϵ^u_{ij}. Therefore, contrary to the $\Delta F = 1$ case, in principle all of these limits can be evaded for one of the couplings by suppressing the other one. Fig. 9 and Fig. 10 show the allowed regions for these parameters obtained from neutral Higgs contribution to $B_{d,s}$–$\overline{B}_{d,s}$, K–$\overline{K}$ and D–$\overline{D}$ mixing (see the Feynman diagram in Fig. 8).

5.3 Lepton-flavor-violating decays: $\tau^-\to\mu^-\mu^+\mu^-$, $\tau^-\to e^-\mu^+\mu^-$ and $\mu\to e^-e^+e^-$

In this section, we investigate the constraints that $\tau^-\to\mu^-\mu^+\mu^-$, $\tau^-\to e^-\mu^+\mu^-$ and $\mu\to e^-e^+e^-$ place on the flavor changing couplings $\epsilon^\ell_{32,23}$, $\epsilon^\ell_{31,13}$ and $\epsilon^\ell_{21,12}$, respectively.

For these decays, the experimental upper limits [84, 85] are

$$\begin{aligned}\mathcal{B}\left[\tau^-\to\mu^-\mu^+\mu^-\right] &\leq 2.1\times 10^{-8}\,,\\ \mathcal{B}\left[\tau^-\to e^-\mu^+\mu^-\right] &\leq 2.7\times 10^{-8}\,,\\ \mathcal{B}\left[\mu^-\to e^-e^+e^-\right] &\leq 1.0\times 10^{-12}\,,\end{aligned} \tag{40}$$

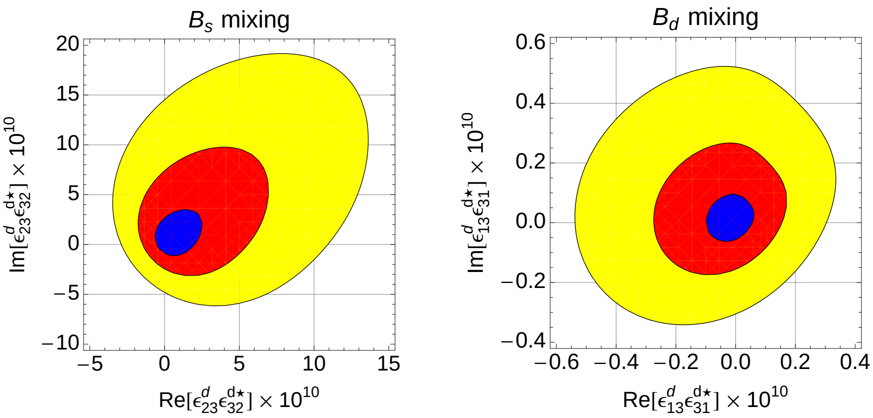

Figure 9: Allowed regions in the complex ϵ^{d}_{ij}-plane from $B_{d,s}$-$\overline{B}_{d,s}$ mixing for $\tan\beta = 50$ and $m_H = 700$ GeV (yellow), $m_H = 500$ GeV (red) and $m_H = 300$ GeV (blue).

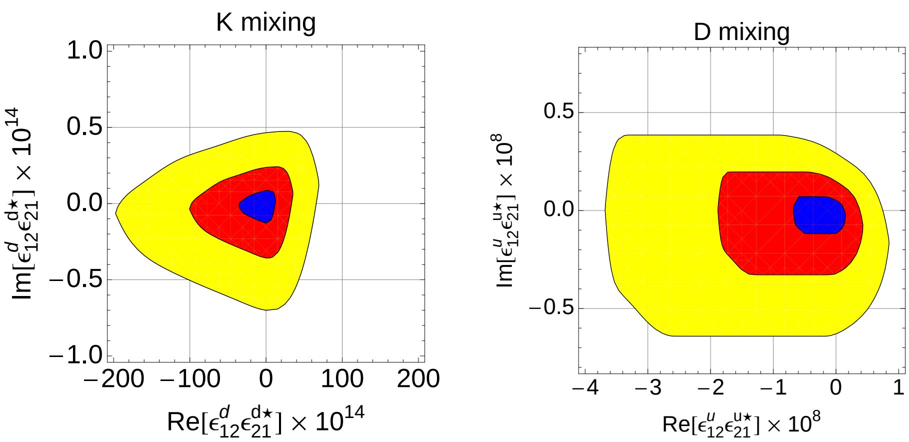

Figure 10: Allowed regions in the complex $\epsilon^{q}_{12}\epsilon^{q\star}_{21}$–plane from $K-\overline{K}$ and $D-\overline{D}$ mixing for $\tan\beta = 50$ and $m_H = 700$ GeV (yellow), $m_H = 500$ GeV (red) and $m_H = 300$ GeV (blue).

at 90% CL. Let us consider the processes $\tau^- \to \mu^-\mu^+\mu^-$ and $\tau^- \to e^-\mu^+\mu^-$ which are shown in Fig. 11. The expressions for the branching-ratio for $\tau^- \to e^-\mu^+\mu^-$ can be written as

$$\mathcal{B}\left[\tau^- \to e^-\mu^+\mu^-\right] = \frac{m_\tau^5}{12(8\pi)^3\Gamma_\tau}\frac{\tan^4\beta}{m_H^4}\left|\left(\frac{m_\mu}{v} - \varepsilon^{\ell}_{22}\right)\right|^2\left(\left|\varepsilon^{\ell}_{31}\right|^2 + \left|\varepsilon^{\ell}_{13}\right|^2\right) \tag{41}$$

where, Γ_τ is the total decay width of the τ-lepton. The branching ratios for $\tau^- \to e^-e^+e^-$ and $\mu^- \to e^-e^+e^-$ can be obtained by an obvious replacement of masses, indices and total decays widths. Note that the full expression for general scalar couplings given in Eq. (116) of the appendix is different for $\tau^- \to e^-\mu^+\mu^-$ than for $\tau^- \to \mu^-\mu^+\mu^-$ and only approaches a common expression in the limit of large $\tan\beta$ and large Higgs masses.

Comparing the type-III 2HDM expression with experiment we obtain the following con-

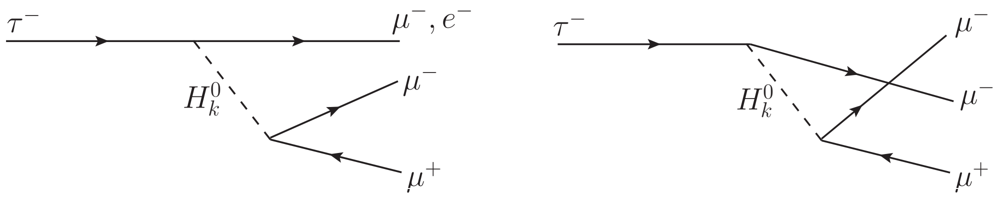

Figure 11: Feynman diagrams contributing to $\tau^- \to \mu^-\mu^+\mu^-$ and $\tau^- \to e^-\mu^+\mu^-$ via neutral Higgs exchange. Note that for $\tau^- \to \mu^-\mu^+\mu^-$ (or $\mu \to e^-e^+e^-$) two distinct diagrams exist which come with a relative minus sign due to the exchange of the two fermion lines.

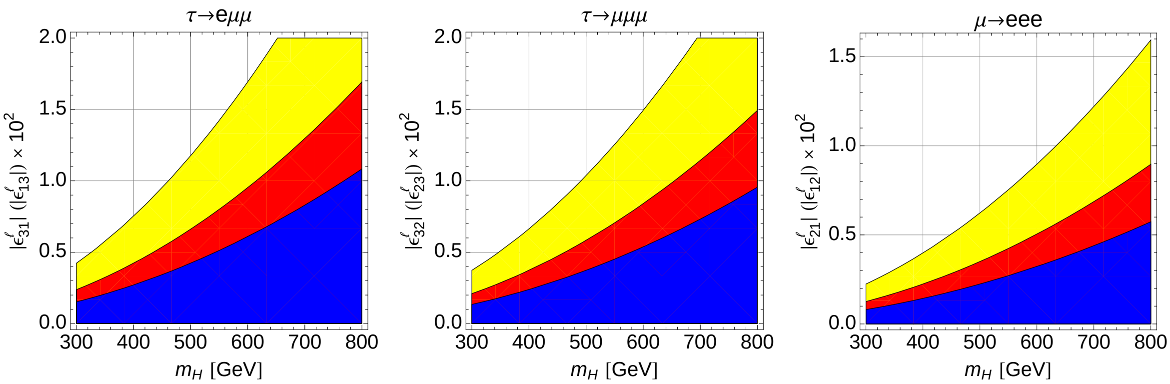

Figure 12: Allowed regions for the absolute value of $\epsilon^\ell_{13,31}$, $\epsilon^\ell_{23,32}$ and $\epsilon^\ell_{12,21}$ for $\tan\beta = 30$ (yellow), $\tan\beta = 40$ (red) and $\tan\beta = 50$ (blue) from $\tau^- \to e^-\mu^+\mu^-$, $\tau^- \to \mu^-\mu^+\mu^-$ and $\mu^- \to e^-e^+e^-$, respectively. In each plot only one of the elements ϵ^ℓ_{if} or ϵ^ℓ_{fi} is assumed to be different from zero.

straints on ϵ^ℓ_{fi} (assuming $\epsilon^\ell_{jj} = 0$)

$$\begin{aligned}
\left|\epsilon^\ell_{12}\right|^2 + \left|\epsilon^\ell_{21}\right|^2 &\leq (2.3\times 10^{-3})^2 \left(\frac{m_H/500\,\mathrm{GeV}}{\tan\beta/50}\right)^4 \frac{\mathcal{B}\left[\mu^- \to e^-e^+e^-\right]}{1.0\times 10^{-12}}\,,\\
\left|\epsilon^\ell_{13}\right|^2 + \left|\epsilon^\ell_{31}\right|^2 &\leq (4.2\times 10^{-3})^2 \left(\frac{m_H/500\,\mathrm{GeV}}{\tan\beta/50}\right)^4 \frac{\mathcal{B}\left[\tau^- \to e^-\mu^+\mu^-\right]}{2.7\times 10^{-8}}\,,\\
\left|\epsilon^\ell_{23}\right|^2 + \left|\epsilon^\ell_{32}\right|^2 &\leq (3.7\times 10^{-3})^2 \left(\frac{m_H/500\,\mathrm{GeV}}{\tan\beta/50}\right)^4 \frac{\mathcal{B}\left[\tau^- \to \mu^-\mu^+\mu^-\right]}{2.1\times 10^{-8}}\,.
\end{aligned} \tag{42}$$

These constraints are also illustrated in Fig. 12 for the experimental limits given in Eq. (40).

6 Loop-contributions to FCNC processes

We observed in the previous section that all elements ϵ^d_{ij}, ϵ^ℓ_{ij} (with $i \neq j$) and $\epsilon^u_{12,21}$ must be extremely small due to the constraints from tree-level neutral Higgs contributions to FCNC processes. Furthermore, the constraints on ϵ^q_{ij} and ϵ^q_{ji} get even more stringent if both of them are non-zero at the same time due to the bounds from $\Delta F = 2$ processes. Nevertheless, the elements $\epsilon^u_{13,23}$ and $\epsilon^u_{31,32}$ are still unconstrained because we have no data from neutral current top decays. In addition, also the flavor-conserving elements ϵ^f_{ii} are not constrained from neutral Higgs contributions to FCNC processes.

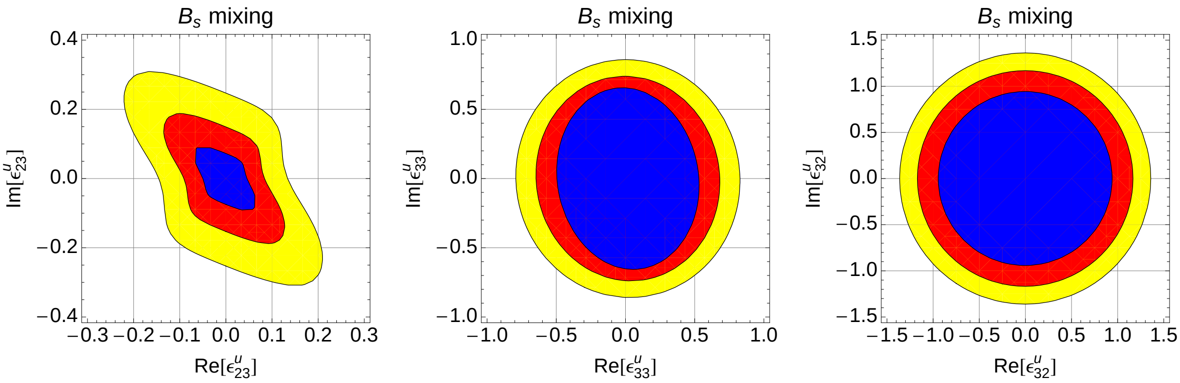

Figure 13: Allowed regions in the complex ϵ^u_{ij}-plane from B_s mixing for $\tan\beta = 50$ and $m_H = 700\,\text{GeV}$ (yellow), $m_H = 500\,\text{GeV}$ (red) and $m_H = 300\,\text{GeV}$ (blue).

In this section, we study the constraints from Higgs mediated loop contributions to FCNC observables. First, in Sec. 6.1 we consider the $\Delta F = 2$ processes, B_s–$\overline{B}_s$, B_d–$\overline{B}_d$ and $K-\overline{K}$ mixing and then examine the constraints on $\epsilon^u_{13,23}$ and $\epsilon^u_{31,32}$ from $b \to s(d)\gamma$. Also ϵ^u_{22} (ϵ^u_{33}) can be constrained from these processes due to the relative $\tan\beta$ enhancement compared to m_c (m_t) in the quark-quark-Higgs vertices. In this analysis, we neglect the effects of the elements ϵ^d_{ij}, which means that we assume the absence of large accidental cancellations between different contributions.

Also $\Delta F = 0$ processes (electric dipole moments) place relevant constraints on the type-III 2HDM parameter space, as we will see in Sec 6.6.

6.1 $B_s-\overline{B}_s$, $B_d-\overline{B}_d$ and $K-\overline{K}$ mixing

For the charged Higgs contributions to $\Delta F = 2$ processes we calculated the complete set of Wilson Coefficients in a general R_ξ-gauge. The result is given, together with our conventions for the Hamiltonian, in the appendix. For the QCD evolution we used the NLO running of the Wilson coefficients of Ref. [74, 75].

For computing the allowed regions in parameter space we used the same procedure as explained in the last section. The results are shown in Fig. 13, 14 and 15 and can be summarized as follows: B_s–$\overline{B}_s$ (B_d–$\overline{B}_d$) mixing gives constraints on ϵ^u_{23} (ϵ^u_{13}) which are of the order of 10^{-1} (10^{-2}) for our typical values of $\tan\beta$ and m_H. In addition, B_d–$\overline{B}_d$ mixing also constrains ϵ^u_{23} to a similar extent as B_s–$\overline{B}_s$ mixing. The constraints on ϵ^u_{33}, ϵ^u_{32} and ϵ^u_{31} are all very weak (of order one). Also Kaon mixing gives comparable bounds on Abs$[\epsilon^u_{23}]$ and the bounds on Abs$[\epsilon^u_{22}]$ are of the order 10^{-1}.

6.2 Radiative B meson decays: $b \to s\gamma$ and $b \to d\gamma$

The radiative B decay $b \to s\gamma$ ($b \to d\gamma$) imposes stringent constraints on the element ϵ^u_{23} (ϵ^u_{13}) while also in this case the constraints on ϵ^u_{32} (ϵ^u_{31}) are very weak due to the light charm (up) quark involved (see left diagram in Fig. 16). For these processes both a neutral and a charged Higgs contribution occur. Since the flavor off-diagonal elements $\epsilon^d_{13,23}$ and $\epsilon^d_{31,32}$ are already stringently constrained from tree-level decays we neglect the neutral Higgs contribution here.

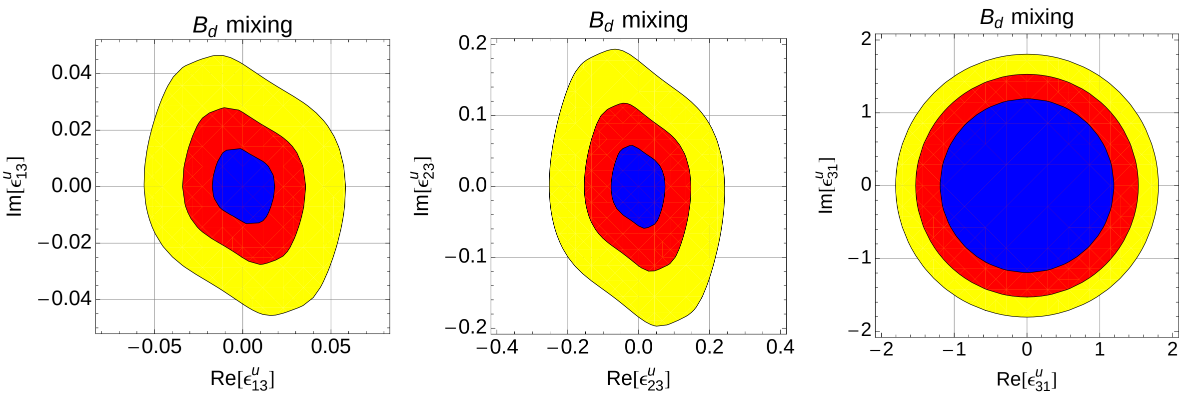

Figure 14: Allowed regions in the complex ϵ^u_{ij}-plane from B_d mixing for $\tan\beta = 50$ and $m_H = 700\,\text{GeV}$ (yellow), $m_H = 500\,\text{GeV}$ (red) and $m_H = 300\,\text{GeV}$ (blue).

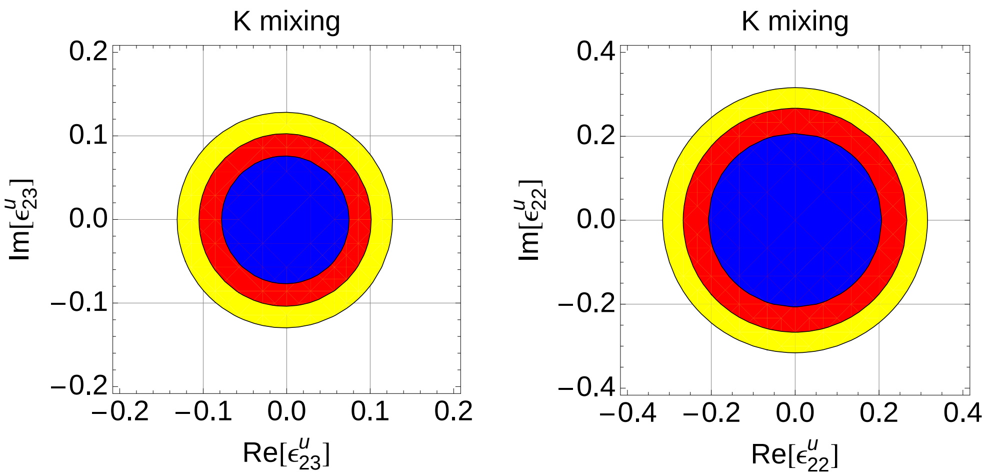

Figure 15: Allowed regions in the complex ϵ^u_{ij}-plane from $K-\overline{K}$ mixing for $\tan\beta = 50$ and $m_H = 700\,\text{GeV}$ (yellow), $m_H = 500\,\text{GeV}$ (red) and $m_H = 300\,\text{GeV}$ (blue). The constraints are practically independent of $\tan\beta$.

We give the explicit results for the Higgs contributions to the Wilson coefficients governing $b \to s(d)\gamma$ in the appendix.

For $B \to X_s\gamma$, we obtain the constraints on the 2HDM of type III parameters ϵ^u_{ij} by using $\mathcal{B}\left[B \to X_s\gamma\right]$ from Ref. [86] (BABAR) and Ref. [87, 88] (BELLE). Combined and extrapolated to a photon energy cut of 1.6 GeV, the HFAG value is [89]

$$\mathcal{B}\left[B \to X_s\gamma\right]\Big|^{\text{exp}}_{E_\gamma > 1.6\,\text{GeV}} = (3.43 \pm 0.21 \pm 0.07) \times 10^{-4}\,. \tag{43}$$

In order to estimate the possible size of NP we use the NNLO SM calculation of Ref. [48] (again for a photon energy cut of 1.6 GeV)

$$\mathcal{B}\left[B \to X_s\gamma\right]^{\text{SM}} = (3.15 \pm 0.23) \times 10^{-4}\,, \tag{44}$$

and calculate the ratio

$$R^{b\to s\gamma}_{\text{exp}} = \frac{\mathcal{B}\left[B \to X_s\gamma\right]\big|^{\text{exp}}}{\mathcal{B}\left[B \to X_s\gamma\right]\big|^{\text{SM}}}\,. \tag{45}$$

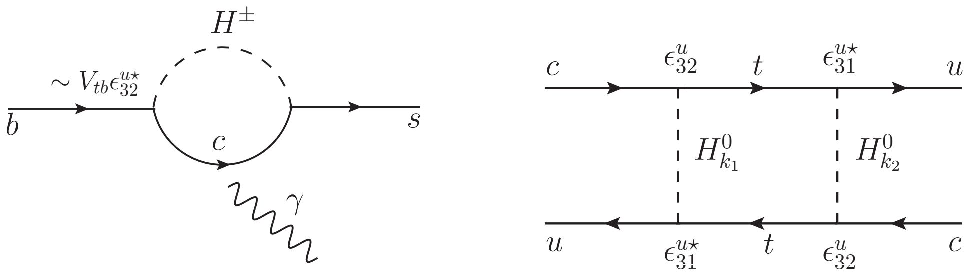

Figure 16: Left: Feynman diagram contributing to $b \to s\gamma$ via a charm-loop containing $\epsilon^{u\star}_{32}$. The contribution is suppressed, since the small charm mass enters either form the propagator or from the charged Higgs coupling to the charm and strange quark. Right: Feynman diagram showing a neutral Higgs box contribution to $D-\overline{D}$ mixing arising if ϵ^u_{31} and ϵ^u_{32} are simultaneously different from zero.

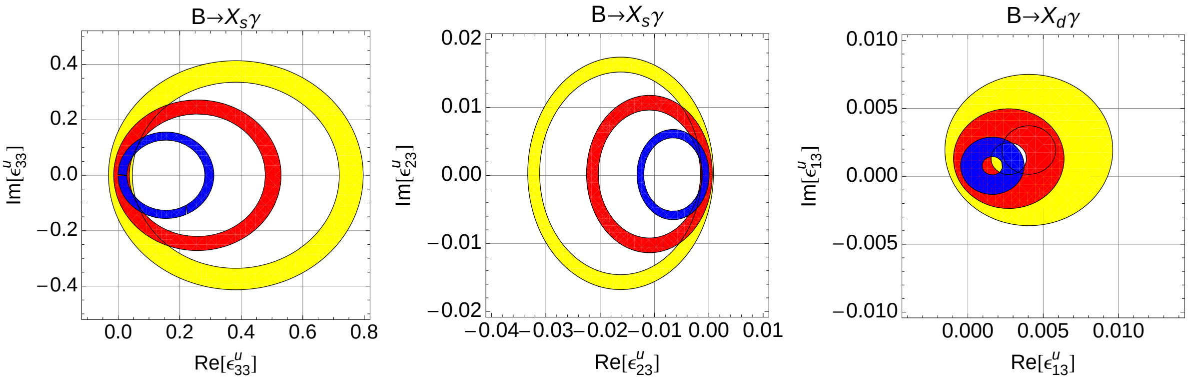

Figure 17: Allowed regions for ϵ^u_{ij} from $B \to X_{s(d)}\gamma$, obtained by adding the $2\,\sigma$ experimental error and theoretical uncertainty linear for $\tan\beta = 50$ and $m_H = 700\,\text{GeV}$ (yellow), $m_H = 500\,\text{GeV}$ (red) and $m_H = 300\,\text{GeV}$ (blue).

This leads to a certain range for $R^{b\to s\gamma}_{\text{exp}}$. Now, we require that in our leading-order calculation the ratio

$$R^{b\to s\gamma}_{\text{theory}} = \frac{\mathcal{B}\left[B \to X_s\gamma\right]\big|^{\text{2HDM}}}{\mathcal{B}\left[B \to X_s\gamma\right]\big|^{\text{SM}}} \tag{46}$$

lies within this range. In this way, we obtain the constraints on our model parameters ϵ^u_{ij} as illustrated in Fig. 17 and Fig. 18.

The analysis for $b \to d\gamma$ is performed in an analogous way. In addition we use here the fact that most of the hadronic uncertainities cancel in the CP-averaged branching ratio for $B \to X_d\gamma$ [90, 91]. The current experimental value of the BABAR collaboration [92, 93] for the CP averaged branching ratio reads

$$\mathcal{B}\left[B \to X_d\gamma\right]\big|^{\text{exp}}_{E_\gamma > 1.6\,\text{GeV}} = (1.41 \pm 0.57) \times 10^{-5}\,. \tag{47}$$

Here we take into account a conservative estimate of the uncertainty coming from the extrapolation in the photon energy cut [94]. For the theory prediction we use the NLL SM predictions

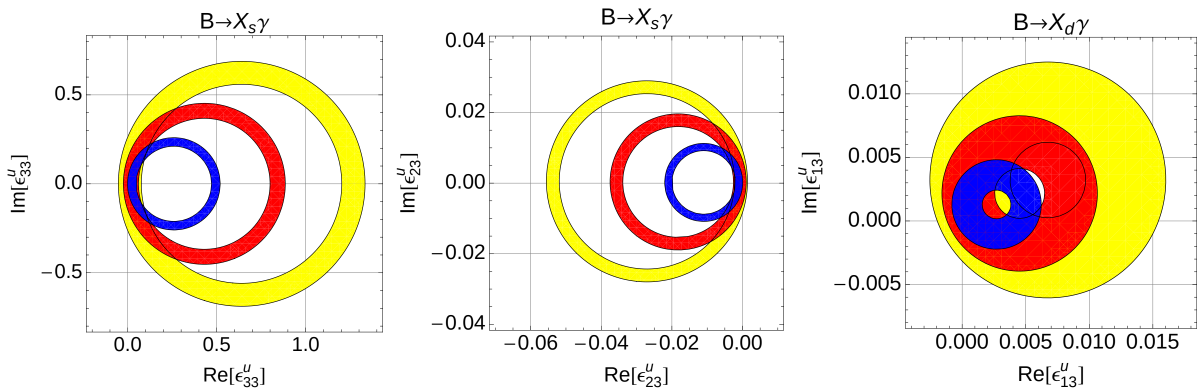

Figure 18: Allowed regions for ϵ^u_{ij} from $B \to X_{s(d)}\gamma$, obtained by adding the $2\,\sigma$ experimental error and theoretical uncertainty linear for $\tan\beta = 30$ and $m_H = 700\,\text{GeV}$ (yellow), $m_H = 500\,\text{GeV}$ (red) and $m_H = 300\,\text{GeV}$ (blue).

of the CP-averaged branching ratio $\mathcal{B}(B \to X_d\gamma)|_{E_\gamma > 1.6\,\text{GeV}}$ of Ref. [95, 96], which was recently updated in Ref. [94] and reads

$$\mathcal{B}\,[B \to X_d\gamma]|^{\text{SM}}_{E_\gamma>1.6\,\text{GeV}} = (1.54^{+0.26}_{-0.31}) \times 10^{-5}\,. \tag{48}$$

After defining the ratios $R^{b\to d\gamma}_{\text{exp}}$ and $R^{b\to d\gamma}_{\text{theory}}$ we continue as in the case of $\mathcal{B}\,[B \to X_s\gamma]$ in order to constrain ϵ^u_{13}.

As can be seen from Fig.17 and Fig. 18, the constraints that $B \to X_{s(d)}\gamma$ enforces on $\epsilon^u_{23(13)}$ are stronger than the ones from $B_{s(d)}$ mixing. Even ϵ^u_{33} can be restricted to a rather small range.

While in the 2HDM of type II $b \to s\gamma$ enforces a lower limit on the charged Higgs mass of 360 GeV [49] this constraint can get weakened in the 2HDM of type III: The off-diagonal element ϵ^u_{23} can lead to a destructive interference with the SM (depending on its phase) and thus reduce the 2HDM contribution. Lighter charged Higgs masses are also constrained from $b \to d\gamma$ but also this constraint can be avoided by ϵ^u_{13}.

6.3 Neutral Higgs box contributions to $D-\overline{D}$ mixing

Nearly all the loop-induced neutral Higgs contributions to FCNC processes can be neglected because the elements involved are already stringently constrained from tree-level processes. However, there is one exception: since the constraints on $\epsilon^u_{31,32}$ are particularly weak (because of the light charm or up quark entering the loop) this can give a sizable effect in $D-\overline{D}$ mixing via a neutral Higgs box[12] (see Fig. 16). As we will use ϵ^u_{31} and ϵ^u_{32} in Sec. 7 for explaining the mentioned deviations from the SM prediction in $B \to \tau\nu$, $B \to D\tau\nu$ and $B \to D^*\tau\nu$ it is interesting to ask if all processes can be explained simultaneously without violating $D-\overline{D}$ mixing. In principle also charged Higgs contributions to $D-\overline{D}$ mixing arise but we find that they are very small compared to the H^0_k contributions. The explicit expression for the Wilson coefficients can be found in the appendix.

[12]In principle, one can also get contribution to $\bar{D}^0 \to \mu^+\mu^-$ through H^0_k box and penguin contributions if the elements ϵ^u_{32} and ϵ^u_{31} are simultaneously non-zero. However, we observe that they are negligible.

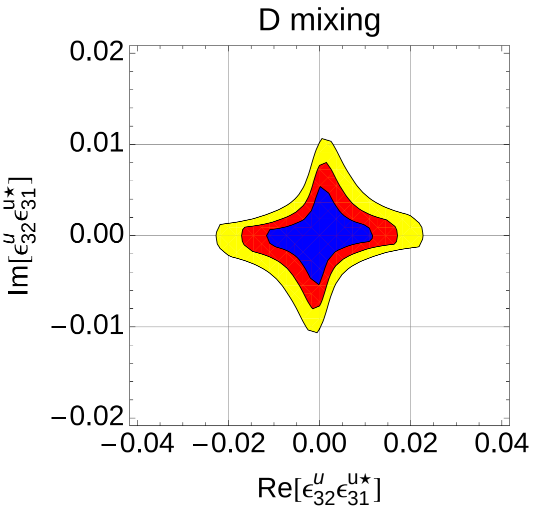

Figure 19: Allowed region in the complex $\epsilon^u_{32}\epsilon^{u\star}_{31}$–plane obtained from neutral Higgs box contributions to $D-\overline{D}$ mixing for $\tan\beta = 50$ and $m_H = 700\,\text{GeV}$ (yellow), $m_H = 500\,\text{GeV}$ (red) and $m_H = 300\,\text{GeV}$ (blue).

Fig. 19 shows the allowed regions in the complex $\epsilon^u_{32}\epsilon^{u\star}_{31}$–plane. The constraints are again obtained by using the recent UTfit [83] analysis for the D–$\overline{D}$ system.

6.4 Radiative lepton decays : $\mu \to e\gamma$, $\tau \to e\gamma$ and $\tau \to \mu\gamma$

The bounds on $\epsilon^\ell_{13,31}$ and $\epsilon^\ell_{23,32}$ from the radiative lepton decays $\tau \to e\gamma$ and $\tau \to \mu\gamma$ (using the experimental values given in Table 8) turn out to be significantly weaker than the ones from $\tau^- \to \mu^-\mu^+\mu^-$ and $\tau^- \to e^-\mu^+\mu^-$. Concerning $\mu \to e\gamma$ we expect constraints which are at least comparable to the ones from $\mu^- \to e^-e^+e^-$ since $\mu \to e\gamma$ does not involve the small electron Yukawa coupling entering $\mu^- \to e^-e^+e^-$. In fact, using the new MEG results [97] the constraints from $\mu \to e\gamma$ turn out to be stronger than the ones from $\mu^- \to e^-e^+e^-$ (see Fig. 20). Note that the constraints from $\mu^- \to e^-e^+e^-$ can be avoided if $v_u\epsilon^\ell_{11} \approx m_e$ while the leading contribution to $\mu \to e\gamma$ vanishes for $v_u\epsilon^\ell_{22} \approx m_\mu$.

Process	Experimental bounds
$\mathcal{B}\,[\tau \to \mu\gamma]$	$\leq 4.5 \times 10^{-8}$ [98, 99]
$\mathcal{B}\,[\tau \to e\gamma]$	$\leq 1.1 \times 10^{-7}$ [98]
$\mathcal{B}\,[\mu \to e\gamma]$	$\leq 5.7 \times 10^{-13}$ [97]

Table 8: Experimental upper limits on the branching ratios of lepton-flavor violating decays.

In principle, for $\mu \to e\gamma$ a simplified expression for the branching ratio in the large $\tan\beta$ limit and $v \ll m_H$ could also be given. However, due to the large logarithm with a relative big prefactor (last term of Eq. (96)) this is only a good approximation for very heavy Higgses and we therefore use the full expression in our numerical analysis.

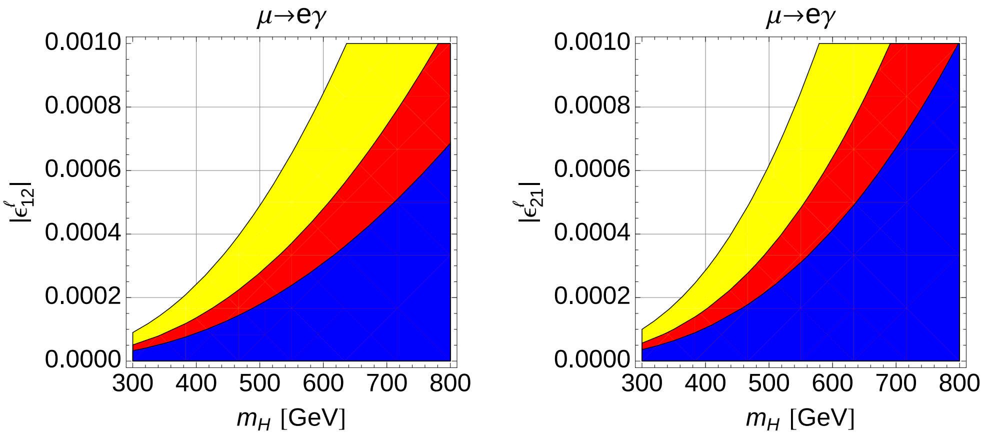

Figure 20: Allowed region for ϵ^ℓ_{12} (left plot) and ϵ^ℓ_{21} (right plot) from $\mu \to e\gamma$ for $\tan\beta = 30$ (yellow), $\tan\beta = 40$ (red) and $\tan\beta = 50$ (blue).

We will return to the radiative lepton decays in Sec. 8 and correlate them to the decays $\tau^- \to \mu^-\mu^+\mu^-$, $\tau^- \to e^-\mu^+\mu^-$ and $\mu^- \to e^-e^+e^-$.

6.5 $B_s \to \mu^+\mu^-$

Setting $\epsilon^q_{ij} = 0$ only the loop induced charged Higgs contribution to $B_s \to \mu^+\mu^-$ (and $B_d \to \mu^+\mu^-$) exist. This contribution (see Eq. (24)) gets altered in the presence of non-zero elements ϵ^ℓ_{ij}, e.g. ϵ^ℓ_{22}. In the large $\tan\beta$ limit, the loop induced result in Eq. (24) is modified to

$$C_S^{bs} = C_P^{bs} = -\frac{m_b\, V_{tb}^\star V_{ts}}{2}\,\frac{m_\mu - v_u\epsilon^\ell_{22}}{2M_W^2}\,\tan^2\beta\,\frac{\log\left(m_H^2/m_t^2\right)}{m_H^2/m_t^2 - 1}\,. \tag{49}$$

The resulting constraints on ϵ^ℓ_{22} from $B_s \to \mu^+\mu^-$ are shown in Fig. 21 and the ones from $B_d \to \mu^+\mu^-$ are found to be weaker.

6.6 Electric dipole moments and anomalous magnetic moments

6.6.1 Charged leptons

The same diagrams which contribute to the radiative lepton decays for $\ell_i \neq \ell_f$ also affect the electric dipole moments and the anomalous magnetic moments of leptons for $\ell_i = \ell_f$ (see Fig. 22). For this reason we use the same conventions as in Eq. (93) and express the EDMs of leptons in terms of the coefficients $c^{\ell_f\ell_i}_{L,R}$ of the magnetic dipole operators $O^{\ell_f\ell_i}_{L,R}$ in the following way (using that for flavor conserving transitions $c^{\ell_i\ell_i}_L = c^{\ell_i\ell_i\star}_R$)

$$d_{\ell_i} = 2m_{\ell_i}\,\mathrm{Im}\left[c^{\ell_i\ell_i}_R\right]\,. \tag{50}$$

In SM there is no contribution to the EDMs of leptons at the one-loop level. This is also true in the 2HDM of type II, because the Wilson coefficients are purely real since the phases of the PMNS matrix drop out in the charged Higgs contributions after summing over the massless neutrinos. However, in a 2HDM of type III, one can have neutral Higgs mediated

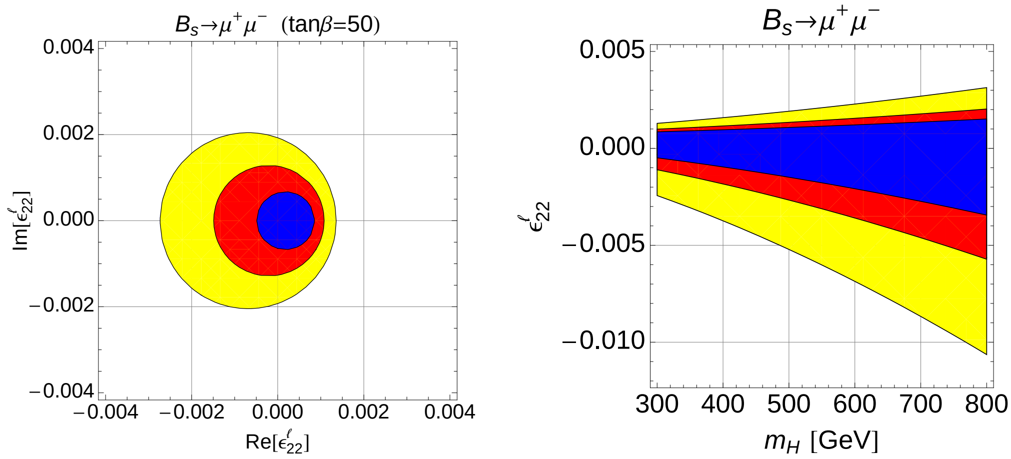

Figure 21: Left: Allowed regions in the complex ϵ^ℓ_{22}–plane from $B_s \to \mu^+\mu^-$ for $\tan\beta = 50$ and $m_H = 700$ GeV (yellow), $m_H = 500$ GeV (red) and $m_H = 300$ GeV (blue). Right: Allowed regions in the ϵ^ℓ_{22}–m_H plane from $B_s \to \mu^+\mu^-$ for $\tan\beta = 30$ (yellow), $\tan\beta = 40$ (red), $\tan\beta = 50$ (blue) and real values of ϵ^ℓ_{22}.

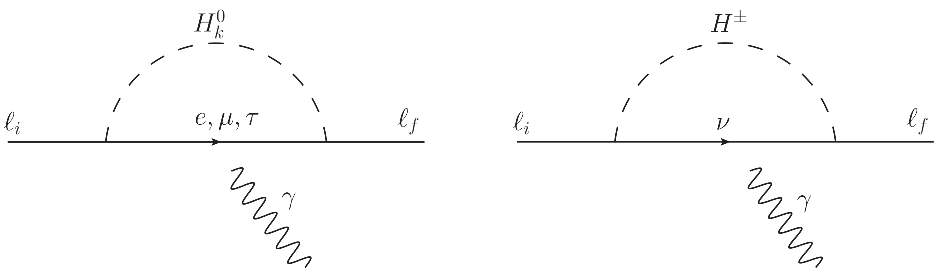

Figure 22: Left: Feynman diagram contributing to EDMs (for $i = f$) or LFV decays (for $i \neq f$) involving a neutral-Higgs boson. Right: Feynman diagram contributing to EDMs (for $i = f$) or LFV decays (for $i \neq f$) involving a charged-Higgs boson.

contributions to EDMs. Note that there is no charged Higgs contribution to the charged lepton EDMs also in the 2HDM of type III because the Wilson coefficients are purely real in this case. Comparing the expression for the EDMs in the 2HDM of type III with the experimental upper bounds on d_e, d_μ and d_τ (see Table 9), one can constrain the parameters ϵ^ℓ_{ij} (or combination of them) if they are complex.

We observe that while d_e enforces strong constraints on the products $\mathrm{Im}\left[\epsilon^\ell_{13}\epsilon^\ell_{31}\right]$ and $\mathrm{Im}\left[\epsilon^\ell_{12}\epsilon^\ell_{21}\right]$ (see Fig. 23), d_μ and d_τ are not capable of placing good constraints on our model parameters.

Similarly, following the conventions in Eq. (93), the anomalous magnetic moments (AMMs) can be written in terms of $c_R^{\ell_i\ell_i}$ as (e > 0)

$$a_{\ell_i} = -\frac{4m^2_{\ell_i}}{e}\,\mathrm{Re}\left[c_R^{\ell_i\ell_i}\right] . \tag{51}$$

The discrepancy between experiment and the SM prediction for the muon magnetic moment

EDMs	$\lvert d_e\rvert$	$\lvert d_\mu\rvert$	d_τ	$\lvert d_n\rvert$
Bounds (e cm)	10.5×10^{-28} [100]	1.9×10^{-19} [101]	$\in [-2.5, 0.8] \times 10^{-17}$ [102]	2.9×10^{-26} [103]

Table 9: Experimental (upper) bounds on electric dipole moments.

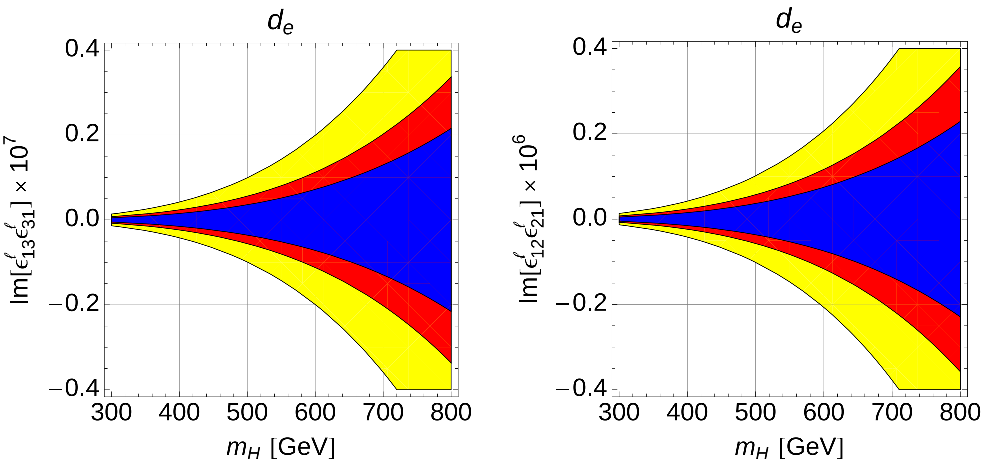

Figure 23: Allowed regions in the Im $\left[\epsilon^\ell_{13}\epsilon^\ell_{31}\right]$-$m_H$ and Im $\left[\epsilon^\ell_{12}\epsilon^\ell_{21}\right]$-$m_H$ planes from neutral Higgs contribution to d_e for $\tan\beta = 50$ (blue), $\tan\beta = 40$ (red) and $\tan\beta = 30$ (yellow). The constraints on Im $\left[\epsilon^\ell_{11}\right]$ are not sizable.

$a_\mu = (g-2)/2$ is [104, 105, 106, 107, 108]

$$\Delta a_\mu = a_\mu^{exp} - a_\mu^{SM} \approx (3 \pm 1) \times 10^{-9}\,. \tag{52}$$

In the 2HDM of type II, the sum of the neutral and charged Higgs mediated diagrams gives the following contribution to a_μ (for $\tan\beta = 50$ and $m_H = 500$ GeV):

$$a_\mu^{\text{2HDM II}} \approx 2.7 \times 10^{-13}\,, \tag{53}$$

which is interfering constructively with the SM. Anyway, it can be seen that the effect is orders of magnitude smaller than the actual sensitivity and it even gets smaller for higher Higgs masses.

Concerning the 2HDM of type III the discrepancy between experiment and the SM prediction given in Eq. (52) could be explained but only with severe fine-tuning. One would need to allow for very large values of ϵ^ℓ_{22} which would not only violate 't Hooft's naturalness criterion but also enhance $B_s \to \mu^+\mu^-$ by orders of magnitude above the experimental limit. If one would try to explain the anomaly using ϵ^ℓ_{23} and ϵ^ℓ_{32} (ϵ^ℓ_{12} and ϵ^ℓ_{21}) one would violate the bounds from $\tau^- \to \mu^-\mu^+\mu^-$ ($\mu^- \to e^-e^+e^-$ or $\mu \to e\gamma$) as illustrated in Fig. 24.

In conclusion, neither a type-II nor a type-III 2HDM can give a sizable effect in a_μ and both models are not capable of explaining the deviation from the SM.

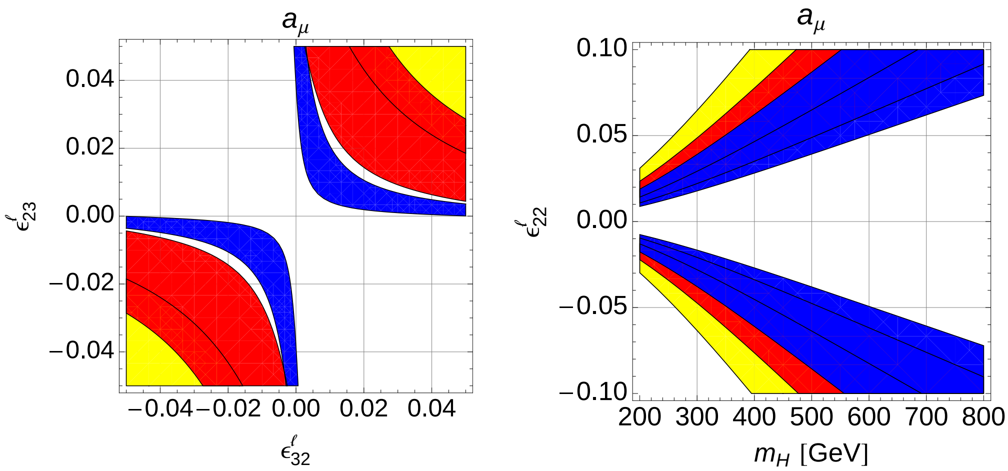

Figure 24: Left: Allowed region in the ϵ^ℓ_{23}–ϵ^ℓ_{32} plane from Δa_μ for real values of ϵ^ℓ_{23}, ϵ^ℓ_{32} and $\tan\beta = 50$, $m_H = 700$ GeV (yellow), $m_H = 500$ GeV (red) and $m_H = 300$ GeV (blue). Right: Allowed region in ϵ^ℓ_{22}–m_H plane from Δa_μ for real values of ϵ^ℓ_{22} and $\tan\beta = 50$ (blue), $\tan\beta = 40$ (red) and $\tan\beta = 30$ (yellow).

6.6.2 Electric dipole moment of the neutron

The neutron electric dipole moment d_n can also provide constraints on the parameters ϵ^q_{ij}. In the SM, there is no contribution to d_n at the 1-loop level since the coefficients are real. This is also true in the type-II 2HDM.

Using the theory estimate of Ref. [109], which is based on the QCD sum-rules calculations of Refs. [110, 111, 112, 113], the neutron EDM can be written as

$$d_n = (1 \pm 0.5)\left[1.4(d_d - 0.25 d_u) + 1.1 e(d^g_d + 0.5 d^g_u)\right] , \tag{54}$$

where, d_u (d_d) is the EDM of the up (down) quark and $d^g_{u(d)}$ define the corresponding chromoelectric dipole moments which stem from the chromomagnetic dipole operator

$$O^{q_f q_i}_{R(L)} = m_{q_i} \bar{q}_f \sigma^{\mu\nu} T^a P_{R(L)} q_i G^a_{\mu\nu} . \tag{55}$$

Similar to EDMs, the (chromo) electric dipole moments of quarks are given as

$$d^{(g)}_{q_i} = 2 m_{q_i} \,\mathrm{Im}\left[c^{q_i q_i}_{R,(g)}\right] . \tag{56}$$

Using the upper limit on d_n (see Table 9) we can constrain some of ϵ^u_{ij} (for $\epsilon^d_{ij} = 0$) as shown in Fig. 25 and 26. These constraints are obtained for the conservative case of assuming a prefactor of 0.5 in Eq. (54). The explicit expressions for $c^{q_i q_i}_{R,(g)}$ stemming from neutral and charged Higgs contributions to $d^{(g)}_{q_i}$ are relegated to the appendix. Note that for the neutron EDM we did not include QCD corrections.

7 Tree-level charged current processes

In this section we study the constraints from processes which are mediated in the SM by a tree-level W exchange and which receive additional contributions from charged Higgs exchange in

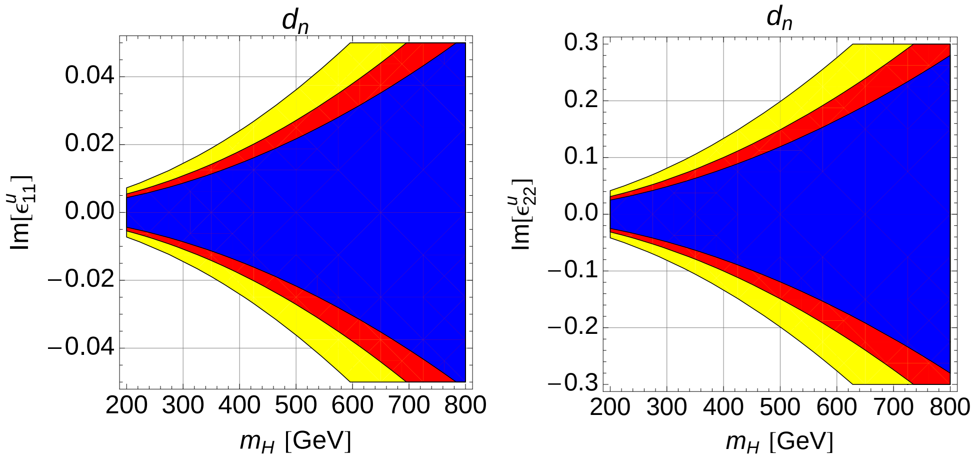

Figure 25: Allowed regions in the $\mathrm{Im}\left[\epsilon^u_{11,22}\right]$–$m_H$ planes from the electric dipole moment of the neutron for $\tan\beta = 50$ (blue), $\tan\beta = 40$ (red) and $\tan\beta = 30$ (yellow). We observe that d_n can not provide good constraints on the real parts of $\epsilon^u_{11,22}$.

2HDMs. We study purely leptonic meson decays, semileptonic meson decays and tau lepton decays. Concerning B meson decays we consider $B \to \tau\nu$, $B \to D\tau\nu$ and $B \to D^*\tau\nu$ which are, as outlined in the introduction, very interesting in the light of the observed deviation from the SM. We consider in addition $D_{(s)} \to \tau\nu$, $D_{(s)} \to \mu\nu$, $K(\pi) \to e\nu$, $K(\pi) \to \mu\nu$ and $\tau \to K(\pi)\nu$ and look for violation of lepton flavor universality via $K(\pi) \to e\nu/K(\pi) \to \mu\nu$ and $\tau \to K(\pi)\nu/K(\pi) \to \mu\nu$. Even though no deviations from the SM have been observed in these channels, they put relevant constraints on the parameter space of the type-III 2HDM.

For purely leptonic decays of a psudoscalar meson M (and also tau decays to mesons) to a lepton ℓ_j and a neutrino ν (which is not detected) the SM prediction is given by

$$\mathcal{B}_{SM}\left[M \to \ell_j\nu\right] = \frac{m_M}{8\pi} G_F^2 m_{\ell_j}^2 \tau_M f_M^2 \left|V_{u_f d_i}\right|^2 \left(1 - \frac{m_{\ell_j}^2}{m_M^2}\right)^2 \left(1 + \delta_{EM}^{M\ell_j}\right), \tag{57}$$

where $\delta_{EM}^{M\ell_j}$ stands for channel dependent electromagnetic corrections (see Table 10), m_M is the mass of the meson involved and m_{u_f} (m_{d_i}) refers to the mass of its constituent up (down) type quark. The expression for $\tau \to M\nu$ differers by the exchange of the meson masses (life time) with the tau masses (life time) and by a factor of 1/2 stemming from spin averaging.

NP via scalar operators can be included very easily:

$$\mathcal{B}_{NP} = \mathcal{B}_{SM} \left| 1 + \frac{m_M^2}{\left(m_{u_f} + m_{d_i}\right) m_{\ell_j}} \frac{C_R^{u_f d_i,\ell_j} - C_L^{u_f d_i,\ell_j}}{C_{SM}^{u_f d_i,\ell_j}} \right|^2 \tag{58}$$

with

$$C_{SM}^{u_f d_i,\ell_j} = 4 G_F V_{u_f d_i}/\sqrt{2}\,. \tag{59}$$

All quantities in Eq. (58) are understood to be at the meson scale m_M. Like for $B_s \to \mu^+\mu^-$, the SM Wilson coefficient is renormalization scale independent and the scalar Wilson coefficients evolve in the same way as the quark masses.

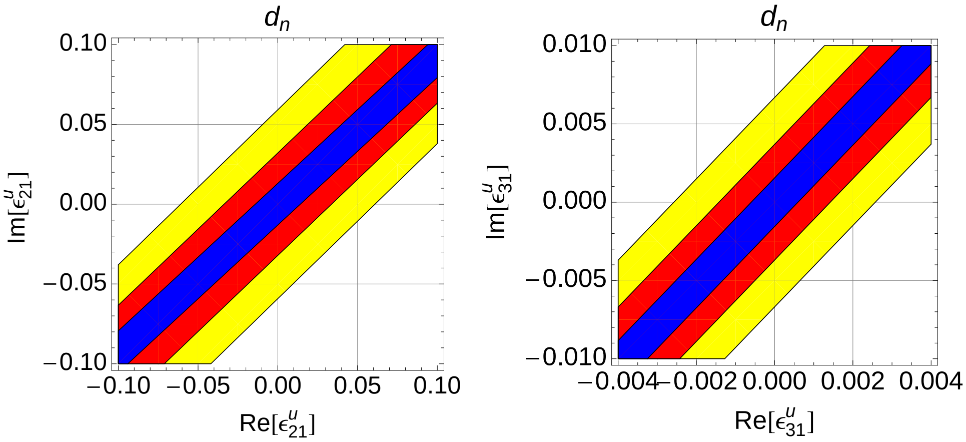

Figure 26: Allowed regions in the complex $\epsilon^u_{21,31}$–planes from d_n for $\tan\beta = 50$ and $m_H = 700$ GeV (yellow), $m_H = 500$ GeV (red) and $m_H = 300$ GeV (blue). We see that the absolute value of ϵ^u_{31} can only be large if it is aligned to V_{ub}, i.e. $\mathrm{Arg}[V_{ub}] = \mathrm{Arg}[\epsilon^u_{31}] \pm \pi$ which is very important when we consider later $B \to \tau\nu$.

In the 2HDM III the Wilson coefficients $C_L^{u_f d_i,\ell_j}$ and $C_R^{u_f d_i,\ell_j}$ are given by (neglecting terms which are not $\tan\beta$ enhanced)

$$
\begin{aligned}
C_R^{u_f d_i,\ell_j} &= -\frac{\tan^2\beta}{m^2_{H^\pm}} \left(V_{fi}\frac{m_{d_i}}{v} - \sum_{j=1}^{3} V_{fj}\epsilon^d_{ji} \right) \left(\frac{m_{\ell_j}}{v} - \sum_{k=1}^{3} \epsilon^{\ell\star}_{kj} \right) , \\
C_L^{u_f d_i,\ell_j} &= \frac{\tan\beta}{m^2_{H^\pm}} \sum_{j=1}^{3} V_{ji}\epsilon^{\star u}_{jf} \left(\frac{m_{\ell_j}}{v} - \sum_{k=1}^{3} \epsilon^{\ell\star}_{kj} \right) .
\end{aligned} \tag{60}
$$

Note that $C_L^{u_f d_i,\ell_j}$ is only proportional to one power of $\tan\beta$ while $C_R^{u_f d_i,\ell_j}$ is proportional to $\tan^2\beta$. The Hamiltonian governing $M \to \ell_j\nu$ ($\tau \to M\nu$) and the Wilson coefficients for general scalar interactions are given in the appendix. It is important to keep in mind that, since we are dealing with lepton flavour-violating terms, we must sum over the neutrinos in the final state because the neutrino is not detected. Note that we did not include the PMNS matrix in both $C_{SM}^{u_f d_i,\ell_j}$ and $C_{L,R}^{u_f d_i,\ell_j}$ for simplifying the expressions, since it cancels in the final expression after summing over the neutrinos.

For semileptonic meson decays $B \to D\tau\nu$ and $B \to D^*\tau\nu$, which have a three-body final state, both the SM prediction and the inclusion of NP is more complicated, as will be discussed in subsection 7.1.1.

7.1 Tauonic charged B meson decays: $B \to \tau\nu$, $B \to D\tau\nu$ and $B \to D^*\tau\nu$

As discussed in the introduction the BABAR collaboration performed an analysis of the semileptonic B decays $B \to D\tau\nu$ and $B \to D^*\tau\nu$ using the full available data set [8, 9]. They find for the ratios

$$
\mathcal{R}(D^{(*)}) = \mathcal{B}(B \to D^{(*)}\tau\nu)/\mathcal{B}(B \to D^{(*)}\ell\nu) , \tag{61}
$$

Ratio	Experimental value	SM prediction	$\delta_{EM}^{M\ell_j}$
$\mathcal{B}[K\to e\nu]/\mathcal{B}[K\to\mu\nu]$	$(2.488\pm0.013)\times10^{-5}$	$(2.472\pm0.001)\times10^{-5}$	-0.0378 ± 0.0004 [61]
$\mathcal{B}[K\to\mu\nu]/\mathcal{B}[\pi\to\mu\nu]$	$(63.55\pm0.11)\times10^{-2}$	$(63.48\pm1.37)\times10^{-2}$	-0.0070 ± 0.0018 [114]
$\mathcal{B}[K\to e\nu]/\mathcal{B}[\pi\to e\nu]$	$(1.285\pm0.008)\times10^{-1}$	$(1.270\pm0.027)\times10^{-1}$	-0.0070 ± 0.0018 [114]
$\mathcal{B}[\pi\to e\nu]/\mathcal{B}[\pi\to\mu\nu]$	$(1.230\pm0.004)\times10^{-4}$	1.234×10^{-4}	$-3.85\,\%$ [115]
$\mathcal{B}[\tau\to K\nu]/\mathcal{B}[\tau\to\pi\nu]$	$(6.46\pm0.10)\times10^{-2}$	$(6.56\pm0.16)\times10^{-2}$	0.0003 ± 0.0044 [116]
$\mathcal{B}[\tau\to\pi\nu]/\mathcal{B}[\pi\to\mu\nu]$	$(10.83\pm0.06)\times10^{-2}$	10.87×10^{-2}	$+1.2\,\%$ [115]
$\mathcal{B}[\tau\to K\nu]/\mathcal{B}[K\to\mu\nu]$	$(1.102\pm0.016)\times10^{-2}$	1.11×10^{-2}	$+2.0\,\%$ [115]

Table 10: Experimental values, SM predictions and electromagnetic corrections (in the SM) for the ratios of charged current processes. The experimental values are obtained by adding the errors of the individual branching ratios given in Ref. [72] in quadrature. The SM predictions include the uncertainties from $\delta_{EM}^{M\ell_j}$ and (if involved) as well as the uncertainties due to CKM factors and decay constants. As always, we add the theory error linear to the experimental ones.

(with $\ell=e,\mu$) the following results:

$$\mathcal{R}(D) \;=\; 0.440\pm0.058\pm0.042\,, \tag{62}$$
$$\mathcal{R}(D^*) \;=\; 0.332\pm0.024\pm0.018\,. \tag{63}$$

Here the first error is statistical and the second one is systematic. Comparing these measurements to the SM predictions

$$\mathcal{R}_{\rm SM}(D) \;=\; 0.297\pm0.017\,, \tag{64}$$
$$\mathcal{R}_{\rm SM}(D^*) \;=\; 0.252\pm0.003\,, \tag{65}$$

we see that there is a discrepancy of $2.0\,\sigma$ for $\mathcal{R}(D)$ and $2.7\,\sigma$ for $\mathcal{R}(D^*)$. For the theory predictions we used the updated results of [8], which rely on the calculations of Refs. [55, 117] based on the results of Refs. [118, 119, 120, 121, 122]. The measurements of both ratios $\mathcal{R}(D)$ and $\mathcal{R}(D^*)$ exceed the SM prediction, and combining them gives a $3.4\,\sigma$ deviation from the SM [8, 9] expectation.

This evidence for the violation of lepton flavour universality in $B\to D\tau\nu$ and $B\to D^*\tau\nu$ is further supported by the measurement of $B\to\tau\nu$ by BABAR [10, 11] and BELLE [12]. Until recently, all measurements of $B\to\tau\nu$ (the hadronic tag and the leptonic tag both from BABAR and BELLE) were significantly above the SM prediction. However, the latest BELLE result for the hadronic tag [13] of $\mathcal{B}[B\to\tau\nu]=(0.72^{+0.27}_{-0.25}\pm0.11)\times10^{-4}$ is in agreement with the SM prediction [14]:

$$\mathcal{B}_{\rm SM}[B\to\tau\nu]=(0.796^{+0.088}_{-0.087})\times10^{-4}\,. \tag{66}$$

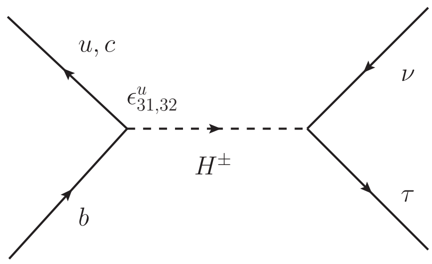

Figure 27: Feynman diagram showing a charged Higgs contributing to $B \to \tau\nu$ and $B \to D^{(*)}\tau\nu$ involving the flavour changing parameters ϵ^u_{31} and ϵ^u_{32} which affect $B \to \tau\nu$ and $B \to D^{(*)}\tau\nu$, respectively.

Averaging all measurements, one obtains the branching ratio

$$\mathcal{B}_{exp}[B \to \tau\nu] = (1.15 \pm 0.23) \times 10^{-4}\,. \tag{67}$$

which now disagrees with the SM prediction by $1.6\,\sigma$ using V_{ub} from the global fit [14].

Combining $\mathcal{R}(D)$, $\mathcal{R}(D^*)$ and $B \to \tau\nu$, we have evidence for violation of lepton flavor universality. Assuming that these deviations from the SM are not statistical fluctuations or underestimated theoretical or systematic uncertainties, it is interesting to ask which model of new physics can explain the measured values [16, 123, 124, 125, 126, 127, 128, 129, 130, 131, 132].

7.1.1 $B \to D\tau\nu$ and $B \to D^*\tau\nu$

Let us first consider the semileptonic decays $B \to D\tau\nu$ and $B \to D^*\tau\nu$. Here the Wilson coefficients $C_R^{qb,\tau}$ and $C_L^{qb,\tau}$ affect $B \to D\tau\nu$ and $B \to D^*\tau\nu$ in the following way [54, 55, 133]:

$$\mathcal{R}(D) = \mathcal{R}_{SM}(D)\left(1 + 1.5\Re\left[\frac{C_R^{cb,\tau} + C_L^{cb,\tau}}{C_{SM}^{cb,\tau}}\right] + 1.0\left|\frac{C_R^{cb,\tau} + C_L^{cb,\tau}}{C_{SM}^{cb,\tau}}\right|^2\right)\,, \tag{68}$$

$$\mathcal{R}(D^*) = \mathcal{R}_{SM}(D^*)\left(1 + 0.12\Re\left[\frac{C_R^{cb,\tau} - C_L^{cb,\tau}}{C_{SM}^{cb,\tau}}\right] + 0.05\left|\frac{C_R^{cb,\tau} - C_L^{cb,\tau}}{C_{SM}^{cb,\tau}}\right|^2\right)\,. \tag{69}$$

For our analysis we add the experimental errors in quadrature and the theoretical uncertainty linear on top of this. There are also efficiency corrections to $\mathcal{R}(D)$ due to the BABAR detector [8] which are important in the case of large contributions from the scalar Wilson coefficients $C_{R,L}^{cb,\tau}$ (i.e. if one wants to explain $\mathcal{R}(D)$ with destructive interference with the SM contribution). As shown in Ref. [123], these corrections can be effectively taken into account by multiplying the quadratic term in $C_{R,L}^{cb,\tau}$ of Eq. (68) by an approximate factor of 1.5 (not included in Eq. (68)).

Since ϵ^d_{33} contributes to $C_R^{cb,\tau}$ (the same Wilson coefficient generated in the type-II 2HDM) it cannot simultaneously explain $\mathcal{R}(D)$ and $\mathcal{R}(D^*)$. Therefore, we are left with ϵ^u_{32}, which contributes to $B \to D\tau\nu$ and $B \to D^*\tau\nu$ as shown in Fig. 27. In the left frame of Fig. 28 we see the allowed region in the complex ϵ^u_{32}-plane, which gives the correct values for $\mathcal{R}(D)$ and $\mathcal{R}(D^*)$ within the $1\,\sigma$ uncertainties for $\tan\beta = 50$ and $m_H = 500$ GeV, and the middle and the right frames correspond to the allowed regions on ϵ^u_{31} from $B \to \tau\nu$.

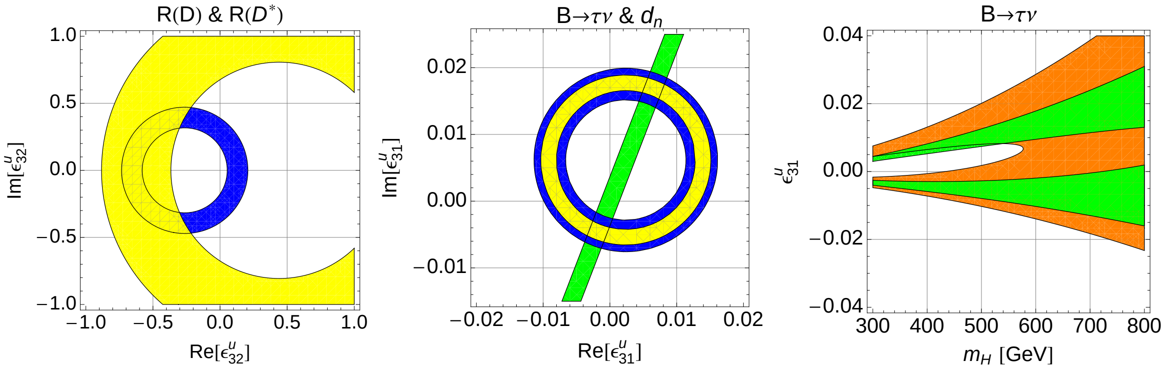

Figure 28: Left: Allowed regions in the complex ϵ^u_{32}–plane from $\mathcal{R}(D)$ (blue) and $\mathcal{R}(D^*)$ (yellow) for $\tan\beta = 50$ and $m_H = 500$ GeV. Middle: Allowed regions in the complex ϵ^u_{31}–plane combining the constraints from $B \to \tau\nu$ (1 σ (yellow) and 2 σ (blue)) and neutron EDM (green) for $\tan\beta = 50$ and $m_H = 500$ GeV. Right: Allowed regions in the m_H–ϵ^u_{31} plane from $B \to \tau\nu$ for real values of ϵ^u_{31} and $\tan\beta = 50$ (green), $\tan\beta = 30$ (orange).

Process	Experimental value (bound)	SM prediction
$\mathcal{B}\left[D_s \to \tau\nu\right]$	$(5.43 \pm 0.31) \times 10^{-2}$	$\left(5.36^{+0.54}_{-0.50}\right) \times 10^{-2}$
$\mathcal{B}\left[D_s \to \mu\nu\right]$	$(5.90 \pm 0.33) \times 10^{-3}$	$\left(5.50^{+0.55}_{-0.52}\right) \times 10^{-3}$
$\mathcal{B}\left[D \to \tau\nu\right]$	$\leq 1.2 \times 10^{-3}$	$(1.10 \pm 0.06) \times 10^{-3}$
$\mathcal{B}\left[D \to \mu\nu\right]$	$(3.82 \pm 0.33) \times 10^{-4}$	$\left(4.15^{+0.22}_{-0.21}\right) \times 10^{-4}$

Table 11: Experimental values (upper bounds) and SM predictions for $D_{(s)} \to \tau\nu$ and $D_{(s)} \to \mu\nu$ processes. The SM prediction for $D_s \to \mu\nu$ mode takes into account the EM correction effects of $+1.0\,\%$ [134, 135, 140].

7.1.2 $B \to \tau\nu$

In principle, $B \to \tau\nu$ can be explained either by using ϵ^d_{33} (as in 2HDMs with MFV) or by ϵ^u_{31} (or by a combination of both of them). However, ϵ^d_{33} alone cannot explain the deviation from the SM without fine tuning, while ϵ^u_{31} is capable of doing this [16].

$B \to \tau\nu$ can also be used to constrain ϵ^ℓ_{13}, ϵ^ℓ_{23} and ϵ^ℓ_{33} as illustrated in Fig. 29. In order to obtain these constraints, we assumed that all other relevant elements (ϵ^d_{33} and ϵ^u_{31}) are zero.

7.2 $D_{(s)} \to \tau\nu$ and $D_{(s)} \to \mu\nu$

Previously, there were some indications for NP in $D_s \to \tau\nu$ [134, 135, 136]. However, using the new experimental values for $\mathcal{B}\left[D_s \to \tau\nu\right]$ (see Table 11) and the improved lattice determination for the decay constant f_{D_s} [137, 138] we find agreement between the SM predictions and experiment. Nevertheless, it is interesting to consider the constraints on the 2HDM of type III parameter space. Charged Higgs contributions to $D_{(s)} \to \tau\nu$ and $D_{(s)} \to \mu\nu$ have been investigated in Ref. [58, 59, 60, 139].

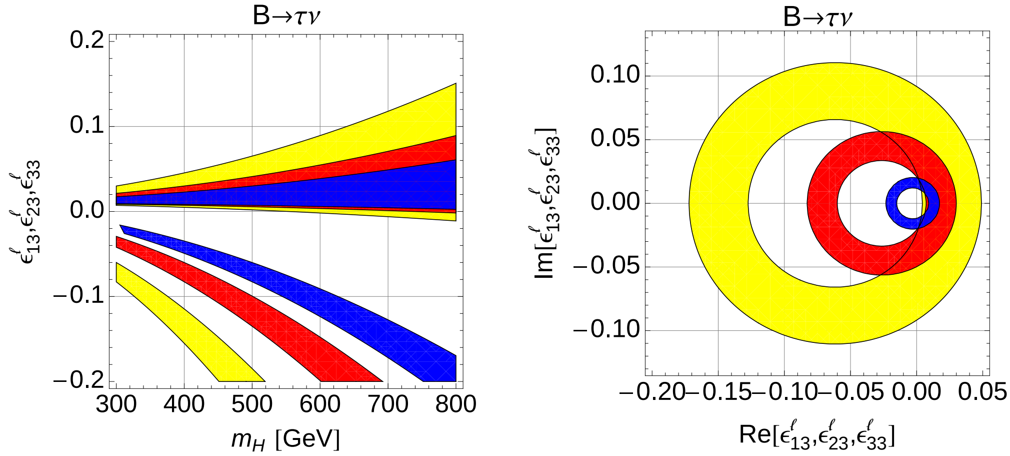

Figure 29: Left: Allowed regions in the m_H–ϵ^ℓ_{i3} plane from $B \to \tau\nu$ for real values of ϵ^ℓ_{i3} and $\tan\beta = 30$ (yellow), $\tan\beta = 40$ (red), $\tan\beta = 50$ (blue). Right: Allowed regions in the complex ϵ^ℓ_{13}, ϵ^ℓ_{23} and ϵ^ℓ_{33}–planes from $B \to \tau\nu$ for $m_H = 700$ GeV (yellow), $m_H = 500$ GeV (red) and $m_H = 300$ GeV (blue).

The most important constraints on the 2HDM of type III parameter space are the ones on ϵ^u_{22} (shown in Fig. 30). $D_{(s)} \to \tau\nu$ and $D_{(s)} \to \mu\nu$ constrains $\mathrm{Re}\,[\epsilon^u_{22}]$ while the constraints on $\mathrm{Im}\,[\epsilon^u_{22}]$ are very weak. In principle, also the ratio $D_{(s)} \to \tau\nu/D_{(s)} \to \mu\nu$ could be used for constraining deviations from lepton flavor universality, but the constraints from $K(\pi) \to e\nu/K(\pi) \to \mu\nu$ and $\tau \to K(\pi)\nu/K(\pi) \to \mu\nu$ turn out to be stronger.

7.3 $K \to \mu\nu/\pi \to \mu\nu$ and $K \to e\nu/\pi \to e\nu$

The ratio $R_{K_{\ell 2},\pi_{\ell 2}} = \mathcal{B}\,[K \to \ell\nu]\,/\mathcal{B}\,[\pi \to \ell\nu]$ ($\ell = e,\mu$) is useful for constraining ϵ^d_{22}, ϵ^ℓ_{i1} and ϵ^ℓ_{i2} because the ratio of the decay constants f_K/f_π is known more precisely than the single decay constants [61].

For obtaining the experimental values we add the errors of the individual branching ratios in quadrature and the SM values take into account the electromagnetic correction. The corresponding values are given in Table. 10. The errors are due to the combined uncertainties in f_K/f_π, the CKM elements and the EM corrections. We obtained the value for V_{us} from $K \to \pi\ell\nu$ (which is much less sensitive to charged Higgs contributions than $K \to \mu\nu/\pi \to \mu\nu$) and V_{ud} by exploiting CKM unitarity.

Fig. 32 illustrates the allowed regions for ϵ^d_{22} by combining the constraints from $K \to \mu\nu/\pi \to \mu\nu$ and $K \to e\nu/\pi \to e\nu$. Like in $D_{(s)} \to \tau\nu$ and $D_{(s)} \to \mu\nu$ the constraints are on the real part of ϵ^d_{22} while the constraints on the imaginary part are very weak. Concerning ϵ^ℓ_{i1} and ϵ^ℓ_{i2} the constraints from $K(\pi) \to e\nu/K(\pi) \to \mu\nu$ will turn out to be more stringent but the latter ones can be avoided in the limit $\frac{m_{\ell_i}}{m_{\ell_j}} = \frac{\epsilon^\ell_{ii}}{\epsilon^\ell_{jj}}$ (see Fig. 31 and Fig. 33).

7.4 $\tau \to K\nu/\tau \to \pi\nu$

The τ is the only lepton which is heavy enough to decay into hadrons. The ratio $\mathcal{B}\,[\tau \to K\nu]/\mathcal{B}\,[\tau \to \pi\nu]$ can be considered for putting constraints on ϵ^u_{21}, ϵ^d_{12} and ϵ^ℓ_{i3}.

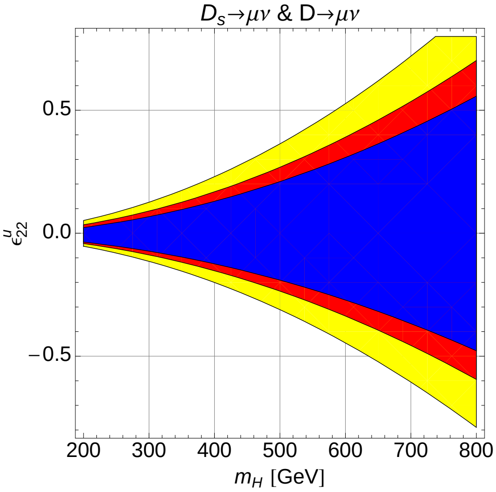

Figure 30: Left: Allowed region in the m_H–ϵ^u_{22}–plane (for real values of ϵ^u_{22}) obtained by combining the constraints from $D \to \mu\nu$ and $D_s \to \mu\nu$ for $\tan\beta = 30$ (yellow), $\tan\beta = 40$ (red) and $\tan\beta = 50$ (blue). While the upper bound on ϵ^u_{22} comes from $D_s \to \mu\nu$, $D \to \mu\nu$ is more constraining for negative values of ϵ^u_{22}. The bounds on the imaginary part of ϵ^u_{22} are very weak. The constraints from $D_s \to \tau\nu$ turn out to be comparable (but a bit weaker) while the ones from $D \to \tau\nu$ are weak.

The experimental and theoretical values for this ratio are given in Table. 10. We observe that the constraints from $\bar{D}^0 \to \mu^+\mu^-$ and $D-\overline{D}$ mixing on ϵ^u_{21} and $K_L \to \mu^+\mu^-$ on ϵ^d_{12} are too stringent so that no sizable effects stemming from these elements are possible. Also concerning ϵ^ℓ_{i3}, as we will see in the following sections, the constraints from $\tau \to \pi\nu/\pi \to \mu\nu$ will be stronger but again the latter ones can be avoided in the MFV limit $\frac{m_{\ell_i}}{m_{\ell_j}} = \frac{\epsilon^\ell_{ii}}{\epsilon^\ell_{jj}}$ (see Fig. 32).

7.5 Tests for lepton flavour universality: $K(\pi) \to e\nu/K(\pi) \to \mu\nu$ and $\tau \to K(\pi)\nu/K(\pi) \to \mu\nu$

$K_{\ell 2}\,(K \to \ell\nu)$ decays ($\ell = e, \mu$) are helicity suppressed in the SM and suffers from large theoretical uncertainties due to the decay constants. However, considering the ratio $R_{K_{\ell 2}} = \mathcal{B}\left[K \to e\nu\right]/\mathcal{B}\left[K \to \mu\nu\right]$ the dependence on decay constants drops out.

In the 2HDM of type II the charged Higgs contributions to $K(\pi) \to e\nu/K(\pi) \to \mu\nu$ and $\tau \to K(\pi)\nu/K(\pi) \to \mu\nu$ drop out. This is also true in the 2HDM of type III (for $\epsilon^\ell_{ij} = 0$ with $i \neq j$) as long as the MFV-like relation $\epsilon^\ell_{22}/m_\mu{=}\epsilon^\ell_{11}/m_e$ is not violated.

7.5.1 $K \to e\nu/K \to \mu\nu$ and $\pi \to e\nu/\pi \to \mu\nu$

$K \to e\nu/K \to \mu\nu$ is a very precise test of lepton flavor universality [141] (see table. 10). Including NP entering via scalar operators modifies this ratio according to Eq. (58).

We find strong constraints on ϵ^ℓ_{i2} (which affect the coupling to the muon) and the constraints on ϵ^ℓ_{i1} (where the coupling of the electron is involved) are even more stringent. Like for $D_{(s)} \to \tau\nu$ and $D_{(s)} \to \mu\nu$ the constraints are much better for the real part of ϵ^ℓ_{ij} than

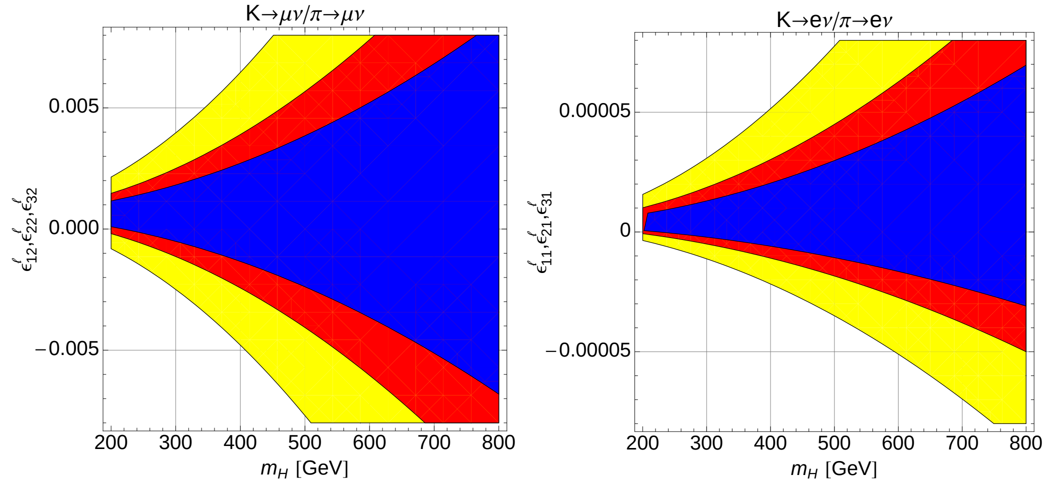

Figure 31: Allowed regions in the m_H–$\epsilon^\ell_{i1,i2}$–plane from $K \to \mu\nu/\pi \to \mu\nu$ and $K \to e\nu/\pi \to e\nu$ for real values of $\epsilon^\ell_{i1,i2}$ and $\tan\beta = 30$ (yellow), $\tan\beta = 40$ (red) and $\tan\beta = 50$ (blue). The constraints are weaker than the ones from $K(\pi) \to e\nu/K(\pi) \to \mu\nu$ and $\tau \to K(\pi)\nu/K(\pi) \to \mu\nu$ but cannot be avoided assuming the MFV limit $(\frac{m_{\ell_i}}{m_{\ell_j}} = \frac{\epsilon^\ell_{ii}}{\epsilon^\ell_{jj}})$.

the imaginary part. Note that these constraints are obtained assuming that only one element ϵ^ℓ_{ij} is non-zero. In the case ϵ^ℓ_{22}/m_μ=ϵ^ℓ_{11}/m_e where lepton flavor universality is restored no constraints can be obtained.

Alternatively, the ratio $\pi \to e\nu/\pi \to \mu\nu$ can test lepton flavor universality. We find that the constraints from $\pi \to e\nu/\pi \to \mu\nu$ are comparable with the ones from $K \to e\nu/K \to \mu\nu$. Our results are illustrated in Fig. 33.

7.5.2 $\tau \to K\nu/K \to \mu\nu$ and $\tau \to \pi\nu/\pi \to \mu\nu$

The ratios $\tau \to K\nu/K \to \mu\nu$ and $\tau \to \pi\nu/\pi \to \mu\nu$ are very similar to $K(\pi) \to e\nu/K(\pi) \to \mu\nu$: all dependencies on decay constants and CKM elements drop out and they are only sensitive to NP which violates lepton-flavour universality. The corresponding experimental and the theoretical values for these ratios are given in Table. 10.

We find that the constraints on ϵ^ℓ_{i3} from $\tau \to \pi\nu/\pi \to \mu\nu$ are stronger than the ones from $\tau \to K\nu/K \to \mu\nu$ and they are shown in Fig. 34.

8 Upper limits and correlation for LFV processes

In Sec. 5 we found that the neutral current lepton decays $\tau^- \to \mu^-\mu^+\mu^-$ and $\tau^- \to e^-\mu^+\mu^-$ give more stringent bounds on the elements $\epsilon^\ell_{32,23}$ and $\epsilon^\ell_{31,13}$ than the radiative decays $\tau \to \mu\gamma$ and $\tau \to e\gamma$. Also the LFV neutral meson decays $B_{s,d} \to \tau\mu$, $B_{s,d} \to \tau e$, $B_{s,d} \to \mu e$ cannot be arbitrarily large in the type-III 2HDM due to the constraints from $B_{s,d} \to \mu^+\mu^-$ and $\tau^- \to \mu^-\mu^+\mu^-$, $\tau^- \to e^-\mu^+\mu^-$, $\mu^- \to e^-e^+e^-$ (assuming again the absence of large cancellations)[13].

[13]see e.g. Ref. [142, 143, 144] for an analysis of NP in $B_{s,d} \to \tau\mu$.

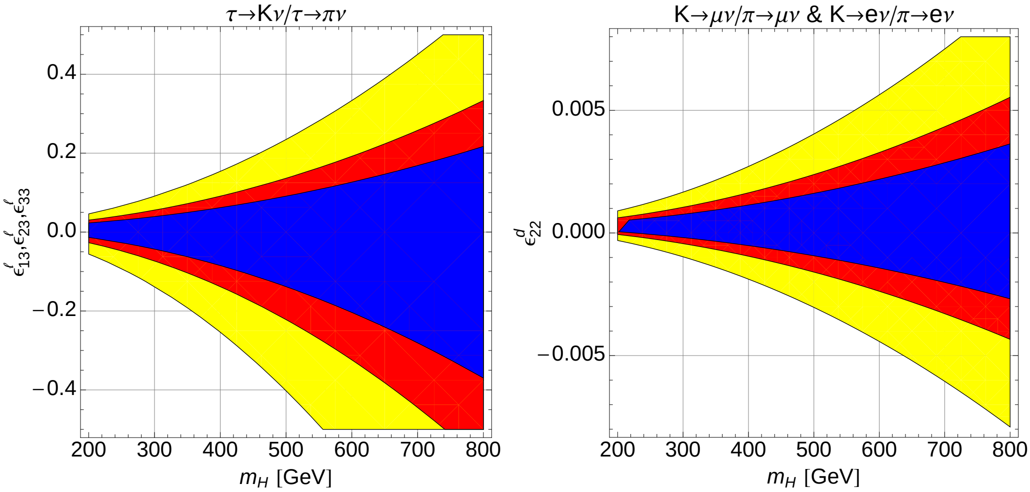

Figure 32: Left: Allowed regions in the m_H–ϵ^ℓ_{i3}–plane from $\tau \to K\nu/\tau \to \pi\nu$. Right: Allowed regions in the m_H–ϵ^d_{22}–plane obtained by combining the constraints from $K \to \mu\nu/\pi \to \mu\nu$ and $K \to e\nu/\pi \to e\nu$ for real values of ϵ^d_{22}. In both plots $\tan\beta = 30$ (yellow), $\tan\beta = 40$ (red) and $\tan\beta = 50$ (blue).

Therefore, in this section we study the upper limits on $B_{s,d} \to \tau\mu$, $B_{s,d} \to \tau e$, $B_{s,d} \to \mu e$ and the correlation among $\tau^- \to \mu^-\mu^+\mu^-$, $\tau^- \to e^-\mu^+\mu^-$, $\mu^- \to e^-e^+e^-$ and $\tau \to \mu\gamma$, $\tau \to e\gamma$, $\mu \to e\gamma$ in the type-III 2HDM.

8.1 Neutral meson decays: $B_{s,d} \to \tau\mu$, $B_{s,d} \to \tau e$ and $B_{s,d} \to \mu e$

In the SM (with massless neutrinos) the branching ratios for these decays vanish. Also in the 2HDM of type II these decays are not possible (even beyond tree-level). In the type-III 2HDM, these decay modes are generated in the presence of flavor-violating terms ϵ^ℓ_{ij} and there exists even a tree-level neutral Higgs contribution to $B_s \to \ell_i^+\ell_j^-$ ($B_d \to \ell_i^+\ell_j^-$) if also $\epsilon^d_{23,32} \neq 0$ ($\epsilon^d_{13,31} \neq 0$).

Observables	$\mathcal{B}(B_s \to \mu e)$	$\mathcal{B}(B_d \to \mu e)$	$\mathcal{B}(B_d \to \tau\mu)$	$\mathcal{B}(B_d \to \tau e)$
Upper bounds	2.0×10^{-7} [145]	6.4×10^{-8} [145]	2.2×10^{-5} [146]	2.8×10^{-5} [146]

Table 12: Upper limits (90 % CL) on the branching ratios of the lepton flavor-violating B meson decays.

In the large $\tan\beta$ limit, $v \ll m_H$ and neglecting the smaller lepton mass, the corresponding expressions for these branching ratios take the simple form

$$\mathcal{B}\left[B_q \to \ell_i^+\ell_j^-\right] \approx N^q_{ij}\left(\frac{\tan\beta/50}{m_H/500\,\mathrm{GeV}}\right)^4 2\left[\left|\epsilon^\ell_{ji}\right|^2\left|\epsilon^d_{q3}\right|^2 + \left|\epsilon^\ell_{ij}\right|^2\left|\epsilon^d_{3q}\right|^2\right], \tag{70}$$

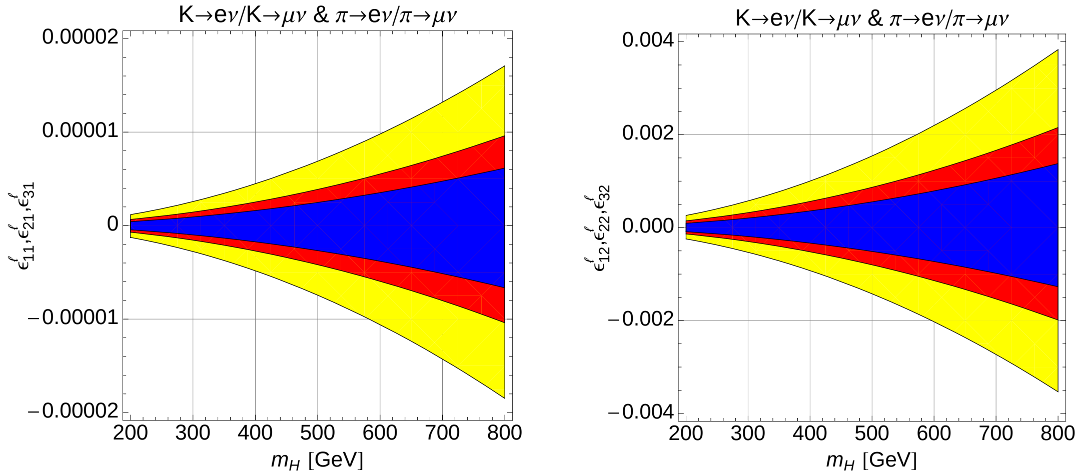

Figure 33: Allowed regions in the m_H–ϵ^ℓ_{ij}–plane obtained by combining the constraints from $K \to e\nu/K \to \mu\nu$ and $\pi \to e\nu/\pi \to \mu\nu$ for real values of ϵ^ℓ_{ij} and $\tan\beta = 30$ (yellow), $\tan\beta = 40$ (red) and $\tan\beta = 50$ (blue). The constraints on ϵ^ℓ_{i1} (affecting the electron coupling) are more stringent than the constraints on ϵ^ℓ_{i2} (which affect the muon coupling).

with $q = d, s$, $N^q_{ji} = N^q_{ij}$ and

$$\begin{aligned}
N^s_{21} &\approx 2.1 \times 10^7 \frac{f_{B_s}}{0.229\,\text{GeV}}\,,\\
N^d_{21} &\approx 1.6 \times 10^7 \frac{f_{B_d}}{0.196\,\text{GeV}}\,,\\
N^s_{31,32} &\approx 1.7 \times 10^7 \frac{f_{B_s}}{0.229\,\text{GeV}}\,,\\
N^d_{31,32} &\approx 1.2 \times 10^7 \frac{f_{B_d}}{0.196\,\text{GeV}}\,.
\end{aligned} \tag{71}$$

Note that the expressions for the branching ratios are not symmetric in ϵ^ℓ_{ij} and ϵ^ℓ_{ji}. Since experimentally both $B_q \to \ell_i^+\ell_j^-$ and $B_q \to \ell_i^-\ell_j^+$ are combined we compute the average

$$\mathcal{B}\left[B_q \to \ell_i\ell_j\right] = \left(\mathcal{B}\left[B_q \to \ell_i^+\ell_j^-\right] + \mathcal{B}\left[B_q \to \ell_j^+\ell_i^-\right]\right)/2\,.$$

In order to obtain the upper limits we insert the biggest allowed values for Abs $\left[\epsilon^{d,\ell}_{ij}\right]$. For $\epsilon^d_{23,32}$ ($\epsilon^d_{13,31}$) we use the biggest allowed absolute value compatible with the bounds from $B_s \to \mu^+\mu^-$ ($B_d \to \mu^+\mu^-$). As we can see from Fig. 4 (Fig. 5) the absolute value for ϵ^d_{32} (ϵ^d_{31}) can be bigger than ϵ^d_{23} (ϵ^d_{13}). For the leptonic parameters $\epsilon^\ell_{13,31}$ and $\epsilon^\ell_{23,32}$ we use the constraints obtained from $\tau^- \to \mu^-\mu^+\mu^-$, $\tau^- \to e^-\mu^+\mu^-$ (see Sec. 5.3)

$$\begin{aligned}
\left|\epsilon^\ell_{31,13}\right| &\leq 4.2 \times 10^{-3} \left(\frac{m_H/500\,\text{GeV}}{\tan\beta/50}\right)^2\,,\\
\left|\epsilon^\ell_{32,23}\right| &\leq 3.7 \times 10^{-3} \left(\frac{m_H/500\,\text{GeV}}{\tan\beta/50}\right)^2\,,
\end{aligned} \tag{72}$$

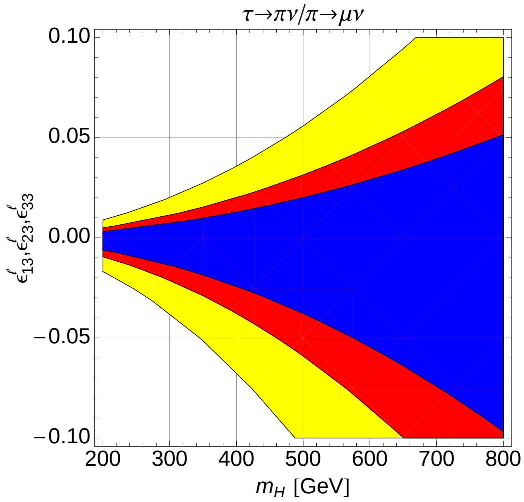

Figure 34: Allowed regions in the m_H–ϵ^ℓ_{i3}–plane from $\tau \to \pi\nu/\pi \to \mu\nu$ for real values of ϵ^ℓ_{i3} and $\tan\beta = 30$ (yellow), $\tan\beta = 40$ (red), $\tan\beta = 50$ (blue). The bounds on the imaginary parts are very weak.

while for $\epsilon^\ell_{12,21}$ we use the combined constraints from $\mu^- \to e^-e^+e^-$ and from $\mu \to e\gamma$ (see Sec. 6.4).

Our results are shown in Fig. 35 (see Table 12 for the current experimental limits). We see that for bigger Higgs masses larger values for the branching ratios are possible.

8.2 Radiative lepton decays: $\tau \to \mu\gamma$, $\tau \to e\gamma$ and $\mu \to e\gamma$.

In Sec. 5.3 and Sec. 6.4 we found that the radiative lepton decays $\tau \to \mu\gamma$ and $\tau \to e\gamma$ give less stringent bounds on the parameters $\epsilon^\ell_{23,32}$ and $\epsilon^\ell_{13,31}$ than the processes $\tau^- \to \mu^-\mu^+\mu^-$ and $\tau^- \to e^-\mu^+\mu^-$ while the constraints on $\epsilon^\ell_{12,21}$ from $\mu \to e\gamma$ are stronger than the ones from $\mu^- \to e^-e^+e^-$.

There are however interesting correlations between these decays in the type-III 2HDM. In the large $\tan\beta$ limit and for $v \ll m_H$ we obtain the following relation

$$\frac{\mathcal{B}\left[\ell_i \to \ell_f\gamma\right]}{\mathcal{B}\left[\ell_i^- \to \ell_f^-\ell_j^+\ell_j^-\right]} = \frac{\alpha_{em}}{24\pi}\frac{\left|m_{\ell_i}/v - \epsilon^\ell_{ii}\right|^2}{\left|m_{\ell_j}/v - \epsilon^\ell_{jj}\right|^2}\frac{\left(\left|\epsilon^\ell_{if}\right|^2 + 4\left|\epsilon^\ell_{fi}\right|^2\right)}{\left(\left|\epsilon^\ell_{if}\right|^2 + \left|\epsilon^\ell_{fi}\right|^2\right)}\,. \tag{73}$$

As already noted in Sec. 6.4, we stress that this formula is only a good approximation for very heavy Higgs due to the large logarithmic term in the expression for $\ell_i \to \ell_f\gamma$ (see Eq. (96)). Therefore, the relation in Eq. (73) gets modified for lighter Higgs masses as shown in Fig. 36. We see that, as expected, for very large Higgs masses the ratios approach

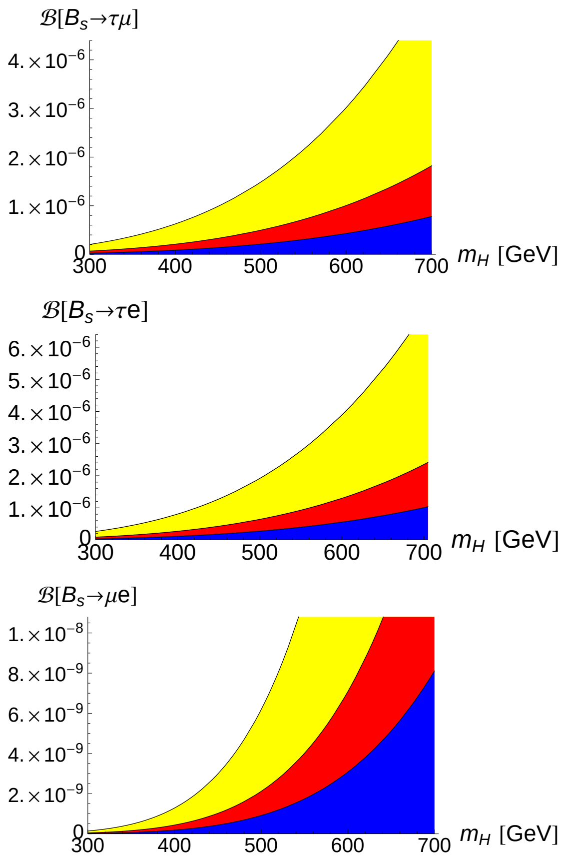

Figure 35: Upper limits on the branching ratios of the lepton flavor violating B meson decays as a function of m_H for $\tan\beta = 30$ (yellow), $\tan\beta = 40$ (red) and $\tan\beta = 50$ (blue).

$$\begin{aligned} \frac{\mathcal{B}\left[\ell_i \to \ell_f \gamma\right]}{\mathcal{B}\left[\ell_i^- \to \ell_f^- \ell_j^+ \ell_j^-\right]} &= \frac{\alpha_{em}}{24\pi} \frac{m_{\ell_i}^2}{m_{\ell_j}^2} \quad \text{for} \quad \epsilon_{if}^{\ell} \neq 0\,, \\ \frac{\mathcal{B}\left[\ell_i \to \ell_f \gamma\right]}{\mathcal{B}\left[\ell_i^- \to \ell_f^- \ell_j^+ \ell_j^-\right]} &= \frac{\alpha_{em}}{6\pi} \frac{m_{\ell_i}^2}{m_{\ell_j}^2} \quad \text{for} \quad \epsilon_{fi}^{\ell} \neq 0\,, \end{aligned} \tag{74}$$

where, we assumed that $\epsilon_{jj}^{\ell}/\epsilon_{ii}^{\ell} = m_{\ell_j}/m_{\ell_i}$ and that only one flavor changing element ϵ_{fi}^{ℓ}, ϵ_{if}^{ℓ} is different from zero.

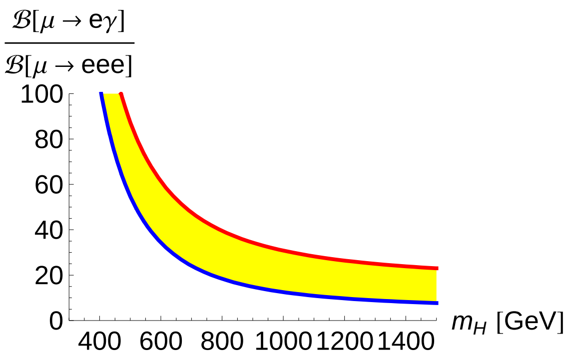

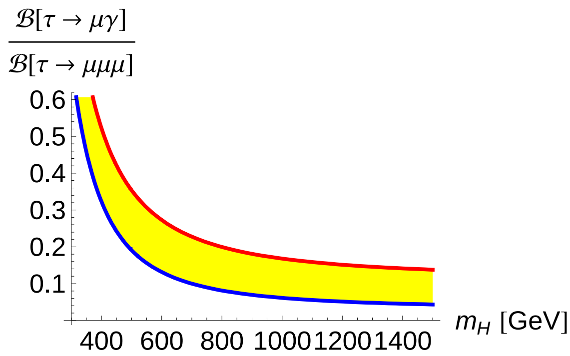

Figure 36: Left: $\frac{\mathcal{B}[\mu\to e\gamma]}{\mathcal{B}[\mu^-\to e^-e^+e^-]}$ as a function of m_H assuming that only ϵ^ℓ_{12} (red) or ϵ^ℓ_{21} (blue) is different from zero for $\tan\beta = 50$. Right: $\frac{\mathcal{B}[\tau\to\mu\gamma]}{\mathcal{B}[\tau^-\to\mu^-\mu^+\mu^-]}$ as a function of m_H assuming that only ϵ^ℓ_{23} (red) or ϵ^ℓ_{32} (blue) is different from zero for $\tan\beta = 50$.

For scenarios in which both ϵ^ℓ_{23} and ϵ^ℓ_{32} (ϵ^ℓ_{12} and ϵ^ℓ_{21}) are different from zero the 2HDM of type III predicts the ratio $\frac{\mathcal{B}[\tau\to\mu\gamma]}{\mathcal{B}[\tau^-\to\mu^-\mu^+\mu^-]}$ $\left(\frac{\mathcal{B}[\mu\to e\gamma]}{\mathcal{B}[\mu^-\to e^-e^+e^-]}\right)$ to be within the yellow region. These ratios are to a good approximation independent of $\tan\beta$ for $\tan\beta \gtrsim 20$. The behavior of $\frac{\mathcal{B}[\tau\to e\gamma]}{\mathcal{B}[\tau^-\to e^-\mu^+\mu^-]}$ (not shown here) is very similar to the case of $3\to 2$ transitions.

9 Conclusions

In this article we studied in detail the flavor phenomenology of a 2HDM with general Yukawa couplings. Motivated by the fact that the 2HDM of type III is the decoupling limit of the MSSM we assumed a MSSM-like Higgs potential. In our analysis we proceeded in several steps:

1. We gave order of magnitude constraints on the parameters $\epsilon^{q,\ell}_{ij}$ from 't Hooft's naturalness criterion and found that all couplings except $\epsilon^u_{i3,3i}$ and $\epsilon^u_{21,22}$ should be much smaller than one.

2. Considering tree-level FCNC processes we constrained the elements ϵ^d_{ij} ($i\neq j$) and $\epsilon^u_{12,21}$ from neutral meson decays to muons and from $\Delta F = 2$ processes, finding that they are tiny for the values of m_H and $\tan\beta$ under investigation (assuming $\epsilon^\ell_{ij} = 0$). In the lepton sector the absolute values of all flavor off-diagonal elements ϵ^ℓ_{ij} were constrained from $\tau^-\to\mu^-\mu^+\mu^-$, $\tau^-\to e^-\mu^+\mu^-$ and $\mu^-\to e^-e^+e^-$ to be very small.

3. After having found that the off-diagonal elements ϵ^d_{ij} must be very small due to constraints from tree-level contributions to FCNC processes we considered charged Higgs contributions to $K-\overline{K}$, $B_s-\overline{B}_s$, $B_d-\overline{B}_d$ mixing and $b\to s(d)\gamma$ arising at the one-loop level. In these contributions the so far unconstrained elements $\epsilon^u_{i3,3i}$ (and also ϵ^u_{22}) enter for the first time and we found that, setting $\epsilon^d_{ij} = 0$ (with $i\neq j$), $\epsilon^u_{13,23}$ should be rather small. Furthermore, the electric dipole moment of the neutron and of the charged leptons constrain ϵ^u_{11}, ϵ^u_{22}, ϵ^u_{21}, ϵ^u_{31} and ϵ^ℓ_{ij}, respectively. Respecting all other constraints, no sizable effect in a_μ is possible.

4. Keeping in mind the constraints from the previous steps, we considered the possible effects in charged current processes. Here we found that tests for lepton flavor univer-

Observable	Results
Neutral meson decays to muons	
$B_s \to \mu^+\mu^-$	$\left\|\epsilon^d_{32}\right\| \leq 3.0\times10^{-5}$, $\left\|\epsilon^d_{23}\right\| \leq 1.9\times10^{-5}$, $\left\|\epsilon^\ell_{22}\right\| \leq 2.0\times10^{-3}$
$B_d \to \mu^+\mu^-$	$\left\|\epsilon^d_{31}\right\| \leq 1.1\times10^{-5}$, $\left\|\epsilon^d_{13}\right\| \leq 9.4\times10^{-6}$
$K_L \to \mu^+\mu^-$	$\left\|\epsilon^d_{21}\right\| \leq 1.6\times10^{-6}$, $\left\|\epsilon^d_{12}\right\| \leq 1.6\times10^{-6}$
$\bar{D}^0 \to \mu^+\mu^-$	$\|\epsilon^u_{21}\| \leq 3.0\times10^{-2}$, $\|\epsilon^u_{12}\| \leq 3.0\times10^{-2}$
$\boldsymbol{\Delta F = 2}$ **processes**	
$B_s - \overline{B}_s$ mixing	$\left\|\epsilon^d_{23}\epsilon^{d\star}_{32}\right\| \leq 9.2\times10^{-10}$, $\|\epsilon^u_{23}\| \leq 0.18$, $\|\epsilon^u_{32}\| \leq 1.7$, $\|\epsilon^u_{33}\| \leq 0.7$
$B_d - \overline{B}_d$ mixing	$\left\|\epsilon^d_{13}\epsilon^{d\star}_{31}\right\| \leq 3.9\times10^{-11}$, $\|\epsilon^u_{23}\| \leq 0.2$, $\|\epsilon^u_{13}\| \leq 0.04$, $\|\epsilon^u_{31}\| \leq 1.9$
$K - \overline{K}$ mixing	$\left\|\epsilon^d_{12}\epsilon^{d\star}_{21}\right\| \leq 1.0\times10^{-12}$, $\|\epsilon^u_{22}\| \leq 0.25$, $\|\epsilon^u_{23}\| \leq 0.14$
$D - \overline{D}$ mixing	$\|\epsilon^u_{12}\epsilon^{u\star}_{21}\| \leq 2.0\times10^{-8}$, $\|\epsilon^u_{32}\epsilon^{u\star}_{31}\| \leq 0.02$
Radiative $\boldsymbol{B}$ decays	
$b \to s\gamma$	$\|\epsilon^u_{23}\| \leq 0.024$, $\|\epsilon^u_{33}\| \leq 0.55$
$b \to d\gamma$	$\|\epsilon^u_{13}\| \leq 7.0\times10^{-3}$
Radiative lepton decays	
$\mu \to e\gamma$	$\left\|\epsilon^\ell_{12}\right\| \leq 1.7\times10^{-4}$, $\left\|\epsilon^\ell_{21}\right\| \leq 2.2\times10^{-4}$, $55 \leq \frac{\mathcal{B}[\mu\to e\gamma]}{\mathcal{B}[\mu^-\to e^-e^+e^-]} \leq 86$
$\tau \to e\gamma$	$0.19 \leq \frac{\mathcal{B}[\tau\to e\gamma]}{\mathcal{B}[\tau^-\to e^-\mu^+\mu^-]} \leq 0.35$
$\tau \to \mu\gamma$	$0.19 \leq \frac{\mathcal{B}[\tau\to \mu\gamma]}{\mathcal{B}[\tau^-\to \mu^-\mu^+\mu^-]} \leq 0.35$
Neural current lepton decays	
$\mu^- \to e^-e^+e^-$	$\left\|\epsilon^\ell_{12,21}\right\| \leq 2.3\times10^{-3}$
$\tau^- \to e^-\mu^+\mu^-$	$\left\|\epsilon^\ell_{13,31}\right\| \leq 4.2\times10^{-3}$
$\tau^- \to \mu^-\mu^+\mu^-$	$\left\|\epsilon^\ell_{23,32}\right\| \leq 3.7\times10^{-3}$

Table 13: Results obtained in the type-III 2HDM from various processes for $\tan\beta = 50$ and $m_H = 500$ GeV.

sality constrain the differences $\epsilon^\ell_{ii}/m_{\ell_i} - \epsilon^\ell_{jj}/m_{\ell_j}$. Most importantly, the unconstrained elements ϵ^u_{31} and ϵ^u_{32} enter the processes $B \to \tau\nu$ and $B \to D^{(*)}\tau\nu$ directly (without CKM suppression) and can remove the tension between experiment and theory prediction observed in the SM simultaneously.

5. Finally we gave upper limits on the lepton flavor violating neutral B meson decays in the 2HDM of type III and correlated the radiative lepton decays to $\tau^- \to \mu^-\mu^+\mu^-$, $\tau^- \to e^-\mu^+\mu^-$ and $\mu^- \to e^-e^+e^-$.

In Table 13 and 14 we list all processes which have been under consideration and quote the constraints placed on the parameters $\epsilon^{q,\ell}_{ij}$ for our benchmark point $m_H = 500$ GeV and $\tan\beta = 50$.

In summary, combining the constraints from Table 13 and 14 the following bounds on the absolute values of the parameters ϵ^q_{ij} and ϵ^ℓ_{ij} (for our benchmark point with $m_H = 500$ GeV

Observable	**Results**
Charged current processes	
$B \to \tau\nu$	$2.7 \times 10^{-3} \leq \lvert\epsilon^u_{31}\rvert \leq 2.0 \times 10^{-2}$, $\left\lvert\epsilon^\ell_{i3}\right\rvert \leq 6.0 \times 10^{-2}$
$B \to D\tau\nu$ & $B \to D^\star\tau\nu$	$0.43 \leq \lvert\epsilon^u_{32}\rvert \leq 0.74$
$D_s \to \tau\nu$ & $D_{(s)} \to \mu\nu$	$\lvert\mathrm{Re}\,[\epsilon^u_{22}]\rvert \leq 0.2$
$D \to \tau\nu$	–
$K \to \mu(e)\nu/\pi \to \mu(e)\nu$	$\left\lvert\mathrm{Re}\left[\epsilon^d_{22}\right]\right\rvert \leq 1.0 \times 10^{-3}$
$K(\pi) \to e\nu/K(\pi) \to \mu\nu$	$\left\lvert\mathrm{Re}\left[\epsilon^\ell_{i1}\right]\right\rvert \leq 2.0 \times 10^{-6}$, $\left\lvert\mathrm{Re}\left[\epsilon^\ell_{i2}\right]\right\rvert \leq 5.0 \times 10^{-4}$
$\tau \to K(\pi)\nu/K(\pi) \to \mu\nu$	$-4.0 \times 10^{-2} \leq \mathrm{Re}\left[\epsilon^\ell_{i3}\right] \leq 2.0 \times 10^{-2}$
$\tau \to K\nu/\tau \to \pi\nu$	$\left\lvert\epsilon^\ell_{i3}\right\rvert \leq 0.14$
EDMs and anomalous magnetic moments	
d_e	$\left\lvert\mathrm{Im}\left[\epsilon^\ell_{12}\epsilon^\ell_{21}\right]\right\rvert \leq 2.5 \times 10^{-8}$, $\left\lvert\mathrm{Im}\left[\epsilon^\ell_{13}\epsilon^\ell_{31}\right]\right\rvert \leq 2.5 \times 10^{-9}$
d_μ	–
d_τ	–
d_n	$\lvert\mathrm{Im}\,[\epsilon^u_{11}]\rvert \leq 2.2 \times 10^{-2}$, $\lvert\mathrm{Im}\,[\epsilon^u_{22}]\rvert \leq 1.1 \times 10^{-1}$, $\mathrm{Arg}[\epsilon^u_{31}] = \mathrm{Arg}[V_{ub}] \pm \pi$
a_μ	Deviation from the SM cannot be explained
LVF B meson decays	
$B_s \to \tau\mu$	$\mathcal{B}\,[B_s \to \tau\mu] \leq 2.0 \times 10^{-7}$
$B_s \to \mu e$	$\mathcal{B}\,[B_s \to \mu e] \leq 9.2 \times 10^{-10}$
$B_s \to \tau e$	$\mathcal{B}\,[B_s \to \tau e] \leq 2.8 \times 10^{-7}$
$B_d \to \tau\mu$	$\mathcal{B}\,[B_d \to \tau\mu] \leq 2.1 \times 10^{-8}$
$B_d \to \mu e$	$\mathcal{B}\,[B_d \to \mu e] \leq 9.2 \times 10^{-11}$
$B_d \to \tau e$	$\mathcal{B}\,[B_d \to \tau e] \leq 2.8 \times 10^{-8}$

Table 14: Results obtained in the type-III 2HDM from various processes for $\tan\beta = 50$ and $m_H = 500$ GeV.

and $\tan\beta = 50$) are obtained:

$$\begin{aligned}
\left\lvert\epsilon^u_{ij}\right\rvert &\leq \begin{pmatrix} 3.4 \times 10^{-4} & 3.0 \times 10^{-2} & 7.0 \times 10^{-3} \\ 3.0 \times 10^{-2} & 1.4 \times 10^{-1} & 2.4 \times 10^{-2} \\ 2.0 \times 10^{-2} & 7.4 \times 10^{-1} & 5.5 \times 10^{-1} \end{pmatrix}_{ij} \\
\left\lvert\epsilon^d_{ij}\right\rvert &\leq \begin{pmatrix} 1.3 \times 10^{-4} & 1.6 \times 10^{-6} & 9.4 \times 10^{-6} \\ 1.6 \times 10^{-6} & 2.6 \times 10^{-4} & 2.0 \times 10^{-5} \\ 1.1 \times 10^{-5} & 3.0 \times 10^{-5} & 1.4 \times 10^{-2} \end{pmatrix}_{ij} \\
\left\lvert\epsilon^\ell_{ij}\right\rvert &\leq \begin{pmatrix} 2.9 \times 10^{-6} & 1.7 \times 10^{-4} & 4.2 \times 10^{-3} \\ 2.2 \times 10^{-4} & 6.1 \times 10^{-4} & 3.7 \times 10^{-3} \\ 4.2 \times 10^{-3} & 3.7 \times 10^{-3} & 1.0 \times 10^{-2} \end{pmatrix}_{ij}
\end{aligned} \tag{75}$$

These bounds hold in the absence of large cancellations between different contributions. Note that in Eq. (75) we applied the naturalness bounds in case they were stronger than the experimental limits.

It is interesting that $B \to \tau\nu$, $B \to D\tau\nu$ and $B \to D^*\tau\nu$ can be explained simultaneously in the 2HDM of type III without violating bounds from other observables and without significant fine-tuning. It remains to be seen if these tensions with the SM remain when updated experimental results and improved theory predictions will be available in the future. In order to further test the model and constrain the parameters ϵ^u_{32} (ϵ^u_{31}) we propose to study $H^0, A^0 \to \bar{t}c$ ($H^0, A^0 \to \bar{t}u$) at the LHC.

Acknowledgments : This work is supported by the Swiss National Science Foundation. We thank Jernej Kamenik and Ulrich Nierste for collaboration in the early stages of this work. A.C. also thanks Jernej Kamenik for useful comments on the manuscript.

10 Appendix

In this appendix, we collect the Wilson coefficients (to the relevant precision at the matching scale) which are needed for the calculation of $b \to s(d)\gamma$, $\Delta F = 2$ processes (i.e. neutral meson mixing), leptonic neutral meson decays ($\Delta F = 1$ processes), $B \to \tau\nu$, $B \to D\tau\nu$, $B \to D^*\tau\nu$, $D_{(s)} \to \ell\nu_\ell$, $K(\pi) \to \ell\nu_\ell$, $\tau \to K(\pi)\nu$, LFV radiative lepton transitions, EDMs of charged leptons and neutron, as well as the AMM of the muon. In addition, we give general expressions for some branching ratios, the explicit form of the loop functions entering our results and summarize the input parameters used in our analysis in tabular form.

10.1 Loop functions

We give the explicit form of the loop functions entering our results. In the limit of vanishing external momentum the one and two-point Passarino Veltman functions [147] are defined as

$$\begin{aligned} A_0\left(m^2\right) &= \frac{16\pi^2}{i}\mu^{4-d}\int \frac{d^dk}{(2\pi)^d}\frac{1}{\left(k^2-m^2\right)}\,, \\ B_0\left(m_1^2,m_2^2\right) &= \frac{16\pi^2}{i}\mu^{4-d}\int \frac{d^dk}{(2\pi)^d}\frac{1}{\left(k^2-m_1^2\right)\,\left(k^2-m_2^2\right)}\,, \end{aligned} \tag{76}$$

where μ is the renormalization scale.

The loop functions C_0 (three-point) and D_0 (four-point) are defined in analogy to B_0, but with three and four propagators, respectively. Evaluating these loop functions yields (with $d = 4 - 2\varepsilon$)

$$\begin{aligned} A_0\left(m^2\right) &= m^2\left[1+\frac{1}{\varepsilon}-\gamma_E+\ln\left(4\pi\right)+\ln\left(\frac{\mu^2}{m^2}\right)\right]+O\left(\varepsilon\right)\,, \\ B_0\left(m_1^2,m_2^2\right) &= 1+\frac{1}{\varepsilon}-\gamma_E+\ln\left(4\pi\right)+\frac{m_1^2\ln\left(\frac{\mu^2}{m_1^2}\right)-m_2^2\ln\left(\frac{\mu^2}{m_2^2}\right)}{m_1^2-m_2^2}+O\left(\varepsilon\right)\,, \end{aligned} \tag{77}$$

$$\begin{aligned} C_0\left(m_1^2,m_2^2,m_3^2\right) &= \frac{B_0\left(m_1^2,m_2^2\right)-B_0\left(m_1^2,m_3^2\right)}{m_2^2-m_3^2} \\ &= \frac{m_1^2m_2^2\ln\left(\frac{m_1^2}{m_2^2}\right)+m_3^2m_2^2\ln\left(\frac{m_2^2}{m_3^2}\right)+m_3^2m_1^2\ln\left(\frac{m_3^2}{m_1^2}\right)}{\left(m_1^2-m_2^2\right)\,\left(m_3^2-m_1^2\right)\,\left(m_2^2-m_3^2\right)}\,, \\ D_0\left(m_1^2,m_2^2,m_3^2,m_4^2\right) &= \frac{C_0\left(m_1^2,m_2^2,m_3^2\right)-C_0\left(m_1^2,m_2^2,m_4^2\right)}{m_3^2-m_4^2}\,. \end{aligned} \tag{78}$$

Here, the one and the two-point loop functions A_0, B_0 are UV-divergent and ε is the UV-regulator.

At various places also the functions C_2 and D_2 appear, which have, compared to C_0 and D_0, an additional factor k^2 in the numerator of the integrand. These functions read

$$\begin{aligned} &C_2\left(m_1^2,m_2^2,m_3^2\right) = B_0\left(m_1^2,m_2^2\right)+m_3^2\,C_0\left(m_1^2,m_2^2,m_3^2\right)\,, \\ &D_2\left(m_1^2,m_2^2,m_3^2,m_4^2\right) = C_0\left(m_1^2,m_2^2,m_3^2\right)+m_4^2\,D_0\left(m_1^2,m_2^2,m_3^2,m_4^2\right)\,. \end{aligned} \tag{79}$$

10.2 Radiative $b \to s(d)\gamma$ decays

Concering new physics contributions to $b \to s(d)\gamma$, we work in leading logarithmic (LL) precision in this paper. As mentioned before, we use these processes to constrain certain elements ϵ^{u}_{ij}. For this purpose, we put the $\epsilon^{d}_{ij}-$couplings (which are already constrained to be very small) to zero. When also neglecting the mass of the strange quark and further neglecting operators with mass dimension higher than six, we obtain the same effective Hamiltonian as in the SM, reading for $b \to s\gamma$ (see e.g. Ref. [47]).

$$\mathcal{H}_{eff}^{b\to s\gamma} = -\frac{4G_F}{\sqrt{2}} V_{tb}V_{ts}^{\star} \sum_i C_i\, O_i\,. \tag{80}$$

For $b \to d\gamma$ the CKM structure is slightly more complicated (see e.g. Ref. [95]). In our approximation only the Wilson coefficients C_7 and C_8 of the operators

$$O_7 = \frac{e}{16\pi^2} m_b \bar{s}\sigma^{\mu\nu} P_R b F_{\mu\nu} \quad ; \qquad O_8 = \frac{g_s}{16\pi^2} m_b \bar{s}\sigma^{\mu\nu} T^a P_R b G^a_{\mu\nu} \tag{81}$$

get new physics contributions. They are induced through charged Higgs bosons propagating in the loop (neutral Higgs boson exchange leads to power suppressed contributions which we neglect). For $b \to s\gamma$ the new physics contributions read (with $y_j = m^2_{u_j}/m^2_{H^+}$ and $\lambda_t = V_{tb}\, V^{\star}_{ts}$)

$$\begin{aligned}
C_7^{NP} &= \frac{v^2}{\lambda_t}\frac{1}{m_b}\sum_{j=1}^{3} \Gamma^{RLH^{\pm}\star}_{u_j d_2}\Gamma^{LRH^{\pm}}_{u_j d_3}\frac{C^0_{7,XY}(y_j)}{m_{u_j}} \\
&+ \frac{v^2}{\lambda_t}\sum_{j=1}^{3} \Gamma^{RLH^{\pm}\star}_{u_j d_2}\Gamma^{RLH^{\pm}}_{u_j d_3}\frac{C^0_{7,YY}(y_j)}{m^2_{u_j}}\,, \\
C_8^{NP} &= \frac{v^2}{\lambda_t}\frac{1}{m_b}\sum_{j=1}^{3} \Gamma^{RLH^{\pm}\star}_{u_j d_2}\Gamma^{LRH^{\pm}}_{u_j d_3}\frac{C^0_{8,XY}(y_j)}{m_{u_j}} \\
&+ \frac{v^2}{\lambda_t}\sum_{j=1}^{3} \Gamma^{RLH^{\pm}\star}_{u_j d_2}\Gamma^{RLH^{\pm}}_{u_j d_3}\frac{C^0_{8,YY}(y_j)}{m^2_{u_j}}\,,
\end{aligned} \tag{82}$$

while for $b \to d\gamma$ the label d_2 and $\lambda_t = V_{tb}\, V^{\star}_{ts}$ have to be replaced by d_1 and $\lambda_t = V_{tb}\, V^{\star}_{td}$, respectively. The functions $C^0_{7,XY}$, $C^0_{7,YY}$, $C^0_{8,XY}$ and $C^0_{8,YY}$ were introduced in Ref. [47]; their explicit form reads

$$\begin{aligned}
C^0_{7,XY}(y_j) &= \frac{y_j}{12}\left[\frac{-5y_j^2 + 8y_j - 3 + (6y_j - 4)\ln y_j}{(y_j-1)^3}\right] \quad , \\
C^0_{8,XY}(y_j) &= \frac{y_j}{4}\left[\frac{-y_j^2 + 4y_j - 3 - 2\ln y_j}{(y_j-1)^3}\right] \quad , \\
C^0_{7,YY}(y_j) &= \frac{y_j}{72}\left[\frac{-8y_j^3 + 3y_j^2 + 12y_j - 7 + (18y_j^2 - 12y_j)\ln y_j}{(y_j-1)^4}\right] \quad , \\
C^0_{8,YY}(y_j) &= \frac{y_j}{24}\left[\frac{-y_j^3 + 6y_j^2 - 3y_j - 2 - 6y_j\ln y_j}{(y_j-1)^4}\right] \quad .
\end{aligned} \tag{83}$$

In Eq. (82) we retained the contributions from internal up- and charm-quarks, although these contributions are subleading.

10.3 Wilson coefficients for $\Delta F = 2$ processes

The extended Higgs sector of our 2HDM of type-III also leads to extra contributions to $\Delta F = 2$ processes (B_s, B_d, Kaon and D mixing) which can be matched onto the effective Hamiltonian

$$\mathcal{H}_{eff}^{\Delta F=2} = \sum_{j=1}^{5} C_j\, O_j + \sum_{j=1}^{3} C_j'\, O_j' + h.c.\,, \tag{84}$$

where the operators read in the case of B_s mixing

$$\begin{aligned} O_1 &= (\bar{s}_\alpha \gamma^\mu P_L b_\alpha)\,(\bar{s}_\beta \gamma^\mu P_L b_\beta)\,, & O_2 &= (\bar{s}_\alpha P_L b_\alpha)\,(\bar{s}_\beta P_L b_\beta)\,, \\ O_3 &= (\bar{s}_\alpha P_L b_\beta)\,(\bar{s}_\beta P_L b_\alpha)\,, & O_4 &= (\bar{s}_\alpha P_L b_\alpha)\,(\bar{s}_\beta P_R b_\beta)\,, \\ O_5 &= (\bar{s}_\alpha P_L b_\beta)\,(\bar{s}_\beta P_R b_\alpha)\,. \end{aligned} \tag{85}$$

α and β are color indices and the primed operators can be obtained from $O_{1,2,3}$ by interchanging L and R. Similarly, the corresponding operator bases for B_d, Kaon and D mixing follow from Eq. (85) through simple adjustment of the indices.

In the following subsections we present the contributions to these Wilson coefficients arising from: 1.) one-loop box diagrams with charged Higgs boson exchange; 2.) tree-level contributions induced by neutral Higgs boson exchange; 3.) box diagrams involving neutral Higgs bosons, relevant in the case of D mixing.

10.3.1 Charged Higgs box contributions

For definiteness, let us consider B_s mixing. The corresponding Wilson coefficients for B_d and Kaon mixing follow by a simple adjustment of the indices. We have performed our calculation in a general R_ξ gauge. The non-vanishing Wilson coefficients from pure charged Higgs boxes are given by

$$\begin{aligned} C_1 &= \frac{-1}{128\pi^2} \sum_{j,k=1}^{3} \Gamma_{u_j d_2}^{RL\,H^\pm\star} \Gamma_{u_j d_3}^{RL\,H^\pm} \Gamma_{u_k d_2}^{RL\,H^\pm\star} \Gamma_{u_k d_3}^{RL\,H^\pm} D_2\left(m_{u_j}^2, m_{u_k}^2, m_{H^\pm}^2, m_{H^\pm}^2\right), \\ C_2 &= \frac{-1}{32\pi^2} \sum_{j,k=1}^{3} m_{u_j} m_{u_k} \Gamma_{u_j d_2}^{LR\,H^\pm\star} \Gamma_{u_j d_3}^{RL\,H^\pm} \Gamma_{u_k d_2}^{LR\,H^\pm\star} \Gamma_{u_k d_3}^{RL\,H^\pm} D_0\left(m_{u_j}^2, m_{u_k}^2, m_{H^\pm}^2, m_{H^\pm}^2\right), \\ C_4 &= \frac{-1}{16\pi^2} \sum_{j,k=1}^{3} m_{u_j} m_{u_k} \Gamma_{u_j d_2}^{LR\,H^\pm\star} \Gamma_{u_j d_3}^{RL\,H^\pm} \Gamma_{u_k d_2}^{RL\,H^\pm\star} \Gamma_{u_k d_3}^{LR\,H^\pm} D_0\left(m_{u_j}^2, m_{u_k}^2, m_{H^\pm}^2, m_{H^\pm}^2\right), \\ C_5 &= \frac{1}{32\pi^2} \sum_{j,k=1}^{3} \Gamma_{u_j d_2}^{LR\,H^\pm\star} \Gamma_{u_j d_3}^{LR\,H^\pm} \Gamma_{u_k d_2}^{RL\,H^\pm\star} \Gamma_{u_k d_3}^{RL\,H^\pm} D_2\left(m_{u_j}^2, m_{u_k}^2, m_{H^\pm}^2, m_{H^\pm}^2\right). \end{aligned} \tag{86}$$

The sum of the charged Higgs$-W^{\pm}$ and charged Higgs$-$Goldstone-boson boxes is given by

$$
\begin{aligned}
C_1 &= \frac{g_2^2}{32\pi^2}\sum_{j,k=1}^{3}\Bigg(m_{u_j}m_{u_k}V_{j2}^{\star}V_{k3}\Gamma_{u_jd_3}^{RL\,H^{\pm}}\Gamma_{u_kd_2}^{RL\,H^{\pm}\star}\\
&\quad\times\frac{4M_W^2 D_0\left(M_W^2,m_{H^{\pm}}^2,m_{u_j}^2,m_{u_k}^2\right)-D_2\left(M_W^2,m_{H^{\pm}}^2,m_{u_j}^2,m_{u_k}^2\right)}{4M_W^2}\Bigg)\\
C_4 &= \frac{1}{16\pi^2}\frac{g_2^2}{2}\sum_{j,k=1}^{3}\Bigg(V_{j3}V_{k2}^{\star}\Gamma_{u_jd_2}^{LR\,H^{\pm}\star}\Gamma_{u_kd_3}^{LR\,H^{\pm}}\\
&\quad\times\frac{C_2\left(\xi M_W^2,m_{H^{+}}^2,m_{u_j}^2\right)-C_2\left(m_{H^{+}}^2,m_{u_j}^2,m_{u_k}^2\right)+m_{u_k}^2C_0\left(\xi M_W^2,m_{H^{\pm}}^2,m_{u_k}^2\right)}{M_W^2}\Bigg)
\end{aligned}
\tag{87}
$$

We stress here, that we want to use B_s mixing only to constrain certain $\epsilon_{ij}^{u}-$couplings, because the $\epsilon_{ij}^{d}-$quantities are already contrained to be very small. We therefore only took systematically into account those contributions to the Wilson coefficients which stay different from zero in the limit $\epsilon_{ij}^{d}\to 0$. At first sight, the Wilson coefficient C_4 seems to be gauge dependent. However, when using the unitarity of the CKM matrix (entering the expression for C_4 both, explicitly and implicitly through the $\Gamma-$quantities), we find that the $\xi-$dependent terms are always proportional to an element ϵ_{ij}^{d}, which we put to zero in our analysis. Also note that our result agrees with the one of Ref. [148]. The only difference is that we neglected gauge dependent terms corresponding to higher dimensional operators. The Wilson coefficients of the primed operators can be obtained by interchanging L and R in the corresponding unprimed ones.

10.3.2 Tree-level H_k^0 contribution

The Wilson coefficients from neutral Higgs mediated tree-level contributions to B_s mixing read:

$$
\begin{aligned}
C_2^{H_k^0} &= \sum_{k=1}^{3}\frac{-1}{2m_{H_k^0}^2}\left(\Gamma_{d_3d_2}^{LR\,H_k^0\star}\right)^2\\
C_2'^{\,H_k^0} &= \sum_{k=1}^{3}\frac{-1}{2m_{H_k^0}^2}\left(\Gamma_{d_2d_3}^{LR\,H_k^0}\right)^2\\
C_4^{H_k^0} &= \sum_{k=1}^{3}\frac{-1}{m_{H_k^0}^2}\Gamma_{d_2d_3}^{LR\,H_k^0}\,\Gamma_{d_3d_2}^{LR\,H_k^0\star}
\end{aligned}
\tag{88}
$$

The corresponding coefficients for B_d, Kaon and D mixing follow by a careful adjustment of the indices.

Note that in the limit of large $\tan\beta$ and $m_A \gg v$, $C_2^{H_k^0}$ and $C_2'^{\,H_k^0}$ vanish and we only get a contribution to $C_4^{H_k^0}$.

10.3.3 Neutral Higgs box contribution to D mixing

The Wilson coefficients resulting from the neutral Higgs box contribution to D mixing are given as

$$
\begin{aligned}
C_1 &= \frac{-1}{128\pi^2} \sum_{j_1,j_2=1}^{3} \sum_{k_1,k_2=1}^{3} \Gamma^{LR\,H^0_{k_1}\star}_{u_2 u_{j_1}} \Gamma^{LR\,H^0_{k_2}}_{u_1 u_{j_1}} \Gamma^{LR\,H^0_{k_2}\star}_{u_2 u_{j_2}} \Gamma^{LR\,H^0_{k_1}}_{u_1 u_{j_2}} D_2\left(m^2_{u_{j_1}}, m^2_{u_{j_2}}, m^2_{H^0_{k_1}}, m^2_{H^0_{k_2}}\right), \\
C_2 &= \frac{-1}{32\pi^2} \sum_{j_1,j_2=1}^{3} \sum_{k_1,k_2=1}^{3} m_{u_{j_1}} m_{u_{j_2}} \Gamma^{LR\,H^0_{k_1}\star}_{u_{j_1} u_1} \Gamma^{LR\,H^0_{k_2}\star}_{u_2 u_{j_1}} \Gamma^{LR\,H^0_{k_1}\star}_{u_{j_2} u_1} \Gamma^{LR\,H^0_{k_2}\star}_{u_2 u_{j_2}} \\
&\times\ D_0\left(m^2_{u_{j_1}}, m^2_{u_{j_2}}, m^2_{H^0_{k_1}}, m^2_{H^0_{k_2}}\right), \\
C_3 &= 0\,, \\
C_4 &= \frac{-1}{16\pi^2} \sum_{j_1,j_2=1}^{3} \sum_{k_1,k_2=1}^{3} m_{u_{j_1}} m_{u_{j_2}} \Gamma^{LR\,H^0_{k_1}\star}_{u_{j_1} u_1} \Gamma^{LR\,H^0_{k_2}\star}_{u_2 u_{j_1}} \Gamma^{LR\,H^0_{k_2}}_{u_{j_2} u_2} \Gamma^{LR\,H^0_{k_1}}_{u_1 u_{j_2}} \\
&\times\ D_0\left(m^2_{u_{j_1}}, m^2_{u_{j_2}}, m^2_{H^0_{k_1}}, m^2_{H^0_{k_2}}\right), \qquad (89) \\
C_5 &= \frac{-1}{128\pi^2} \sum_{j_1,j_2=1}^{3} \sum_{k_1,k_2=1}^{3} \Gamma^{LR\,H^0_{k_1}\star}_{u_{j_1} u_1} \Gamma^{LR\,H^0_{k_2}}_{u_{j_1} u_2} \Gamma^{LR\,H^0_{k_1}}_{u_1 u_{j_2}} \Gamma^{LR\,H^0_{k_2}\star}_{u_2 u_{j_2}} D_2\left(m^2_{u_{j_1}}, m^2_{u_{j_2}}, m^2_{H^0_{k_1}}, m^2_{H^0_{k_2}}\right).
\end{aligned}
$$

The indices j_1, j_2 describe the internal up-type quarks while k_1, k_2 stand for neutral Higgs indices (H^0, h^0, A^0). Moreover, the primed Wilson coefficients can be obtained from above by the replacement $L \leftrightarrow R$ in the couplings.

10.4 Semileptonic and leptonic meson decays and tau decays: $B \to (D^{(*)})\tau\nu$, $D_{(s)} \to \ell\nu_\ell$, $K(\pi) \to \ell\nu_\ell$ and $\tau \to K(\pi)\nu$ processes

These processes are governed by the effective Hamiltonian

$$
\mathcal{H}_{\text{eff}} = C^{u_f d_i,\ell_j}_{\text{SM}} O^{u_f d_i,\ell_j}_{\text{SM}} + C^{u_f d_i,\ell_j}_{L} O^{u_f d_i,\ell_j}_{L} + C^{u_f d_i,\ell_j}_{R} O^{u_f d_i,\ell_j}_{R} + \text{h.c.}\,, \qquad (90)
$$

with the operators defined as

$$
\begin{aligned}
O^{u_f d_i,\ell_j}_{\text{SM}} &= \bar{u}_f \gamma_\mu P_L d_i\, \bar{\ell}_j \gamma_\mu P_L \nu\,, \\
O^{u_f d_i,\ell_j}_{R} &= \bar{u}_f P_R d_i\, \bar{\ell}_j P_L \nu\,, \qquad (91) \\
O^{u_f d_i,\ell_j}_{L} &= \bar{u}_f P_L d_i\, \bar{\ell}_j P_L \nu\,.
\end{aligned}
$$

Here, for tauonic B meson decays $\ell_j = \tau$, $d_i = b$ and $u_f = u$ $(u_f = c)$ for $B \to \tau\nu$ $(B \to D\tau\nu$ and $B \to D^*\tau\nu$). For $D_s \to \ell_j\nu$ $(D \to \ell_j\nu)$, $u_f = c$ and $d_i = s$ (d), for $\tau \to K(\pi)\nu$, $\ell_j = \tau$, $u_f = u$ and $d_i = s$ (d) and for $K(\pi) \to \ell_j\nu$ we have $\ell_j = \mu, e$, $u_f = u$ and $d_i = s$ (d). The Wilson coefficients in 2HDM of type III at the matching scale read

$$
\begin{aligned}
C^{u_f d_i,\ell_j}_{\text{SM}} &= \frac{4G_F}{\sqrt{2}}\, V_{u_f d_i}\,, \\
C^{u_f d_i,\ell_j}_{R} &= \frac{-1}{m^2_{H^\pm}}\, \Gamma^{LR\,H^\pm}_{u_f d_i}\, \Gamma^{LR\,H^\pm\star}_{\nu\ell_j}\,, \qquad (92) \\
C^{u_f d_i,\ell_j}_{L} &= \frac{-1}{m^2_{H^\pm}}\, \Gamma^{RL\,H^\pm}_{u_f d_i}\, \Gamma^{LR\,H^\pm\star}_{\nu\ell_j}\,.
\end{aligned}
$$

10.5 Lepton flavour violation (LFV): $\ell_i \to \ell_f \gamma$ processes

The radiative lepton decays $\ell_i \to \ell_f \gamma$ ($\ell = e, \mu$ or τ) are induced by one-loop penguin diagrams with internal neutral or charged Higgs bosons. The result for the one-loop decay amplitude can be written as a tree-level matrix element of the effective Hamiltonian

$$\mathcal{H}_{eff} = c_R^{\ell_f \ell_i}\, O_R^{\ell_f \ell_i} + c_L^{\ell_f \ell_i}\, O_L^{\ell_f \ell_i}\,, \tag{93}$$

where $c_R^{\ell_f \ell_i}$ and $c_L^{\ell_f \ell_i}$ are the effective Wilson coefficients of the magnetic dipole operators

$$O_{R(L)}^{\ell_f \ell_i} = m_{\ell_i} \bar{\ell}_f \sigma_{\mu\nu} P_{R(L)} \ell_i F^{\mu\nu}\,. \tag{94}$$

With these conventions, the branching ratio for the radiative lepton decays $\ell_i \to \ell_f \gamma$ reads

$$\mathcal{B}\left[\ell_i \to \ell_f \gamma\right] = \frac{m_{\ell_i}^5}{4\pi\, \Gamma_{\ell_i}} \left(|c_R^{\ell_f \ell_i}|^2 + |c_L^{\ell_f \ell_i}|^2 \right)\,. \tag{95}$$

The neutral Higgs ($H_k^0 = H^0, h^0, A^0$) penguin contribution to $c_R^{\ell_f \ell_i}$ is given by

$$\begin{aligned} c_{R\,H_k^0}^{\ell_f \ell_i} = \sum_{k,j=1}^{3} \frac{-e}{192\pi^2 m_{H_k^0}^2} &\left[\Gamma_{\ell_f \ell_j}^{LR\,H_k^0} \Gamma_{\ell_i \ell_j}^{LR\,H_k^0\star} + \frac{m_{\ell_f}}{m_{\ell_i}} \Gamma_{\ell_j \ell_f}^{LR\,H_k^0\star} \Gamma_{\ell_j \ell_i}^{LR\,H_k^0} \right. \\ &\left. - \frac{m_{\ell_j}}{m_{\ell_i}} \Gamma_{\ell_f \ell_j}^{LR\,H_k^0} \Gamma_{\ell_j \ell_i}^{LR\,H_k^0} \left(9 + 6 \ln\left(\frac{m_{\ell_j}^2}{m_{H_k^0}^2} \right) \right) \right]\,, \end{aligned} \tag{96}$$

and $c_L^{\ell_f \ell_i}$ can be obtained from $c_R^{\ell_f \ell_i}$ by interchanging L and R. Similarly, for the charged Higgs penguin contributions we find

$$\begin{aligned} c_{L\;\;H^\pm}^{\ell_f \ell_i} &= \frac{e}{384\pi^2 m_{H^\pm}^2} \sum_{j=1}^{3} \Gamma_{\nu_j \ell_i}^{LR\,H^\pm} \Gamma_{\nu_j \ell_f}^{LR\,H^\pm\star}\,, \\ c_{R\;\;H^\pm}^{\ell_f \ell_i} &= \frac{m_{\ell_f}}{m_{\ell_i}} \frac{e}{384\pi^2 m_{H^\pm}^2} \sum_{j=1}^{3} \Gamma_{\nu_j \ell_i}^{LR\,H^\pm} \Gamma_{\nu_j \ell_f}^{LR\,H^\pm\star}\,. \end{aligned} \tag{97}$$

10.6 Wilson coefficients for EDMs and the anomalous magnetic moment of the muon

10.6.1 Wilson coefficients for EDMs of charged leptons and the anomalous magnetic moment of the muon

As in the case of the LFV processes discussed in the previous section, we again have both neutral and charged Higgs penguin contributions to the flavor conserving radiative transitions $\ell_i \to \ell_i \gamma$. The corresponding effective Hamiltonian is obtained from Eq. (93) and Eq. (94) by identifying ℓ_f with ℓ_i. The contribution to the effective Wilson coefficients related to neutral Higgs bosons (propagating in the loop) reads

$$\begin{aligned} c_{R\;\;H_k^0}^{\ell_i \ell_i} &= \sum_{k,j=1}^{3} \frac{-e}{192\pi^2 m_{H_k^0}^2} \left[\Gamma_{\ell_i \ell_j}^{LR\,H_k^0\star} \Gamma_{\ell_i \ell_j}^{LR\,H_k^0} + \Gamma_{\ell_j \ell_i}^{LR\,H_k^0\star} \Gamma_{\ell_j \ell_i}^{LR\,H_k^0} \right. &(98) \\ &\quad \left. - \frac{m_{\ell_j}}{m_{\ell_i}} \Gamma_{\ell_i \ell_j}^{LR\,H_k^0} \Gamma_{\ell_j \ell_i}^{LR\,H_k^0} \left(9 + 6 \ln\left(\frac{m_{\ell_j}^2}{m_{H_k^0}^2} \right) \right) \right]\,, \\ c_{L\;\;H_k^0}^{\ell_i \ell_i} &= c_{R\;\;H_k^0}^{\ell_i \ell_i \star}\,, &(99) \end{aligned}$$

while the charged Higgs penguin contribution leads to the (real) coefficients

$$c_{L\;H^\pm}^{\ell_i\ell_i} = c_{R\;H^\pm}^{\ell_i\ell_i} = \frac{e}{384\pi^2 m_{H^\pm}^2}\sum_{j=1}^{3}\Gamma_{\nu_j\ell_i}^{LR\,H^\pm}\Gamma_{\nu_j\ell_i}^{LR\,H^\pm\star}\,. \tag{100}$$

10.6.2 Wilson coefficients for neutron EDM

In this section we consider the transitions $d\to d\gamma(g)$ and $u\to u\gamma(g)$ (denoted by $d_d^{(g)}$ and $d_u^{(g)}$) which are the building blocks for the electric dipole moment d_n of the neutron. As we are only interested in a rough estimate of d_n, we do not include QCD corrections to these building blocks. In this approximation the latter can be described by the effective Hamiltonian

$$\begin{aligned}\mathcal{H}_{eff}^{dd,uu} = \;& c_R^{dd}\, m_d\, \bar d\sigma_{\mu\nu}P_R d\, F^{\mu\nu} + c_L^{dd}\, m_d\, \bar d\sigma_{\mu\nu}P_L d\, F^{\mu\nu} + \\ & c_{R,g}^{dd} m_d\, \bar d\sigma_{\mu\nu}P_R T^a d\, G^{a,\mu\nu} + c_{L,g}^{dd}\, m_d\, \bar d\sigma_{\mu\nu}P_L T^a d\, G^{a,\mu\nu} + (d\to u)\,.\end{aligned} \tag{101}$$

The effective Wilson coefficients $c_{R,L}^{dd,uu}$ and $c_{R,L,g}^{dd,uu}$ again receive neutral and charged Higgs contributions. The neutral contributions of the Wilson coefficients (involved in $d_d^{(g)}$) read

$$\begin{aligned}c_R^{dd,H_k^0} = \sum_{k,j=1}^{3}\frac{eQ_d}{192\pi^2 m_{H_k^0}^2}\Big[&\Gamma_{dd_j}^{LR\,H_k^0\star}\Gamma_{dd_j}^{LR\,H_k^0} + \Gamma_{d_jd}^{LR\,H_k^0\star}\Gamma_{d_jd}^{LR\,H_k^0} \\ &- \frac{m_{d_j}}{m_d}\Gamma_{dd_j}^{LR\,H_k^0}\Gamma_{d_jd}^{LR\,H_k^0}\left(9+6\ln\left(\frac{m_{d_j}^2}{m_{H_k^0}^2}\right)\right)\Big]\,,\end{aligned} \tag{102}$$

$$\begin{aligned}c_{R,g}^{dd,H_k^0} = \sum_{k,j=1}^{3}\frac{g_s}{192\pi^2 m_{H_k^0}^2}\Big[&\Gamma_{dd_j}^{LR\,H_k^0\star}\Gamma_{dd_j}^{LR\,H_k^0} + \Gamma_{d_jd}^{LR\,H_k^0\star}\Gamma_{d_jd}^{LR\,H_k^0} \\ &- \frac{m_{d_j}}{m_d}\Gamma_{dd_j}^{LR\,H_k^0}\Gamma_{d_jd}^{LR\,H_k^0}\left(9+6\ln\left(\frac{m_{d_j}^2}{m_{H_k^0}^2}\right)\right)\Big]\,,\end{aligned} \tag{103}$$

and $c_{L,(g)}^{dd,H_k^0} = c_{R,(g)}^{dd,H_k^0\,\star}$. The charged Higgs penguin contributions to the Wilson coefficients (involved in $d_d^{(g)}$) read

$$\begin{aligned}c_R^{dd,H^\pm} = \sum_{j=1}^{3}\frac{-e}{16\pi^2\, m_{u_j}^2}\Bigg[&\Gamma_{du_j}^{LR\,H^\pm\star}\Gamma_{du_j}^{LR\,H^\pm}\, C_{7,YY}^0\left(\frac{m_{u_j}^2}{m_{H^+}^2}\right) + \Gamma_{u_jd}^{LR\,H^\pm\star}\Gamma_{u_jd}^{LR\,H^\pm}\, C_{7,YY}^0\left(\frac{m_{u_j}^2}{m_{H^+}^2}\right) \\ &+\Gamma_{du_j}^{LR\,H^\pm}\Gamma_{u_jd}^{LR\,H^\pm}\frac{m_{u_j}}{m_d}\, C_{7,XY}^0\left(\frac{m_{u_j}^2}{m_{H^+}^2}\right)\Bigg]\,,\end{aligned} \tag{104}$$

$$\begin{aligned}c_{R,g}^{dd,H^\pm} = \sum_{j=1}^{3}\frac{-g_s}{16\pi^2\, m_{u_j}^2}\Bigg[&\Gamma_{du_j}^{LR\,H^\pm\star}\Gamma_{du_j}^{LR\,H^\pm}\, C_{8,YY}^0\left(\frac{m_{u_j}^2}{m_{H^+}^2}\right) + \Gamma_{u_jd}^{LR\,H^\pm\star}\Gamma_{u_jd}^{LR\,H^\pm}\, C_{8,YY}^0\left(\frac{m_{u_j}^2}{m_{H^+}^2}\right) \\ &+\Gamma_{du_j}^{LR\,H^\pm}\Gamma_{u_jd}^{LR\,H^\pm}\frac{m_{u_j}}{m_d}\, C_{8,XY}^0\left(\frac{m_{u_j}^2}{m_{H^+}^2}\right)\Bigg]\,,\end{aligned} \tag{105}$$

and $c_{L,(g)}^{dd,H^\pm} = c_{R,(g)}^{dd,H^\pm\,\star}$.

The analogous expressions for $c_{R,(g)}^{uu,H^\pm,H_k^0}$, which are involved in the expressions of $d_u^{(g)}$ are given as

$$
\begin{aligned}
c_R^{uu,H_k^0} = \sum_{j,k=1}^{3} \frac{-e\,Q_u}{16\pi^2\, m_{u_j}^2} & \left[\Gamma_{uu_j}^{LR\,H_k^0\star}\Gamma_{uu_j}^{LR\,H_k^0}\, C_{8,YY}^0\left(\frac{m_{u_j}^2}{m_{H_k^0}^2}\right) + \Gamma_{u_ju}^{LR\,H_k^0\star}\Gamma_{u_ju}^{LR\,H_k^0}\, C_{8,YY}^0\left(\frac{m_{u_j}^2}{m_{H_k^0}^2}\right)\right. \\
& \left. +\Gamma_{uu_j}^{LR\,H_k^0}\Gamma_{u_ju}^{LR\,H_k^0}\frac{m_{u_j}}{m_u}\, C_{8,XY}^0\left(\frac{m_{u_j}^2}{m_{H_k^0}^2}\right)\right], \qquad (106)
\end{aligned}
$$

$$
\begin{aligned}
c_{R,g}^{uu,H_k^0} = \sum_{j,k=1}^{3} \frac{-g_s}{16\pi^2\, m_{u_j}^2} & \left[\Gamma_{uu_j}^{LR\,H_k^0\star}\Gamma_{uu_j}^{LR\,H_k^0}\, C_{8,YY}^0\left(\frac{m_{u_j}^2}{m_{H_k^0}^2}\right) + \Gamma_{u_ju}^{LR\,H_k^0\star}\Gamma_{u_ju}^{LR\,H_k^0}\, C_{8,YY}^0\left(\frac{m_{u_j}^2}{m_{H_k^0}^2}\right)\right. \\
& \left. +\Gamma_{uu_j}^{LR\,H_k^0}\Gamma_{u_ju}^{LR\,H_k^0}\frac{m_{u_j}}{m_u}\, C_{8,XY}^0\left(\frac{m_{u_j}^2}{m_{H_k^0}^2}\right)\right], \qquad (107)
\end{aligned}
$$

$$
\begin{aligned}
c_R^{uu,H^\pm} = \sum_{j=1}^{3} \frac{-e}{1152\pi^2\, m_{H^+}^2} & \left[5\,\Gamma_{ud_j}^{LR\,H^\pm\star}\Gamma_{ud_j}^{LR\,H^\pm} + 5\,\Gamma_{d_ju}^{LR\,H^\pm\star}\Gamma_{d_ju}^{LR\,H^\pm}\right. \\
& \left. -\Gamma_{ud_j}^{LR\,H^\pm}\Gamma_{d_ju}^{LR\,H^\pm}\frac{m_{d_j}}{m_u}\, 12\,\ln\left(\frac{m_{d_j}^2}{m_{H^+}^2}\right)\right], \qquad (108)
\end{aligned}
$$

$$
\begin{aligned}
c_{R,g}^{uu,H^\pm} = \sum_{j=1}^{3} \frac{g_s}{192\pi^2\, m_{H^+}^2} & \left[\Gamma_{ud_j}^{LR\,H^\pm\star}\Gamma_{ud_j}^{LR\,H^\pm} + \Gamma_{d_ju}^{LR\,H^\pm\star}\Gamma_{d_ju}^{LR\,H^\pm}\right. \\
& \left. -\Gamma_{ud_j}^{LR\,H^\pm}\Gamma_{d_ju}^{LR\,H^\pm}\frac{m_{d_j}}{m_u}\left(9+6\ln\left(\frac{m_{d_j}^2}{m_{H^+}^2}\right)\right)\right]. \qquad (109)
\end{aligned}
$$

Again, we have $c_{L,(g)}^{uu,H_k^0} = c_{R,(g)}^{uu,H_k^0\,\star}$ and $c_{L,(g)}^{uu,H^\pm} = c_{R,(g)}^{uu,H^\pm\,\star}$. The loop functions $C_{7,8,XY,YY}^0(y_j)$ are given in Eq. (83).

10.7 Leptonic decays of neutral mesons

The effective Hamiltonian $\mathcal{H}_{eff}$ which includes the full set of operators for the general decays $PS(\bar{q}_f q_i) \to \ell_A^+ \ell_B^-$ (PS refers to the pseudo-scalar meson) reads

$$
\mathcal{H}_{eff}^{\Delta F=1} = -\frac{G_F^2 M_W^2}{\pi^2}\left[C_V^{q_fq_i} O_V^{q_fq_i} + C_A^{q_fq_i} O_A^{q_fq_i} + C_S^{q_fq_i} O_S^{q_fq_i} + C_P^{q_fq_i} O_P^{q_fq_i} + \text{primed}\right] + \text{h.c.} \qquad (110)
$$

where the operators (together with their primed counterparts) are defined as

$$
\begin{aligned}
\mathcal{O}_V^{q_fq_i} &= (\bar{q}_f\gamma_\mu P_L q_i)\,(\bar{\ell}_B\gamma^\mu\ell_A)\,, & \mathcal{O}_A^{q_fq_i} &= (\bar{q}_f\gamma_\mu P_L q_i)\,(\bar{\ell}_B\gamma^\mu\gamma_5\ell_A)\,, \\
\mathcal{O}_V^{'q_fq_i} &= (\bar{q}_f\gamma_\mu P_R q_i)\,(\bar{\ell}_B\gamma^\mu\ell_A)\,, & \mathcal{O}_A^{'q_fq_i} &= (\bar{q}_f\gamma_\mu P_R q_i)\,(\bar{\ell}_B\gamma^\mu\gamma_5\ell_A)\,, \\
\mathcal{O}_S^{q_fq_i} &= (\bar{q}_f P_L q_i)\,(\bar{\ell}_B\ell_A)\,, & \mathcal{O}_P^{q_fq_i} &= (\bar{q}_f P_L q_i)\,(\bar{\ell}_B\gamma_5\ell_A)\,, \\
\mathcal{O}_S^{'q_fq_i} &= (\bar{q}_f P_R q_i)\,(\bar{\ell}_B\ell_A)\,, & \mathcal{O}_P^{'q_fq_i} &= (\bar{q}_f P_R q_i)\,(\bar{\ell}_B\gamma_5\ell_A)\,.
\end{aligned} \qquad (111)
$$

Making use of the hadronic matrix elements

$$
\begin{aligned}
\langle 0|\bar{q}_f \gamma_\mu \gamma_5 q_i|PS\rangle &= i f_{PS}\, p^\mu_{PS}\,, \\
\langle 0|\bar{q}_f \gamma_5 q_i|PS\rangle &= -i f_{PS} \frac{M^2_{PS}}{(m_{q_f}+m_{q_i})}\,,
\end{aligned}
\tag{112}
$$

one obtains the branching ratio

$$
\begin{aligned}
\mathcal{B}\left[PS(\bar{q}_f q_i) \to \ell_A^+ \ell_B^-\right] = \frac{G_F^4 M_W^4}{32\pi^5} f\left(x_A^2, x_B^2\right) M_{PS}\, f_{PS}^2\, (m_{l_A}+m_{l_B})^2\, \tau_{PS} \\
\times \Bigg\{ \left| \frac{M^2_{PS}\left(C_P^{q_f q_i} - C_P^{\prime q_f q_i}\right)}{\left(m_{q_f}+m_{q_i}\right)(m_{l_A}+m_{l_B})} - \left(C_A^{q_f q_i} - C_A^{\prime q_f q_i}\right)\right|^2 \times \left[1-(x_A - x_B)^2\right] \\
+ \left| \frac{M^2_{PS}\left(C_S^{q_f q_i} - C_S^{\prime q_f q_i}\right)}{(m_{q_f}+m_{q_i})(m_{l_A}+m_{l_B})} + \frac{(m_{l_A}-m_{l_B})}{(m_{l_A}+m_{l_B})}\left(C_V^{q_f q_i} - C_V^{\prime q_f q_i}\right)\right|^2 \times \left[1-(x_A + x_B)^2\right] \Bigg\}\,,
\end{aligned}
\tag{113}
$$

where the function $f(x_i, x_j)$ and the ratio x_i are defined as [149]

$$
f(x_i, x_j) = \sqrt{1 - 2(x_i + x_j) + (x_i - x_j)^2}\,, \quad x_i = \frac{m_{\ell_i}}{M_{PS}}\,.
$$

10.7.1 Wilson coefficients

- *Tree level neutral Higgs contributions to $PS(\bar{q}_f q_i) \to \ell_A^+ \ell_B^-$ in the 2HDM of type III*

  The non-vanishing Wilson coefficients of the operators in Eq. (110) induced through tree-level neutral Higgs ($H_k^0 = H^0, h^0, A^0$) exchange read

$$
\begin{aligned}
C_S^{q_f q_i} &= \frac{\pi^2}{2G_F^2 M_W^2} \sum_{k=1}^{3} \frac{1}{m^2_{H_k^0}} \left(\Gamma^{LR\, H_k^0}_{\ell_B \ell_A} + \Gamma^{RL\, H_k^0}_{\ell_B \ell_A}\right) \Gamma^{RL\, H_k^0}_{q_f q_i} \\
C_P^{q_f q_i} &= \frac{\pi^2}{2G_F^2 M_W^2} \sum_{k=1}^{3} \frac{1}{m^2_{H_k^0}} \left(\Gamma^{LR\, H_k^0}_{\ell_B \ell_A} - \Gamma^{RL\, H_k^0}_{\ell_B \ell_A}\right) \Gamma^{RL\, H_k^0}_{q_f q_i} \\
C_S^{\prime q_f q_i} &= \frac{\pi^2}{2G_F^2 M_W^2} \sum_{k=1}^{3} \frac{1}{m^2_{H_k^0}} \left(\Gamma^{LR\, H_k^0}_{\ell_B \ell_A} + \Gamma^{RL\, H_k^0}_{\ell_B \ell_A}\right) \Gamma^{LR\, H_k^0}_{q_f q_i} \\
C_P^{\prime q_f q_i} &= \frac{\pi^2}{2G_F^2 M_W^2} \sum_{k=1}^{3} \frac{1}{m^2_{H_k^0}} \left(\Gamma^{LR\, H_k^0}_{\ell_B \ell_A} - \Gamma^{RL\, H_k^0}_{\ell_B \ell_A}\right) \Gamma^{LR\, H_k^0}_{q_f q_i}\,.
\end{aligned}
\tag{114}
$$

- *Loop-induced charged Higgs contributions to $B_s \to \mu^+\mu^-$ in the 2HDM of type II*

  As mentioned earlier, we also include in our analysis the 2HDM of type II loop-induced charged Higgs contributions to $B_s \to \mu^+\mu^-$ from Ref. [52]:

$$
C_S^{bs} \;=\; C_P^{bs} = -\frac{m_b V_{tb}^* V_{ts}}{2} \frac{m_\mu}{2M_W^2} \tan^2\beta\, \frac{\log\left(m_H^2/m_t^2\right)}{m_H^2/m_t^2 - 1}\,,
\tag{115}
$$

  where m_b and m_t are understood to be running masses evaluated at the matching scale.

10.8 Flavour-changing lepton decays

The general expressions for the branching ratios of $\tau^- \to e^-\mu^+\mu^-$ and $\tau^- \to \mu^-\mu^+\mu^-$ have the form

$$
\begin{aligned}
\mathcal{B}\left[\tau^- \to e^-\mu^+\mu^-\right] = \frac{m_\tau^5}{12(8\pi)^3\Gamma_\tau} \Bigg(& \left|\frac{\Gamma_{\tau e}^{LR\,H_k^0\star}\Gamma_{\mu\mu}^{LR\,H_k^0}}{m_{H_k^0}^2}\right|^2 + \left|\frac{\Gamma_{e\tau}^{LR\,H_k^0\star}\Gamma_{\mu\mu}^{LR\,H_k^0}}{m_{H_k^0}^2}\right|^2 \\
& + \left|\frac{\Gamma_{\tau e}^{LR\,H_k^0}\Gamma_{\mu\mu}^{LR\,H_k^0}}{m_{H_k^0}^2}\right|^2 + \left|\frac{\Gamma_{e\tau}^{LR\,H_k^0}\Gamma_{\mu\mu}^{LR\,H_k^0}}{m_{H_k^0}^2}\right|^2 \Bigg) \\
\mathcal{B}\left[\tau^- \to \mu^-\mu^+\mu^-\right] = \frac{m_\tau^5}{12(8\pi)^3\Gamma_\tau}\frac{1}{2} \Bigg(& 2\left|\frac{\Gamma_{\tau\mu}^{LR\,H_k^0\star}\Gamma_{\mu\mu}^{LR\,H_k^0}}{m_{H_k^0}^2}\right|^2 + 2\left|\frac{\Gamma_{\mu\tau}^{LR\,H_k^0\star}\Gamma_{\mu\mu}^{LR\,H_k^0}}{m_{H_k^0}^2}\right|^2 \\
& + \left|\frac{\Gamma_{\tau\mu}^{LR\,H_k^0}\Gamma_{\mu\mu}^{LR\,H_k^0}}{m_{H_k^0}^2}\right|^2 + \left|\frac{\Gamma_{\mu\tau}^{LR\,H_k^0}\Gamma_{\mu\mu}^{LR\,H_k^0}}{m_{H_k^0}^2}\right|^2 \Bigg) \, .
\end{aligned}
\tag{116}
$$

Note that the (not explicitly denoted) sum over the Higgses must be performed before taking the various absolute values in Eq. (116).

10.9 Input parameters

In this section we list our input parameters in tabular form.

Parameter	Value (GeV)
$\overline{m}_u(2\text{ GeV})$	0.00219 ± 0.00015 [150]
$\overline{m}_d(2\text{ GeV})$	0.00467 ± 0.00020 [150]
$\overline{m}_s(2\text{ GeV})$	0.095 ± 0.006 [150]
$\overline{m}_c(m_c)$	1.28 ± 0.04 [151]
$\overline{m}_b(m_b)$	4.243 ± 0.043 [89]
$\overline{m}_t(m_t)$	$165.80 \pm 0.54 \pm 0.72$ [14]

Parameter	Value
M_W	80.40 GeV
M_Z	91.19 GeV
$\alpha_s(M_Z)$	0.119
G_F	1.16637×10^{-5} GeV^{-2}
$\alpha_{em}{}^{-1}$	137
v	174.10 GeV

Table 15: Left: Input values for the quark masses used in our article. In the numerical analysis, we used the NNLO expressions in α_s for the running (see for example Ref. [152]) in order to obtain the quark-mass values at higher scales. Right: Electroweak parameters and the strong coupling constant used in our analysis. Concerning the running of α_s we used NNLO expressions (given for example in Ref. [72]).

Parameter	Value
f_{B_s}/f_B	$1.221 \pm 0.010 \pm 0.033$ [14]
f_D	218.9 ± 11.3 MeV [138]
f_{D_s}	$249 \pm 2 \pm 5$ MeV [14]
f_{D_s}/f_D	1.188 ± 0.025 [138]
f_K	$156.3 \pm 0.3 \pm 1.9$ MeV [14]
f_K/f_π	1.193 ± 0.005 [150]

Meson massses	Values (GeV)
$m_{B^\pm(B^0)}$	5.279
m_{B_s}	5.367
$m_{D^\pm(D^0)}$	1.870 (1.865)
m_{D_s}	1.969
$m_{K^\pm(K^0)}$	0.494 (0.498)
$m_{\pi^\pm(\pi^0)}$	0.140 (0.135)

Table 16: Left: Values for decay constants of Ref. [14] obtained by averaging the lattice results of Ref. [138, 153, 154, 155, 156, 157, 158, 159, 160, 161, 162, 163, 164, 165]. Right: Meson masses according to the particle data group (see online update of Ref. [72]).

References

[1] T. Lee, "A Theory of Spontaneous T Violation," *Phys.Rev.*, vol. D8, pp. 1226–1239, 1973.

[2] J. F. Gunion, H. E. Haber, G. L. Kane, and S. Dawson, "THE HIGGS HUNTER'S GUIDE," *Front.Phys.*, vol. 80, pp. 1–448, 2000.

[3] G. Branco, P. Ferreira, L. Lavoura, M. Rebelo, M. Sher, *et al.*, "Theory and phenomenology of two-Higgs-doublet models," *Phys.Rept.*, vol. 516, pp. 1–102, 2012, 1106.0034.

[4] J. E. Kim, "Light Pseudoscalars, Particle Physics and Cosmology," *Phys.Rept.*, vol. 150, pp. 1–177, 1987.

[5] R. Peccei and H. R. Quinn, "CP Conservation in the Presence of Instantons," *Phys.Rev.Lett.*, vol. 38, pp. 1440–1443, 1977.

[6] M. Trodden, "Electroweak baryogenesis: A Brief review," 1998, hep-ph/9805252.

[7] H. E. Haber and G. L. Kane, "The Search for Supersymmetry: Probing Physics Beyond the Standard Model," *Phys.Rept.*, vol. 117, pp. 75–263, 1985.

[8] B. Aubert *et al.*, "Evidence for an excess of $B \to D^{(*)}\tau\nu$ decays," 2012, 1205.5442.

[9] J. Lees *et al.*, "Measurement of an Excess of $B \to D^{(*)}\tau\nu$ Decays and Implications for Charged Higgs Bosons," 2013, 1303.0571.

[10] J. Lees *et al.*, "Evidence of $B \to \tau\nu$ decays with hadronic B tags," 2012, 1207.0698.

[11] B. Aubert *et al.*, "A Search for $B^+ \to \ell^+\nu_\ell$ Recoiling Against $B^- \to D^0\ell^-\bar{\nu}X$," *Phys.Rev.*, vol. D81, p. 051101, 2010.

[12] K. Hara *et al.*, "Evidence for $B^- \to \tau^-\bar{\nu}$ with a Semileptonic Tagging Method," *Phys.Rev.*, vol. D82, p. 071101, 2010, 1006.4201.

[13] I. Adachi *et al.*, "Measurement of $B^- \to \tau^-\bar{\nu}_\tau$ with a Hadronic Tagging Method Using the Full Data Sample of Belle," 2012, 1208.4678.

[14] J. Charles *et al.*, "CP violation and the CKM matrix: Assessing the impact of the asymmetric B factories," *Eur.Phys.J.*, vol. C41, pp. 1–131, 2005, hep-ph/0406184.

[15] G. D'Ambrosio, G. F. Giudice, G. Isidori, and A. Strumia, "Minimal flavour violation: An effective field theory approach," *Nucl. Phys.*, vol. B645, pp. 155–187, 2002, hep-ph/0207036.

[16] A. Crivellin, C. Greub, and A. Kokulu, "Explaining $B \to D\tau\nu$, $B \to D^*\tau\nu$ and $B \to \tau\nu$ in a 2HDM of type III," *Phys.Rev.*, vol. D86, p. 054014, 2012, 1206.2634.

[17] A. J. Buras, M. V. Carlucci, S. Gori, and G. Isidori, "Higgs-mediated FCNCs: Natural Flavour Conservation vs. Minimal Flavour Violation," *JHEP*, vol. 1010, p. 009, 2010, 1005.5310.

[18] G. Blankenburg and G. Isidori, " $B \to \tau\nu$ in multi-Higgs models with MFV," 2011, 1107.1216.

[19] C. Hamzaoui, M. Pospelov, and M. Toharia, "Higgs mediated FCNC in supersymmetric models with large tan Beta," *Phys.Rev.*, vol. D59, p. 095005, 1999, hep-ph/9807350.

[20] K. S. Babu and C. F. Kolda, "Higgs mediated $B^0 \to \mu^+\mu^-$ in minimal supersymmetry," *Phys. Rev. Lett.*, vol. 84, pp. 228–231, 2000, hep-ph/9909476.

[21] M. S. Carena, D. Garcia, U. Nierste, and C. E. Wagner, "Effective Lagrangian for the $\bar{t}bH^+$ interaction in the MSSM and charged Higgs phenomenology," *Nucl.Phys.*, vol. B577, pp. 88–120, 2000, hep-ph/9912516.

[22] G. Isidori and A. Retico, "Scalar flavor changing neutral currents in the large tan beta limit," *JHEP*, vol. 0111, p. 001, 2001, hep-ph/0110121.

[23] A. J. Buras, P. H. Chankowski, J. Rosiek, and L. Slawianowska, " $\Delta M_{d,s}, B^0_{d,s} \to \mu^+\mu^-$ and $B \to X_s\gamma$ in supersymmetry at large $\tan\beta$," *Nucl. Phys.*, vol. B659, p. 3, 2003, hep-ph/0210145.

[24] L. Hofer, U. Nierste, and D. Scherer, "Resummation of $\tan(\beta)$-enhanced supersymmetric loop corrections beyond the decoupling limit," *JHEP*, vol. 0910, p. 081, 2009, 0907.5408.

[25] G. Isidori and A. Retico, "$B_{s,d} \to \ell^+\ell^-$ and $K_L \to \ell^+\ell^-$ in SUSY models with nonminimal sources of flavor mixing," *JHEP*, vol. 0209, p. 063, 2002, hep-ph/0208159.

[26] A. Crivellin, "Effective Higgs Vertices in the generic MSSM," *Phys. Rev.*, vol. D83, p. 056001, 2011, 1012.4840.

[27] D. Noth and M. Spira, "Supersymmetric Higgs Yukawa Couplings to Bottom Quarks at next-to-next-to-leading Order," *JHEP*, vol. 06, p. 084, 2011, 1001.1935.

[28] A. Crivellin and C. Greub, "Two-loop SQCD corrections to Higgs-quark-quark couplings in the generic MSSM," 2012, 1210.7453.

[29] Y. Okada, M. Yamaguchi, and T. Yanagida, "Upper bound of the lightest Higgs boson mass in the minimal supersymmetric standard model," *Prog.Theor.Phys.*, vol. 85, pp. 1–6, 1991.

[30] H. E. Haber and R. Hempfling, "Can the mass of the lightest Higgs boson of the minimal supersymmetric model be larger than m_Z?," *Phys.Rev.Lett.*, vol. 66, pp. 1815–1818, 1991.

[31] J. R. Ellis, G. Ridolfi, and F. Zwirner, "Radiative corrections to the masses of supersymmetric Higgs bosons," *Phys.Lett.*, vol. B257, pp. 83–91, 1991.

[32] A. Brignole, "Radiative corrections to the supersymmetric charged Higgs boson mass," *Phys.Lett.*, vol. B277, pp. 313–323, 1992.

[33] P. H. Chankowski, S. Pokorski, and J. Rosiek, "Complete on-shell renormalization scheme for the minimal supersymmetric Higgs sector," *Nucl.Phys.*, vol. B423, pp. 437–496, 1994, hep-ph/9303309.

[34] A. Dabelstein, "The One loop renormalization of the MSSM Higgs sector and its application to the neutral scalar Higgs masses," *Z.Phys.*, vol. C67, pp. 495–512, 1995, hep-ph/9409375.

[35] A. Pilaftsis and C. E. Wagner, "Higgs bosons in the minimal supersymmetric standard model with explicit CP violation," *Nucl.Phys.*, vol. B553, pp. 3–42, 1999, hep-ph/9902371.

[36] M. S. Carena, J. R. Ellis, A. Pilaftsis, and C. Wagner, "Renormalization group improved effective potential for the MSSM Higgs sector with explicit CP violation," *Nucl.Phys.*, vol. B586, pp. 92–140, 2000, hep-ph/0003180.

[37] A. Freitas, E. Gasser, and U. Haisch, "Supersymmetric large tan(β) corrections to $\Delta_{M_{d,s}}$ and $B_{d,s} \to \mu^+\mu^-$ revisited," *Phys.Rev.*, vol. D76, p. 014016, 2007, hep-ph/0702267.

[38] M. Gorbahn, S. Jager, U. Nierste, and S. Trine, "The supersymmetric Higgs sector and $B - \bar{B}$ mixing for large $\tan\beta$," *Phys.Rev.*, vol. D84, p. 034030, 2011, 0901.2065.

[39] A. Crivellin, L. Hofer, and J. Rosiek, "Complete resummation of chirally-enhanced loop-effects in the MSSM with non-minimal sources of flavor-violation," 2011, 1103.4272.

[40] J. Rosiek, "Complete set of Feynman rules for the MSSM: Erratum," 1995, hep-ph/9511250.

[41] S. L. Glashow and S. Weinberg, "Natural Conservation Laws for Neutral Currents," *Phys.Rev.*, vol. D15, p. 1958, 1977.

[42] T. Miki *et al.*, "Effects of charged Higgs boson and QCD corrections in $\bar{B} \to D\tau\bar{\nu}_\tau$," pp. 116–124, 2002, hep-ph/0210051.

[43] A. Wahab El Kaffas, P. Osland, and O. M. Ogreid, "Constraining the Two-Higgs-Doublet-Model parameter space," *Phys.Rev.*, vol. D76, p. 095001, 2007, 0706.2997.

[44] O. Deschamps, S. Descotes-Genon, S. Monteil, V. Niess, S. T'Jampens, *et al.*, "The Two Higgs Doublet of Type II facing flavour physics data," *Phys.Rev.*, vol. D82, p. 073012, 2010, 0907.5135.

[45] S. Bertolini, F. Borzumati, A. Masiero, and G. Ridolfi, "Effects of supergravity induced electroweak breaking on rare B decays and mixings," *Nucl.Phys.*, vol. B353, pp. 591–649, 1991.

[46] M. Ciuchini, G. Degrassi, P. Gambino, and G. Giudice, "Next-to-leading QCD corrections to $B \to X_s\gamma$: Standard model and two Higgs doublet model," *Nucl.Phys.*, vol. B527, pp. 21–43, 1998, hep-ph/9710335.

[47] F. Borzumati and C. Greub, "2HDMs predictions for $\bar{B} \to X_s\gamma$ in NLO QCD," *Phys.Rev.*, vol. D58, p. 074004, 1998, hep-ph/9802391.

[48] M. Misiak, H. Asatrian, K. Bieri, M. Czakon, A. Czarnecki, *et al.*, "Estimate of $\mathcal{B}(\bar{B} \to X_s\gamma)$ at $O(\alpha_s^2)$," *Phys.Rev.Lett.*, vol. 98, p. 022002, 2007, hep-ph/0609232.

[49] T. Hermann, M. Misiak, and M. Steinhauser, "$\bar{B} \to X_s\gamma$ in the Two Higgs Doublet Model up to Next-to-Next-to-Leading Order in QCD," 2012, 1208.2788.

[50] X. He, T. Nguyen, and R. Volkas, "B MESON RARE DECAYS IN TWO HIGGS DOUBLETS MODELS," *Phys.Rev.*, vol. D38, p. 814, 1988.

[51] W. Skiba and J. Kalinowski, "$B_s \to \tau^+\tau^-$ decay in a two Higgs doublet model," *Nucl.Phys.*, vol. B404, pp. 3–19, 1993.

[52] H. E. Logan and U. Nierste, " $B_{s,d} \to \ell^+\ell^-$ in a two Higgs doublet model," *Nucl.Phys.*, vol. B586, pp. 39–55, 2000, hep-ph/0004139.

[53] W.-S. Hou, "Enhanced charged Higgs boson effects in $B^- \to \tau\bar{\nu}, \mu\bar{\nu}$, and $b \to \tau\bar{\nu}X$," *Phys.Rev.*, vol. D48, pp. 2342–2344, 1993.

[54] A. Akeroyd and S. Recksiegel, "The Effect of $H^\pm$ on $B^\pm \to \tau^\pm\nu_\tau$ and $B^\pm \to \mu^\pm\nu_\mu$," *J.Phys.G*, vol. G29, pp. 2311–2317, 2003, hep-ph/0306037.

[55] S. Fajfer, J. F. Kamenik, and I. Nisandzic, "On the $B \to D^*\tau\nu_\tau$ Sensitivity to New Physics," 2012, 1203.2654.

[56] M. Tanaka, "Charged Higgs effects on exclusive semitauonic B decays," *Z.Phys.*, vol. C67, pp. 321–326, 1995, hep-ph/9411405.

[57] U. Nierste, S. Trine, and S. Westhoff, "Charged-Higgs effects in a new $B \to D\tau\nu$ differential decay distribution," *Phys.Rev.*, vol. D78, p. 015006, 2008, 0801.4938.

[58] A. Akeroyd, "Effect of $H^\pm$ on $D_s^+ \to \mu\nu$ and $D_s^+ \to \tau\nu$," *Prog.Theor.Phys.*, vol. 111, pp. 295–299, 2004, hep-ph/0308260.

[59] A. Akeroyd and C. H. Chen, "Effect of $H^\pm$ on $B \to \tau\nu_\tau$ and $D_s^+ \to \tau, \mu\nu$," *Phys.Rev.*, vol. D75, p. 075004, 2007, hep-ph/0701078.

[60] A. Akeroyd and F. Mahmoudi, "Constraints on charged Higgs bosons from $D_s^+ \to \mu\nu$ and $D_s^+ \to \tau\nu$," *JHEP*, vol. 0904, p. 121, 2009, 0902.2393.

[61] M. Antonelli *et al.*, "Precision tests of the Standard Model with leptonic and semileptonic kaon decays," 2008, 0801.1817.

[62] M. Baak, M. Goebel, J. Haller, A. Hoecker, D. Ludwig, K. Moenig, M. Schott and J. Stelzer, Eur. Phys. J. C **72** (2012) 2003 [arXiv:1107.0975 [hep-ph]].

[63] S. Chatrchyan *et al.*, "Search for neutral Higgs bosons decaying to tau pairs in pp collisions at $\sqrt{s} = 7$ TeV," *Phys.Lett.*, vol. B713, pp. 68–90, 2012, 1202.4083.

[64] A. Pich and P. Tuzon, "Yukawa Alignment in the Two-Higgs-Doublet Model," *Phys.Rev.*, vol. D80, p. 091702, 2009, 0908.1554.

[65] M. Jung, A. Pich, and P. Tuzon, "Charged-Higgs phenomenology in the Aligned two-Higgs-doublet model," *JHEP*, vol. 1011, p. 003, 2010, 1006.0470.

[66] F. Mahmoudi and O. Stal, "Flavor constraints on the two-Higgs-doublet model with general Yukawa couplings," *Phys.Rev.*, vol. D81, p. 035016, 2010, 0907.1791.

[67] E. Iltan, "Electric dipole moments of charged leptons and lepton flavor violating interactions in the general two Higgs doublet model," *Phys.Rev.*, vol. D64, p. 013013, 2001, hep-ph/0101017.

[68] T. Cheng and M. Sher, "Mass Matrix Ansatz and Flavor Nonconservation in Models with Multiple Higgs Doublets," *Phys.Rev.*, vol. D35, p. 3484, 1987.

[69] R. Aaij *et al.*, "First evidence for the decay $B_s \to \mu^+\mu^-$," 2012, 1211.2674.

[70] A. J. Buras, J. Girrbach, D. Guadagnoli, and G. Isidori, "On the Standard Model prediction for $BR(B_{s,d} \to \mu^+\mu^-)$," 2012, 1208.0934.

[71] G. Isidori and R. Unterdorfer, "On the short distance constraints from $K_{L,S} \to \mu^+\mu^-$," *JHEP*, vol. 0401, p. 009, 2004, hep-ph/0311084.

[72] J. Beringer *et al.*, "Review of Particle Physics (RPP)," *Phys.Rev.*, vol. D86, p. 010001, 2012.

[73] T. Inami and C. Lim *Prog. Theor. Phys*, vol. 65, p. 297, 1981.

[74] M. Ciuchini, E. Franco, V. Lubicz, G. Martinelli, I. Scimemi, *et al.*, "Next-to-leading order QCD corrections to $\Delta F = 2$ effective Hamiltonians," *Nucl.Phys.*, vol. B523, pp. 501–525, 1998, hep-ph/9711402.

[75] A. J. Buras, M. Misiak, and J. Urban, "Two loop QCD anomalous dimensions of flavor changing four quark operators within and beyond the standard model," *Nucl.Phys.*, vol. B586, pp. 397–426, 2000, hep-ph/0005183.

[76] M. Bona *et al.*, "Model-independent constraints on Δ F=2 operators and the scale of new physics," *JHEP*, vol. 0803, p. 049, 2008, 0707.0636.

[77] D. Becirevic, M. Ciuchini, E. Franco, V. Gimenez, G. Martinelli, *et al.*, "$B_d - \bar{B}_d$ mixing and the $B_d \to J/\psi K_s$ asymmetry in general SUSY models," *Nucl.Phys.*, vol. B634, pp. 105–119, 2002, hep-ph/0112303.

[78] M. Ciuchini, V. Lubicz, L. Conti, A. Vladikas, A. Donini, *et al.*, "Delta M(K) and epsilon(K) in SUSY at the next-to-leading order," *JHEP*, vol. 9810, p. 008, 1998, hep-ph/9808328.

[79] V. Lubicz and C. Tarantino, “Flavour physics and Lattice QCD: Averages of lattice inputs for the Unitarity Triangle Analysis,” *Nuovo Cim.*, vol. B123, pp. 674–688, 2008, 0807.4605.

[80] D. Becirevic, V. Gimenez, G. Martinelli, M. Papinutto, and J. Reyes, “Combined relativistic and static analysis for all Delta B=2 operators,” *Nucl.Phys.Proc.Suppl.*, vol. 106, pp. 385–387, 2002, hep-lat/0110117.

[81] M. Ciuchini, G. D’Agostini, E. Franco, V. Lubicz, G. Martinelli, *et al.*, “2000 CKM triangle analysis: A Critical review with updated experimental inputs and theoretical parameters,” *JHEP*, vol. 0107, p. 013, 2001, hep-ph/0012308.

[82] A. Lenz, U. Nierste, J. Charles, S. Descotes-Genon, A. Jantsch, *et al.*, “Anatomy of New Physics in $B - \bar{B}$ mixing,” *Phys.Rev.*, vol. D83, p. 036004, 2011, 1008.1593.

[83] M. Bona *et al.*, “The UTfit Collaboration Average of D meson mixing data: Spring 2012,” 2012, 1206.6245.

[84] K. Hayasaka, K. Inami, Y. Miyazaki, K. Arinstein, V. Aulchenko, *et al.*, “Search for Lepton Flavor Violating Tau Decays into Three Leptons with 719 Million Produced $\tau^+\tau^-$ Pairs,” *Phys.Lett.*, vol. B687, pp. 139–143, 2010, 1001.3221.

[85] U. Bellgardt *et al.*, “Search for the Decay $\mu^+ \to e^+e^+e^-$,” *Nucl.Phys.*, vol. B299, p. 1, 1988.

[86] S. Stone, “Planery talk at the international conference on high energy physics (ichep 2012), melbourne, australia,” *Planery talk at the International Conference on High Energy Physics (ICHEP 2012), Melbourne, Australia,*, July 4-11th, 2012.

[87] B. Collaboration, “Precision measurement of the $b \to x_s\gamma$ photon energy spectrum, branching fraction, and direct cp asymmetry $a_{CP}(b \to x_{s+d}\gamma)$,” 07 2012, 1207.2690v1,1207.5772.

[88] J. Lees *et al.*, “Exclusive Measurements of $b \to s\gamma$ Transition Rate and Photon Energy Spectrum,” 2012, 1207.2520.

[89] Y. Amhis *et al.*, “Averages of b-hadron, c-hadron, and τ-lepton properties as of early 2012,” 2012, 1207.1158.

[90] M. Benzke, S. J. Lee, M. Neubert, and G. Paz, “Factorization at Subleading Power and Irreducible Uncertainties in $\bar{B} \to X_s\gamma$ Decay,” *JHEP*, vol. 1008, p. 099, 2010, 1003.5012.

[91] T. Hurth and M. Nakao, “Radiative and Electroweak Penguin Decays of B Mesons,” *Ann.Rev.Nucl.Part.Sci.*, vol. 60, pp. 645–677, 2010, 1005.1224.

[92] P. del Amo Sanchez *et al.*, “Study of $B \to X\gamma$ decays and determination of $|V_{td}/V_{ts}|$,” *Phys.Rev.*, vol. D82, p. 051101, 2010, 1005.4087.

[93] W. Wang, “ $b \to s\gamma$ and $b \to d\gamma$ (B factories) ,” 2011, 1102.1925.

[94] A. Crivellin and L. Mercolli, “ $B \to X_d\gamma$ and constraints on new physics,” *Phys.Rev.*, vol. D84, p. 114005, 2011, 1106.5499.

[95] A. Ali, H. Asatrian, and C. Greub, "Inclusive decay rate for $B \to X_d\gamma$ in next-to-leading logarithmic order and CP asymmetry in the standard model," *Phys.Lett.*, vol. B429, pp. 87–98, 1998, hep-ph/9803314.

[96] T. Hurth, E. Lunghi, and W. Porod, "Untagged $\bar{B} \to X_{s+d}\gamma$ CP asymmetry as a probe for new physics," *Nucl.Phys.*, vol. B704, pp. 56–74, 2005, hep-ph/0312260.

[97] J. Adam *et al.*, "New constraint on the existence of the $\mu^+ \to e^+\gamma$ decay," 2013, 1303.0754.

[98] B. Aubert *et al.*, "Searches for Lepton Flavor Violation in the Decays $\tau^\pm \to e^\pm\gamma$ and $\tau^\pm \to \mu^\pm\gamma$," *Phys.Rev.Lett.*, vol. 104, p. 021802, 2010, 0908.2381.

[99] K. Hayasaka *et al.*, "New search for $\tau \to \mu\gamma$ and $\tau \to e\gamma$ decays at Belle," *Phys.Lett.*, vol. B666, pp. 16–22, 2008, 0705.0650.

[100] J. Hudson, D. Kara, I. Smallman, B. Sauer, M. Tarbutt, *et al.*, "Improved measurement of the shape of the electron," *Nature*, vol. 473, pp. 493–496, 2011.

[101] G. Bennett *et al.*, "An Improved Limit on the Muon Electric Dipole Moment," *Phys.Rev.*, vol. D80, p. 052008, 2009, 0811.1207.

[102] K. Inami *et al.*, "Search for the electric dipole moment of the tau lepton," *Phys.Lett.*, vol. B551, pp. 16–26, 2003, hep-ex/0210066.

[103] C. Baker, D. Doyle, P. Geltenbort, K. Green, M. van der Grinten, *et al.*, "An Improved experimental limit on the electric dipole moment of the neutron," *Phys.Rev.Lett.*, vol. 97, p. 131801, 2006, hep-ex/0602020.

[104] J. Hisano, M. Nagai, P. Paradisi, and Y. Shimizu, "Waiting for $\mu \to e\gamma$ from the MEG experiment," *JHEP*, vol. 0912, p. 030, 2009, 0904.2080.

[105] M. Passera, "The Standard model prediction of the muon anomalous magnetic moment," *J.Phys.*, vol. G31, pp. R75–R94, 2005, hep-ph/0411168.

[106] M. Passera, "Status of the standard model prediction of the muon $g - 2$," *Nucl.Phys.Proc.Suppl.*, vol. 155, pp. 365–368, 2006, hep-ph/0509372.

[107] M. Davier, "The Hadronic contribution to $(g - 2)_\mu$," *Nucl.Phys.Proc.Suppl.*, vol. 169, pp. 288–296, 2007, hep-ph/0701163.

[108] K. Hagiwara, A. Martin, D. Nomura, and T. Teubner, "Improved predictions for $g-2$ of the muon and $\alpha_{QED}(M_Z^2)$," *Phys.Lett.*, vol. B649, pp. 173–179, 2007, hep-ph/0611102.

[109] A. J. Buras, G. Isidori, and P. Paradisi, "EDMs versus CPV in $B_{s,d}$ mixing in two Higgs doublet models with MFV," *Phys.Lett.*, vol. B694, pp. 402–409, 2011, 1007.5291.

[110] D. A. Demir, O. Lebedev, K. A. Olive, M. Pospelov, and A. Ritz, "Electric dipole moments in the MSSM at large tan beta," *Nucl.Phys.*, vol. B680, pp. 339–374, 2004, hep-ph/0311314.

[111] M. Pospelov and A. Ritz, "Neutron EDM from electric and chromoelectric dipole moments of quarks," *Phys.Rev.*, vol. D63, p. 073015, 2001, hep-ph/0010037.

[112] D. A. Demir, M. Pospelov, and A. Ritz, "Hadronic EDMs, the Weinberg operator, and light gluinos," *Phys.Rev.*, vol. D67, p. 015007, 2003, hep-ph/0208257.

[113] K. A. Olive, M. Pospelov, A. Ritz, and Y. Santoso, "CP-odd phase correlations and electric dipole moments," *Phys.Rev.*, vol. D72, p. 075001, 2005, hep-ph/0506106.

[114] M. Antonelli, V. Cirigliano, G. Isidori, F. Mescia, M. Moulson, *et al.*, "An Evaluation of $|V_{us}|$ and precise tests of the Standard Model from world data on leptonic and semileptonic kaon decays," *Eur.Phys.J.*, vol. C69, pp. 399–424, 2010, 1005.2323.

[115] R. Decker and M. Finkemeier, "Radiative corrections to the decay $\tau \to \pi(K)\nu_\tau$," *Phys.Lett.*, vol. B316, pp. 403–406, 1993, hep-ph/9307372.

[116] S. Banerjee, "Lepton Universality, $|V_{us}|$ and search for second class current in tau decays," 2008, 0811.1429.

[117] J. F. Kamenik and F. Mescia, " $B \to D\tau\nu$ Branching Ratios: Opportunity for Lattice QCD and Hadron Colliders," *Phys.Rev.*, vol. D78, p. 014003, 2008, 0802.3790.

[118] J. Korner and G. Schuler, "Exclusive Semileptonic Decays of Bottom Mesons in the Spectator Quark Model," *Z.Phys.*, vol. C38, p. 511, 1988.

[119] J. Korner and G. Schuler, "LEPTON MASS EFFECTS IN SEMILEPTONIC B MESON DECAYS," *Phys.Lett.*, vol. B231, p. 306, 1989.

[120] J. Korner and G. Schuler, "Exclusive Semileptonic Heavy Meson Decays Including Lepton Mass Effects," *Z.Phys.*, vol. C46, p. 93, 1990.

[121] P. Heiliger and L. Sehgal, "SEMILEPTONIC DECAYS OF B MESONS INTO $\tau\nu_\tau$," *Phys.Lett.*, vol. B229, p. 409, 1989.

[122] X.-Y. Pham, "New method for determination of the $D \to \bar{K}^* e\nu$ axial form-factors without resort to angular distributions," *Phys.Rev.*, vol. D46, p. R1909, 1992.

[123] S. Fajfer, J. F. Kamenik, I. Nisandzic, and J. Zupan, "Implications of lepton flavor universality violations in B decays," 2012, 1206.1872.

[124] N. Deshpande and A. Menon, "Hints of R-parity violation in B decays into $\tau\nu$," 2012, 1208.4134.

[125] X.-G. He and G. Valencia, "B decays with τ-leptons in non-universal left-right models," 2012, 1211.0348.

[126] A. Celis, M. Jung, X.-Q. Li, and A. Pich, "Sensitivity to charged scalars in $B \to D^{(*)}\tau\nu_\tau$ and $B \to \tau\nu_\tau$ decays," 2012, 1210.8443.

[127] M. Tanaka and R. Watanabe, "New physics in the weak interaction of $\bar{B} \to D^{(*)}\tau\bar{\nu}$," 2012, 1212.1878.

[128] J. A. Bailey, A. Bazavov, C. Bernard, C. Bouchard, C. DeTar, *et al.*, "Refining new-physics searches in $B \to D\tau\nu$ decay with lattice QCD," *Phys.Rev.Lett.*, vol. 109, p. 071802, 2012, 1206.4992.

[129] A. Datta, M. Duraisamy, and D. Ghosh, "Diagnosing New Physics in $b \to c\,\tau\,\nu_\tau$ decays in the light of the recent BaBar result," *Phys.Rev.*, vol. D86, p. 034027, 2012, 1206.3760.

[130] D. Becirevic, N. Kosnik, and A. Tayduganov, "$\bar{B} \to D\tau\bar{\nu}_\tau$ vs. $\bar{B} \to D\mu\bar{\nu}_\mu$," *Phys.Lett.*, vol. B716, pp. 208–213, 2012, 1206.4977.

[131] P. Ko, Y. Omura, and C. Yu, "$B \to D^{(*)}\tau\nu$ and $B \to \tau\nu$ in chiral $U(1)'$ models with flavored multi Higgs doublets," 2012, 1212.4607.

[132] P. Biancofiore, P. Colangelo, and F. De Fazio, "On the anomalous enhancement observed in $B \to D^{(*)}\,\tau\,\bar{\nu}_\tau$ decays," 2013, 1302.1042.

[133] Y. Sakaki and H. Tanaka, "Constraints of the Charged Scalar Effects Using the Forward-Backward Asymmetry on $B \to D^{(*)}\tau\bar{\nu}_\tau$," 2012, 1205.4908.

[134] B. A. Dobrescu and A. S. Kronfeld, "Accumulating evidence for nonstandard leptonic decays of D_s mesons," *Phys.Rev.Lett.*, vol. 100, p. 241802, 2008, 0803.0512.

[135] J. Alexander *et al.*, "Measurement of $B(D_s^+ \to \ell^+\nu)$ and the Decay Constant $f_{D_s^+}$ From 600 $/pb^{-1}$ of $e^\pm$ Annihilation Data Near 4170 MeV," *Phys.Rev.*, vol. D79, p. 052001, 2009, 0901.1216.

[136] P. Onyisi *et al.*, "Improved Measurement of Absolute Branching Fraction of $D_s^+ \to \tau\nu_\tau$," *Phys.Rev.*, vol. D79, p. 052002, 2009, 0901.1147.

[137] J. N. Simone, "The decay constants f_{D_s} and f_{D^+} form lattice QCD," *Int.J.Mod.Phys.Conf.Ser.*, vol. 02, pp. 92–96, 2011.

[138] A. Bazavov *et al.*, "*B*- and *D*-meson decay constants from three-flavor lattice QCD," *Phys.Rev.*, vol. D85, p. 114506, 2012, 1112.3051.

[139] V. G. M. J. Barranco, D. Delepine and L. Lopez-Lozano, "Constraining New Physics with D meson decays," 2013, 1303.3896.

[140] G. Burdman, J. T. Goldman, and D. Wyler, "Radiative leptonic decays of heavy mesons," *Phys.Rev.*, vol. D51, pp. 111–117, 1995, hep-ph/9405425.

[141] A. Masiero and P. Paradisi, "The B - TAU FCNC connection in SUSY Unified Theories," *J.Phys.Conf.Ser.*, vol. 53, pp. 248–254, 2006, hep-ph/0609262.

[142] A. Dedes, J. R. Ellis, and M. Raidal, "Higgs mediated $B^0_{s,d} \to \mu\tau$, $e\tau$ and $\tau \to 3\mu$, $e\mu\mu$ decays in supersymmetric seesaw models," *Phys.Lett.*, vol. B549, pp. 159–169, 2002, hep-ph/0209207.

[143] A. Dedes, J. Rosiek, and P. Tanedo, "Complete One-Loop MSSM Predictions for $B^0 \to \ell^+\ell'^-$ at the Tevatron and LHC," *Phys.Rev.*, vol. D79, p. 055006, 2009, 0812.4320.

[144] D. Boubaa, A. Datta, M. Duraisamy, and S. Khalil, "Predictions for $B \to \tau\bar{\mu} + \mu\bar{\tau}$," 2012, 1211.5168.

[145] T. Aaltonen *et al.*, "Search for the Decays $B^0_{(s)} \to e^+\mu^-$ and $B^0_{(s)} \to e^+e^-$ in CDF Run II," *Phys.Rev.Lett.*, vol. 102, p. 201801, 2009, 0901.3803.

[146] B. Aubert *et al.*, "Searches for the decays $B^0 \to \ell^\pm \tau^\mp$ and $B^+ \to \ell^+ \nu$ ($\ell = e, \mu$) using hadronic tag reconstruction," *Phys.Rev.*, vol. D77, p. 091104, 2008, 0801.0697.

[147] G. Passarino and M. J. G. Veltman, Nucl. Phys. B **160** (1979) 151.

[148] W. Altmannshofer, A. J. Buras, and D. Guadagnoli, "The MFV limit of the MSSM for low $\tan(\beta)$: Meson mixings revisited," *JHEP*, vol. 0711, p. 065, 2007, hep-ph/0703200.

[149] P. H. Chankowski and L. Slawianowska, " $B^0_{s,d} \to \mu^+\mu^-$ decay in the MSSM," *Phys.Rev.*, vol. D63, p. 054012, 2001, hep-ph/0008046.

[150] G. Colangelo, S. Durr, A. Juttner, L. Lellouch, H. Leutwyler, *et al.*, "Review of lattice results concerning low energy particle physics," *Eur.Phys.J.*, vol. C71, p. 1695, 2011, 1011.4408.

[151] B. Blossier *et al.*, "Average up/down, strange and charm quark masses with Nf=2 twisted mass lattice QCD," *Phys.Rev.*, vol. D82, p. 114513, 2010, 1010.3659.

[152] A. J. Buras, "Weak Hamiltonian, CP violation and rare decays," pp. 281–539, 1998, hep-ph/9806471.

[153] B. Blossier *et al.*, "Pseudoscalar decay constants of kaon and D-mesons from $N_f = 2$ twisted mass Lattice QCD," *JHEP*, vol. 0907, p. 043, 2009, 0904.0954.

[154] C. Bernard, C. E. DeTar, L. Levkova, S. Gottlieb, U. Heller, *et al.*, "Status of the MILC light pseudoscalar meson project," *PoS*, vol. LAT2007, p. 090, 2007, 0710.1118.

[155] E. Follana, C. Davies, G. Lepage, and J. Shigemitsu, "High Precision determination of the pi, K, D and D(s) decay constants from lattice QCD," *Phys.Rev.Lett.*, vol. 100, p. 062002, 2008, 0706.1726.

[156] C. Aubin, J. Laiho, and R. S. Van de Water, "Light pseudoscalar meson masses and decay constants from mixed action lattice QCD," *PoS*, vol. LATTICE2008, p. 105, 2008, 0810.4328.

[157] S. Beane, P. Bedaque, K. Orginos, and M. Savage, "f_K/f_π in Full QCD with Domain Wall Valence Quarks," *Phys.Rev.*, vol. D75, p. 094501, 2007, hep-lat/0606023.

[158] S. Durr, Z. Fodor, C. Hoelbling, S. Katz, S. Krieg, *et al.*, "The ratio F_K/F_π in QCD," *Phys.Rev.*, vol. D81, p. 054507, 2010, 1001.4692.

[159] C. Bernard *et al.*, "Lattice calculation of heavy light decay constants with two flavors of dynamical quarks," *Phys.Rev.*, vol. D66, p. 094501, 2002, hep-lat/0206016.

[160] A. Bazavov *et al.*, "The D_s and D^+ Leptonic Decay Constants from Lattice QCD," *PoS*, vol. LAT2009, p. 249, 2009, 0912.5221.

[161] C. Davies, C. McNeile, E. Follana, G. Lepage, H. Na, *et al.*, "Update: Precision D_s decay constant from full lattice QCD using very fine lattices," *Phys.Rev.*, vol. D82, p. 114504, 2010, 1008.4018.

[162] P. Dimopoulos *et al.*, "Lattice QCD determination of m_b, f_B and f_{B_s} with twisted mass Wilson fermions," *JHEP*, vol. 1201, p. 046, 2012, 1107.1441.

[163] E. Gamiz, C. T. Davies, G. P. Lepage, J. Shigemitsu, and M. Wingate, "Neutral B Meson Mixing in Unquenched Lattice QCD," *Phys.Rev.*, vol. D80, p. 014503, 2009, 0902.1815.

[164] C. McNeile, C. Davies, E. Follana, K. Hornbostel, and G. Lepage, "High-Precision f_{B_s} and HQET from Relativistic Lattice QCD," *Phys.Rev.*, vol. D85, p. 031503, 2012, 1110.4510.

[165] C. Albertus, Y. Aoki, P. Boyle, N. Christ, T. Dumitrescu, *et al.*, "Neutral B-meson mixing from unquenched lattice QCD with domain-wall light quarks and static b-quarks," *Phys.Rev.*, vol. D82, p. 014505, 2010, 1001.2023.

Acknowledgements

First of all, I would like to express my deepest gratitudes to Christoph Greub for offering me the opportunity for this thesis and for his continuous support and advices. His knowledge and endless patience have had an enormous influence on this thesis as well as on my scientific work in general. I am really indebted to him more than he knows. I would also like to thank Hrachia M. Asatrian and Andreas Crivellin for their close collaborations as well as Prof. Daniel Wyler for being the co-referee for my thesis.

Furthermore, I thank all members of the institute for providing me a very pleasant working atmosphere. I owe special thanks to Christof Schüpbach and my office mate Peter Stoffer for numerous interesting discussions within or beyond Physics and for their invaluable computer support. I further thank all my friends in Bern who made my stay pleasant.

Last but not least, special thanks go to my family for their continuous support throughout my life. There are no words to describe my appreciation and gratitudes I feel for them.

Erklärung

gemäss Art. 28 Abs. 2 RSL 05

Name, Vorname:	Kokulu, Ahmet
Matrikelnummer:	09-121-435
Studiengang:	Physik
	Bachelor ☐ Master ☐ Dissertation ☒
Titel der Arbeit:	Flavor phenomenology of rare processes in the Standard Model and beyond
Leiter der Arbeit:	Prof. Dr. Christoph Greub

Ich erkläre hiermit, dass ich diese Arbeit selbständig verfasst und keine anderen als die angegebenen Quellen benutzt habe. Alle Stellen, die wörtlich oder sinngemäss aus Quellen entnommen wurden, habe ich als solche gekennzeichnet. Mir ist bekannt, dass andernfalls der Senat gemäss Artikel 36 Absatz 1 Buchstabe o des Gesetzes vom 5. September 1996 über die Universität zum Entzug des auf Grund dieser Arbeit verliehenen Titels berechtigt ist.

Bern, 03.09.2013

Ahmet Kokulu

Curriculum vitæ

Personal Data

Name	**Kokulu, Ahmet**
Date of birth	January 15, 1985
Nationality	Turkish
Marital status	Single
Private address	Wankdorffeldstrasse 85, CH-3014 Bern, Switzerland phone: +41 76 607 65 90
Work address	Albert Einstein Center for Fundamental Physics, Institute for Theoretical Physics, Sidlerstrasse 5, CH-3012 Bern, Switzerland phone: +41 31 631 82 98 email: akokulu@itp.unibe.ch

Education

2010 - today	University of Bern Ph.D. student of Prof. Dr. Ch. Greub
September 2008	Middle East Technical University (METU) Master of Science in Physics: $\eta - \eta'$ *mixing in Chiral perturbation theory* supervised by Prof. Dr. Altuğ Özpineci
2001- 2006	METU Department of Physics Bachelor of Science in Physics
1998 - 2001	High school in Harbiye, Antakya/Turkey
1994 - 1997	Secondary school in Gümüşgöze, Antakya/Turkey
1989 - 1994	Primary school in Gümüşgöze, Antakya/Turkey